SPATIOTEMPORAL EFFECTS OF DIETARY BIOACTIVES ON LGR5^{+} STEM CELLS DURING COLON TUMORIGENESIS

A Dissertation

by

EUN JOO KIM

Submitted to the Office of Graduate and Professional Studies of
Texas A&M University
in partial fulfillment of the requirements for the degree of

DOCTOR OF PHILOSOPHY

Chair of Committee,	Robert S. Chapkin
Committee Members,	David W. Threadgill
	Rajesh C. Miranda
	Robin Fuchs-Young
Head of Department,	Warren E. Zimmer

December 2017

Major Subject: Medical Sciences

ABSTRACT

To better understand how the stem cells respond to environmental factors such as diet and carcinogen, we investigated the chemo-protective effects of dietary agents (n-3 PUFA and curcumin) on DNA damage response in colonic stem cells isolated from Lgr5-EGFP-IRES-CreER^{T2} knock in mice injected with AOM. We demonstrated that n-3 PUFA and curcumin synergize to promote targeted apoptosis of damaged Lgr5^{+} stem cells in part by enhancing p53 signaling in Lgr5^{+} stem cells at the tumor initiation stage. In addition, at the pre-tumor stage of tumorigenesis in colon cancer, we demonstrated n-3 PUFA and curcumin combination synergistically reduces nuclear β-catenin levels in aberrant crypt foci, a surrogate marker of colon cancer. In order to assess the dose-dependency of n-3 PUFA and curcumin action, we also calculated the median effective concentration and the Human equivalent dose of n-3 PUFA + curcumin required to remove DNA damaged Lgr5^{+} stem cells by targeted apoptosis.

In order to further elucidate the effects of oncogenesis on the biophysical properties of the colonocyte plasma membrane at the pre tumor stage, we generated CDX2P-CreER^{T2}-Apc$^{580S/+}$; Kras$^{LSL-G12D/+}$ (ACK) transgenic mice. Our findings demonstrate for the first time that oncogenic Apc and Kras increase plasma membrane order by perturbing cholesterol homeostasis and promoting cell proliferation. Genes associated with cholesterol uptake and *de*

novo synthesis of cholesterol are enhanced in ACK mice. This process is associated with the upregulation of Myc signaling, a well-known upstream mediator of cholesterol homeostasis. Our preliminary findings also indicate that the addition of exogenous cholesterol can dose-dependently promote cell proliferation in colonic cell lines and mouse colonic organoids. In complementary experiments, we also investigated the chemo-protective effects of dietary agents on cholesterol homeostasis and plasma membrane order in ACK mice. Our findings indicate that perturbed plasma membrane order and cholesterol homeostasis is ameliorated by n-3 PUFA + curcumin feeding.

In summary, our results indicate for the first time that fish oil plus curcumin synergistically reduce colon cancer risk in part by modulating (i) p53 signaling in $Lgr5^{+}$ stem cells, and (ii) plasma membrane properties implicated in the regulation of the colon cancer cells and tumor development.

DEDICATION

I would like to dedicate this work to my family, which without their constant support and unconditional love I would not be writing these words.

ACKNOWLEDGEMENTS

Above all, I am deeply grateful to Dr. Robert S. Chapkin for supporting and guiding my doctoral studies presented here. His insights have been fundamental for all of this research and invaluable at every step for all my work. He has always been patient and supportive, and has shown complete faith in my abilities for which I am very grateful. At any time, the doors of his office were open for discussions on any question or problem that I had and I will always be grateful for his guidance. I would likewise like to thank my committee members: Dr. David W. Threadgill, Dr. Rajesh C. Miranda and Dr. Robin Fuchs-Young. Their insight and direction was indispensable in developing this body of work. I am also thankful for the aid of all of the members of the Chapkin lab. They were always willing to provide a helping hand when it was most needed. Lastly, I appreciate the love and support of my family. I know that none of this would have been possible without them.

CONTRIBUTORS AND FUNDING SOURCES

Contributors

This work was supervised by a dissertation committee consisting of Professor Dr. Robert S. Chapkin [advisor] and Professor Dr. Robin Fuchs-Young of the Department of Molecular and Cellular Medicine and Professor Dr. David W. Threadgill of the Department of Veterinary Pathobiology and Professor Dr. Rajesh C. Miranda of the Department of Neuroscience and Experimental Therapeutics.

Funding Sources

The work was supported by National Institutes of Health (CA164623, CA129444, CA168312 and P30ES023512); American Institute for Cancer Research and National Institutes of Health (R35CA197707, RO1CA168312 and P30ES023512).

TABLE OF CONTENTS

LIST OF FIGURES

LIST OF TABLES

1. INTRODUCTION

1.1 Colon cancer

Colorectal cancer (CRC) is the second leading cause of cancer-related death in developed countries, and almost half of the population will develop at least one benign intestinal tumor during their lifetime (Jemal et al., 2011). There has been a steady decline in the incidence of CRC in patients age 50 years or older, but the opposite trend has been observed for young adults. For patients 20 to 34 years, the incidence rates of localized, regional, and distant colon and rectal cancers have increased. An increasing incidence rate was also observed for patients with rectal cancer aged 35 to 49 years. Based on current trends, in 2030, the incidence rates for colon and rectal cancers will increase by 90.0% and 124.2%, respectively, in patients 20 to 34 years and by 27.7% and 46.0%, respectively, in patients 35 to 49 years (Bailey et al., 2015). Despite recent advances in early detection and therapeutic intervention, CRC remains one of the most deadly cancers in the United States (Jemal et al., 2011). While surgical removal leads to high cure rates of localized disease, metastatic CRCs are typically associated with a poor prognosis with the majority of patients dying within two years upon diagnosis, resulting in a five-year survival rate of just 10% (Markowitz et al., 2002). Therefore, developing strategies for prevention and treatment of this pernicious disease is of the utmost importance. Both genetic and environmental factors modulate colon cancer risk (Kim et al., 2016a; Tomasetti and Vogelstein, 2015; Wu et al., 2016). Additionally, many modifiable

factors, including diet, exercise, and smoking play a role in more than 50% of colon cancer cases (Beyaz et al., 2016; Kim et al., 2016b).

1.1.1 Histological progression of colon cancer

Formation of colon cancer is a multi-step process that results from a systematic accumulation of both genetic and epigenetic perturbations that cause normal colonic epithelial cells to transform and progress into cancer (Di Gregorio et al., 1997). Colonic transformation progressing through multiple distinct histologically abnormal stages.

Aberrant crypts foci: Aberrant crypts foci (ACF) are putative early stage biomarkers of colonic carcinogenesis, and consist of hyperplastic epithelium (Takayama et al., 1998). ACF are defined as crypts with dysplastic microadenomas, with enlarged, elongated, intermittent stratified nuclei with loss of polarity, mucin depletion and dysplasia) as defined by (Di Gregorio et al., 1997). It currently remains unclear whether ACF serve as precursors for human colon cancer, although many studies have shown that ACF incidence increases with increased risk factors for colon cancer (Hata et al., 2004; Iwamoto et al., 2000; Rudolph et al., 2005).

Polyps: Polyps are macroscopic growths of hyperplastic or dysplastic cells that can be observed in the colon. Polyps contain a short stalk with a raised, nodular foci of hyperplastic epithelium (Di Gregorio et al., 1997). They share many of the cellular features of dysplasia but are more nodular and

elevated above the surrounding epithelium. Some polyps are innocuous, whereas others can develop into cancer. Polyps are classified as either hyperplastic, adenomatous, or serrated (Noffsinger, 2009). Hyperplastic polyps are traditionally classified as benign lesions. However, it has been clearly demonstrated that adenomatous polyps and adenomas can develop into carcinomas subsequent to a well-established accumulation of molecular alterations (Vogelstein et al., 1988; Vogelstein et al., 1989). Recently, it has been shown that serrated polyps can also serve as precursors to colon cancer. The molecular alterations that contribute to this pathway of tumorigenesis, termed the serrated neoplasia pathway, are distinct from those affiliated with the adenoma-to-carcinoma conversion (Noffsinger, 2009). Although some polyps serve as precursors for cancer, polyps are considered benign growths because they have not yet broken through the basement membrane.

Adenomas: Adenomas are nodular, raised, circumscribed foci of neoplastic epithelial cells arising from the mucosa (Di Gregorio et al., 1997). In this case, epithelial cells form irregularly branching tortuous glands that do not extend beyond the muscularis mucosa. Typically, the stroma contain small numbers of neutrophils and lymphocytes (Di Gregorio et al., 1997; Naini and Odze, 2013; Suzui et al., 2013). The transformation from adenoma to carcinoma takes an average of eight to twelve years, but most adenomas are thought to never develop into cancer (Saif and Chu, 2010).

Carcinoma: Once one of these abnormal growths breaches the

basement membrane and begins infiltrating into the surrounding tissue, it is classified as a carcinoma and is considered malignant (Di Gregorio et al., 1997). Colon carcinomas can penetrate into underlying stromal layers and smooth muscle and eventually metastasize to distal locales. The major site of colon cancer metastasis is the liver (Chambers et al., 2002).

1.1.2 Molecular progression of cancer by intrinsic and extrinsic factors

Early insights into the central role of the genome in cancer development emerged in the late nineteenth and early twentieth centuries from studies by David von Hansemann and Theodor Boveri (Stratton et al., 2009). Examination of dividing cancer cells under the microscope, these pioneers documented the presence of bizarre chromosomal aberrations. This led to the proposal that cancers are abnormal clones of cells characterized by and caused by abnormalities of hereditary material. Following the discovery of DNA as the molecular substrate of inheritance (Avery et al., 2000) and determination of its structure (Watson and Crick, 1953), this speculation was supported by the demonstration that agents that damage DNA and generate mutations can also cause cancer (Loeb and Harris, 2008).

1.1.3 Molecular progression of colon cancer by intrinsic factors

Colorectal tumorigenesis often begins with precursor lesions in the colonic epithelium, and is driven by a series of genetic and epigenetic alterations (Fearon and Vogelstein, 1990; Vogelstein and Kinzler, 2004). One

of the earliest genetic changes is the loss of the Apc tumor suppressor gene, which antagonizes β-catenin signaling and is mutated in the majority of CRCs (Moran et al., 2010). Another key early event is the activation of the oncogenic Kras, which is mutated in over one-third of CRCs (Jancik et al., 2010; Vogelstein and Kinzler, 2004). Genetic instability has also been implicated to contribute to colorectal tumorigenesis (Grady and Carethers, 2008; Lengauer et al., 1997).

1.1.4 Molecular progression of colon cancer by extrinsic factors (alkylating agents)

Alkylating agents are a ubiquitous family of reactive chemicals that transfer alkyl carbon groups onto a broad range of biological molecules, thereby altering their structure and potentially disrupting their function. Alkylating agents are practically unavoidable due to their abundance in the environment and within living cells. Major sources of external alkylating agents include constituents of air, water and food such as biological byproducts (e.g., abiotic plant material) and pollutants (e.g. tobacco smoke and fuel combustion products) (Ballschmiter, 2003; Hamilton et al., 2003; Hecht, 1999). Internally, alkylating agents can arise as byproducts of oxidative damage or from cellular methyl donors such as S-adenosylmethionine, a common cofactor in biochemical reactions (Rydberg and Lindahl, 1982; Taverna and Sedgwick, 1996). Due to the cytotoxic, teratogenic and carcinogenic effects caused by

alkylation damage, alkylating agents pose significant threats to human health.

Azoxymethane (AOM), an alkylating agent, and its metabolic precursor, 1, 2-dimethylhydrazine (DMH), are commonly used carcinogens to study the molecular mechanisms of colon carcinogenesis in rodents (Femia and Caderni, 2008; Magnuson et al., 2000; Rosenberg et al., 2009). These preferred model carcinogens induce colonic tumors that exhibit pathological features known to be associated with human sporadic colorectal cancer (Corpet and Pierre, 2005). DMH and AOM are pro-carcinogens, which require metabolic activation by cytochrome P450 (P450) enzymes, primarily CYP2E1 (Sohn et al., 2001). DMH undergoes N-oxidation to form AOM, which, upon hydroxylation, yields methylazoxymethanol (MAM). MAM is unstable, with a half-life of ~12 hr. It subsequently decomposes to yield formaldehyde and a highly reactive methyldiazonium ion, which alkylates the DNA bases, resulting in the formation of DNA adducts, including O6-methylguanine (O^6-mG) and N7-methylguanine (N7-mG) (Rosenberg et al., 2009). Persistence of O^6-mG can lead to mutations in oncogenes and the initiation of tumorigenesis (Takahashi and Wakabayashi, 2004).

The prevailing hypothesis is that the liver plays a critical role in DMH/AOM bioactivation in vivo and that the reactive intermediates produced by the liver are transported to the colon via the blood or bile to induce carcinogenicity (Fiala, 1977; Pozharisski et al., 1975; Zedeck et al., 1977). This is a plausible hypothesis, given that the colon generally possesses much lower

levels of P450 enzymes, relative to the liver.

Due to their chemical reactivity as a methylating agent, AOM produce significant levels of 7meG, 3meA and O6meG lesions as the primary alkylated DNA adducts. Alkylation of oxygen atoms within DNA bases generates the important premutagenic lesion O6-methylguanine (O^6meG) (6~8%) and, to lower extent, O4-methylthymine (0.3%) (Beranek, 1990). Among the oxygen atoms of DNA, the O^6-position of guanine represents a major site of methylation by S_N1-type alkylating agents to generate O^6meG. Even though alkyl lesions are generated to a much lesser extent than N-alkyl adducts, the induction of O^6meG lesions by alkylating agents is of great biological relevance because O^6meG can readily mispair with thymine during DNA replication to cause many of the mutagenic and cytotoxic biological effects of alkylating agents. Alkylating agents can also modify other nitrogen and oxygen atoms in DNA besides the aforementioned sites to generate additional toxic and mutagenic lesions.

The major repair mechanisms for alkylation damage include direct DNA repair by the AlkB dioxygenase enzyme and the O^6-methylguanine-DNA methyltransferase (MGMT) repair protein; and by the multistep pathways of base excision repair (BER) and nucleotide excision repair (NER). Among these repairing mechanisms, MGMT directly repairs O^6meG and O^6Cl-ethylG lesions via transfer of the alkyl group to its active site cysteine residue (Sedgwick et al., 2007). If DNA damage is not repaired by MGMT, O^6MeG adducts have

dramatic biological consequences that include cytotoxicity, mutagenicity, clastogenicity and carcinogenicity (Becker et al., 1996; Kaina et al., 1991). Owing to their mispairing properties, persistent O^6MeG lesions favor the incorporation of thymine instead of cytosine, which results in G:C to A:T transition mutations (Swann, 1990).

The formed O^6MeG:T mispair is also recognized by the mismatch excision repair (MMR) system (Duckett et al., 1996), leading to a variety of downstream effects. Upon activation, the MMR system initiates a futile repair process that finally results in the generation of DNA single-strand breaks with subsequent collapse of the replication fork, giving rise to DNA double-strand breaks (DSBs) (Mojas et al., 2007; Ochs and Kaina, 2000). O^6MeG-triggered DSBs are repaired via homologous recombination, which was shown to enhance cell survival at the expense of increased rates of sister chromatid exchanges (Roos et al., 2009). Non-repaired DSBs trigger cell death and the formation of chromosomal aberrations (Roos et al., 2009). The O^6-MeG:T mispair leads to apoptotic cell death via DSB formation in the second replication cycle following damage induction (Quiros et al., 2010). G:C to A:T transition mutations induced by AOM is clinically relevant because AOM hyper-activates β-catenin and Kras signaling, which are dysregulated in sporadic colorectal cancer in humans (Hata et al., 2004; Takahashi and Wakabayashi, 2004).

Both the homologous recombination (HR) and non-homologous end

joining (NHEJ) pathways repair DSBs; HR uses homologous DNA (sister chromatids) as a template to resynthesize DNA across the break, which results in sister chromatid exchanges (SCEs); whereas, NHEJ joins the DNA ends with little or no homology. The translesion DNA synthesis (TLS) pathway uses low-fidelity DNA polymerases to bypass lesions that stall high-fidelity replicative polymerases, thereby alleviating any blocks during DNA replication. Importantly, HR generally results in error-free repair, whereas NHEJ and TLS are usually error-prone repair mechanisms that can give rise to mutations (Deans and West, 2011; Kee and D'Andrea, 2010; Lange et al., 2011).

Finally, DNA adducts introduced by alkylating agents can compromise genome integrity by inducing mutagenesis (promoting cancer induction) and/or blocking essential biological processes such as DNA replication and transcription (leading to cell death). Moreover, certain lesions can also be processed into cytotoxic products that can engage other DNA repair pathways or induce programmed cell death. Thus, alkylating agents are able to modify a variety of biological molecules to generate a spectrum of lesions that can elicit a number of biological effects.

1.1.5 Location of colon cancer

Colon cancer can arise in either the right side (proximal) or left side (distal) of the colon. Interestingly, research findings have implicated differing genetic alterations as the cause of colonic transformation in left-sided

compared to right-sided colorectal cancers (Iacopetta, 2002; Meza et al., 2010; Sugai et al., 2006). Microsatellite instability has been shown to be primarily located in right-sided cancers, whereas chromosomal instability is more common in left-sided colon cancer (Lindblom, 2001). CpG island methylator phenotype (CIMP) incidence most often occurs in right-sided colon cancers (Hawkins et al., 2002). Furthermore, mutations in Tp53 and Kras genes occur predominantly in left-sided carcinomas (Bleeker et al., 2000; Sugai et al., 2006). The differences between left- and right-sided colon cancers provide evidence for different mechanisms contributing to colonic transformation.

1.1.6 Apc-Kras Molecular progression of colon cancer by intrinsic factors

CRC develops through a series of well-characterized histopathological changes resulting from specific mutations in selected oncogenes and tumor suppressor genes. At least four sequential genetic changes need to occur to ensure CRC evolution (Fearon and Vogelstein, 1990). One oncogene, Kras, as well as the tumor suppressor genes adenomatous polyposis coli (Apc), Smad4 and Tp53, are the main targets of these genetic changes. Of note, mutations in the Apc gene are responsible for familial adenomatous polyposis and also have a rate-limiting role in the initiation of the majority of sporadic CRCs. The major tumor suppressor function of the Apc protein is a negative regulator of Wnt signaling, where it forms part of the β-catenin destruction complex, comprising Axin, Glycogen synthase kinase-3 beta (Gsk3β) and Casein Kinase 1 (Ck1).

Mutations in Apc lead to β-catenin stabilization and, consequently, to the deregulation of the Wnt pathway through the activation of T-cell factor (Tcf)/ lymphocyte enhancer binding factor (Lef) target genes such as Myc (Gregorieff and Clevers, 2005). Approximately, 80% of colon cancers have biallelic Apc mutations (Kinzler and Vogelstein, 1996; Sparks et al., 1998), often with complete lack of expression from one allele and expression of a truncated form from the other. Most of genetically modified mice carrying different mutations in the Apc gene (Taketo, 2006) show an intestinal tumor predisposition phenotype and develop few to many adenomas. Remarkably, Myc deletion suppresses all the phenotypes of the Apc tumor suppressor loss and halts intestinal regeneration (Ashton et al., 2010; Sansom et al., 2007).

Kras is another important and frequently mutated gene during colorectal carcinogenesis. Kras mutations are found in 35–42% of CRCs and advanced adenomas (Pretlow and Pretlow, 2005; Worthley and Leggett, 2010). Genetic and biochemical studies have firmly established the central role of Kras-dependent signaling in regulating colorectal tumor cell proliferation, growth, survival, invasion and metastasis formation (Pretlow and Pretlow, 2005; Smakman et al., 2005). The most studied Kras effector pathways are the Raf-Mek-Erk mitogen-activated protein kinase (MAPK) and the phosphatidylinositol 3-kinase (PI3K)-AKT effector pathways (Worthley and Leggett, 2010) with inhibitors of components of both pathways currently under clinical evaluation (Dasari and Messersmith, 2010; Deng et al., 2004; Dienstmann and Tabernero,

2011; Ikenoue et al., 2005; Li et al., 2006a). As Kras and Braf mutations are mutually exclusive in colorectal tumors (Rajagopalan et al., 2002; Yuen et al., 2002), aberrant activation of Braf signaling is considered critical for Kras-mediated colorectal oncogenesis (Yuen et al., 2002).

1.1.7 Myc - oncogene metabolic disease

Multiple studies have used a candidate gene approach to address the nature of the Wnt/Tcf4 target gene program in CRC. Among these, Myc (He et al., 1998) is an essential component of this program in transformed intestinal epithelial cells. The Myc proto-oncogene is aberrantly overexpressed in over half of human cancers (Dang, 2012). For example, proto-oncogene Myc is overexpressed in approximately 70% of colorectal tumors (Erisman et al., 1985). It is one of the most frequently amplified oncogenes in human cancers and a member of the larger Myc family (Brodeur et al., 1984; Nau et al., 1985). Dysregulation of Myc, such as amplification, chromosome translocation or loss of upstream repressors, have been detected in many human cancers (Beroukhim et al., 2010; He et al., 1998).

Compelling evidence has underscored the multifaceted role of Myc in controlling cancer metabolism. Myc persistently emerges as a global growth regulator that drives glucose metabolism, glutamine metabolism, fatty acid synthesis, oxidative phosphorylation, nucleotide synthesis and ribosomal biogenesis (Hsieh et al., 2015).

1.2 Lgr5^{+} stem cells

1.2.1 Wnt signals drive self-renewal of the healthy intestinal epithelium

The first genetic mouse experiment linking Wnt signaling with adult stem cell biology involved the deletion of the Tcf4/Tcf7l2 gene (Korinek et al., 1998). Tcf4 constitutes the nuclear effector of Wnt signaling that, when bound by the key regulated protein β-catenin, will activate Wnt target gene expression. Absence of this transcription factor completely blocks development of the intestinal crypts. The same phenotype was reported for transgenic mice in which Wnt signaling was inhibited using Dickkopf-1 (Dkk1) (Kuhnert et al., 2004; Pinto et al., 2003), Dkk1 being a secreted Wnt antagonist (Glinka et al., 1998). Along these lines, the induced deletion in adult mice of the β-catenin gene (Fevr et al., 2007; Ireland et al., 2004) or Tcf4 (van Es et al., 2012) blocks all crypt stem cell activity.

As the mirror image of this phenomenon, it was found that the colon cancer tumor suppressor Apc serves as a negative regulator of β-catenin stability. Levels of free cytoplasmic β-catenin are normally exceedingly low but rapidly increase upon Wnt signaling, after which β-catenin can engage and activate Tcf4. Apc was observed to bind β-catenin (Rubinfeld et al., 1993; Su et al., 1993). In Apc mutant colon cancer cells, β-catenin levels are aberrantly increased (Munemitsu et al., 1995), leading to the inappropriate activation of Tcf4 target genes (Korinek et al., 1997). The same effect occurs when the β-catenin gene sustains activating point mutations (Morin et al., 1997; Rubinfeld et al., 1997). The Wnt/Tcf4-driven genetic program in colon cancer was first determined by microarray in 2002 (van de

Wetering et al., 2002).

1.2.2 Intestinal crypt homeostasis and structure

The epithelium of the intestine forms a single-cell-layer barrier between the hazardous chemical and biological contents of the gut lumen and the host. Likely because of this, the intestinal epithelium undergoes intense self-renewal. With a renewal cycle of 4–5 days, it is the fastest proliferating tissue in adult animals (Clevers, 2013; de Lau et al., 2014). The epithelium of the small intestine is organized into repetitive units, consisting of villi that protrude into the lumen and are surrounded at their base by the crypts of Lieberku¨hn, invaginations into the underlying connective tissue. Villi serve to maximize the surface epithelium for the uptake of nutrients. New epithelial cells are constantly birthed in the crypts. While having an overall similar setup, the colon differs from the small intestine by the absence of villi, creating a flat surface epithelium. While typical Paneth cells are missing in the colon, deep-crypt-secretory cells have been proposed to represent their colonic counterpart (Altmann, 1983). Indeed, it has recently been shown that a c-Kit positive population of goblet cells resides directly adjacent to $Lgr5^+$ stem cells at the colonic crypt bottom. This cell type produces Notch ligands and EGF similar to Paneth cells, and that it can functionally support $Lgr5^+$ stem cells in organoid cultures (Rothenberg et al., 2012). Colonic transit amplifying (TA) cells differentiate toward the goblet and absorptive cell lineages.

1.2.3 Leucine-rich repeat-containing G-protein coupled receptor 5 (Lgr5) stem cells

Two types of representative stem cells are currently defined in intestinal crypts: cycling crypt base columnar (CBC) cells (Barker et al., 2007) and quiescent "+4" cells (Potten et al., 1997). Lgr5 is a Wnt target gene that marks proliferative stem cells in several Wnt-dependent stem cell compartments, that is, the small intestine and colon (Barker et al., 2007), the stomach (Barker et al., 2010) and the hair follicle (Jaks et al., 2008). Rapidly cycling $Lgr5^{+}$ stem cells fuel the rapid turnover of the adult intestinal epithelium (Sato et al., 2009; Schepers et al., 2011), and its properties are not shared by other crypt cells (Barker and Clevers, 2010; Li and Clevers, 2010).

Lgr4 and Lgr6 are Lgr5 homologs, encode orphan 7-transmembrane receptors that are close relatives of the receptors for follicle stimulating hormone (FSH), luteinizing hormone (LH) and thyroid- stimulating hormone (TSH) (Barker and Clevers, 2010). Lgr6, marks multipotent stem cells in the epidermis (Snippert et al., 2010), whereas the expression of Lgr4 marks a much broader expressing crypt cell type, including $Lgr5^{+}$ stem cells (Van Schoore et al., 2005).

Homozygous disruption of Lgr5 results in neonatal lethality due to ankyloglossia, a fusion of the tongue to the floor of the oral cavity (Morita et al. 2004). The origin of this abnormality corresponds with the expression of Lgr5 in the epithelium of the tongue and in the mandible of developing embryos.

Conditional deletion of Lgr5 in the intestines of adult mice revealed no overt phenotype, while deletion of Lgr4 reduced the proliferation of CBC cells in intestinal crypts (de Lau et al. 2011). The combined removal of Lgr4 and Lgr5 aggravated this phenotype, abolishing the crypt stem cell compartment. Gene expression profiling indicated that removal of Lgr4 and Lgr5 specifically affected expression of the Wnt-driven crypt program, implying a functional connection between the two Lgrs and the Wnt pathway. Finally, homozygous mutant Lgr6 mice displayed no apparent phenotype (Snippert et al. 2010).

1.2.4 Lgr5 ligands

It has been demonstrated that Lgr4 and Lgr5 function as receptors of the R-spondin family of stem cell factors to potentiate Wnt/β-catenin signaling (Carmon et al., 2011; de Lau et al., 2011; Glinka et al., 2011). R-spondins (RSPOs) are a group of four secreted proteins (RSPO1–4) that share an overall identity of 40–60% at the amino acid sequence level and are comprised of similar domains (Kim et al., 2006). They were originally identified as Wnt agonists based on their robust, positive effect on Wnt/ β-catenin signaling (Kazanskaya et al., 2004; Nam et al., 2006). Stimulation of Lgr4 or Lgr5 with any of the four RSPOs greatly potentiates β-catenin dependent transcription induced by Wnt3a, with RSPO2 and RSPO3 showing the highest potency and affinity (Carmon et al., 2011).

Upon binding of Wnt to the Frizzled/Low-density lipoprotein receptor-

related protein receptor complex (Fz/LRP), Wnt target genes are activated, including Lgr5. Two other Wnt target genes, Rnf43 and Znrf3, encode transmembrane E3 ligases containing a cytoplasmic RING domain (Koo et al., 2012) and serve as components of a negative feedback loop. Enzymatic interaction of the Rnf43/Znrf3-associated RING domain with the Fz/LRP complex leads to polyubiquitination of the intracellular loops of the 7TM domain of Fz. The resulting endocytosis of Fz/Lrp abrogates Wnt signaling (Glinka et al., 2011). However, when R-spondin is present, it is recruited to Lgr5 or its homolog, Lgr4, which enables R-spondin to interact with Rnf43/Znrf3. As a consequence, Wnt/Fz/Lrp receptor complexes persist on the plasma membrane, enhancing Wnt signal strength and duration (animation at http://www.nymus3d.nl/video/rspondin) (de Lau et al., 2014).

Taken together, Lgr5 and Lgr4 receptors serve to efficiently recruit R-spondin ligands and bring these into position for interaction with Rnf43/Znrf3. This interaction leads to membrane clearance of the Ring finger proteins, the consequent persistence of surface Frizzled receptors, and the boosting of Wnt signal strength (de Lau et al., 2014).

1.2.5 Lgr5 in cancer

The expression of Lgr5 occurs in stem cells at sites of active proliferation and is the direct consequence of active Wnt signaling. The transformation of $Lgr5^{+}$ stem cells drives intestinal neoplasia in the $Apc^{flox/flox}$ mouse model,

indicating that Lgr5$^+$ crypt stem cells are the cell-of-origin of cancer (Barker et al., 2009). Not unexpectedly, Lgr5 expression occurs also in human colon cancer (van de Wetering et al. 2002; McClanahan et al. 2006). Likely as a result of Wnt pathway mutations, Lgr5 is also strongly expressed in cancers of the ovary, liver, and lung (Yamamoto et al. 2003; McClanahan et al. 2006; Zucman-Rossi et al. 2007; Tanese et al. 2008).

1.3 Lipids and cellular membrane biology

1.3.1 Cellular lipid classes

Lipid metabolism involves a very large number of metabolic reactions spanning different compartments in eukaryotic cells, resulting in the formation of a diverse group of chemical compounds (Nielsen, 2009). Lipids can be divided into the following classes: (1) fatty acids (FAs) that mainly serve as intermediates in lipid biosynthesis; (2) free sterols, e.g., cholesterol, that serve as structural components in membranes; (3) sterol esters that are formed from FAs and sterols and serve as lipid storage compounds, mainly as lipid bodies; (4) triacylglycerols (TAG) that are formed from glycerol and FAs that serve as lipid storage, mainly in lipid bodies; (5) phospholipids/phosphoglycerides (PLs) that are formed from FAs, glycerol and an alcohol moiety, e.g., inositol, choline or ethanolamine, that serve as structural components of membranes; and (6) sphingolipids that contain a sphingosine backbone and a very long chain FA. These

phospholipids serve as structural components at the cell surface as well as key signaling roles, e.g., regulation of endocytosis, ubiquitin dependent proteolysis and cell cycle control (Nielsen, 2009; Rohrig and Schulze, 2016). Despite the large chemical variety of lipids, they all have the same key carbon precursor, namely acetyl-CoA, and all initial steps of lipid/cholesterol biosynthesis occur in the cytosol (Rohrig and Schulze, 2016). Lipid biosynthesis involves two branches from acetyl-CoA, one leading to sterols and the other leading to FAs that serve as building blocks for biosynthesis of TAG, phospholipids, sterol esters and sphingolipids.

1.3.2 Composition of cellular membranes

Eukaryotic cells contain different types of membranes, including the plasma, endosomal, nuclear and mitochondrial membranes. The specific lipid composition of these membranes influences function, and since these membranes carry out vastly different functions, inherently their composition is extremely diverse (van Meer et al., 2008). Their heterogeneous composition is the result of *de novo* lipid synthesis (Kennedy pathway) and exogenous substrate availability (Lands' cycle). Unlike proteins that are directly encoded in the genome, lipid composition is the result of an indirect influence of biosynthetic enzymes and exogenous substrate availability.

1.3.3 Plasma membrane and signal transduction

The plasma membrane is composed of a heterogeneous mixture of lipids/cholesterol and proteins whose distinct organization maintains efficient signal transduction. Lipid rafts, enriched in sphingolipids, cholesterol and associated proteins, are special plasma membrane microdomains with an increased structural order, which are designated liquid ordered domains in plasma membranes (Sezgin et al., 2017). These lipid rafts are believed to be dynamic and small (5–200 nm) membrane microdomains, which play a critical role as sorting platforms for many membrane-associated proteins (Frisz et al., 2013; Hancock, 2006; Kraft, 2013; Levental and Veatch, 2016; Lingwood and Simons, 2010). Importantly, these domains are generally below the resolution of light microscopy (~200 nm). However, using specialized forms of microscopy that rely on non-radiative transfer of energy or single molecule localization, it is now possible to directly observe nanoscale dynamics of membrane lipids in living cells (Eggeling et al., 2009; Sahl et al., 2014). For example, the increased accessibility of super-resolution microscopy techniques has shed new light on the nanoscale organization of membrane proteins (Sezgin, 2017; Wang et al., 2014).

According to the emerging membrane biology picture, protein and lipid nanoclusters can be organized to form domains that are capable of facilitating signaling events (Ariotti et al., 2014; Garcia-Parajo et al., 2014;

Zhou and Hancock, 2015). The formation of these nanoclusters is believed to be driven by cortical actin and/or proximal transmembrane proteins (Garcia-Parajo et al., 2014). Currently, protein-protein, lipid-lipid and protein-lipid nanoclusters are considered a predominant feature of the plasma membrane and appear to mediate critical signaling processes (Ariotti et al., 2014), including signal integration and cross talk of the transduction of oncogenic Ras and the epidermal growth factor receptor (EGFR) (Ariotti et al., 2014; Janosi et al., 2012; Zhou et al., 2012) regulated pathways. This is noteworthy, because there is emerging evidence that drugs and select membrane active dietary components, which we term membrane targeted dietary bioactives (MTDBs), e.g., n-3 PUFA and curcumin, can attenuate Ras and EGFR (Ariotti et al., 2014; Nussinov et al., 2015) activity by modulating nanocluster organization. It also has been suggested that disrupting clustering/dimerization of membrane associated proteins can lead to attenuation of downstream oncogenic signaling and the suppression of tumor growth (Fuentes et al., 2017).

1.3.4 The role of cholesterol in plasma membrane physiology

Approximately 90% of cellular cholesterol resides in the plasma membrane (Kim et al., 1991; Lange et al., 1989; Ueland et al., 1986), and increases in cholesterol promote plasma membrane order (Montero et al., 2008). This is significant, because highly ordered/rigid lipid rafts are

increased in many types of cancer (Li et al., 2006; Patra, 2008) and some multidrug-resistant cancers (Yang et al., 2009; Yi et al., 2013). The term 'rigidity' refers to the packing of the lipids in the membrane, and cholesterol favors the production of more tightly pack "rigid" domains. This increased rigidity associated with increased lipid rafts typically facilitates efficient cellular signaling. Interestingly, multidrug-resistant cells have remodeled their membrane to be in a state that is more rigid and thus receptive to activation (Li et al., 2015; Raghavan et al., 2015).

1.3.5 Cellular function of membrane cholesterol

Cholesterol is an essential component of higher eukaryotic membranes and plays an important role in cell membrane organization, dynamics and function (Bloch, 1983). It is the end product of a sterol biosynthetic pathway involving more than 20 enzymes (Singh et al., 2013). According to the 'Bloch hypothesis', the sterol biosynthetic pathway parallels sterol evolution. In other words, the cholesterol biosynthetic pathway has evolved to optimize properties of eukaryotic cell membranes for specific biological functions (Hedlund et al., 2011). As an important membrane component, cholesterol helps to generate a semi-permeable barrier between cellular compartments and to regulate membrane fluidity. Cholesterol favors the formation of highly packed and ordered, rigid domains. A common term used for the ordered domains is "lipid-rafts"

(Levental and Veatch, 2016; Sezgin et al., 2017). From a functional perspective, the cholesterol / phospholipid composition of cellular membranes is known to influence lipid raft formation and the ability of plasma membrane receptors / signaling proteins to function properly (Griffié et al., 2015; Hou et al., 2016; Phillips et al., 2009).

1.3.6 Membrane cholesterol in stem cells

In preclinical studies, diet-induced obesity (DIO) augments self-renewal of intestinal $Lgr5^+$ stem cells, the cells-of-origin of intestinal cancer (Barker et al., 2007, 2009), and bestows a stemness related phenotype, e.g., organoid-initiating capacity in non-stem cell progenitors (Beyaz et al., 2016). This is consistent with recent work from our lab indicating that DIO promotes colonic $Lgr5^+$ stem cell expansion during cancer initiation (DeClercq et al., 2015). In comparison, in preclinical models of atherosclerosis, inactivation of cholesterol efflux transporters (ABCA1 and ABCG1) increases the number of circulating hematopoietic stem cells (HSPCs) (Feng et al., 2012; Gomes et al., 2010; Yvan-Charvet et al., 2007) and activate inflammatory cells (Lang and Cimato, 2014). From a mechanistic perspective, the Wnt/β-catenin pathway maintains a stem cell/progenitor phenotype in many cell types (Pinto and Clevers, 2005). Interestingly, recent evidence indicates that cholesterol selectively activates canonical Wnt signaling (Sheng et al., 2014). This is noteworthy,

because Wnt positively regulates cholesterol uptake for growth of cancer cells (Scott et al., 2015). Collectively, these findings suggest that lipid metabolism may play a critical role in stem cell signaling, thereby modulating cancer risk.

1.3.7 Plasma membrane/ cholesterol in cancer and anti-cancer therapy

There is evidence suggesting that disruption of lipid rafts in cancer can lead to increased responsiveness to anti-cancer therapies (Fedida-Metula et al., 2012; Irwin et al., 2011). Additionally, some anti-cancer drugs have beneficial effects through alteration of the protein content of lipid rafts (George and Wu, 2012; Hryniewicz-Jankowska et al., 2014). In colon cancer, lipid rafts have been shown to function in cell death (apoptosis)-mediated signaling (Lacour et al., 2004; Rebillard et al., 2007), cell entry/bioavailability of bioactive compounds (Adachi et al., 2007) and localization of key proteins involved in immune response (Bene et al., 2004). These findings indicate that lipids can no longer be ignored in the structures of membrane complexes, due to their ability to fine-tune and stabilize different signaling interfaces (Barrera et al., 2013; Levental et al., 2016; Lin et al., 2016). For several viruses, a dependence on cholesterol for virus entry and/or morphogenesis has been shown. Cholesterol depletion of virus-infected cells affects integrity of the virus envelope, causes disruption of the viral envelope, and adversely affects virus

infectivity (Barman and Nayak, 2007; Imhoff et al., 2007). For this reason, there is considerable interest in identifying alternative strategies for lowering cholesterol, micronutrient supplementation and pharmaceutical development.

1.3.8 Role of mitochondrial membrane/ cholesterol in cancer and anti-cancer therapy

Mitochondria are cholesterol-poor organelles which contain 0.5 to 3% of the cholesterol content found in plasma membranes (Maxfield and Tabas, 2005; Soccio and Breslow, 2004). Interestingly, expression of oncogenic Ras results in the down regulation of the cholesterol transporter ATP-binding cassette transporter A1/cholesterol exporter (ABCA1) (Smith and Land, 2012), a key player in cholesterol metabolism. As a result, cholesterol accumulates in the mitochondria, which inhibits the release of death promoting molecules (Smith and Land, 2012). Similarly, mitochondria from rat or human hepatocellular carcinoma (HC) cells (HCC) or primary tumors from patients with HC exhibit increased mitochondrial cholesterol levels (Montero et al., 2008). Elevated cholesterol in mitochondria membranes may decrease membrane fluidity. This in turn, may inhibit mitochondrial permeability transition (MPT), decreasing the capacity of the pro-cell death/apoptotic Bax protein to oligomerize and penetrate into the

mitochondrial outer membrane, which will ultimately promote cancer cell survival (Colell et al., 2003; Montero et al., 2008).

1.4 n-3 PUFA and curcumin

1.4.1 Effect of n-3 PUFA and curcumin on colon cancer

It is clear that select extrinsic bioactives, e.g., n-3 polyunsaturated fatty acids (n-3 PUFA) and curcumin, independently reduce aberrant crypt foci (ACF) and polyp formation in humans (Carroll et al., 2011; West et al., 2010) and combinations of the two have been reported to exert synergistic effects related to the suppression of chronic inflammation and cell proliferation and the promotion of apoptosis in breast and pancreatic cancers (Altenburg et al., 2011; Jia et al., 2011; Saw et al., 2010; Siddiqui et al., 2013; Swamy et al., 2008). From a mechanistic perspective, the combination of n-3 PUFA and curcumin has been shown to suppress NFκB activation in mouse colonic mucosa (Jia et al., 2011) in part by altering plasma membrane composition (Kim et al., 2009), which is required for activation of the apoptotic pathways (Beneteau et al., 2008; Gajate and Mollinedo, 2011). The suppression of inflammatory mediators such as COX-2, inducible nitric oxide synthase (iNOS), prostaglandin E_2 (PGE_2), 5-lipoxygenase (5-LOX) and cytosolic phospholipase A_2 ($cPLA_2$) has also been linked to the synergistic action of curcumin and n-3 PUFA, e.g., docosahexaenoic acid (DHA) (Saw et al., 2010; Swamy et al., 2008).

DHA and curcumin synergistically induce p53 activation (Altenburg et al., 2011; Siddiqui et al., 2013), a well-known tumor suppressor (Stracquadanio et al., 2016; Vogelstein et al., 2000). This is noteworthy, because p53 functions in part to inhibit NFκB activity, thereby inducing apoptosis in human colon cancer cells (Shao et al., 2000) (Puszynski et al., 2009). In contrast, the loss of p53 during tumor progression promotes an NFκB dependent inflammatory microenvironment (Schwitalla et al., 2013b), which is a critical event in the commitment of stem cells to apoptosis following DNA damage (Davidson et al., 2015; Dumitru et al., 2012).

1.4.2 n-3 PUFA and curcumin disrupt plasma membrane order

The two lipid bilayers of the plasma membrane each have unique interactions. The cytofacial (inner) leaflet interacts directly with the actin cytoskeleton. The exofacial (outer) leaflet is the site for ligand-receptor interactions, as well as glycosylated protein interactions. Several classes of MTDBs, because of size, hydrophobic/hydrophilic interactions, or steric hindrances, do not readily intercalate or incorporate into the phospholipid membrane.

Both DHA and curcumin are capable of modulating plasma membrane structure and EGFR function (Soung and Chung, 2011; Turk et al., 2012), which regulates colon cancer stem cell proliferation (Feng et al., 2012). In addition, there is emerging evidence that n-3 PUFA, can attenuate Ras and

EGFR (Ariotti et al., 2014; Nussinov et al., 2015) activity by modulating nanocluster organization. With respect to its membrane targeting properties, curcumin associates with the head group region of the phospholipid bilayer (Barry et al., 2009; Hung et al., 2008), whereas n-3 PUFA interact with the tail group region within rafts (Shaikh et al., 2004; Shaikh et al., 2015; Shaikh et al., 2009a). It also has been suggested that disrupting clustering/dimerization of membrane associated proteins can lead to attenuation of downstream oncogenic signaling and the suppression of tumor growth (Fuentes et al., 2017).

1.4.3 Clinical impact of lipids and cholesterol in cancer

According to emerging findings, lipids and membrane biology in part underlie the impact of diet on cancer prevention (Fuentes et al., 2017; Hou et al., 2016). With regard to human health, high cholesterol intake is known to increase colorectal cancer risk (Järvinen et al., 2001). Increased free cholesterol (1.5-fold) and esterified cholesterol (2-fold) in tumor tissue as compared to normal tissue has been reported in human colon cancer patients (Dessì et al., 1994). Interestingly, an inverse relationship between serum cholesterol levels and the risk for colon cancer has been reported (Broitman et al.; Forones et al.). In terms of colon cancer patients, liver metastases are significantly associated with elevated low-density lipoprotein (LDL) cholesterol levels and LDL receptor (LDLR) expression

levels are upregulated and associated with progression of colorectal cancer (Wang et al., 2017a). Epidemiologic studies suggest that statins, a cholesterol synthesis inhibitor, prevent certain malignancies (Hindler et al., 2006), including melanoma (Downs et al., 1998), breast (Boudreau et al., 2004; Cauley et al., 2003), colon (Cardwell et al., 2014; Lakha et al., 2012; Poynter et al., 2005), and prostate cancer (Shannon et al., 2005). Interestingly, elevated mitochondrial cholesterol in cancer cells (Montero et al., 2008) is associated with the suppression of programmed cell death (apoptosis) and the promotion of malignant cell transformation (Smith and Land, 2012) and chemotherapy resistance (Montero et al., 2008). In addition, apoptosis resistance was restored by cholesterol synthesis inhibitors and cholesterol depletion agents establishing a cause-and-effect relationship between mitochondrial membrane cholesterol (membrane order) and membrane-mediated apoptotic signal (Montero et al., 2008).

1.5 Current study

The major objective of this research is to determine the response of $Lgr5^+$ stem cells to extrinsic (carcinogen and diet compounds) and intrinsic factors (oncogenic Apc and Kras), mediators of CRC. The evidence discussed herein strongly suggests that n-3 PUFA and curcumin have broad-acting effects on mammalian physiology and fast cycling $Lgr5^+$ stem cells. Our data specifically address the effects of n- 3 PUFA and curcumin on the response of

Lgr5^{+} stem cells to alkylation-induced DNA damage. In addition, we have assessed the effects of the oncogenes and MTDBs on plasma membrane physiology. This study also elucidated the mechanism by which DHA and curcumin functions in chemoprevention.

2. HOMEOSTATIC RESPONSES OF COLONIC LGR5$^+$ STEM CELLS TO CARCINOGEN*

2.1 Introduction

The transformation of Lgr5$^+$ stem cells drives intestinal neoplasia in the *Apc*$^{flox/flox}$ mouse model, indicating that Lgr5$^+$ crypt stem cells are the cell-of-origin of cancer (Barker et al., 2009). Colon cancer has been suggested to follow a cancer stem cell (CSC) hierarchical model (Asfaha et al., 2015; Li et al., 2011). Although cycling Lgr5$^+$ stem cells fuel the rapid turnover of the adult intestinal epithelium (Sato et al., 2009; Schepers et al., 2011), and its properties are not shared by other crypt cells (Barker and Clevers, 2010; Li and Clevers, 2010), the role of Lgr5$^+$ cells in colorectal cancer (CRC) pathogenesis has not been well investigated. Therefore, it is important to identify the properties of Lgr5$^+$ cells at the initiation stage of colon tumorigenesis because transformation of Lgr5+ stem cells is an extremely efficient route towards initiating intestinal cancer (Barker et al., 2009). Recently, DNA damage responses in Lgr5$^+$ cells have been reported (Hua et al., 2012; Li et al., 2011; Metcalfe et al., 2014), however to date, colonic Lgr5$^+$ cytokinetics have not been examined in the

*This chapter is reprinted with permission from "Homeostatic responses of colonic LGR5 + stem cells following acute in vivo exposure to a genotoxic carcinogen" by Eunjoo Kim; Laurie A Davidson; Roger S Zoh; Martha E Hensel; Bhimanagouda S Patil; Guddadarangavvanahally K Jayaprakasha; Evelyn S Callaway; Clinton D Allred; Nancy D Turner; Brad R Weeks & Robert S Chapkin. Carcinogenesis 2016, 37(2):206-214. doi: https://doi.org/10.1093/carcin/bgv250. Copyright (2016) by Oxford Journals.

context of an alkylating agent induced DNA damage model of CRC. Critical to the prevention of colon cancer is the removal of O^6-methylguanine (O^6meG) DNA adducts, either through repair, for example, via O^6-methylguanine-DNA methyltransferase (MGMT) or targeted apoptosis (Meikrantz et al., 1998). MGMT is an inducible repair enzyme (Boldogh et al., 1998) that acts by transferring the methyl group from guanine in DNA to a cysteine residue on the repair protein (Montesano et al., 1990), resulting in rapid removal of promutagenic O^6-meG DNA adducts and the irreversible inactivation of the repair enzyme (Boldogh et al., 1998).

Cells with unrepaired DNA adducts may be eliminated through the activation of the apoptotic cascade, resulting in their selective removal (Thompson, 1995). In general, during the initiation of tumorigenesis following carcinogen exposure, there is an immediate apoptotic response to DNA damage in the colonic epithelium (Hirose et al., 1996). This is consistent with the fact that O^6-meG DNA lesions trigger apoptosis (Meikrantz et al., 1998).

The life-time risk of cancer is strongly correlated with the total number of stem cell divisions (Tomasetti and Vogelstein, 2015). Although the effect of DNA alkylating agent administration on O^6-meG DNA adduct repair, apoptosis and proliferation in colonic crypts has been reported in preclinical models (Hong et al., 1999; Hong et al., 2000; Hua et al., 2012; Metcalfe et al., 2014), there is no information on the interrelationship among these phenotypes in DNA damaged adult colonic $Lgr5^+$ stem cells. We therefore determined how colonic

Lgr5$^+$ stem cells respond to the administration of azoxymethane (AOM), a well-characterized experimental colon carcinogen and DNA alkylating agent (Hawks and Magee, 1974), in terms of O^6-meG DNA adduct removal by MGMT, apoptosis, and cell cycle arrest. In this study, we provide evidence that Lgr5$^+$ stem cells exhibit elevated AOM induced-DNA damage compared to differentiated cells. We also show that Lgr5$^+$ stem cells profoundly induce MGMT to delete O^6meG and promote untargeted apoptosis upon AOM exposure. These data document for the first time how the rapidly cycling Lgr5$^+$ stem cell population responds to environmental factors at the initiation stage of colon tumorigenesis.

2.2 Material and methods

2.2.1 Animals, diet, and study design

The animal use protocol was approved by the University Animal Care Committee of Texas A&M University and conformed to NIH guidelines. Lgr5-EGFP-IRES-CreER^{T2} (Barker et al., 2009) knock-in mice 6-7 wk old were acclimated for 1 wk and then provided with a semi-purified diet (Table 1) for 3 wk prior to injection with AOM (Sigma Chemical (St. Louis, MO); 10 mg/kg body weight). Mice were injected with EdU (Life Technologies) 2 h prior to sacrifice. Twelve (n=8) and 24 hr (n=8) following a single intraperitoneal injection of AOM, animals were euthanized by CO_2 asphyxiation. Control mice (n=3) received a single saline injection. Immediately after termination, the colon was rapidly

removed, flushed with ice-cold saline and immediately fixed in 4% paraformaldehyde for immunofluorescence (IF) analyses. Figure 1 shows the timeline of the treatments and the experimental design.

Ingredients	Diet (g)
Sucrose	42
Casein	20
DL-methionine	0.3
Mineral mix	3.5
Vitamin mix	1
Choline Chloride	0.2
Corn Starch	22
Cellulose	6
Corn oil	5
Total	100

Table 1. Experimental diets.

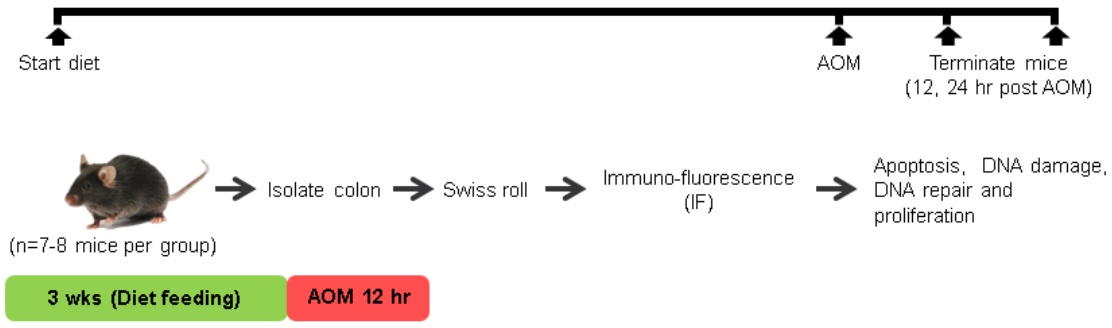

Figure 1. Timeline of treatments and the experimental design. Lgr5-EGFP-IRES-CreER^{T2} mice were provided with corn oil diet for 3 weeks prior to carcinogen injection. Mice were subsequently injected one time with AOM or saline at 10 mg/kg body weight. 12 or 24 hr following injection, mice were terminated and the colon was extracted for stem cell isolation.

2.2.2 In vivo DNA damage and repair measurement

Formalin-fixed paraffin-embedded 4 μm colon sections were deparaffinized, rehydrated through graded ethanol and stained with antibodies using standard procedures. DNA double strand breaks (DSBs) were measured by IF using a rabbit monoclonal phospho-gamma H2AX (γH2AX) Ser139 antibody (9718, Cell Signaling; dilution 1:200), $Lgr5^+$ stem cells were labeled using goat polyclonal GFP antibody (ab6673, Abcam; dilution 1:400) and O^6meG DNA adduct removal was estimated by the induction of MGMT expression using a mouse monoclonal MGMT antibody (ab54306, Abcam; prediluted). Secondary antibodies were anti-rabbit Alexa 647 (711-605-152, Jackson ImmunoResearch: dilution 1:400) for γH2AX, anti-goat 488 (705-545-147, Jackson ImmunoResearch) for GFP and anti-mouse Alexa 546 (A10036, Life Technologies) for MGMT. The DNA damage (or repair) index was determined by dividing the number of γH2AX (or MGMT) positive cells by the total number of cells in each crypt column and multiplying by 100.

2.2.3 In vitro apoptosis measurement

To investigate whether alkylating agent-induced DNA damage triggered apoptotic cell death in colonic $Lgr5^+$ stem cells, apoptotic bodies were visualized using the TACS 2 TdT-Fluor *in situ* apoptosis detection kit (Trevigen) as per the manufacturer's instructions. Negative control slides were incubated without TdT enzyme. The apoptotic index was determined by dividing the

number of apoptotic cells by the total number of cells in the crypt column and multiplying by 100.

2.2.4 In vivo measurement of cell proliferation

To investigate the effects of alkylating agent-induced DNA damage on cell cycle in colonic epithelial cells, proliferative activity was measured using the Click-iT EdU Alexa Fluor 555 Imaging kit (Life Technologies) as per the manufacturer's instructions. Negative control slides were incubated without Alexa Fluor.

2.2.5 Slide scoring

Images of colonic crypts were captured on an inverted TE 300 Nikon Eclipse fluorescence microscope equipped with 40x/1.30 Nikon Plan Fluor oil immersion objective and a Photometrics Cool snap EZ digital CCD camera. The external light source was powered by a mercury lamp. Images were processed using NIS Image software, version 3.2 (Nikon). A total of 426 GFP^{high} crypts from 8 mice were counted at 12 and 24 hr post AOM exposure and 150 GFP^{high} crypts from 3 saline injected mice (control) were examined.

2.2.6 Statistics

GraphPad Prism6 was used to analyze DNA adduct removal, apoptosis and proliferation and to produce graphs. Two-way analysis of variance

(ANOVA) was used to determine the effect of carcinogen in $Lgr5^+$ stem cells compared to differentiated cells over time. Comparisons between different time points were analyzed using one-way ANOVA.

2.3 Results

2.3.1 $Lgr5^+$ stem cells are preferentially damaged by carcinogen

To elucidate the unique properties of colonic $Lgr5^+$ stem cells in terms of their response to DNA damage, we assessed $Lgr5^+$ stem cell homeostasis in the context of AOM-induced tumorigenesis. $Lgr5^+$ stem cells and differentiated cells were tracked using the Lgr5-EGFP-IRES- $CreER^{T2}$ knock-in mouse. In this model, GFP expression is driven by the Lgr5 locus, leading to high GFP expression in $Lgr5^+$ stem cells (GFP^{high}), which is distinguishable from $Lgr5^-$ cells (GFP^{neg}) within crypts (Barker et al., 2007). Fluorescence microscopy was used to visualize GFP^{high} ($Lgr5^+$) cells by fluorescence within the context of the colonic crypt. In addition, sequencing results confirmed that GFP^{high} cells highly expressed Lgr5 and other stem cell markers, whereas GFP^{neg} cells expressed differentiated cell markers, e.g., Atoh1 (Table 2).

Marker genes	Fold change (GFP^{high} / GFP^{neg})	P-value
Lgr5	9.88	6.29E-88
Nr2e3	5.40	2.60E-26
Msi1	4.38	7.32E-17
Ascl2	3.83	6.05E-18
Troy	3.65	8.86E-13
Sox4	3.22	2.04E-11
Hes1	1.52	1.92E-07
Bmi1	1.43	5.26E-06
Atoh1	0.67	1.01E-05

Table 2. Representative differentially expressed genes in GFP^{high} versus GFP^{neg} cells. Cells were sorted by GFP intensity and subsequently sequenced.

O^6-meG is the dominant mutagenic adduct introduced by AOM (Kondo et al., 2010). O^6-meG:T mispairs can stall DNA replication when not repaired before replication, resulting in double strand breaks (DSBs) (Karran and Bignami, 1992). DSBs are always followed by phosphorylation of γH2AX (Kuo and Yang, 2008). Hence, γH2AX foci in the nucleus are a useful marker of the DSBs induced by S-phase dependent genotoxins during replication (Kuo and Yang, 2008; Staszewski et al., 2008). We hypothesized that AOM would induce more DSBs in GFP^{high} cells compared to GFP^{neg}, due to the fact that $Lgr5^+$ cells are actively proliferating and AOM induced-DSBs are formed during replication (Staszewski et al., 2008). We therefore assessed the cytotoxic effects of AOM by quantifying γH2AX (phospho S139) labeling. As shown in Figure 2A, γH2AX levels in the proximal colon were barely detectable similar to saline control indicating that the distal colon is the primary target of AOM. Following AOM

exposure, colonic cells in the distal colon were intensely stained for γH2AX at 12 h, which persisted through the 24 hr time point. DNA damage levels were 5.7-fold higher (P<0.01) in GFP^{high} stem cells as compared to GFP^{neg} cells (Figure 2B).

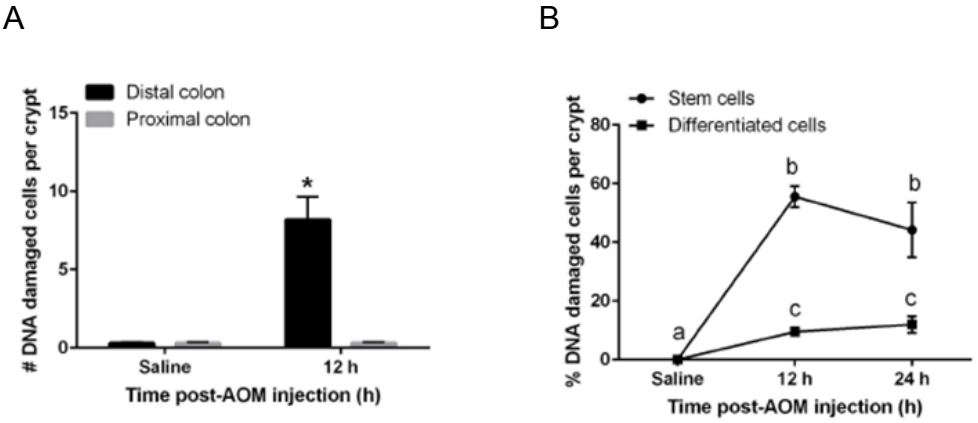

Figure 2. Carcinogen (AOM)-induced DNA DSBs in mouse colonic crypts at 12 and 24 hr post-AOM injection. (**A**) Quantitative comparison of the number of γH2AX $^{+}$ (DNA damaged) cells per crypt in the distal and proximal colon in saline versus AOM injected mice. (**B**) Quantitative comparison of the % of γH2AX $^{+}$ stem cells (GFP ^{high}) and differentiated cells (GFP ^{neg}) per crypt. A total of 426 Lgr5 GFP $^{+}$crypts from eight mice were counted at 12 hr, 150 Lgr5 GFP $^{+}$ crypts from three mice were counted at 24 hr and 150 crypts from three saline control mice were examined. DAPI stained nuclei along the mouse colonic crypt were counted and stem cells were determined by counting cells double stained for GFP and DAPI within Lgr5 GFP $^{+}$ crypts. Statistically significant differences between time points were determined using two-way ANOVA followed by Fisher's LSD multiple comparison testing. Different letters or * indicate significant differences between treatment groups ($p < 0.05$).

2.3.2 *Lgr5^{+} stem cells preferentially promote damage-induced apoptosis in response to carcinogen*

It has been reported that O^6-meG can generate stalled replication and DSBs, resulting in the induction of apoptosis (Karran and Bignami, 1992). In addition, stem cells exhibit a lower apoptotic threshold due to mitochondrial priming (Dumitru et al., 2012; Liu et al., 2013). This is noteworthy, because an excess number of stem cells can cause cancer (Verzi and Shivdasani, 2010) and "apoptosis resistance" has been reported in normal and cancer stem cells (Kruyt and Schuringa, 2010). Therefore, we quantified the levels of AOM-induced apoptotic GFP^{high} and GFP^{neg} cells per crypt in the distal colon. For this purpose, we used the TUNEL assay to colocalize apoptosis with γH2AX and GFP (Lgr5^{+} cells). To corroborate the frequency of epithelial cells undergoing apoptosis, paraffin-embedded sections were also assessed by H&E staining (Figures 3A&C).

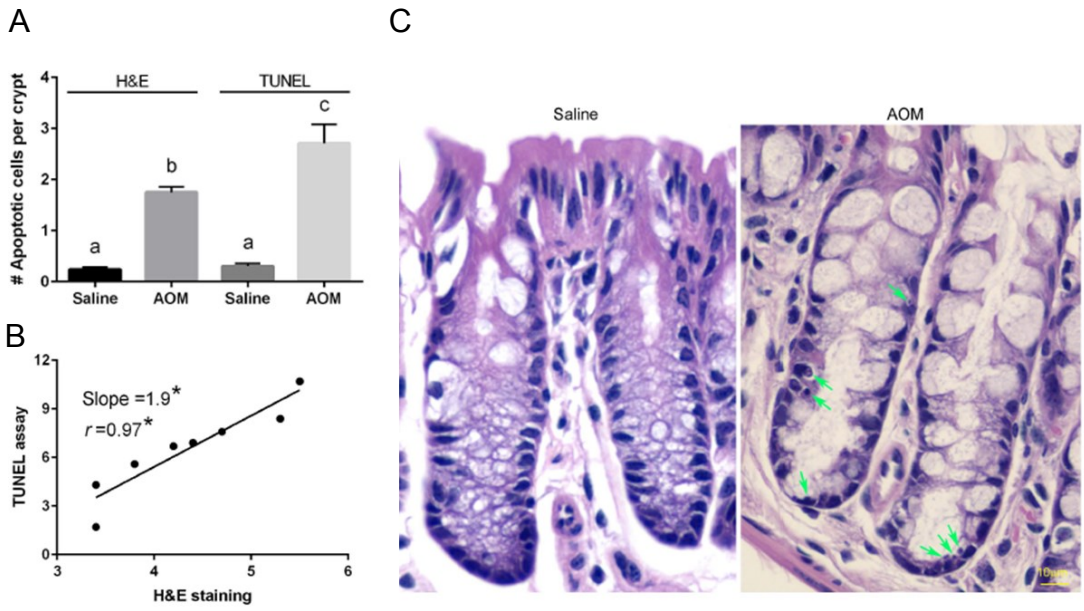

Figure 3. Quantitative comparison of the number of apoptotic cells per crypt measured by H&E and TUNEL (**A**) Quantitative comparison of the number of apoptotic cells per crypt measured by H&E and TUNEL in the distal colon in saline versus AOM injected mice (12 hr). (**B**) Association between the number of apoptotic cells per crypt in TUNEL assay and H&E. (**C**) Representative image of AOM-induced apoptotic cells at 12 hr post AOM injection as seen by H&E. Refer to Figure 2 legend for statistics.

Consistent with previous findings (Hu et al., 2002), H&E and TUNEL data were highly correlated (Figure 3B). GFP^{high} cells preferentially exhibited AOM-induced apoptosis, e.g., 4.7-fold higher levels ($P<0.0001$), compared to GFP^{neg} cells at 12 hr (Figures 4). In contrast, apoptosis in GFP^{neg} cells after exposure to carcinogen was more modest. Next, using linear regression analysis, we determined whether AOM-induced apoptosis was associated with the levels of

DNA damage induced by AOM. As shown in Figure 4C, only GFP^{high} cells exhibited proportionally increased apoptosis (slope=0.42, p=0.03) in response to DNA damage, whereas GFP^{neg} cells were non-responsive. We subsequently quantified the number of damaged $Lgr5^{+}$ stem cells that were targeted for apoptotic deletion, i.e., GFP^{high}, $TUNEL^{+}$, $\gamma H2AX^{+}$ triple positive cells, since the selective deletion of damaged $Lgr5^{+}$ stem cells by promoting apoptosis could mitigate the clonal expansion of DNA-damaged $Lgr5^{+}$ stem cells. As shown in Figure 4D, no statistically significant differences between GFP^{high} cells and GFP^{neg} cells (p=0.54) were observed in terms of targeted apoptosis ($TUNEL^{+}$, $\gamma H2AX^{+}$ cells) both at 12 and 24 hr. However, $\gamma H2AX^{-}$, GFP^{high} cells exhibited a 7.7-fold higher induction of apoptosis (non-targeted apoptosis - $TUNEL^{+}$, $\gamma H2AX^{-}$ cells) as compared to $\gamma H2AX^{-}$, GFP^{neg} cells at 12 hr (p=0.001) (Figure 4D right). These data indicate that the majority (63%) of induced apoptosis in GFP^{high} cells was non-targeted. Specifically, 28% of GFP^{high} cells exhibited non-targeted apoptosis (12 hr, Figure 4D right) and 13% exhibited targeted apoptosis (12 hr, Figure 4D left).

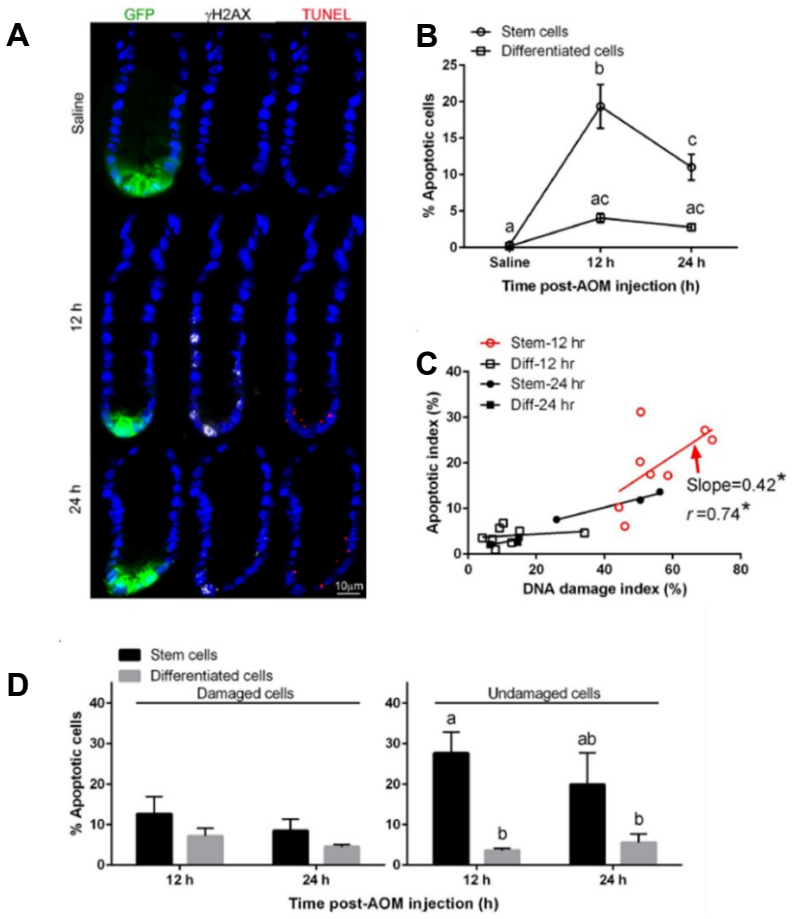

Figure 4. Comparison of AOM-induced apoptosis in stem cells and differentiated cells. (**A**) Representative images (objective, 40×) of GFP^{+} (GFP ^{high} stem cells, green), γH2AX^{+} (DSBs, white) and TUNEL^{+} (apoptotic body, red) cells are shown. For comparative purposes, immunofluorescence staining of colonic crypts in the distal colon in saline (control) and AOM injected mice is shown. (**B**) % TUNEL^{+} (apoptotic) stem cells and differentiated cells per crypt. (**C**) Association between the % of AOM-induced apoptotic cells and % of γH2AX^{+} cells per crypt in stem and differentiated (Diff) cells. Each point represents an individual animal. The *P* value was calculated using an *F* test. Correlation computes the value of the Pearson correlation coefficient, *r*, ranges from −1 to +1. The linear regression was fitted using GraphPad Prism 6.0. Apoptotic index = # of TUNEL^{+} stem or differentiated cells/total # of stem or differentiated cells per crypt X 100 at 12 and 24 hr post-AOM injection; Damage index = # of γH2AX^{+} stem or differentiated cells/total # of stem or differentiated cells per crypt X 100 at 12 and 24 hr post-AOM injection. Slope where the difference from zero is statistically significant is marked in red (Stem, 12 hr). (**D**) (left panel) % targeted apoptosis (double positive TUNEL^{+} and γH2AX^{+} stem or differentiated cells/γH2AX^{+} stem or differentiated cells) at 12 and 24 hr post-AOM injection; (right panel) % nontargeted apoptosis (TUNEL^{+} and γH2AX^{-} stem or differentiated cells/γH2AX $^{-}$ stem or differentiated cells) at 12 and 24 hr post-AOM injection. Different letters or * indicate significant differences between treatment groups ($p < 0.05$). Refer to Figure 2 legend for animal numbers.

2.3.3 AOM exposure promotes an apoptosis-bystander effect (BE) in Lgr5$^+$ stem cells.

In order to further shed mechanistic insight into the cause of the non-targeted apoptosis stem cell phenotype (TUNEL$^+$, γH2AX$^-$, Lgr5$^+$, Figure 4D), we defined BE-dependent apoptosis as apoptotic cells without DNA damage adjacent to damaged or apoptotic/damaged cells. In comparison, BE-independent apoptosis was defined as apoptotic cells with no adjacent damaged cells (Figure 5A, left). Our findings indicate that TUNEL$^+$, γH2AX$^-$, Lgr5$^+$ stem cells were predominantly (70%) localized to regions adjacent to γH2AX$^+$ cells (Figure 5B, left). The proximity of γH2AX$^+$ cells to TUNEL$^+$, γH2AX$^-$ Lgr5$^+$ stem cells suggest the involvement of AOM-induced BE (Figures 5A&B, *right*).

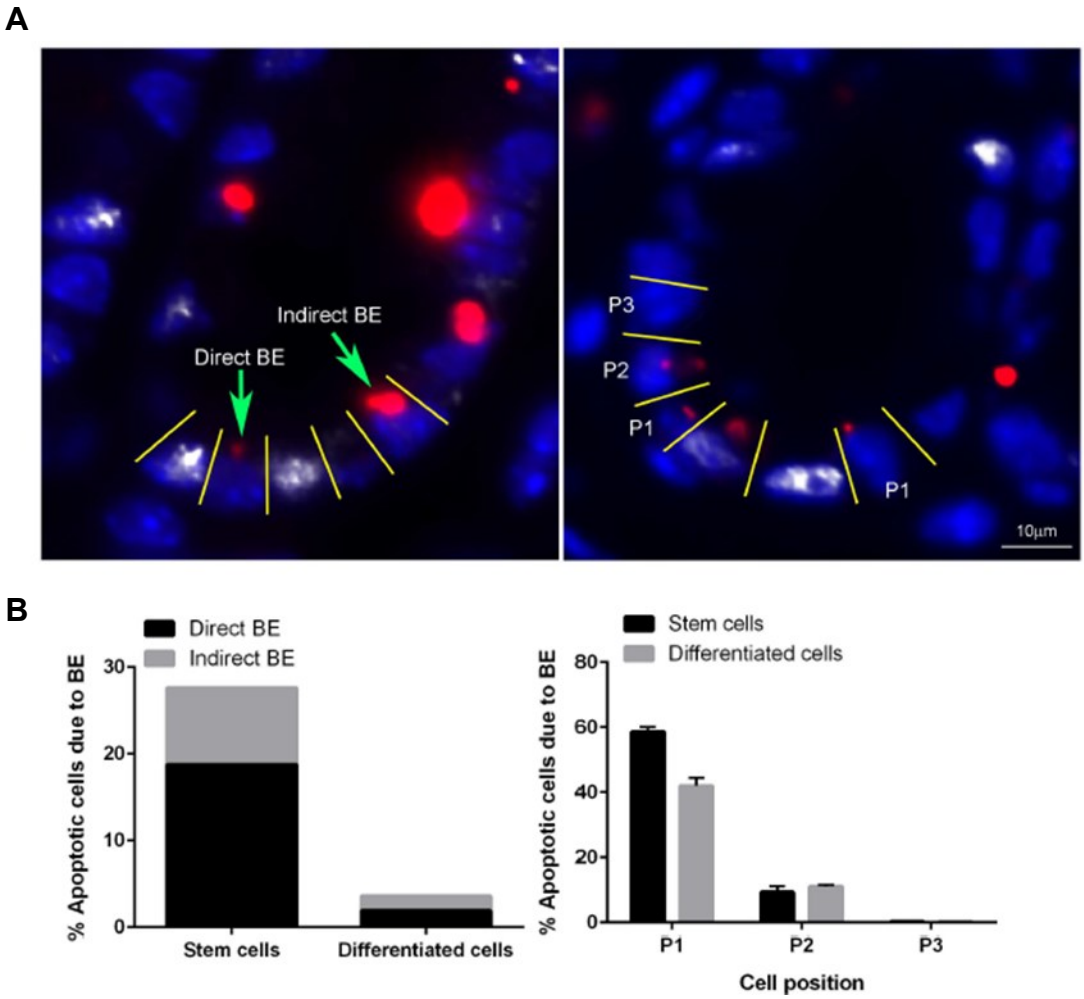

Figure 5. Bystander effect. (**A**) Representative image of direct BE (apoptotic cell located one or two cells away from damaged cell) and indirect BE (apoptotic cells with no damaged cells in the field of interest) at 12 hr post-AOM injection. An apoptotic cell immediately adjacent to a damaged cell is defined as P1; an apoptotic cell located one cell away from a damaged cell is defined as P2 (*right*). Representative images (objective, 40×) of TUNEL$^+$ (apoptotic body, red) cells next to γH2AX$^+$ (DSBs, white) cells are shown counter-stained with DAPI (blue). (**B**) Percentage of BE-dependent and BE-independent apoptotic Lgr5$^+$ stem versus differentiated cells (left) and percentage of BE-dependent apoptotic cells in relation to its proximity to a damaged cell.

2.3.4 Lgr5^{+} stem cells up-regulate DNA repair enzyme expression in response to carcinogen.

The major pathway for the repair of the O^6meG is via the MGMT mechanism (Pegg and Byers, 1992). Because this alkyltransferase is induced by alkylating agents, quantitative immunohistochemical analysis can be used to estimate MGMT activity upon AOM injection (Zaidi et al., 1996). As shown in Figure 6A&B, MGMT expression in GFP^{high} cells in the distal colon was increased by 18.5-fold 24 hr after AOM injection, whereas in GFP^{neg} cells, no induction was detected. Using linear regression analysis, both GFP^{high} cells (slope=1.08, p=0.03) and GFP^{neg} cells (slope=0.87, p=0.006) at 24 hr exhibited an induction of MGMT expression that was associated with the amount of DNA damage induced by AOM (Figure 6C), whereas at 12 h, no statistical differences were detected both in Lgr5^{+} stem and differentiated cells. Next, we quantified the number of damaged cells expressing MGMT, i.e., exhibiting targeted repair (GFP^{high}, γH2AX^{+} and MGMT^{+} triple positive), since the removal of mutagenic and cytotoxic adducts via induced-MGMT expression is negatively associated with G to A mutations in K-ras in colorectal tumorigenesis (Esteller et al., 2000). With respect to the γH2AX^{+} cell compartment, only γH2AX^{+} cells exhibited a statistically induced MGMT expression in GFP^{high} cells at 24 hr, whereas no significant changes were detected in GFP^{neg} cells (Figure 6D left). In comparison, MGMT expression in γH2AX^{-} cells was negligible both in GFP^{high} and GFP^{neg} cells (Figure 6D right).

DSBs can be repaired by at least four independent pathways including, homologous repair (HR), non-homologous end joining (NHEJ), alternative-NHEJ (alt-NHEJ), and single-strand annealing (SSA) (Ciccia and Elledge, 2010). Therefore, we used BRCA1 and Rad51 as markers of HR to define AOM-induced post-replicative repair process of Lgr5+ stem cells. BRCA1 and Rad51 are well known markers for post-replication repair, especially HR in the presence of radiation Rad51 (Hua et al., 2012). However, we were not able to detect an induction of HR marked by BRCA1 and Rad51 (Figure 7).

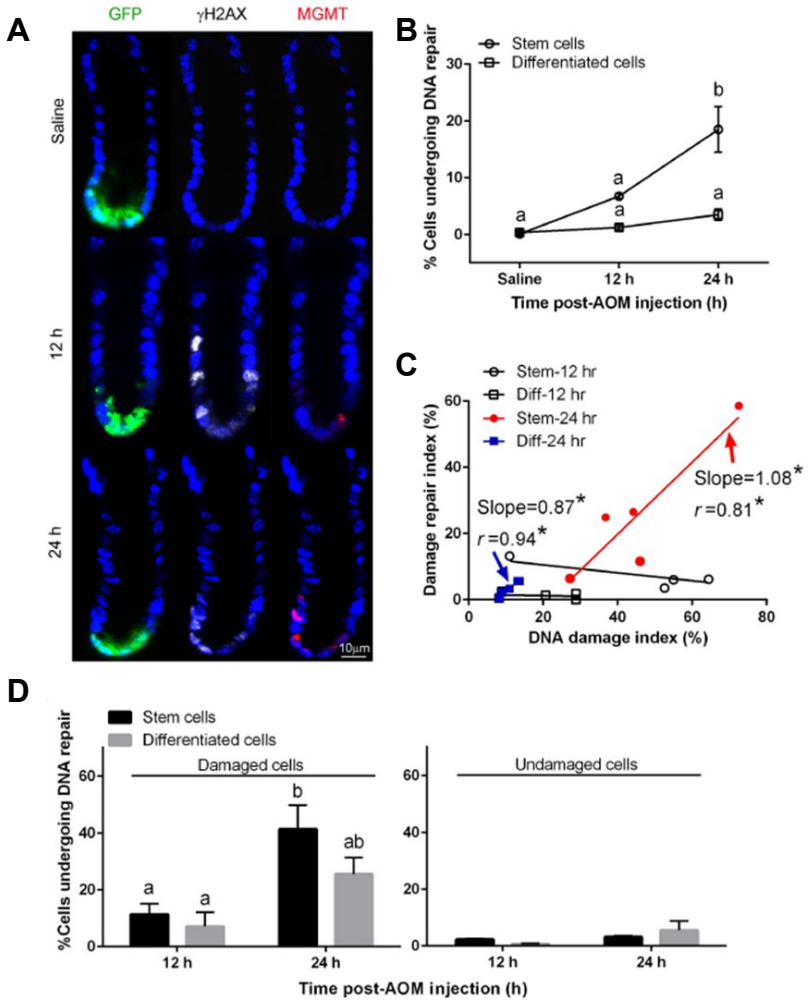

Figure 6. Comparison of AOM-induced MGMT expression in stem cells and differentiated cells. (**A**) Representative images (objective, 40×) of GFP$^+$ (Lgr5 $^+$ stem cells), γH2AX$^+$ (DSBs) and MGMT$^+$ (repair enzyme) cells are shown. For comparative purposes, immunofluorescence staining of colonic crypt in the distal colon in saline (control) and AOM injected mice is shown. (**B**) % MGMT$^+$ stem cells and differentiated cells per crypt. (**C**) Association between the % of AOM-induced MGMT$^+$ (DNA repair) cells and % of γH2AX$^+$ cells per crypt in stem and differentiated (Diff) cells. Repair index = # of MGMT$^+$ stem or differentiated cells/total # of stem or differentiated cells per crypt X 100 at 12 and 24 hr post-AOM injection; DNA damage index = # of γH2AX$^+$ stem or differentiated cells/total # of stem or differentiated cells per crypt X 100 at 12 and 24 hr post-AOM injection. Slope where the difference from zero is statistically significant is marked in red (Stem, 24 hr) or blue (Diff, 24 hr). (**D**) (left panel) % of γH2AX$^+$ cells expressing MGMT (both γH2AX$^+$ and MGMT$^+$ stem or differentiated cells/γH2AX $^+$ stem or differentiated cells) at 12 and 24 hr (right) post-AOM injection; (right panel) % of γH2AX$^-$ cells expressing MGMT (both γH2AX$^-$ and MGMT$^+$ stem or differentiated cells/γH2AX$^-$ stem or differentiated cells) at 12 and 24 hr post-AOM injection. Different letters or * indicate significant differences between treatment groups ($p < 0.05$). Refer to Figure 2 legend for animal numbers.

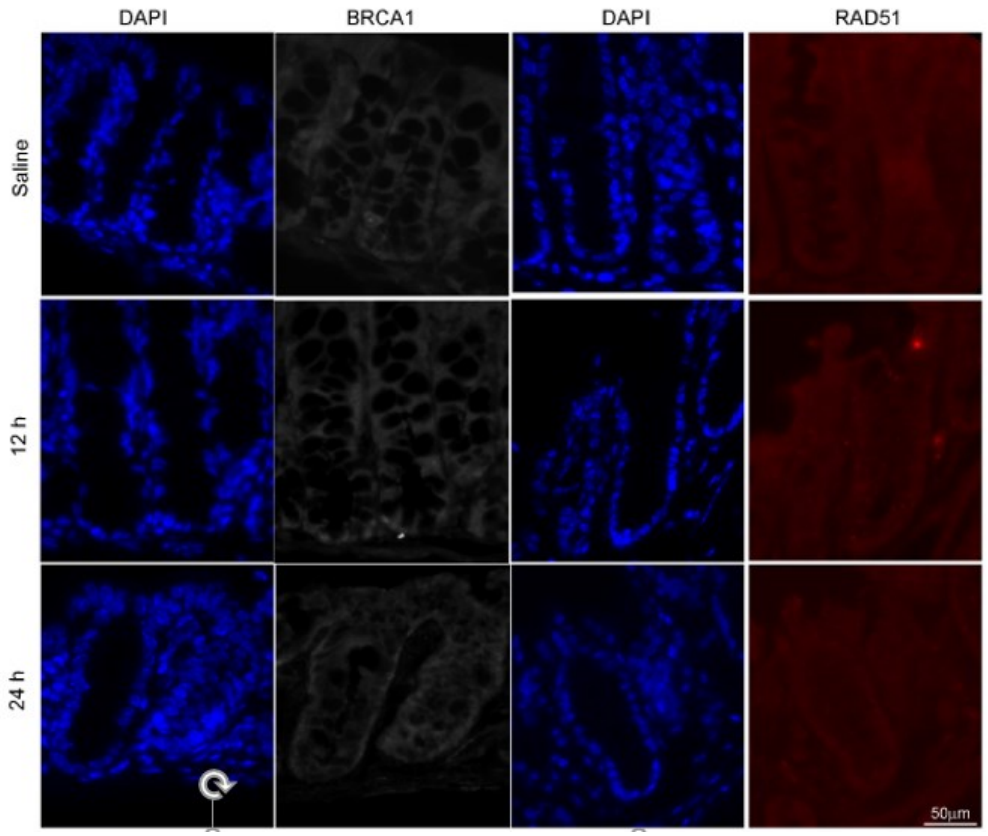

Figure 7. Breast cancer genes 1 (BRCA1) and RAD51 recombinase (RAD51) expression in mouse colonic crypts at 12 and 24 hr post AOM injection. Representative images (objective, 40X) of BRCA1^{+} (white) and RAD51^{+} (red) cells are shown counter-stained with DAPI (blue). Saline represents control sections.

2.3.5 Lgr5^{+} cells exhibit increased proliferation following AOM exposure

Elevated crypt epithelial cell proliferation is considered a risk factor for colon cancer (Chapkin and Lupton, 1999). For example, assessment of colonic crypt cell proliferation, including detection of an increased proliferative state

and expansion of the proliferative zone, are considered putative intermediate markers of colon cancer risk (Colussi et al., 2001). Furthermore, it has been shown that alkylating agent exposure results in increased colonic crypt cellularity, colonic crypt cell proliferation and the crypt proliferative zone (Richards, 1977). Therefore, we determined whether AOM injection results in increased GFP^{high} cell proliferation in the presence of AOM in the distal colon. As shown in Figures 8A&B, no reduction in cell cycle was observed immediately following AOM injection (12 hr) both in GFP^{high} and GFP^{neg} cells. However, a significant increase in cell proliferation (EdU labeling) was detected in GFP^{hjgh} cells at 24 hr (Figure 8B) and the increase in proliferation was associated with the induction of DNA damage (slope=0.98, p=0.01) as assessed by linear regression analysis (Figure 8C). In contrast, this association was not detected in GFP^{neg} cells. Figure 8D (left) also shows that the percentage of GFP^{hjgh}, $\gamma H2AX^{+}$, EdU^{+} triple positive $Lgr5^{+}$ stem cells increased overtime. This is consistent with the fact that $Lgr5^{+}$ cells are actively cycling and have a greater chance of accumulating DNA double breaks as compared to differentiated cells (Staszewski et al., 2008). The percentage of $\gamma H2AX^{-}$, EdU^{+} cells did not exhibit a cell type or temporal response (Figure 8D right).

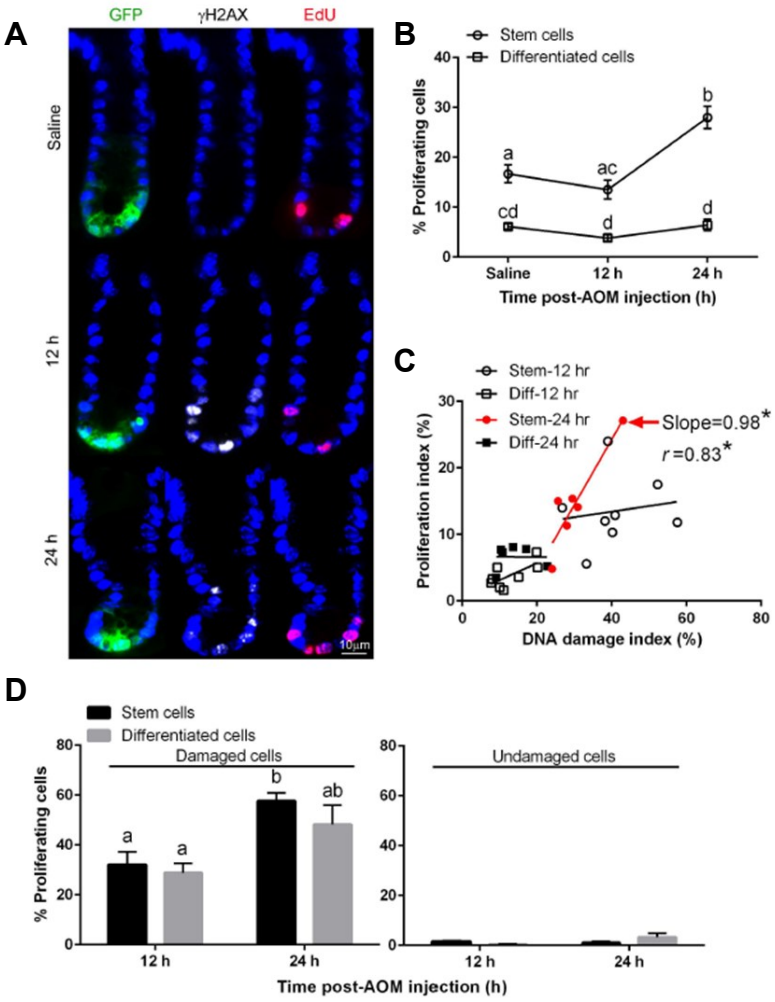

Figure 8. Comparison of AOM-induced proliferation in stem cells and differentiated cells. (**A**) Representative images (objective, 40×) of GFP$^+$ (Lgr5$^+$ stem cells), γH2AX$^+$ (DSBs) and EdU$^+$ (proliferation) cells are shown. For comparative purposes, immunofluorescence staining of colonic crypts in the distal colon in saline (control) and AOM injected mice is shown. (**B**) % EdU$^+$ stem cells and differentiated cells per crypt. (**C**) Association between the % of AOM-induced proliferating cells and % of γH2AX$^+$ cells per crypt in both stem and differentiated (Diff) cells. Proliferating index = # of EdU$^+$ stem or differentiated cells/total # of stem or differentiated cells per crypt X 100 at 12 and 24 hr post-AOM injection; DNA damage index = # of γH2AX$^+$ stem or differentiated cells/total # of stem or differentiated cells per crypt X 100 at 12 and 24 hr post-AOM injection. Slope where the difference from zero is statistically significant is marked in red (stem, 24 hr). (**D**) (left panel) % of γH2AX$^+$ cells also positive for EdU (both γH2AX$^+$ and EdU$^+$ stem or differentiated cells/γH2AX$^+$ stem or differentiated cells) at 12 and 24 hr post-AOM injection; (right panel) % of γH2AX$^-$ cells positive for EdU (both γH2AX$^-$ and EdU$^+$ stem or differentiated cells/γH2AX$^-$ stem or differentiated cells) at 12 and 24 hr post-AOM injection. Different letters or * indicate significant differences between treatment groups ($p < 0.05$). Refer to Figure 1 legend for animal numbers.

2.4 Discussion

Historically, alkylating agents are known to produce gastrointestinal tumors in rodents (Hawks and Magee, 1974; James and Autrup, 1983), and to cause cancer in humans as a result of lifetime environmental exposures (Hall et al., 1991). Of the spectrum of adducts produced by AOM, O^6MeG accounts for ~8% of the total DNA methyl adducts, is stable and persists in the absence of the DNA repair enzyme MGMT (Kondo et al., 2010). If left unrepaired, this adduct remains in the genome, triggering a futile repair loop which can eventually result in highly toxic double-strand breaks (DSBs), which are intermediates in apoptotic and DSB repair pathways (Karran and Bignami, 1992). DSBs are the most dominant cytotoxic effect generated by AOM (Kondo et al., 2010), and are typically detected at 12 hr following exposure (Hong et al., 2000). This form of alkylation-induced DNA damage is clinically relevant because AOM hyper-activates β-catenin and K-ras signaling, which are dysregulated in sporadic colorectal cancer in humans (Hata et al., 2004; Takahashi and Wakabayashi, 2004). In addition, this preclinical model recapitulates the pathogenesis of human sporadic colon cancer (Deschner and Long, 1977).

Colon cancer has been suggested to follow a cancer stem cell (CSC) hierarchical model (Barker et al., 2009; Chandler and Lagasse, 2010). Several studies have monitored DNA damage in stem cells, including MNNG-induced (Tominaga et al., 1997) and radiation-induced (Asfaha et al., 2015; Bhanja et

al., 2009) mouse stem cells, and small intestinal Lgr5$^+$ stem cells at the initiation stage of tumorigenesis (Metcalfe et al., 2014). Moreover, the transformation of actively cycling, long-lived intestinal Lgr5$^+$ stem cells drives intestinal cancer (Barker et al., 2007). Overexpression of Lgr5 has been shown to occur in human colorectal adenomas and cancers (Fan et al., 2010), as well as in other solid tumors (McClanahan et al., 2006). However, to date, no investigation has determined the *in vivo* effect of AOM exposure with respect to colonic Lgr5$^+$ stem cells. In the present study, we report for the first time the biological properties of AOM-damaged colonic Lgr5$^+$ stem cells at the initiation stage of tumorigenesis. For this purpose, the relationship between DNA damage, apoptosis, repair, and cell cycle arrest was examined in Lgr5$^+$ stem cells versus differentiated cells within the colonic crypt at 12 and 24 hr following the administration of carcinogen.

We have previously demonstrated that (a) AOM induces DNA damage to a greater degree in actively proliferating cells at the base of the crypt (Hong et al., 1999); (b) AOM-induced apoptosis is primarily targeted to the base of the crypt (Hong et al., 1999); and (c) AOM-induced MGMT protein expression increases over time in the bottom one-third of the crypt as compared to the differentiated cell compartment (Hong et al., 2000). In the present study, we extend these findings by demonstrating that: DNA damage occurs to a greater degree in Lgr5$^+$ stem cells (located at the base of the crypt) as compared to the differentiated cell compartment (Figure 2). It is assumed that AOM induced

γH2AX phosphorylation occurs during DNA replication in rapidly cycling Lgr5$^+$ stem cells before the damage has been repaired, i.e., restored to normal (O'Neill, 2000). This finding is consistent with the fact that alkylating agent-induced γH2AX foci are selectively formed in proliferating cells (Staszewski et al., 2008). In addition, we also demonstrate that colonic Lgr5$^+$ stem cells uniquely respond to AOM by inducing preferential apoptosis (Figure 4B), which is positively associated with induced γH2AX (Figure 4C), whereas differentiated cells do not exhibit this response. These findings are consistent with the fact that stem cells exhibit a rapid apoptotic response due to mitochondrial priming in a p53 dependent manner (Liu et al., 2013). It is noteworthy that AOM-induced apoptosis is p53-dependent whereas spontaneous apoptosis is p53-independent (Hu et al., 2005). However, it remains to be determined whether the induced apoptosis in Lgr5$^+$ stem cells is promoted due to p53-dependent mitochondrial priming.

Interestingly, “untargeted” apoptosis (TUNEL$^+$, γH2AX$^-$) in Lgr5$^+$ stem cells (Figure 4D right) was 2.2-fold higher than “targeted” apoptosis (TUNEL$^+$, γH2AX$^+$) (Figure 4D left), implying an inefficient removal of damaged Lgr5$^+$ stem cells via programmed cell death. Apoptotic cell death might be considered protective, because it selectively eliminates damaged cells that can contribute to carcinogenesis. However, untargeted cell death in the presence of residual DNA damage could promote cell proliferation and generate defective progenitor cells, which is potentially a tumor-promoting factor (Hua et al., 2012). It has also

been demonstrated that untargeted apoptosis can mediate DNA damage and induce chromosomal instability in neighboring cells (Coquerelle et al., 1995; Yang et al., 2013). Therefore, primary prevention strategies resulting in a favorable enhancement of apoptosis in damaged $Lgr5^{+}$ stem cells would be expected to reduce colon cancer risk.

Data in Figure 4D indicate that the majority of apoptosis occurs in undamaged GFP^{high} $Lgr5^{+}$ stem cells following AOM exposure. Based on the proximity of $\gamma H2AX^{+}$ cells to $TUNEL^{+}$, $\gamma H2AX^{-}$ $Lgr5^{+}$ stem cells, we have proposed the involvement of an AOM-induced BE (Figure 5). This unexpected outcome suggests that undamaged 'bystander' $Lgr5^{+}$ stem cells are being indirectly influenced by the intestinal niche. For example, numerous studies have shown that irradiated/damaged colonic cells can induce secondary apoptosis (Furlong et al., 2013) and γH2AX foci in non-irradiated cells via bystander effects (Dickey et al., 2011). This process, in part, may be mediated by lipid rafts (Burdak-Rothkamm et al., 2007) via the absorption of exosomes by naïve bystander cells (Al-Mayah et al., 2012) or intestinal commensal bacteria by triggering macrophages (Yang et al., 2013). It is noteworthy that bystander cells exhibit a significant pro-apoptotic gene expression profile compared to cells directly impacted by radiation (Furlong et al., 2013). From a mechanistic perspective, soluble mediators induced by AOM such as PGE_2 may partly mediate this process (Riehl et al., 2006; Zhou et al., 2005).

Additional studies are required to further elucidate the mechanism of the alkylation-induced bystander effects.

With respect to cell proliferation, we also determined that $Lgr5^+$ stem cells exhibiting DNA damage were actively cycling (Figure 8D left), and that proliferation was positively associated with DNA damage (Figure 8C), implying that $Lgr5^+$ stem cells have a high potential to accumulate mutations which enhance the risk of tumorigenesis. These findings provide a model for future therapeutic studies designed to ameliorate the effects of DNA damage in $Lgr5^+$ stem cells. Importantly, the level of $\gamma H2AX^+$, GFP^{high} cells (56%) per crypt was 4.1-fold higher (Figure 2) than EdU^+, GFP^{high} cells (14%) per crypt (Figure 8B) at 12 hr. This implies that DSBs may also be formed independently of cell division. γH2AX induced by bystander effects might explain the relatively high number of $\gamma H2AX^+$, GFP^{high} cells compared to $\gamma H2AX^+$, GFP^{high}. This may in part be mediated by apurinic (AP) sites generated from release of N-methylpurines which can be converted into DSBs by the activity of the AP endonuclease (Coquerelle et al., 1995).

A goal of the present study was to assess the localization of the MGMT repair enzyme in both the $Lgr5^+$ stem cell and differentiated cell compartments, which is not possible when using scraped mucosa for enzyme assays. MGMT methylation status has been shown to influence the risk of colon cancer development (Kycler et al., 2012) and it is known that MGMT expression is regulated by p53 in human astrocytic cells (Blough et al., 2007) and human

brain tumors (Russell et al., 1995). This is noteworthy because p53 in Lgr5$^+$ stem cells is a critical regulator of AOM/DSS induced tumorigenesis [unpublished data] and MGMT has been shown to function similarly in humans and rats (Gerson et al., 1995). Therefore, it was interesting to note that Lgr5$^+$ stem cells preferentially induced MGMT in response to DNA damage as compared to differentiated cells. It is possible that this increased expression may represent both an increase in protein expression and also an accumulation of inactive protein targeted for degradation, a distinction that would have to be further evaluated by measuring enzyme activity. Our findings also indicate that Lgr5$^+$ stem cells can modulate cancer risk by promoting DNA repair (Figures 6B&C) and by promoting targeted apoptosis (Figure 5D left). Interestingly, we did not detect evidence of an AOM-induced post-replicative repair process in Lgr5$^+$ stem cells (Figure 7). Collectively these results help clarify the homeostatic responses of Lgr5$^+$ stem cells at the initiation stage of tumorigenesis.

In summary, we demonstrate for the first time that colonic Lgr5$^+$ stem cells actively induce repair enzyme following AOM-induced DNA damage. This phenotype is consistent with the enhanced xenobiotic resistance reported in normal stem cells, attributed in part to a more efficient DNA repair response (Kenyon and Gerson, 2007). Importantly, the stem-like state is deeply linked to resilience and stress response, a relationship that appears to hold for their neoplastic counterpart, the cancer stem cell (CSC) (Dean et al., 2005;

Donnenberg and Donnenberg, 2005; Medema, 2013; Pisco and Huang, 2015). Thus, we propose that the monitoring of $Lgr5^+$ stem cell targeting responses provides a powerful tool to interrogate primary prevention strategies, e.g., diet and exercise, to specifically eradicate damaged $Lgr5^+$ stem cells. Ultimately, this strategy will provide a better understanding of the origin of colon cancer and the development of diagnostic tests that can detect cancer development at its earliest stages, which will improve overall survival.

3. EFFECT OF n-3 PUFA AND CURCUMIN ON TARGETING DNA DAMAGED LGR5^{+} STEM CELL*

3.1 Introduction

Numerous epidemiological studies have established strong evidence that many cancers including colon cancer have substantial risk proportions attributed to extrinsic factors such as diet, smoking and obesity (Kesse et al., 2006; Potter, 1999; Wu et al., 2016). High fat diet (HFD)-induced obesity augments stemness and tumorigenicity of intestinal progenitors (Beyaz et al., 2016; Schulz et al., 2014). In addition, epithelial colonic G protein-coupled receptor 5 (Lgr5)$^{+}$ stem cells respond to HFD (DeClercq et al., 2015) and genotoxic carcinogen, e.g., azoxymethane (AOM) (Kim et al., 2016a), during the cancer initiation stage. It has been also demonstrated that colonic Lgr5^{+} stem cells are preferentially damaged by AOM compared to differentiated cells (Kim et al., 2016a). A functional consequence of this status could enhance tumorigenesis. Thus, induction of apoptosis in DNA damaged Lgr5^{+} stem cells is likely to be a useful marker for successful cancer prevention, and may hold

*This chapter is reprinted with permission from "Rapidly cycling Lgr5+ stem cells are exquisitely sensitive to extrinsic dietary factors that modulate colon cancer risk" by Eunjoo Kim; Laurie A Davidson; Roger S Zoh; Martha E Hensel; Michael L Salinas; Bhimanagouda S Patil; Guddadarangavvanahally K Jayaprakasha; Evelyn S Callaway; Clinton D Allred; Nancy D Turner; Brad R Weeks & Robert S Chapkin. Cell Death and Disease 2016, 7(11):e2460. doi: 10.1038/cddis.2016.269. Copyright (2016) by Nature Publishing Group.

promise for identifying novel and improved cancer chemo-preventive agents. For example, it has been shown that nonsteroidal anti-inflammatory drugs (NSAIDs) can induce apoptosis in $Lgr5^{+}$ stem cells and suppress adenoma formation in $APC^{Min/+}$ mice (Leibowitz et al., 2014; Qiu et al., 2010). Long-term use of NSAIDs, in particular COX-2-specific inhibitors, is associated with side effects, which has stimulated the development of new targets and combination strategies for cancer chemoprevention (Meyskens et al., 2008).

It is clear that select extrinsic bioactives, e.g., n-3 polyunsaturated fatty acids (n-3 PUFA) and curcumin (Cur), independently reduce aberrant crypt foci (ACF) and polyp formation in humans (Carroll et al., 2011; West et al., 2010) and combinations of the two have been reported to exert synergistic effects related to the suppression of chronic inflammation and cell proliferation and the promotion of apoptosis in breast and pancreatic cancers (Altenburg et al., 2011; Jia et al., 2011; Saw et al., 2010; Siddiqui et al., 2013; Swamy et al., 2008). From a mechanistic perspective, the combination of n-3 PUFA and curcumin has been shown to suppress NFκB activation in mouse colonic mucosa (Jia et al., 2011) in part by altering plasma membrane composition (Kim et al., 2009), which is required for activation of the apoptotic pathways (Beneteau et al., 2008; Gajate and Mollinedo, 2011). The suppression of inflammatory mediators such as COX-2, inducible nitric oxide synthase (iNOS), prostaglandin E_2 (PGE_2), 5-lipoxygenase (5-LOX) and cytosolic phospholipase A_2 ($cPLA_2$) has

also been linked to the synergistic action of curcumin and n-3 PUFA, e.g., docosahexaenoic acid (DHA) (Saw et al., 2010; Swamy et al., 2008).

DHA and curcumin synergistically induce p53 activation (Altenburg et al., 2011; Siddiqui et al., 2013), a well-known tumor suppressor (Stracquadanio et al., 2016; Vogelstein et al., 2000). This is noteworthy, because p53 functions in part to inhibit NFκB activity, thereby inducing apoptosis in human colon cancer cells (Shao et al., 2000) (Puszynski et al., 2009). In contrast, the loss of p53 during tumor progression promotes an NFκB dependent inflammatory microenvironment (Schwitalla et al., 2013b), which is a critical event in the commitment of stem cells to apoptosis following DNA damage (Davidson et al., 2015; Dumitru et al., 2012). Unfortunately, the properties of extrinsic chemo-protective natural compounds known to enhance the p53 signaling pathway in colonic adult stem cells from the perspective of cancer initiation and progression have not been determined.

In this study, we assessed the chemo-protective effects of diet on $Lgr5^+$ stem cell homeostasis in the context of AOM-induced tumorigenesis at both the initiation and pre-tumor stages. Our novel data provide evidence that curcumin combined with n-3 PUFA synergistically reduces AOM-induced nuclear β–catenin levels in ACF in part by promoting p53-dependent signaling and targeted apoptosis in damaged $Lgr5^+$ stem cells at the initiation stage. We also provide evidence that DNA damaged $Lgr5^+$ stem cells are highly responsive to the combination diet compared to DNA damaged differentiated cells. Our

findings demonstrate for the first time that rapidly cycling $Lgr5^+$ stem cells are exquisitely sensitive to extrinsic dietary factors which modulate colon cancer risk.

3.2 Material and methods

3.2.1 Animals and study design

The animal use protocol was approved by the University Animal Care Committee of Texas A&M University and conformed to NIH guidelines. Lgr5-EGFP-IRES-$CreER^{T2}$ knock-in mice (Barker et al., 2009), 6-7 wk old, were acclimated for 1 wk and then maintained on a semi-purified diet (Figure 9A) for 3 wks prior to injection with AOM (Sigma, St. Louis, MO, 10 mg/kg body weight). Mice were injected with AOM once a week for 6 wks and euthanized by CO_2 asphyxiation at 17 wks (n=7~8 per group) after the last AOM injection (Figure 9B). In complementary experiments, mice were injected with a single dose of AOM and euthanized 12 (n=8) or 24 hr (n=8) later (Figure 9C). Control mice (n=3) received a single saline injection. Mice were injected with EdU (Life Technologies) 2 h prior to sacrifice. Immediately after termination, the distal colon was rapidly removed, flushed with ice-cold saline and a longitudinal section of the distal colon was immediately fixed in 4% paraformaldehyde for hematoxylin and eosin (H&E) staining and immunofluorescence analyses. Figure 9B&C shows the timeline of the treatments and the experimental design.

3.2.2 Diets

Diet sources have been previously reported (Kim et al., 2009). A complete diet containing 5% corn oil (containing n-6 PUFA) was used as a baseline control, i.e., contained no n-3 PUFA or curcumin. The control diet was supplemented with 1% (w/w) curcumin (n-6 PUFA + Cur) to determine the effect of curcumin. A diet containing 4% (w/w) Menhaden fish oil (enriched in n-3 PUFA) was used to assess the effect of n-3 PUFA alone, while a fish oil + curcumin (n-3 PUFA + Cur) diet was used to determine the additive/synergistic effects of these dietary bioactives. Both n-3 PUFA and n-3 PUFA + Cur diets contained 1% corn oil (w/w) to ensure that essential fatty acid requirements were met (Figure 9A). Mice were provided with fresh diet every day and the feeders were removed and washed daily. Animals had free access to food and water at all times and 24 hr food intakes were measured after 1 week of receiving the diets (Figure 9D). Body weights were recorded each week (Figure 9E) and weight gain was not affected by the experimental diets. The fatty acid composition of the diets was analyzed by gas chromatography and the level of curcumin was quantified by ^{1}H NMR (Jayaprakasha et al., 2013). The fatty acid composition of the crypt was quantified by gas chromatography (Fan et al., 2003) and the level of curcumin was quantified by HPLC (Cuomo et al., 2011; Jayaprakasha et al., 2013).

3.2.3 In vivo DNA damage and repair measurement

Longitudinal sections of paraffin-embedded colon sections (4 μm) were deparaffinized, rehydrated through graded ethanol and stained with antibodies using standard procedures. DNA double strand breaks were measured by immunofluorescence using a rabbit monoclonal phospho-gamma H2AX (γH2AX) Ser139 antibody (9718, Cell Signaling; dilution 1:200). $Lgr5^+$ stem cells were labeled using goat polyclonal GFP antibody (ab6673, Abcam; dilution 1:400) and O^6meG DNA adduct removal was estimated by the induction of O^6-methylguanine-methyl transferase (MGMT) expression using a mouse monoclonal MGMT antibody (ab54306, Abcam; prediluted). Secondary antibodies were anti-rabbit Alexa 647 (711-605-152, Jackson ImmunoResearch: dilution 1:400) for γH2AX, anti-goat 488 (705-545-147, Jackson ImmunoResearch) for GFP and anti-mouse Alexa 546 (A10036, Life Technologies) for MGMT. Negative control slides were incubated without primary antibody. The DNA damage (or repair) index was determined by dividing the number of $\gamma H2AX^+$ (or $MGMT^+$) cells by the total number of cells in each crypt column and multiplying by 100.

3.2.4 Slide scoring of in vivo apoptosis

To investigate whether alkylating agent-induced DNA damage resulted in apoptotic cell death in colonic $Lgr5^+$ stem cells, free 3'OH DNA termini were labeled using the TUNEL procedure according to the manufacturer's

recommendations using the TACS 2 TdT-Fluor *in situ* apoptosis detection kit (4810-30-K and 4810-30-R, Trevigen) and detected with Streptavidin-CY3 (438315, Life Technologies). Negative control slides were incubated without TdT enzyme. The apoptotic index was determined by dividing the number of apoptotic cells by the total number of cells in the crypt column and multiplying by 100. To corroborate the frequency of epithelial cells undergoing apoptosis, paraffin-embedded sections were also assessed by H&E staining by a blinded pathologist with both assays showing similar results.

A

Ingredients	Diet (g/100 g)			
	n-6 PUFA	n-6 PUFA+Cur	n-3 PUFA	n-3 PUFA+Cur
Sucrose	42	41	42	41
Casein	20	20	20	20
DL-methionine	0.3	0.3	0.3	0.3
AIN-76 Mineral mix	3.5	3.5	3.5	3.5
AIN-76 Vitamin mix	1	1	1	1
Choline Chloride	0.2	0.2	0.2	0.2
Corn Starch	22	22	22	22
Cellulose	6	6	6	6
Curcumin	0	1	0	1
Fish oil	0	0	4	4
Corn oil	5	5	1	1
Total	100	100	100	100

B

C

D

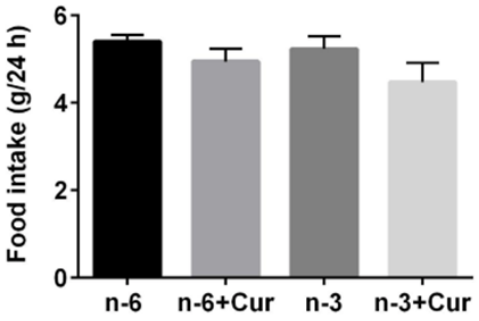

E

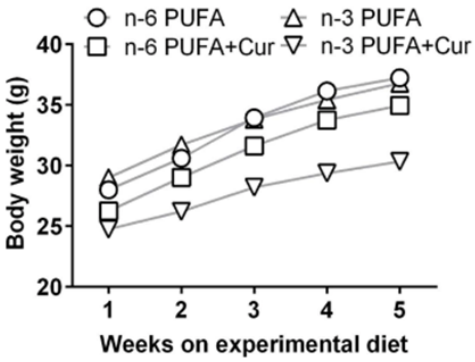

F

Bioactives in mouse experimental diet		n-6 PUFA	n-6 PUFA +Cur	n-3 PUFA	n-3 PUFA +Cur
Fatty acids (ug/g crypt wet weight)	20:5n-3 (EPA)	-	-	19.29 ± 4.54	43.29 ± 11.97
	22:5n-3 (DPA)	-	-	0.80 ± 0.30	1.96 ± 0.56
	22:6n-3 (DHA)	-	-	7.92 ± 1.77	19.34 ± 5.83
Curcumin (ug/g crypt wet weight)		-	4.26 ± 0.95	-	1.08 ± 0.08

Figure 9. Timeline of treatments and the experimental design. (A) Experimental diet composition. Timeline of the treatments at pre-tumor stage **(B)** and initiation stage **(C)** of tumorigenesis. **(D)** Food intake and **(E)** body weight gain. **(F)** Amount of fatty acids and curcumin in colonic crypts (n=4). n-6: n-6 PUFA, n-6+Cur: n-6 PUFA + curcumin, n-3: n-3 PUFA, and n-3+Cur: n-3 PUFA + curcumin.

3.2.5 In vivo measurement of cell proliferation

To investigate the effects of alkylating agent-induced DNA damage on cell cycle activity in colonic epithelial cells, proliferating cells were measured using the Click-iT EdU Alexa Fluor 555 Imaging kit (Life Technologies) as per manufacturer's instructions. Negative control slides were incubated without Alexa Fluor. The proliferation index was determined by dividing the number of proliferating cells by the total number of cells in the crypt column and multiplying by 100.

3.2.6 In vivo measurement of Bax expression

To measure the chemo-protective effect of diet and carcinogen on Bax expression in the colon, $Lgr5^+$ stem cells were labeled using goat polyclonal GFP antibody (ab6673, Abcam; dilution 1:400) and rabbit monoclonal total Bax antibody (14796, Cell Signaling; dilution 1:400). Secondary antibodies were anti-goat 488 (705-545-147, Jackson ImmunoResearch) for GFP and anti-rabbit Alexa 647 (711-605-152, Jackson ImmunoResearch: dilution 1:400) for Bax. Negative control slides were incubated without Alexa Fluor. For each high power field (objective, 40X), GFP positive crypts were assessed by defining regions of interest for analysis. GFP staining was used to define the region of interest and to assess differentiated cells and stem cells within a crypt. The ratio of Bax expression in $Lgr5^+$ stem/differentiated cells was determined using NIS Image software, version 3.2 (Nikon).

3.2.7 Image acquisition and analysis

All immunofluorescent images of colonic crypts were captured using an inverted TE 300 Nikon Eclipse fluorescence microscope equipped with 40X/1.30 Nikon Plan Fluor oil immersion objective and a Photometrics Cool Snap EZ digital CCD camera and a SOLA external light source. Images were processed using NIS Image software, version 3.2 (Nikon). Greater than 40 GFP positive crypts per animal in each treatment group were examined by one reader. The number of animals used for each assay is described in each figure legend.

3.2.8 Lgr5^{+} stem cell isolation from colonic crypt using fluorescence activated cell sorting (FACS)

Colonic crypts were isolated by the method of Sato et al (Sato et al., 2009) with minor modification. 3 cm of the distal colon was removed and flushed with Ca/Mg free PBS containing P/S. After opening longitudinally, it was placed into 30 mL PBS and vigorously vortexed. The colon is then incubated with 2 mM EGTA in PBS at 37 °C for 15 min followed by another incubation with the 20 mM EGTA in PBS at 37° C for 15 min. Following transfer to chilled Ca/Mg free PBS, colons were vigorously vortexed to release crypts. The crypts were then incubated with 50 μL of DNase (stock concentration- 20 units/mL) in 10 mL of 0.25% trypsin solution at 37 °C for 10 min and single cells were then passed through a 40 μm cell strainer. The cells were counted and resuspended

to a final cell density of 2 x10^6 cells/mL. To examine the global transcriptome in stem vs differentiated cells, isolated colonocytes from the distal colon were sorted based on GFP expression using a Beckman Coulter MoFlo Astrios as previously described (Fan et al., 2014). Approximately 12,000 GFP^{high} cells (stem cells) and 275,000 GFP^{neg} cells (differentiated cells) were sorted for each treated mouse. Cells from wild type mice were used to set the gates for sorting.

3.2.9 RNA sequencing

Total RNA from isolated cells was isolated using RNA nanoprep kit (Zymo Research, R1050) following the manufacturer's protocol. RNA quantity and quality were measured by nanodrop and Agilent 2100 Bioanalyzer (Agilent Technologies, CA) respectively. Isolated total RNA (2 ng) from each sample was subsequently prepared for sequencing using the NuGen Ovation® Single Cell RNA-Seq System (0342HV). Samples were sequenced for 75 cycles with single index reads on the NextSeq 500 (Illumina). Following the removal of all genes with CPM (counts-per-million reads) values less than 1, publicly available R software, EdgeR, was used to identify differentially expressed genes. In total, 15,043 genes were queried to detect differentially expressed genes.

3.2.10 Ingenuity pathway analysis (IPA)

Genes differentially expressed (FDR < 0.05) in GFP^{high} versus GFP^{neg} cells were included in pathway and function analyses (Shah et al., 2011; Triff et al., 2013) using Ingenuity software (IPA; Ingenuity® Systems, http://www.ingenuity.com). Statistical significance of the association between each data set and the canonical pathway was determined based on two parameters: (1) A ratio of the number of genes from the data set that map to the pathway divided by the total number of genes that map to the canonical pathway, and (2) P-values calculated using Fischer's exact test determining the probability that the association between the genes in the data set and the canonical pathway is due to chance alone. The upstream regulator analysis function of IPA was subsequently used to identify potential transcriptional regulators that could explain the observed changes in gene expression. The activation z-score was calculated to predict activation or inhibition of transcriptional regulators based on published findings accessible through the Ingenuity knowledge base. Regulators with a z-score greater than 1.96 or less than -1.96 were considered to be significantly activated or inhibited. Functions and pathways with P-value < 0.05 (Fischer's exact test) were considered to be statistically significant.

3.2.11 ACF quantification

Paraffin-embedded, H&E stained distal colon sections (4 μm) were examined for ACF by a veterinary pathologist. Photomicrographs were taken at 40X. ACF were defined as crypts with more than one of the following features: loss of polarity, nuclear atypia (enlarged nuclei, vesiculated chromatin, crowding), mucin depletion, and crypt multiplicity. Emphasis was placed on aberrant crypt multiplicity as a cardinal change. The presence of ACF adjacent to lymphoid follicles were not considered true ACF because proximity to lymphoid tissue may promote changes related to inflammation. For this study, only crypts with criteria matching Group C (dysplastic microadenomas, with enlarged, elongated and sometimes stratified nuclei with loss of polarity, mucin depletion and dysplasia) as defined by (Di Gregorio et al., 1997) were considered aberrant crypt foci. The number of ACF per section was quantified and the location mapped using mm measurements from the slide corner. In addition, complementary immunohistochemistry was performed to assess co-labeling with β-catenin.

3.2.12 β-catenin subcellular localization in nucleus and cytoplasmic ACF

Serial sections were used to measure the subcellular localization of β-catenin in ACF. To measure the ratio of nuclear to cytosolic β-catenin in ACF, tissue was labeled using a mouse monoclonal β-catenin antibody (610154, BD Transduction; dilution 1:500) (Hata et al., 2004; Yamada et al., 2001).

Secondary antibody was anti-mouse Alexa 546 (A10036, Life Technologies). Nuclear staining was detected by counterstaining cells with 4', 6-Diamidino-2-phenylindole, DAPI (P36935, Life Technologies). Negative control slides were incubated without primary antibody. For each high power field (objective, 40X), ACF areas stained with β-catenin and DAPI were assessed by defining regions of interest for analysis. DAPI staining was used to define the nuclear region of interest and to separate nuclear and cytoplasmic staining within a cell. The ratio of nuclear to cytosolic β-catenin was measured using NIS Image software, version 3.2 (Nikon).

3.2.13 Statistics

Data were analyzed using two-way analysis of variance and the estimated mean groups were subsequently compared using simple t-tests. A Tukey approach was used to adjust the resulting p-values for multiple comparisons. The significant comparisons were obtained based on the adjusted p-values<0.05.

3.3 Results

3.3.1 n-3 PUFA and curcumin synergize to promote targeted apoptosis of damaged Lgr5$^+$ stem cells at the tumor initiation stage

To elucidate the unique properties of colonic Lgr5$^+$ stem cells in terms of their response to bioactive compounds in the presence of carcinogen, we

utilized mice carrying a gene for enhanced green fluorescent protein (EGFP) knocked into the Lgr5 genomic locus (Barker and Clevers, 2007). Mice were fed with n-3 PUFA and curcumin alone or in combination for 3 wks, injected with AOM, and analyzed to measure DNA damage (γH2AX), apoptosis (TUNEL), damage repair (O^6-methylguanine-methyl transferase, MGMT) and proliferation (EdU) in crypts 12 and 24 hr later as previously described (Kim et al., 2016a). Because the integration cassette in this mouse model is epigenetically silent in about 60%–70% of crypts (Barker et al., 2007), we analyzed only GFP positive crypts using fluorescence microscopy. No differences between GFP^{high} and GFP^{neg} crypts in response to carcinogen and bioactive compounds were observed (data not shown). In a separate experiment, levels of n-3 PUFA, n-6 PUFA and curcumin incorporated into colonic crypts were assessed following a 3 wks feeding period (Figure 9F). The data demonstrate that these bioactives were readily incorporated into the target site.

It has been demonstrated that $Lgr5^+$ stem cells are preferentially damaged by AOM in the distal colon compared to differentiated cells (Kim et al., 2016a) and n-3 PUFA reduce AOM-induced DNA adducts (Hong et al., 2000) which cause double strand breaks (DSBs) (Karran and Bignami, 1992). Therefore, to determine the chemo-protective effects of combinatorial bioactives on AOM-induced DNA damage in $Lgr5^+$ stem cells as compared to differentiated cells *in vivo*, we measured γH2AX, a marker of the double strand

breaks (Kuo and Yang, 2008). As shown in Figure 10A, the level of DNA damaged stem cells at 12 hr in both n-3 PUFA and n-3 PUFA + Cur treatments was 50% lower than the n-6 PUFA. In comparison, DNA damage in n-6 PUFA + Cur was 33% lower compared to n-6 PUFA fed mice. Strikingly, by 24 hr, the n-3 PUFA + Cur group maximally decreased damaged $Lgr5^+$ stem cells, i.e., the level was not different from the saline-injected mice.

The deletion of damaged $Lgr5^+$ stem cells, the cells of origin of colon cancer (Barker et al., 2009), is a critical mechanism to prevent tumorigenesis in the intestine (Leibowitz et al., 2014). Since n-3 PUFA (Hong et al., 2003; Hong et al., 2000) and curcumin (Xu et al., 2010) promote apoptosis in 1,2-dimethylhydrazine (DMH) or AOM injected rats, we next investigated the synergistic effects of n-3 PUFA + Cur on the $Lgr5^+$ stem cell acute DNA damage response. Figure 10B shows representative co-localization images of DNA damaged (γH2AX, white) $Lgr5^+$ stem cells (GFP, green) with apoptosis (TUNEL, red), DNA repair (MGMT, red) or cell proliferation (EdU, red). As shown in Figure 11A, immediately following AOM exposure, n-3 PUFA and curcumin either alone or in combination increased apoptosis greater than 1.5 fold in $Lgr5^+$ stem cells (open symbols) at 12 hr compared to n-6 PUFA, whereas the apoptotic response was significantly lower in differentiated cells across all groups (filled symbols).

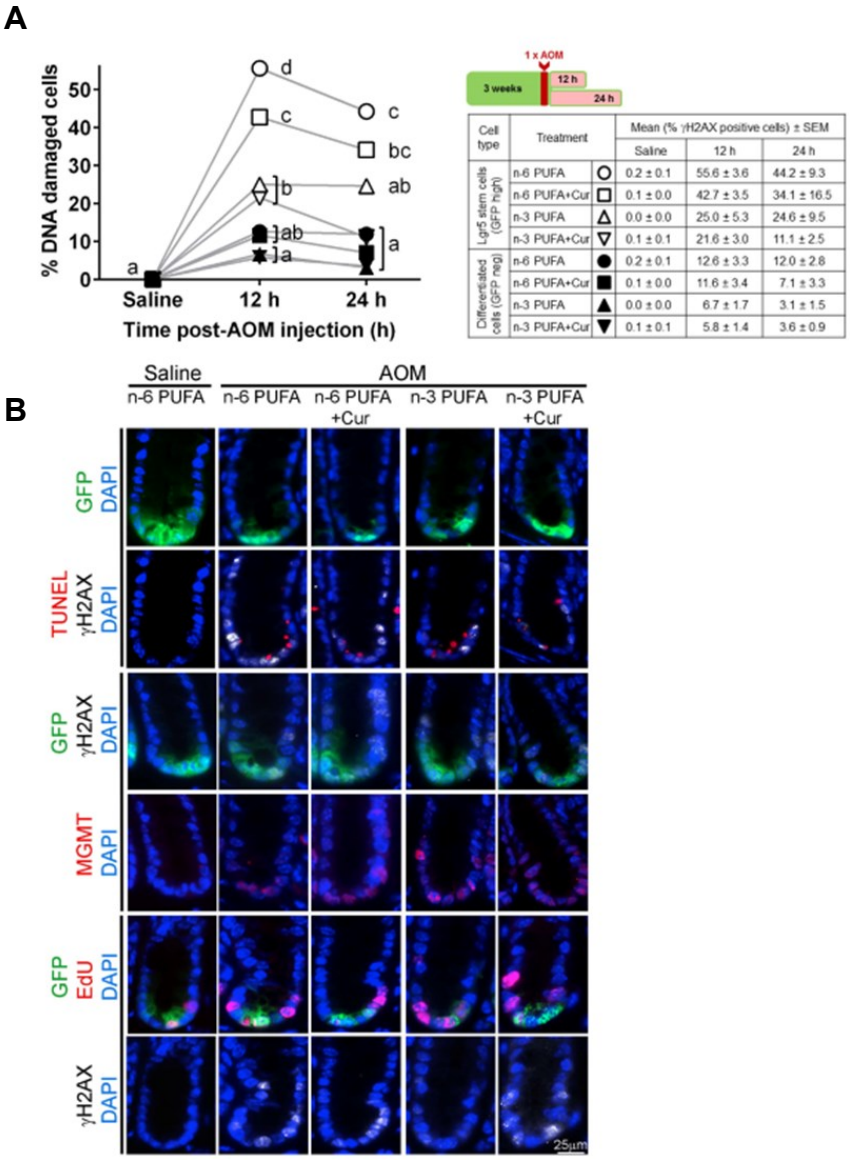

Cell type	Treatment		Mean (% γH2AX positive cells) ± SEM		
			Saline	12 h	24 h
Lgr5 stem cells (GFP high)	n-6 PUFA	○	0.2 ± 0.1	55.6 ± 3.6	44.2 ± 9.3
	n-6 PUFA+Cur	□	0.1 ± 0.0	42.7 ± 3.5	34.1 ± 16.5
	n-3 PUFA	△	0.0 ± 0.0	25.0 ± 5.3	24.6 ± 9.5
	n-3 PUFA+Cur	▽	0.1 ± 0.1	21.6 ± 3.0	11.1 ± 2.5
Differentiated cells (GFP neg)	n-6 PUFA	●	0.2 ± 0.1	12.6 ± 3.3	12.0 ± 2.8
	n-6 PUFA+Cur	■	0.1 ± 0.0	11.6 ± 3.4	7.1 ± 3.3
	n-3 PUFA	▲	0.0 ± 0.0	6.7 ± 1.7	3.1 ± 1.5
	n-3 PUFA+Cur	▼	0.1 ± 0.1	5.8 ± 1.4	3.6 ± 0.9

Figure 10. **Effect of n-3 PUFA ± curcumin on AOM-induced DNA double strand breaks in mouse colonic crypts at 12 and 24 hr post AOM injection. (A)** Comparison of γH2AX$^+$ (DNA damaged) stem and differentiated cells in the distal colon of saline (control) and 12 and 24 hr post AOM injected mice (left). GFP$^+$ crypts from n=8-9 mice at 12 hr, and n=3 for saline and 24 hr were counted. Statistically significant differences between diets and treatments were determined using two-way ANOVA followed by Tukey's multiple comparison test adjustment. Different letters indicate significant differences between treatment groups in each time ($p<0.05$). Means and standard errors of the mean (SEM) in different cell types, diets and treatments are listed in the table (right). Diets are labeled with different symbols and the open symbols refer to stem cells whereas filled symbols refer to differentiated cells. **(B)** Representative images (objective, 40X) of GFP$^+$ (GFP positive Lgr5 stem cells, green), γH2AX$^+$ DNA double strand breaks, white) and TUNEL$^+$ (apoptotic body, red) cells 12 hr after AOM. Representative images of MGMT$^+$ (damage repairing cells, red) and EdU$^+$ (proliferating cells) cells 24 hr following AOM exposure. Saline injected animals serve as the control.

Next, using a simple linear regression analysis, we determined whether there is any association between AOM-induced apoptosis and AOM-induced damage. As shown in Figure 11B (left), n-3 PUFA + Cur (slope=0.65) and n-6 PUFA (slope=0.61) exhibited a significant proportional increase in apoptosis in $Lgr5^+$ stem cells in response to DNA damage at 12 hr. However, n-3 PUFA + Cur exhibited less than 40% of damaged ($\gamma H2AX^+$) $Lgr5^+$ stem cells per crypt (DNA damage index) whereas n-6 PUFA had 40-80% of damaged $Lgr5^+$ stem cells per crypt. These data suggest that $Lgr5^+$ stem cells responded efficiently to n-3 PUFA + Cur treatment in the presence of DNA damage by inducing apoptosis, whereas differentiated cells were not responsive (small symbols within the dotted line). We subsequently quantified the number of damaged $Lgr5^+$ stem cells that were targeted for apoptotic deletion, i.e., GFP^+, $TUNEL^+$, $\gamma H2AX^+$ triple positive cells, since the selective deletion of damaged $Lgr5^+$ stem cells through apoptosis could mitigate the clonal expansion of damaged $Lgr5^+$ stem cells. As shown in Figure 11C (right), 62% of DNA damaged $Lgr5^+$ stem cells were deleted by apoptosis in n-3 PUFA + Cur treated mice at 12 hr, which was 5-fold higher than the n-6 PUFA group. Importantly, n-3 PUFA and curcumin interaction was only detected in $Lgr5^+$ stem cells ($p=0.025$) and not in differentiated cells ($p=0.526$) (Tables 3A&B). These novel findings demonstrate that DNA damaged $Lgr5^+$ stem cells uniquely respond to n-3 PUFA and Cur, and n-3 PUFA and Cur synergize to promote the deletion of DNA damaged $Lgr5^+$ stem cell.

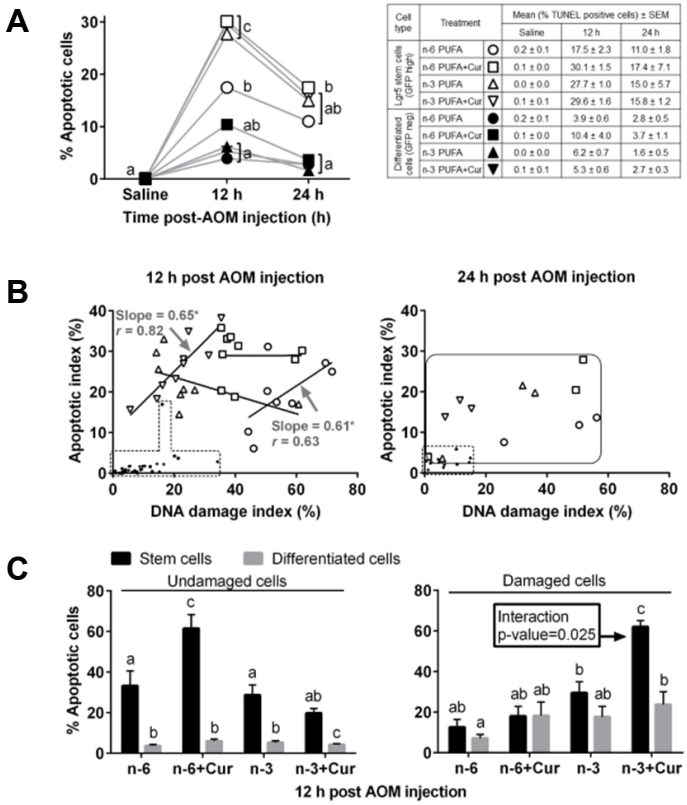

Figure 11. Effect of n-3 PUFA ± curcumin on AOM-induced apoptosis in mouse colonic crypts at 12 and 24 hr post AOM injection. **(A)** Comparison of TUNEL$^+$ (apoptotic) stem and differentiated cells in the distal colon of saline, and 12 and 24 hr post AOM injected mice (left). Refer to Figure 1A legend for animal number and statistical details. Different letters indicate significant ($p<0.05$) differences between treatment groups at each time point. **(B)** Association between AOM-induced apoptotic cells and γH2AX$^+$ cells in stem and differentiated cells at 12 hr (left) and 24 hr (right). Each point represents an individual animal and diets are labeled with different symbols as indicated in the Table in A. Slopes shown are found to be significantly different from 0 at a significant level of 0.05 (n-3 PUFA + Cur and n-6 PUFA stem cells, 12 hr). Data from differentiated cells (12 and 24 hr) and stem cells (24 hr) are highlighted within the dotted lines and solid lines, respectively, instead of showing slope, since none of the slopes differed from zero. Linear regression was performed using GraphPad Prism 6.0. Values represent Pearson correlation coefficients, r, ranges from -1 to +1. P-values were calculated using an F test. Apoptotic index = # of TUNEL$^+$ stem or differentiated cells / total # of stem or differentiated cells per crypt x100 at 12 and 24 hr post AOM injection; Damage index = # of γH2AX$^+$ stem or differentiated cells / total # of stem or differentiated cells per crypt x100 at 12 and 24 hr post AOM injection. **(C)** Percentage of non-targeted apoptosis (# of TUNEL$^+$ and γH2AX$^-$ stem or differentiated cells / total # of γH2AX$^-$ stem or differentiated cells x100) at 12 hr post AOM injection (left). Percentage of targeted apoptosis (# of double positive TUNEL$^+$ and γH2AX$^+$ stem or differentiated cells / total # of γH2AX$^+$ stem or differentiated cells x100) at 12 hr post AOM injection (right). Refer to Figure 10A legend for animal numbers and statistics. Different letters indicate significant ($p<0.05$) differences between treatment groups at each time point. n-6: n-6 PUFA, n-6 + Cur: n-6 PUFA + curcumin, n-3: n-3 PUFA, and n-3 + Cur: n-3 PUFA + curcumin.

A

Comparisons (TukeyHSD test)	Mean difference	Significance (p-value)	95% family-wise confidence level	
			Lower bound	Upper bound
n-3 PUFA vs n-6 PUFA	0.2271	0.062	-0.0088	0.4629
n-6 PUFA+Cur vs n-6 PUFA	0.0682	0.850	-0.1610	0.2974
n-6 PUFA+Cur vs n-3 PUFA	-0.1589	0.256	-0.3881	0.0703
n-3 PUFA+Cur vs n-6 PUFA	0.5775	<0.001	0.3483	0.8067
n-3 PUFA+Cur vs n-3 PUFA	0.3504	0.001	0.1212	0.5796
n-3 PUFA+Cur vs n-6 PUFA+Cur	0.5093	<0.001	0.2869	0.7317

B

Two-way ANOVA - Lgr5⁺ Stem cells					
Source of Variation	Degree of freedom	Sum of squares	Mean squares	F-value	Pr > F
n-3 PUFA	1	1.2048	1.2048	40.032	5.61×10^{-7}
Curcumin	1	0.3711	0.3711	12.331	0.00143
n-3 PUFA+Curcumin	1	0.1687	0.1687	5.605	0.02456

Two-way ANOVA - Differentiated cells					
Source of Variation	Degree of freedom	Sum of squares	Mean squares	F-value	Pr > F
n-3 PUFA	1	0.1024	0.1024	3.394	0.0761
Curcumin	1	0.1628	0.1628	5.396	0.0277
n-3 PUFA+Curcumin	1	0.0125	0.0125	0.413	0.5255

C

Comparisons (TukeyHSD test)	Mean difference	Significance	95% family-wise confidence level	
			Lower bound	Upper bound
n-3 PUFA vs n-6 PUFA	-0.0035	0.999	-0.0706	0.0636
n-6 PUFA+Cur vs n-6 PUFA	0.0105	0.961	-0.0522	0.0732
n-6 PUFA+Cur vs n-3 PUFA	-0.0140	0.940	-0.0858	0.0578
n-3 PUFA+Cur vs n-6 PUFA	-0.6754	<0.001	-0.7612	-0.5896
n-3 PUFA+Cur vs n-3 PUFA	-0.6719	<0.001	-0.7646	-0.5792
n-3 PUFA+Cur vs n-6 PUFA+Cur	-0.6859	<0.001	-0.7754	-0.5964

Two-way ANOVA - β-catenin in ACF				
Source of Variation	Estimate	Stand.Error	T-value	Pr > F
n-3 PUFA	-0.0035	0.0231	-0.152	0.881
Curcumin	0.0105	0.0216	0.487	0.634
n-3 PUFA+Curcumin	-0.6824	0.0385	-17.730	5.47×10^{-11}

Table 3. n-3 PUFA and curcumin interaction. Assessment of statistical interaction between dietary n-3 PUFA and curcumin with respect to the induction of apoptosis in Lgr5⁺ stem cells by Tukey's HSD test **(A&B)** and in stem and differentiated cells by two-way ANOVA **(C)**.

3.3.2 AOM-induced MGMT expression is enhanced by n-3 PUFA and/or curcumin I n damaged Lgr5$^+$ stem cells and differentiated cells.

The major pathway to remove AOM-induced O^6-methylguanine (O^6meG) DNA adducts is via MGMT (Pegg and Byers, 1992). Therefore, the expedited elimination of O^6meG by increasing MGMT activity is likely to be a successful chemoprevention strategy (Niture et al., 2007). Because curcumin induces MGMT protein expression in colon cancer cells (Niture et al., 2007), we estimated MGMT activity using quantitative immuno-histochemical analysis (Zaidi et al., 1996). As shown in Figure 12A, MGMT expression in Lgr5$^+$ stem cells was maximally induced by curcumin with either PUFA diet or the n-3 PUFA treatment at 24 hr as compared to saline treatment. However, only n-3 PUFA + Cur fed animals exhibited an induction in MGMT associated with DNA damage in Lgr5$^+$ stem cells at 24 hr using a simple linear regression analysis (Figure 12B right). In contrast, in differentiated cells (filled symbol), no significant induction was detected at 24 hr (Figure 3A). As shown in Figure 12B (left), at 12 hr post AOM exposure, n-3 PUFA and n-6 PUFA + Cur proportionally increased MGMT expression in Lgr5$^+$ stem cells (n-3 PUFA: slope=2.07, r=0.92 and n-6 PUFA + Cur: slope=0.83, r=0.90), compared to n-3 PUFA and n-3 PUFA + Cur treatment induction of MGMT in differentiated cells (GFP^{neg}) (Figure 12B middle). We subsequently quantified the number of damaged Lgr5$^+$ stem cells that were targeted for damage repair, i.e., GFP$^+$, MGMT$^+$, γH2AX$^+$ triple positive cells, since the deletion of O^6meG in Lgr5$^+$ stem

cells by MGMT could mitigate the clonal expansion of DNA-damaged $Lgr5^+$ stem cells. As shown in Figure 13B (12 hr) and Figure 3C (right, 24 hr), n-3 PUFA + Cur and n-3 PUFA induced MGMT expression in damaged $Lgr5^+$ stem cells as compared to n-6 PUFA. Additionally, damaged differentiated cells also induced MGMT expression, similar to damaged $Lgr5^+$ stem cells both at 12 and 24 hr (Figure 13B and Figure 12C).

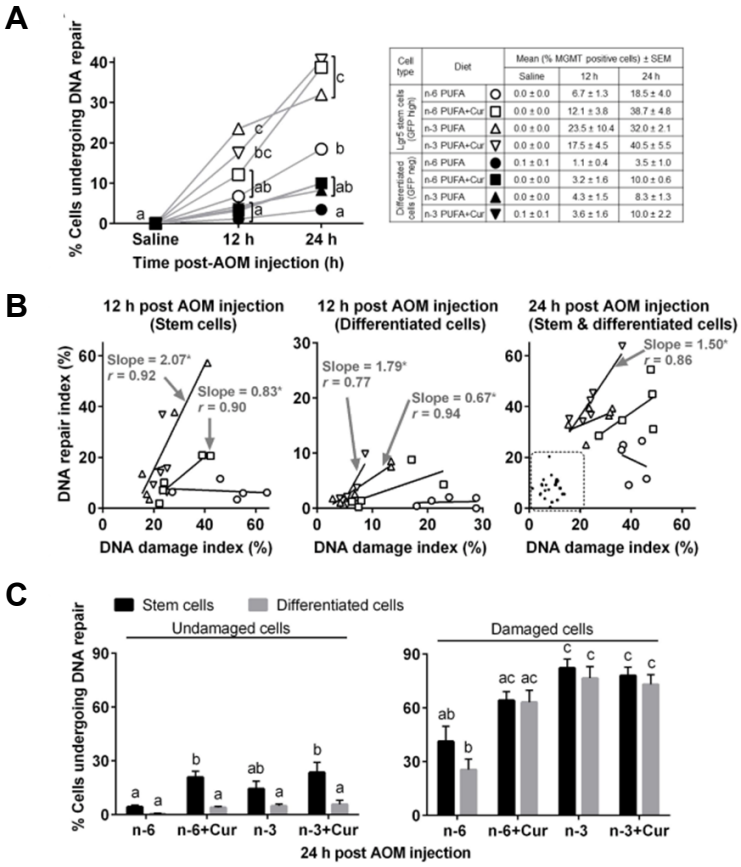

Figure 12. Effect of n-3 PUFA ± curcumin on AOM-induced MGMT expression in mouse colonic crypts at 12 and 24 hr post AOM injection. (A) Comparison of MGMT$^+$ (damage repairing) stem and differentiated cells in the distal colon of saline and 12 and 24 hr post AOM injected mice (left). GFP$^+$ crypts were scored from n=3 per diet in saline treated mice, n=5~6 per diet in AOM injected mice at 12 and 24 hr. Refer to Figure1A legend for statistical details. Different letters indicate significant ($p<0.05$) differences between treatment groups at each time point. **(B)** Association between AOM-induced MGMT expressing cells and γH2AX$^+$ cells in stem and differentiated cells at 12 hr (left and middle) and 24 hr (right). Each point represents an individual animal and diets are labeled with different symbols as indicated in the Table in A. Slopes shown are found to be significantly different from 0 at a significant level of 0.05. Data from differentiated cells (24 hr) are highlighted within the dotted line instead of showing slope because none of the slopes differed from zero. DNA repair index = # of MGMT$^+$ stem or differentiated cells / total # of stem or differentiated cells per crypt x100 at 12 and 24 hr post AOM injection; Damage index = # of γH2AX$^+$ stem or differentiated cells / total # of stem or differentiated cells per crypt x100 at 12 and 24 hr post AOM injection. Refer to Figure 2B legend for statistical details. **(C)** Percentage of undamaged cells expressing MGMT (# of MGMT$^+$ and γH2AX$^-$ stem or differentiated cells / total # of γH2AX$^-$ stem or differentiated cells x100) at 24 hr post AOM injection (left). Percentage of cells expressing MGMT in damaged cells (# of double positive MGMT$^+$ and γH2AX$^+$ stem or differentiated cells / total # of γH2AX$^+$ stem or differentiated cells x100) at 24 hr post AOM injection (right). Refer to Figure 1A legend for statistical details. Different letters indicate significant ($p<0.05$) differences between treatment groups at each time point. n-6: n-6 PUFA, n-6+Cur: n-6 PUFA + curcumin, n-3: n-3 PUFA, and n-3+Cur: n-3 PUFA + curcumin.

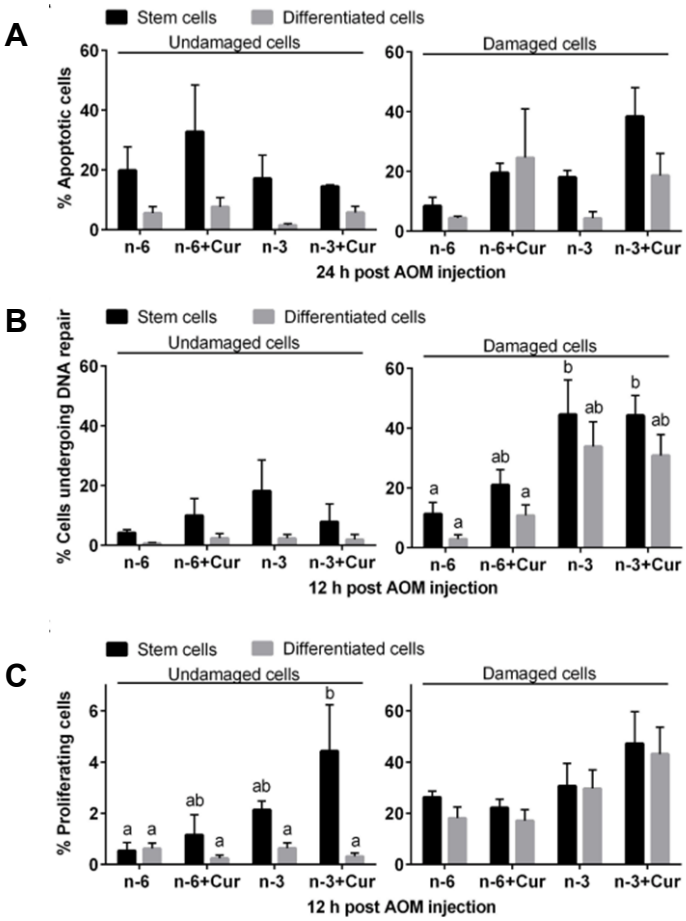

Figure 13. Effect of n-3 PUFA ± curcumin in mouse colonic crypts at 12 and 24 hr post AOM injection (A) Percentage of non-targeted apoptosis (# of TUNEL$^+$ and γH2AX$^-$ stem or differentiated cells / total # of γH2AX$^-$ stem or differentiated cells x 100) at 24 hr post AOM injection (left). Percentage of targeted apoptosis (# of double positive TUNEL$^+$ and γH2AX$^+$ stem or differentiated cells / total # of γH2AX$^+$ stem or differentiated cells x100) at 24 hr post AOM injection (right). Refer to Figure 1A legend for animal number and statistical details. Different letters indicate significant ($p<0.05$) differences between treatment groups. **(B)** Percentage of undamaged cells expressing MGMT (# of MGMT$^+$ and γH2AX$^-$ stem or differentiated cells / total # of γH2AX$^-$ stem or differentiated cells x100) at 12 hr post AOM injection (left). Percentage of damaged cells expressing MGMT (# of double positive MGMT$^+$ and γH2AX$^+$ stem or differentiated cells / total # of γH2AX$^+$ stem or differentiated cells x100) at 12 hr post AOM injection (right). Refer to Figure 1A legend for statistical details and Figure 3A for animal numbers. Different letters indicate significant ($p<0.05$) differences between treatment groups. **(C)** Percentage of undamaged proliferating cells (# of EdU$^+$ and γH2AX$^-$ stem or differentiated cells / total # of γH2AX$^-$ stem or differentiated cells x100) at 12 hr post AOM injection (left). Percentage of damaged proliferating cells (# of double positive EdU$^+$ and γH2AX$^+$ stem or differentiated cells / total # of γH2AX$^+$ stem or differentiated cells x100) at 12 hr post AOM injection (right). GFP$^+$ crypts (n=5 per diet for saline and n=5-6 per diet for 12 and 24 hr post AOM injection) were counted. Refer to Figure 1A legend for statistical details. Different letters indicate significant ($p<0.05$) differences between treatment groups. n-6: n-6 PUFA, n-6+Cur: n-6 PUFA + curcumin, n-3: n-3 PUFA, and n-3+Cur: n-3 PUFA + curcumin.

3.3.3 Crypt regeneration following AOM exposure.

As shown in Figure 10B, proliferating cells were predominantly located at the bottom of crypt where $Lgr5^+$ stem cells and transit amplifying (TA) cells reside, together referred to as the stem cell clonogen (SCC) compartment (Hua et al., 2012). To assess dietary effects on stem cell proliferation, a requirement for crypt regeneration following insult, EdU^+ cells in the colonic crypt were quantified following AOM-induced DNA damage. The percentage of proliferating cells at 12 hr post AOM vs saline injection was not affected across all dietary treatments (Figure 14A). An increase in cell division at 24 hr was only associated with $Lgr5^+$ stem cells, i.e., not in differentiated TA cells (Figure 14A). These findings indicate that colonic $Lgr5^+$ stem cells uniquely respond to cues associated with tissue homeostasis. Surprisingly, there was no significant association between the proliferative index and the level of DNA damage (Figure 14B) and no diet effects were observed with regard to cell proliferation in damaged $Lgr5^+$ stem cells at 12 hr (Figure 13C) and 24 hr (Figure 14C).

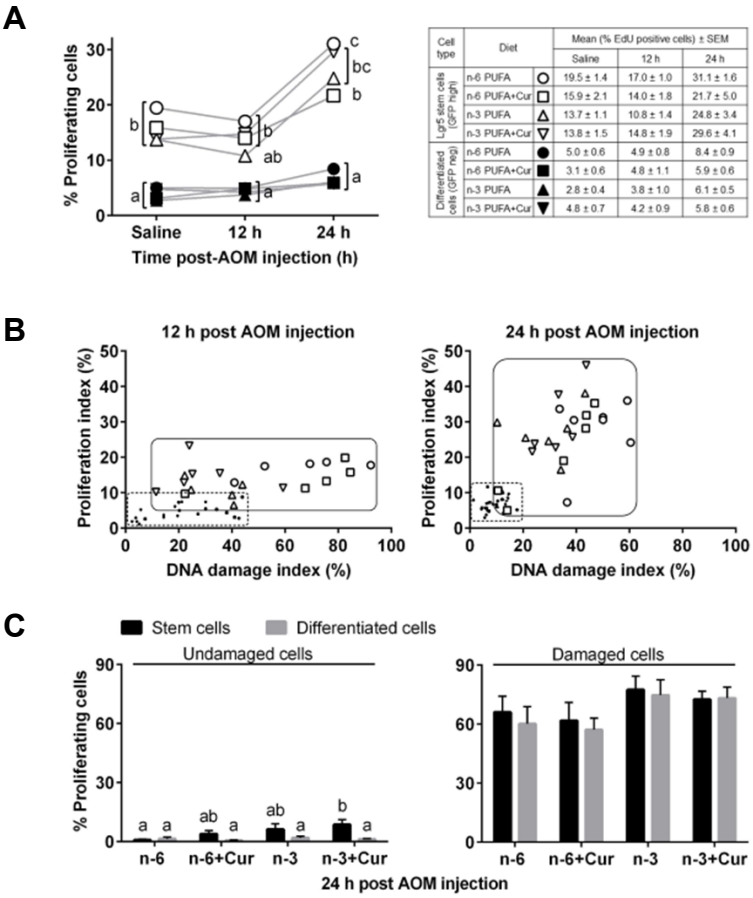

Cell type	Diet	Mean (% EdU positive cells) ± SEM		
		Saline	12 h	24 h
Lgr5 stem cells (GFP high)	n-6 PUFA ○	19.5 ± 1.4	17.0 ± 1.0	31.1 ± 1.6
	n-6 PUFA+Cur □	15.9 ± 2.1	14.0 ± 1.8	21.7 ± 5.0
	n-3 PUFA △	13.7 ± 1.1	10.8 ± 1.4	24.8 ± 3.4
	n-3 PUFA+Cur ▽	13.8 ± 1.5	14.8 ± 1.9	29.6 ± 4.1
Differentiated cells (GFP neg)	n-6 PUFA ●	5.0 ± 0.6	4.9 ± 0.8	8.4 ± 0.9
	n-6 PUFA+Cur ■	3.1 ± 0.6	4.8 ± 1.1	5.9 ± 0.6
	n-3 PUFA ▲	2.8 ± 0.4	3.8 ± 1.0	6.1 ± 0.5
	n-3 PUFA+Cur ▼	4.8 ± 0.7	4.2 ± 0.9	5.8 ± 0.6

Figure 14. Effect of n-3 PUFA ± curcumin on AOM-induced proliferation in mouse colonic crypts at 12 and 24 hr post AOM injection. (A) Comparison of EdU$^+$ (proliferating) stem and differentiated cells in the distal colon of saline, and 12 and 24 hr post AOM injected mice (*left*). GFP$^+$ crypts (n=5 per diet for saline and n=5-6 per diet for 12 and 24 hr post AOM injection) were counted. Refer to Figure 1A legend for statistical details. Different letters indicate significant ($p<0.05$) differences between treatment groups. **(B)** Association between the AOM-induced proliferating cells and γH2AX$^+$ cells in stem and differentiated cells at 12 hr (*left*) and 24 hr (*right*). Each point represents an individual animal and diets are labeled with different symbols as indicated in the Table in A. Data from stem cells and differentiated cells not significantly different from 0 are within the area of the square solid lines and dotted lines, respectively, instead of showing slope since none of the slopes were different from zero. Proliferation index = # of EdU$^+$ stem or differentiated cells / total # of stem or differentiated cells per crypt x100 at 12 and 24 hr post AOM injection; Damage index = # of γH2AX$^+$ stem or differentiated cells / total # of stem or differentiated cells per crypt x100 at 12 and 24 hr post AOM injection. Refer to Figure 2B legend for statistical details. **(C)** Percentage of undamaged proliferating cells (# of EdU$^+$ and γH2AX$^-$ stem or differentiated cells / total # of γH2AX$^-$ stem or differentiated cells x100) at 24 hr post AOM injection (*left*). Percentage of damaged proliferating cells (# of double positive EdU$^+$ and γH2AX$^+$ stem or differentiated cells / total # of γH2AX$^+$ stem or differentiated cells x100) at 24 hr post AOM injection (*right*). Refer to Figure 1A legend for statistical details. Different letters indicate significant ($p<0.05$) differences between treatment groups. n-6: n-6 PUFA, n-6+Cur: n-6 PUFA + curcumin, n-3: n-3 PUFA, and n-3+Cur: n-3 PUFA + curcumin.

3.3.4 Lgr5^{+} stem cells markers are enhanced by carcinogen exposure

To further elucidate the effects of n-3 PUFA + Cur in the presence of AOM on Lgr5^{+} stem cells, global transcriptional differences in early response genes between sorted GFP^{high} (Lgr5^{+}) and GFP^{neg} (differentiated) cells were assessed by RNA sequencing. Mice were fed with the combination of n-3 PUFA and curcumin or control diet (n-6 PUFA) for 3 wks, injected with AOM and euthanized 12 hr later. Table 4 demonstrates that GFP^{high} cells expressed high levels of Lgr5 and other stem cell markers, e.g., Ascl2 and CD44, whereas GFP^{neg} cells expressed progenitor cell markers, e.g., Reg4 and Muc2 as well as Krt20 and Slc26a3, markers highly expressed at the crypt top (Dalerba et al., 2011) (Table 4). Surprisingly, mRNA levels of crypt base columnar cell (CBC) marker genes (Jiao et al., 2008) were rapidly altered by extrinsic factors (Table 5). For example, CD44 mRNA levels in GFP^{high} cells were increased by 5.41-fold (in n-6 PUFA) and 2.88-fold (in n-3 PUFA + Cur) upon AOM exposure, and the enhancement was significantly higher (1.87-fold) in n-6 PUFA versus n-3 PUFA + Cur fed mice. Interestingly, Agr3 mRNA levels in GFP^{high} cells were increased by 108.51-fold by AOM in n-6 PUFA fed mice as compared to 21.10-fold (FDR<0.1) to the n-3 PUFA + Cur group.

Differentiated cell markers were also modulated by extrinsic factors. Alpi, an absorptive enterocyte marker, was mainly found in GFP^{neg} cells (Table 4) and its levels in GFP^{neg} cells were increased by AOM both in n-6 PUFA (1.87-fold FDR) and n-3 PUFA + Cur (1.85-fold FDR) treated mice (Table 5). In

GFP^{high} cells, Alpi levels were increased by AOM only in n-6 PUFA (2.61-fold) (Table 5). This is interesting because Alpi is expressed at the crypt base where cells dedifferentiate into Lgr5 stem cells following targeted depletion of Lgr5 cells (Tetteh et al., 2016), and contributes to intestinal tumorigenesis initiated by dedifferentiation (Schwitalla et al., 2013a). In addition, Kit/CD117, mainly expressed in goblet cells, was also increased by AOM (1.62-fold) only in GFP^{high} cells in n-6 PUFA fed mice. This finding is consistent with the fact that Kit signaling promotes colonic tumor development (Chen et al., 2015). Finally, the colon cancer stem cell marker, Prom1/CD133 (Sahlberg et al., 2014; Snippert et al., 2009) was uniquely up-regulated by n-6 PUFA and AOM co-treatment (Table 5). Specifically, Prom1/CD133 expression in GFP^{high} cells increased following AOM exposure in n-6 PUFA not in n-3 PUFA + Cur treated mice.

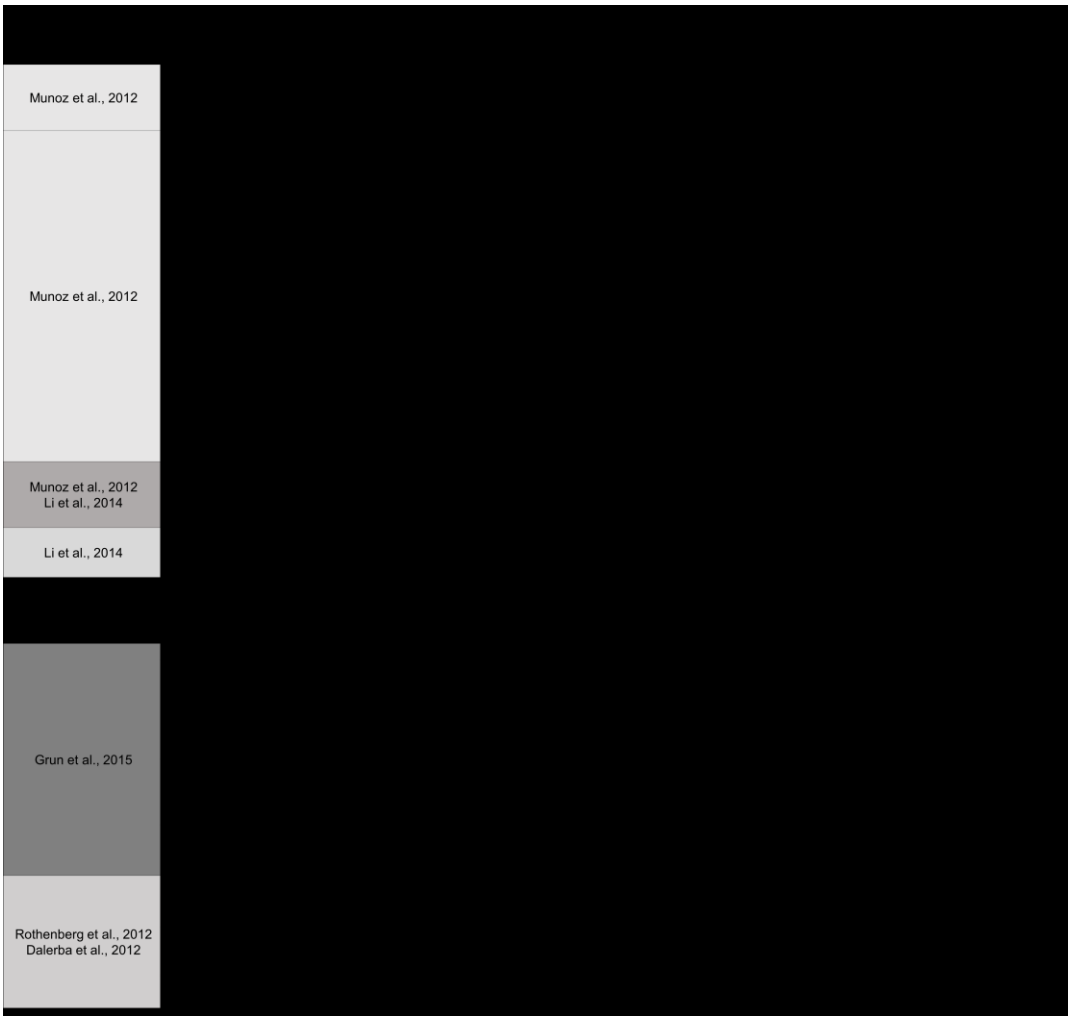

Table 4. Differentially expressed marker genes in GFP^{high} versus GFP^{neg} colonocytes. Fold change of cell type marker gene expression by RNA sequencing of colonic GFP^{high} and GFP^{neg} cells at 12 h post saline exposure, *n*=8 mice per group.

A

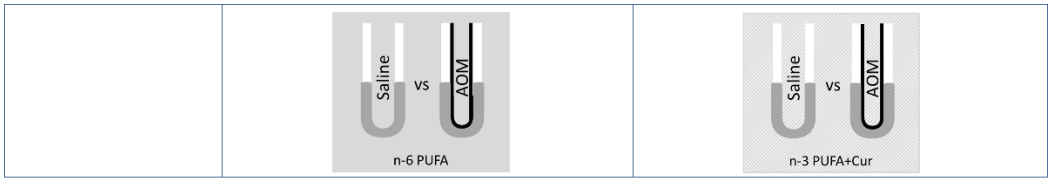

Cell markers	Gene name	Fold change in AOM / saline							
		n6-PUFA				n3-PUFA+Curcumin			
		GFP^{high} (n=4)	FDR	GFP^{neg} (n=4)	FDR	GFP^{high} (n=4)	FDR	GFP^{neg} (n=4)	FDR
Intestinal stem cell signature	Lgr5	1.50	**	1.82	**	1.35	-	0.59	**
	Cd44	5.41	***	2.46	***	2.88	***	1.74	***
	Cdk6	1.62	***	1.16	-	1.30	-	0.95	-
	Msi1	94.92	*	0.66	-	3.74	-	25.97	-
	Agr3	108.51	***	1.45	-	21.10	**	0.79	-
	Slc12a2	1.42	***	0.95	-	0.96	-	0.72	***
Wnt target genes	Axin2	1.46	***	0.94	-	1.05	-	0.91	-
	Sox9	0.88	-	0.85	-	0.75	***	0.93	-
TA cells	Ccnd1	1.36	***	1.13	-	1.33	**	1.41	***
	Cd44	5.41	***	2.46	***	2.88	***	1.74	***
Progenitor cells	Agr2	1.62	***	1.15	-	0.95	-	0.95	-
	Clca3	0.33	***	0.78	-	1.03	-	0.85	-
	Kit	1.37	-	1.00	-	0.86	-	1.02	-
	Muc2	1.93	***	2.30	***	1.38	*	3.50	***
Colorectal cancer cells	Cdx2	2.61	***	1.87	**	1.28	-	1.85	***
	Prom1	1.29	-	2.91	***	0.97	-	1.26	-

B

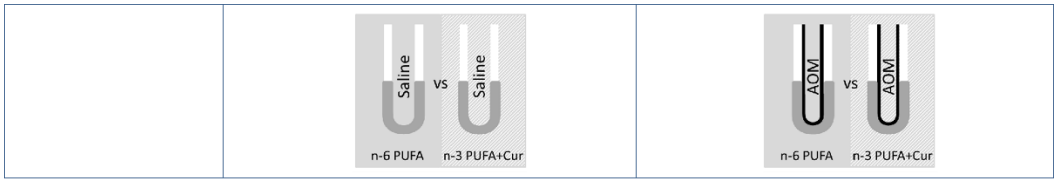

Cell markers	Gene name	Fold change in n-6 PUFA / n-3 PUFA+Curcumin							
		GFP^{high}				GFP^{neg}			
		Saline (n=4)	FDR	AOM (n=4)	FDR	Saline (n=4)	FDR	AOM (n=4)	FDR
Intestinal stem cell signature	Lgr5	0.86	-	0.95	-	0.40	***	1.24	-
	Cd44	1.00	-	1.87	***	1.61	-	2.27	***
	Cdk6	0.88	-	1.10	-	1.02	-	1.26	-
	Msi1	0.11	-	2.79	-	70.46	-	1.79	-
	Agr3	0.24	-	1.26	-	1.09	-	2.02	-
	Slc12a2	0.84	-	1.24	-	0.95	-	1.25	-
Wnt target genes	Axin2	0.57	***	0.79	-	1.09	-	1.14	-
	Sox9	0.86	-	0.99	-	1.10	-	1.01	-
TA cells	Ccnd1	0.99	-	1.02	-	1.25	-	1.00	-
	Cd44	1.00	-	1.87	***	1.61	-	2.27	***
Progenitor cells	Agr2	1.19	-	2.03	***	1.30	-	1.56	**
	Clca3	17.39	***	5.56	***	6.26	***	5.77	***
	Kit	1.05	-	1.68	**	1.36	-	1.33	-
	Muc2	1.75	***	2.45	***	2.53	***	1.66	***
Colorectal cancer cells	Cdx2	0.97	-	1.97	***	1.25	-	1.26	-
	Prom1	1.20	-	1.59	**	0.94	-	2.18	***

Table 5. **Marker genes transcriptionally modulated by extrinsic factors.** Fold change of marker gene expression in colonic GFP^{high} and GFP^{neg} cells in the presence of (**A**) carcinogen (12 hr) and (**B**) bioactive treatments, n=4 mice per group. FDR values <0.05 are given three asterisks (***), FDR values <0.1 are given two asterisks (**), FDR values <0.2 are given one asterisk (*) and any FDR values >0.2 are marked with a dash (-).

3.3.5 Dietary fish oil and curcumin synergistically enhance p53 signaling in stem cells following AOM exposure

RNA Seq was used to identify signaling pathways that were most significantly modulated by extrinsic cues. From a global transcriptome perspective, GFP^{high} stem cells from n-3 PUFA + Cur versus n-6 PUFA (control) fed mice treated with AOM exclusively increased p53, BRCA1, and Polo-like kinase related pathways (z-score>1.96) (Figure 15A). This is relevant because rapid accumulation of p53 is associated with cell death in human colon cancer cells (Paek et al., 2016). A total of twenty-four p53 target genes were increased by extrinsic factors in GFP^{high} and GFP^{neg} cells (Figure 15B). Of the eleven genes uniquely increased by n-3 PUFA + Cur in GFP^{high} cells, Bax was increased 3.53-fold (Figure 15C). This is noteworthy, because human embryonic stem cells have constitutively active Bax at the Golgi, and active Bax translocates from Golgi to mitochondria after DNA damage in a p53-dependent manner, triggering a rapid apoptotic response (Dumitru et al., 2012). To examine whether the increase in mRNA expression was accompanied by enhanced expression at the protein level, we quantified total Bax expression in $Lgr5^{+}$ stem cells and differentiated cells in n-6 PUFA versus n-3 PUFA + Cur

fed mice in the presence of AOM. As shown in Figure 15D, the relative expression of total Bax in GFP^{high}/GFP^{neg} cells was increased 1.3-fold by the administration of n-3 PUFA + Cur at 12 hr post AOM exposure and persisted for up to 24 hr (1.5-fold). In contrast, in n-6 PUFA fed mice, total Bax in GFP^{high}/GFP^{neg} cells was unresponsive at 12 hr, and increased 1.3-fold at 24 hr post AOM injection.

A

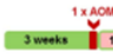

Treatment	AOM			
Bioactive compounds	n-6 PUFA		n-3 PUFA + Curcumin	
Cell type	GFP^{high} cells	GFP^{neg} cells	GFP^{high} cells	GFP^{neg} cells
Canonical pathway	Z-score			
p53 signaling	1	n/a	2.1	0.5
Role of BRCA1 in DNA Damage Response	n/a	n/a	2.3	n/a
Mitotic Roles of Polo-Like Kinase	n/a	n/a	2.6	n/a

B

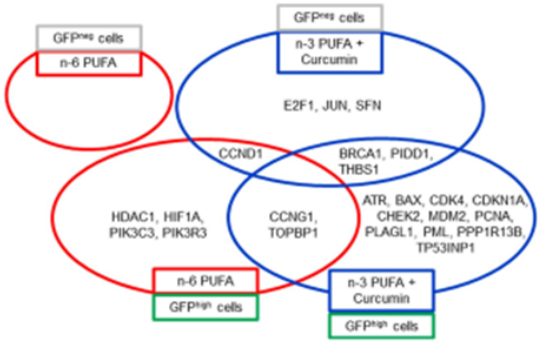

C

Gene name	Description	Fold change in AOM/saline							
		n6-PUFA				n3-PUFA+Curcumin			
		GFP^{high} (n=4)	FDR	GFP^{neg} (n=4)	FDR	GFP^{high} (n=4)	FDR	GFP^{neg} (n=4)	FDR
Trp53	Transformation related protein 53	1.10	-	0.90	-	1.13	-	1.78	-
Atr	Ataxia telangiectasia and Rad3 related	1.04	-	1.05	-	1.90	***	0.89	-
Bax	BCL2-associated X protein	0.88	-	0.59	-	3.53	***	1.38	-
Cdk4	Cyclin-dependent kinase 4	1.39	**	1.02	-	1.52	***	0.98	-
Cdkn1a	Cyclin-dependent kinase inhibitor 1A (P21)	0.64	-	0.82	-	3.16	***	1.77	-
Chek2	Checkpoint kinase 2	0.83	-	1.25	-	2.25	***	0.86	-
Mdm2	Transformed mouse 3T3 cell double minute 2	1.36	-	0.85	-	2.86	***	1.34	-
Pcna	Proliferating cell nuclear antigen	1.38	*	1.14	-	1.79	***	1.09	-
Plagl1	Pleiomorphic adenoma gene-like 1	2.41	-	1.28	-	15.50	***	2.64	-
Pml	Promyelocytic leukemia	0.98	-	1.36	-	1.95	***	1.35	-
Ppp1r13b	Protein phosphatase 1, regulatory (inhibitor) subunit 13B	1.41	*	1.06	-	0.60	***	1.12	-
Trp53inp1	Transformation related protein 53 inducible nuclear protein 1	1.21	-	0.72	-	2.25	***	0.68	-

D

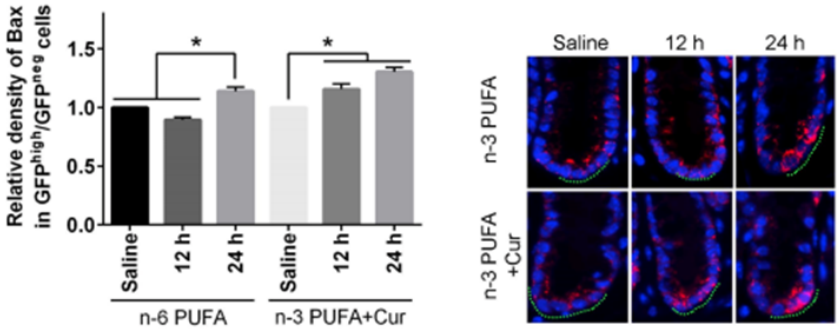

Figure 15. **Lgr5^{+} stem cells exclusively enhance p53 signaling pathway by n-3 PUFA + curcumin in the presence of AOM. (A)** Canonical pathways in cells induced by n-6 PUFA or n-3 PUFA + Cur in the presence of AOM. **(B)** p53-associated genes induced by different groups. **(C)** Genes downstream of p53 in GFP^{high} cells uniquely increased by n-3 PUFA + Cur in the presence of AOM. **(D)** (*left*) Total Bax abundance in cells in n-6 PUFA and n-3 PUFA + Cur. Values were normalized to each respective saline (control) group. * Indicates significant difference between treatment groups ($p<0.05$). (*right*) Representative image of Bax positive (red) cells at 12 hr and 24 hr post AOM exposure. Green dots indicate the location of GFP positive Lgr5 stem cells. Saline injected animals serve as the control.

3.3.6 n-3 PUFA and curcumin combination reduces nuclear β-catenin levels in ACF

Intestinal ACF formation is a surrogate marker of colon cancer both in rodent preclinical models and patients (Hata et al., 2004; Iwamoto et al., 2000). Nuclear to cytoplasmic β-catenin levels are associated with higher mortality in selected groups of colorectal cancer patients (Wanitsuwan et al., 2008) and β-catenin accumulated crypts serve as a premalignant biomarker (Hao et al., 2001; Mi et al., 2009; Mori et al., 2004). As shown in Figure 16A (left), n-3 PUFA ± Cur groups exhibited a significant reduction in the number of ACF per mouse compared to n-6 PUFA and n-3 PUFA + Cur treated mice exhibited a significant reduction (75%) in the incidence of ACF as compared to n-6 PUFA (100% ACF incidence). Figure 16B shows representative images of cross-sectioned ACF (yellow boxes) and Figure 16C shows β-catenin expression (red) in serial cross sections of the same ACF. Subsequently, nuclear to cytosolic β-catenin expression was measured as a biomarker of cancer risk (Figures 16D). β-catenin was predominantly localized to the plasma membrane region of normal colonocytes and negligible nuclear β-catenin was detectable in colonic crypt cells in saline injected animals. In contrast, β-catenin immunoreactivity was present in both the cytoplasm and the nucleus in ACF localized cells as expected (Hao et al., 2001; Mi et al., 2009) (Figure 16C). Surprisingly, only the n-3 PUFA + Cur combination treatment exhibited an inhibitory effect (Figure 16D), i.e., reduced relative density of nuclear/cytosolic β-catenin expression in

ACF (n-3 PUFA x curcumin interaction, $p<0.05$) (Table 3C). These data indicate that n-3 PUFA + Cur synergistically suppressed Wnt signaling in ACF, which may underlie the molecular mechanism of n-3 PUFA and curcumin action in the AOM-induced colon cancer model. Unfortunately, the percentage of GFP^+ Lgr5 cells within the ACF could not be determined due to the mosaic nature of expression in the Lgr5-EGFP-IRES-$CreER^{T2}$ knock-in mouse (Schuijers et al., 2014), i.e., a large fraction of ACF were GFP negative.

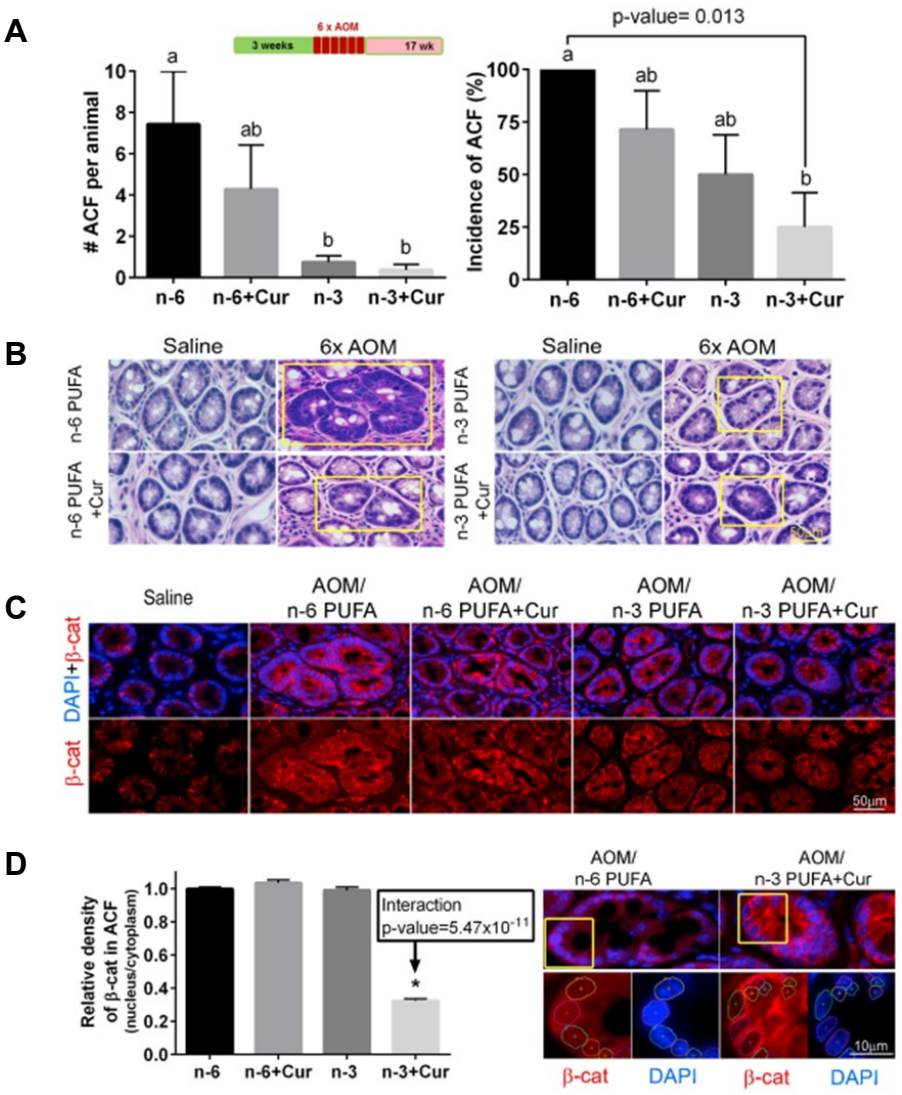

Figure 16. Chemo-protective effect of n-3 PUFA ± curcumin on ACF formation and subcellular localization of β-catenin in ACF. (**A**) (left) Percentage of mice with colonic ACF as affected by diet and (right) the number of ACF per animal (half colon) in the presence of AOM. ACF from n= 7-8 mice were counted 17 wks after 6 AOM injections. Different letters indicate significant ($p<0.05$) differences between treatment groups at each time point. (**B**) H&E stained tissues showing distinct colonic ACF in the center of the image with normal crypts at the periphery in the presence of AOM compared to saline. (**C**) Immunofluorescent images of β-catenin (red) in serially sectioned ACF tissue. Nuclear staining was detected by counterstaining cells with DAPI (blue). (**D**) (left) Quantification of β-catenin expression (staining density) in nucleus/cytoplasm in ACF from mice on the 4 different diets. Values were normalized to the n-6 PUFA (control) group. (right) Representative image of b-catenin (red) translocated into the nucleus in n-6 PUFA vs n-3 PUFA + Cur fed mouse. Magnified image of β-catenin in the nucleus (nuclear DAPI staining is circled). Refer to Figure 1A legend for statistical details. * Indicate significant difference between treatment groups ($p<0.05$). n-6: n-6 PUFA, n-6+Cur: n-6 PUFA + curcumin, n-3: n-3 PUFA, and n-3+Cur: n-3 PUFA + curcumin.

3.4 Discussion

There is an impending chronic disease crisis in our country and it is predicted that if the current trends continue, the number of cancer cases diagnosed annually by 2050 is likely to double as a result of population aging (Vogelstein and Kinzler, 2012). Heading off this escalating burden of age-related illnesses requires an emphasis on primary cancer prevention research and training in cancer-related lifestyle decisions, including diet and exercise (Vogelstein and Kinzler, 2012). Here we describe the effect of beneficial dietary factors on DNA damage-induced responses in $Lgr5^+$ stem cells in the colon. Further justifying our investigation is the fact that these bioactives do not exhibit the side effects such as gastrointestinal bleeding and myocardial complications associated with the administration of anti-cancer drugs (Meyskens et al., 2008; Psaty and Potter, 2006; Solomon et al., 2005; Zell et al., 2009).

DNA damage induced by AOM is directly linked to colon tumorigenesis in the rodent model (Chang et al., 1998). To reduce the risk of tumorigenic transformation of cells, it is critical that DNA damaged cells be deleted (Chang et al., 1998; Rogers and Pegg, 1977) or repaired via MGMT (Zaidi et al., 1995). We have previously demonstrated that colonic $Lgr5^+$ stem cells are highly impacted by AOM exposure, resulting in the promotion of apoptosis and induction of MGMT expression compared to differentiated cells during the first 12-24 hr after AOM exposure (Kim et al., 2016a). In this study, we extend these findings by demonstrating for the first time that n-3 PUFA + Cur combination

maximally promotes targeted apoptosis (Figures 11C) and the induction of MGMT expression in DNA damaged Lgr5$^+$ stem cells (Figure 12B). Consistent with this observation, it has been reported that n-3 PUFA enriched diets enhance targeted apoptosis during colon tumor initiation in part by downregulating Bcl-2 (Hong et al., 2003). In addition, n-3 PUFA may prime colonocytes for damage-induced apoptosis by enhancing the unsaturation of mitochondrial phospholipids, resulting in an increase in oxidative stress and the initiation of the apoptotic cascade (Chapkin et al., 2002; Hong et al., 2002). Curcumin can also induce apoptosis by activating mitochondria-initiated apoptotic pathways (Guo et al., 2013). It has been demonstrated that both n-3 PUFA and curcumin can induce MGMT (Hong et al., 2000; Niture et al., 2007), and MGMT expression is known to be associated with p53 in multiple cell types (Blough et al., 2007; Russell et al., 1995). Interestingly, the combination of DHA and curcumin has an additive effect with regard to the induction of apoptosis in breast cancer and pancreatic cell lines (Altenburg et al., 2011; Swamy et al., 2008). With respect to Lgr5$^+$ stem cell proliferation, only a mild increase was observed at 24 hr post AOM as compared to saline. This finding is consistent with the fact that the crypt must regenerate following the loss of cells in the crypt bottom after carcinogen and radiation exposure (Hong et al., 2015; Hua et al., 2012).

Only mice treated with the combination of n-3 PUFA + Cur exhibited an induction of p53 signaling exclusively in Lgr5$^+$ stem cells in the presence of

AOM. This was exemplified, in part, by the induction of Bax at the mRNA and protein levels, a major mediator of p53-mediated apoptosis. These findings are relevant in view of the fact that human embryonic stem cells (hESCs) have constitutively active Bax at the Golgi and are primed to undergo rapid apoptosis in a p53 dependent manner (Dumitru et al., 2012; Gama and Deshmukh, 2012; Liu et al., 2013) and decreased mitochondrial priming determines chemo-resistance of colon cancer stem cells (Colak et al., 2014). It has also been demonstrated that the absence of an acute apoptotic response to AOM in p53-deficient mice is associated with an increased tumor incidence (Davidson et al., 2015; Hu et al., 2005). Further studies are needed to elucidate the combinatorial effects of diet on the translocation of active Bax from Golgi to mitochondria. Consistent with these observations, curcumin combined with n-3 PUFA synergistically reduced AOM-induced nuclear □-catenin levels in ACF at the pre-tumor stage. This is noteworthy because elevated nuclear □-catenin levels are associated with higher mortality in selected groups of colorectal cancer patients (Hao et al., 2001; Takayama et al., 2001; Wanitsuwan et al., 2008), and various attempts have been made to identify and characterize pharmacological inhibitors of β-catenin (Thakur and Mishra, 2013). Consistent with this notion, it has been shown that n-3 PUFA or curcumin reduce polyps or adenoma in APC mutated mice (Collett et al., 2001; Fini et al., 2010) and inhibit nuclear location of □-catenin in colon cancer cells and breast cancer stem cells (Calviello et al., 2007; Mukherjee et al., 2014).

The potential benefits of using a combination of pleiotropic chemo-protective compounds may also be linked to their combined ability to suppress NFκB activation (Kim et al., 2009), which drives Cox-2 expression (Cai et al., 2011; Charalambous et al., 2003; Cherukuri et al., 2005). In terms of disease progression, Cox-2 is capable of enhancing cell proliferation, angiogenesis, cell migration and invasion as well as inhibiting apoptosis and enhancing tumor growth via cross-talk between Frizzled and the epidermal growth factor receptor (EGFR) (Buchanan et al., 2007). In addition, both DHA and curcumin are capable of modulating plasma membrane structure and EGFR function (Soung and Chung, 2011; Turk et al., 2012), which regulates colon cancer stem cell proliferation (Feng et al., 2012). Curcumin can also inhibit the expression of EGFR in human colon cancer cells (Chen et al., 2006).

In summary, our data broaden and redefine the phenotypic features of the colonic adult stem cell in the presence of external cues. DNA damaged $Lgr5^+$ stem cells uniquely respond to the combination of n-3 PUFA and curcumin, which promote targeted apoptosis in part by enhancing p53 signaling and maximally reducing nuclear β-catenin in ACF. This is a critical area of research because long-lived $Lgr5^+$ stem cells are responsible for maintaining and regenerating intestinal crypts (Kantara et al., 2015). These novel findings demonstrate that $Lgr5^+$ stem cells are uniquely responsive to external dietary cues following the induction of DNA damage during tumor initiation and

progression, providing a therapeutic strategy for eliminating damaged stem cells and reducing colon cancer risk.

4. DOSE EFFECT OF n-3 PUFA AND CURCUMIN ON TARGETED APOPTOSIS

4.1 Introduction

Combination or multicomponent therapy, in which two or more drugs are used together, typically has one or more of the following goals: (i) reduce the frequency at which acquired resistance arises by combining drugs with minimal cross-resistance (ii) lower the dose of drugs with non-overlapping toxicity and similar therapeutic profiles so as to achieve efficacy with fewer side effects; and (iii) achieve enhanced potency by exploiting additivity, or better yet, greater-than-additive effects in the biochemical activities of two drugs (Fitzgerald et al., 2006). There is also a growing interest in drug combinations that might prevent cancer, as summarized in a recent Nature article by Gravitz (Gravitz, 2011). There is also an increasing awareness that the use of synergistic drug combinations in treating cancer can the lower dose of each constituent drug and consequently minimize adverse effects. Thus, to kill cancer cells, combination therapy can be more effective than individual drug use (DeVita et al., 1975).

It has been demonstrated that AOM-induced DNA damaged $Lgr5^{+}$ stem cells, the cells of origin if colon cancer (Barker et al., 2009), are efficiently removed by targeted apoptosis in mice fed a 4% fish oil (1% n-3 PUFA) + 1% curcumin combination diet as compared to fish oil or curcumin alone (Kim et

al., 2016b).

We also demonstrated that curcumin combined with n-3 PUFA synergistically reduces AOM-induced nuclear β-catenin levels in aberrant crypt foci (ACF) (Kim et al., 2016b). In order to determine the clinical relevance of our findings, we extrapolated the animal dose to a human equivalent dose (HED) by applying a conversion based body surface area (BSA) normalization method (Reagan-Shaw et al., 2008). Using this approach, the HED of our experimental diet was 8.6g of n-3 PUFA + 8.5g of curcumin (Figure 17). The FDA has established a generally regarded as safe (GRAS) level of 3g of n-3 PUFA per day. Thus, the HED of the n-3 PUFA (8.6 g) diet used in our mouse study was higher than the FDA recommendation (3g per day). In comparison, curcumin has not yet been approved as a therapeutic agent due to its relatively low bioavailability (Anand et al., 2007).

In this study, we experimentally determined the median effective concentration (ED_{50}) and the HED of n-3 PUFA + curcumin to remove DNA damaged $Lgr5^{+}$ stem cells by targeted apoptosis. We assessed the dietary threshold for phenotypically significant responses by using lower doses of n-3 PUFA and curcumin as described in Figure 17. As part of this effort, we utilized FlowSight image-based flow cytometry. One of the biggest advantages of using the FlowSight system is that sample throughput is increased and potential bias in data analysis can be reduced compared to a traditional fluorescence microscopy.

Our novel data provide evidence that DNA-damaged Lgr5^{+} stem cells are highly responsive to a low dose of the combination curcumin + n-3 PUFA diet. We provide evidence that the low dose combination diet reduces AOM-induced DNA damage in Lgr5^{+} stem cells, implying that a lower HED can utilized in human clinical trials.

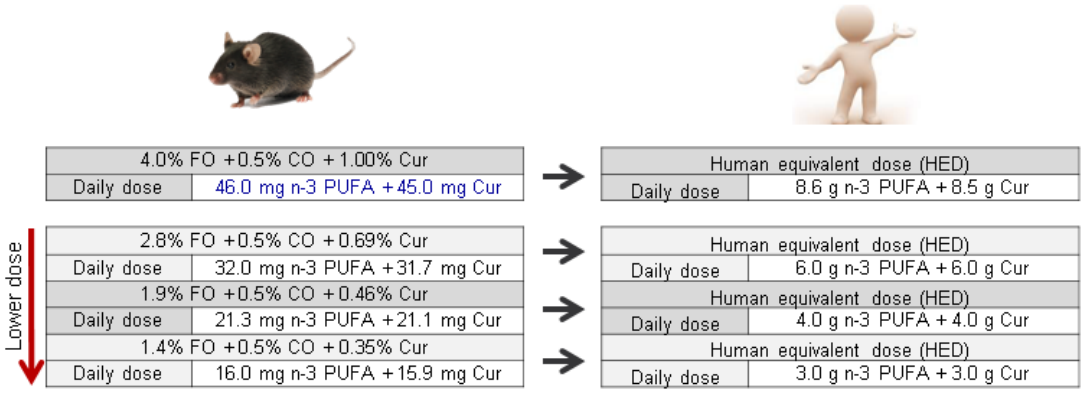

Figure 17. Design of n-3 PUFA and curcumin mouse diets and their human equivalent dose (HED). The animal dose was extrapolated to a HED by applying a conversion based on body surface area (BSA). Lower doses of n-3 PUFA and curcumin in animal diets and corresponding HEDs are listed (marked in red arrow). Daily dose of n-3 PUFA and curcumin from animal diets used in our previous study (Kim et al., 2016b) are marked in blue.

4.2 Material and methods

4.2.1 Animals, diets and study design

The animal use protocol was approved by the University Animal Care Committee of Texas A&M University and conformed to NIH guidelines. Lgr5-EGFP-IRES-CreER^{T2} knock-in mice (Barker et al., 2009), 6-7 wk old, were acclimated for 1 wk and then maintained on a semi-purified diet (Table 6B) for 3 wk prior to injection with AOM (Sigma, St. Louis, MO, 10 mg/kg body weight). Mice (n=7~8 per group) were injected with a single dose of AOM and euthanized 12 hr later. Control mice (n=5) received a single saline injection. Immediately after termination, the distal colon was rapidly removed, flushed with ice-cold saline and a longitudinal section of the distal colon was used for isolating colonocyte. Figure 18A shows the timeline of the treatments and the experimental design. For sample preparation, the profiles of sorted-live GFP^{high} cells and sorted-fixed GFP^{high} cells were assessed. Since fixation was shown to alter the fluorescence signature, to avoid contamination of cell population after PFA fixing step, we initially sorted GFP^{high} and GFP^{neg} live cells using a MoFlow fluorescent cell sorter and then subsequently fixed cells with 4% PFA.

A

Experimental diets			
Chemo-protective diets	Control diets	Ratio of FO : Cur in chemo-protective diets	% total fat in experimental diets
4.0% FO + 0.5% CO + 1.00% Cur	4.5% CO	4 : 1	4.5%
2.8% FO + 0.5% CO + 0.69% Cur	3.3% CO	4 : 1	3.3%
1.9% FO + 0.5% CO + 0.46% Cur	2.4% CO	4 : 1	2.4%
1.4% FO + 0.5% CO + 0.35% Cur	1.9% CO	4 : 1	1.9%

B

Ingredients	Diets (g/100 g)							
	4.5% CO	4.0% FO + 0.5% CO + 1.00% Cur	3.3% CO	2.8% FO + 0.5% CO + 0.69% Cur	2.4% CO	1.9% FO + 0.5% CO + 0.46% Cur	1.9% CO	1.4% FO + 0.5% CO + 0.35% Cur
Sucrose	43	42	44	43	45	44	45	45
Casein	20	20	20	20	20	20	20	20
DL-methionine	0.3	0.3	0.3	0.3	0.3	0.3	0.3	0.3
AIN-76 Mineral mix	3.5	3.5	3.5	3.5	3.5	3.5	3.5	3.5
AIN-76 Vitamin mix	1	1	1	1	1	1	1	1
Choline Chloride	0.2	0.2	0.2	0.2	0.2	0.2	0.2	0.2
Corn Starch	22	22	22	22	22	22	22	22
Cellulose	6	6	6	6	6	6	6	6
Curcumin	0	1	0	1	0	0.46	0	0.35
Fish oil	0	4.0	0	2.8	0	1.9	0	1.4
Corn oil	4.5	0.5	3.3	1	2.4	0.5	1.9	0.5
Total	100	100	100	100	100	100	100	100

Table 6. Dose of n-3 PUFA and curcumin in the experimental mouse diets and their corresponding human equivalent dose (HED). (A) Design of experimental diet and **(B)** diet composition. (FO = fish oil; CO = corn oil; Cur = curcumin)

4.2.2 Diets

Diet sources have been previously reported (Kim et al., 2009). Complete diets containing 1.9~4.5% corn oil (containing n-6 PUFA) were used as a baseline controls, i.e., contained no n-3 PUFA or curcumin. Diets containing 1.4~4.0% (w/w) Menhaden fish oil (containing n-3 PUFA) + 0.23~1% curcumin diets were used to determine the median effective dose (ED_{50}). All fish oil (FO) + curcumin (Cur) diets contained 0.5% corn oil (w/w) to ensure that essential fatty acid requirements were met (Table 6A&B). The four FO + Cur diets listed in Table 6 had different levels of total fat (%), thus the level of total fat (%) in each CO diet was matched to serve as a control. In addition, the ratio of FO :

Cur across all combination (FO + Cur) diets was maintained at a 4 : 1 ratio (Table 6A). Mice were provided with fresh diet every day and the feeders were removed and washed daily. Animals had free access to food and water at all times. The fatty acid composition of the diets was analyzed by gas chromatography and the level of curcumin was quantified by ^{1}H NMR (Jayaprakasha et al., 2013). The fatty acid composition of isolated colonic crypts was quantified by gas chromatography (Fan et al., 2003) and the level of curcumin was quantified by HPLC (Cuomo et al., 2011; Jayaprakasha et al., 2013).

4.2.3 DNA damaged and apoptotic cell staining

To quantify targeted apoptosis in stem cells, isolated colonocytes from the distal colon were sorted based on GFP expression using a Beckman Coulter MoFlo Astrios as previously described (Fan et al., 2014). Dead cells positive for Propidium Iodide (PI, 1μg/mL) staining were excluded from sorting. GFP^{high} cells (stem cells) and GFP^{neg} cells (all cells combined) were sorted and subsequently fixed in 4% PFA for 20 min at room temperature followed by incubation in 100 mM glycine for 30 min to quench paraformaldehyde autofluorescence. After washing with PBS, cells were permeabilized in 70% EtOH for 24 hr at -20◦C followed by rehydration in PBS prior to immunostaining. Fixed and permeabilized cells were subsequently stained with phospho-γH2AX-Alexa Fluor 647 antibody (γH2AX-AF 647, Cell Signaling, 20E3, 1:25

dilution), to detect DNA damaged cells and cleaved caspase3-Alexa Fluor 555 (Cl.caspase-3-AF 555, Cell Signaling, D3E9, 1:50 dilution) antibody to detect apoptotic cells, for 24 hr at 4°C followed by washing with PBS. Stained cells were counterstained with DAPI and quantified by FlowSight imaging flow cytometry.

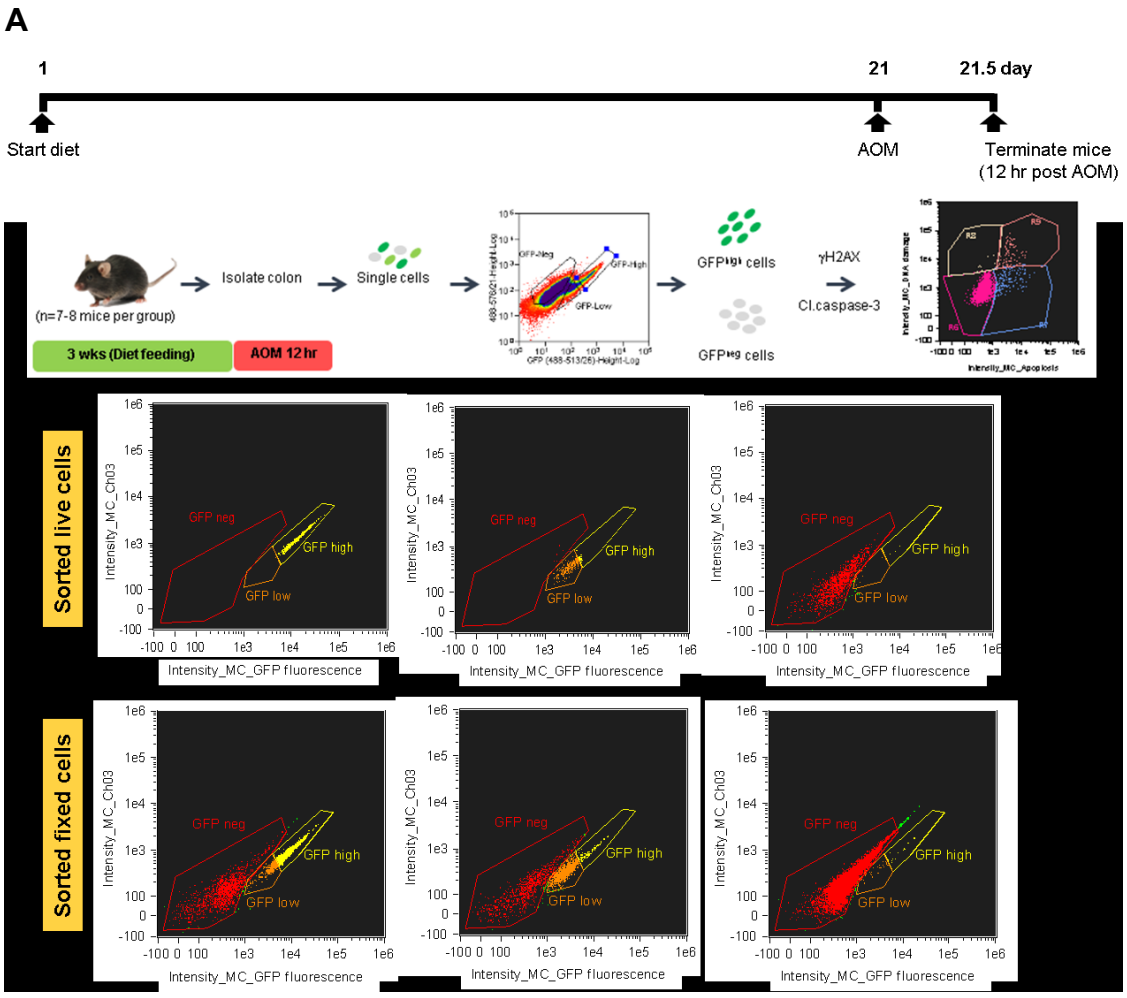

Figure 18. Experimental design and validation. (A) Timeline of the treatments and experimental design. **(B)** Profile of sorted live GFP^{high} cells (left), GFP^{low} cells (middle) and GFP^{neg} cells (right). **(C)** Profile of sorted and fixed GFP^{high} cells (left), GFP^{low} cells (middle) and GFP^{neg} cells (right).

4.2.4 FlowSight

Samples were analyzed with the imaging flowcytometer FlowSight® (Amnis®, EMDMillipore). The 403, 488 and 647 nm lasers were used for excitation. On average, 18,225 events of GFP^{high} cells (Lgr5^{+} stem cells) and

434,301 events of GFP^{neg} cells (all population) per sample were collected. Bright field (430–480 nm), nucleus (405 nm), cleaved caspase-3 (555 nm) and γH2AX (647 nm) channels were used to collect data. Color compensation was not necessary as no overlapping emission spectra were observed. The IDEAS version 6.0 was used for analysis, and image based features and single gating control for each population was achieved.

4.2.5 Statistics

One-way ANOVA followed by Sidak's multiple comparison test adjustment was used to determine the biological effect of FO + Cur dose as compared to each respective CO control diet. The significant comparisons were obtained based on adjusted P-values <0.05.

4.3 Results

4.3.1 Quantification of γH2AX-labeled DNA damaged cells and cleaved caspase-3-labeled apoptotic cells

To elucidate the dose response of colonic $Lgr5^{+}$ stem cells to bioactive compounds in the presence of carcinogen, we utilized mice expressing enhanced green fluorescent protein (EGFP) knocked into the Lgr5 genomic locus (Barker and Clevers, 2007). Mice were fed with different doses of the combination diet (n-3 PUFA and curcumin) described in Table 6 for 3 wks, injected with AOM and euthanized 12 hr later. To examine the response of

Lgr5^{+} stem cells, represented by GFP^{high}, Lgr5^{+} stem cells were sorted based on GFP expression using a Beckman Coulter MoFlo. Bulk (GFP^{neg}) cells were also sorted as a control. Approximately 18,225 GFP^{high} cells (Lgr5^{+} stem cells) and 434,301 GFP^{neg} cells (all cells combined) were sorted for each treated mouse. Isolated GFP^{high} cells and GFP^{neg} cells were subsequently fixed in 4% PFA and analyzed for the purpose of quantifying DNA damage (γH2AX-AF647) and apoptosis (cleaved caspase-3-AF 555, Cl.caspase-3-AF 555) and targeted apoptosis (both γH2AX-AF647 and Cl. caspase-3-AF555) at 12 h post AOM injection. The 4% FO + 1% Cur diet was used to reproduce finding from the previous study and also as a comparison to the lower dose FO + Cur diets.

Using the imaging flowcytometer, focused single cells were identified using gradient root mean square of the bright filed image (Figure 19A) and bright area and aspect ratio (Figure 19B), respectively. Single-labeled samples were prepared and served as serve a positive control for single staining of γH2AX (Figure 20A, *right*) or Cl.caspase-3 (Figure 20B, *right*), respectively. As additional negative antibody controls, samples not incubated with antibodies were used for gating cells negative for γH2AX (Figure 20A, *left*) or Cl.caspase-3 (Figure 20A, *left*). Figure 20C shows representative images of γH2AX^{+} and γH2AX^{-} cells and Figure 20D shows representative images of Cl.caspase-3^{+} and Cl.caspase-3^{-} cells.

The fluorescence intensities of γH2AX-AF 647 and Cl.caspase-3-AF 555, % of DNA damage, apoptosis and targeted apoptosis were determined as

demonstrated in Figure 21A. To provide biological negative controls, colonic cells from saline injected mice (Figure 21B) were used to gate cells negative for γH2AX-AF 647 and Cl.caspase-3-AF 555. Less than 5% of γH2AX$^+$ and/or Cl.caspase-3$^+$ events were detected following the processing of samples. As shown in Figure 21C&D, AOM-induced γH2AX$^+$ and/or Cl.caspase-3$^+$ were detected in both in mice fed FO + Cur and CO diets. Figure 21E shows representative images of cells negative for γH2AX and Cl.caspase-3, as well as cells staining positive for Cl.caspase-3 and/or γH2AX.

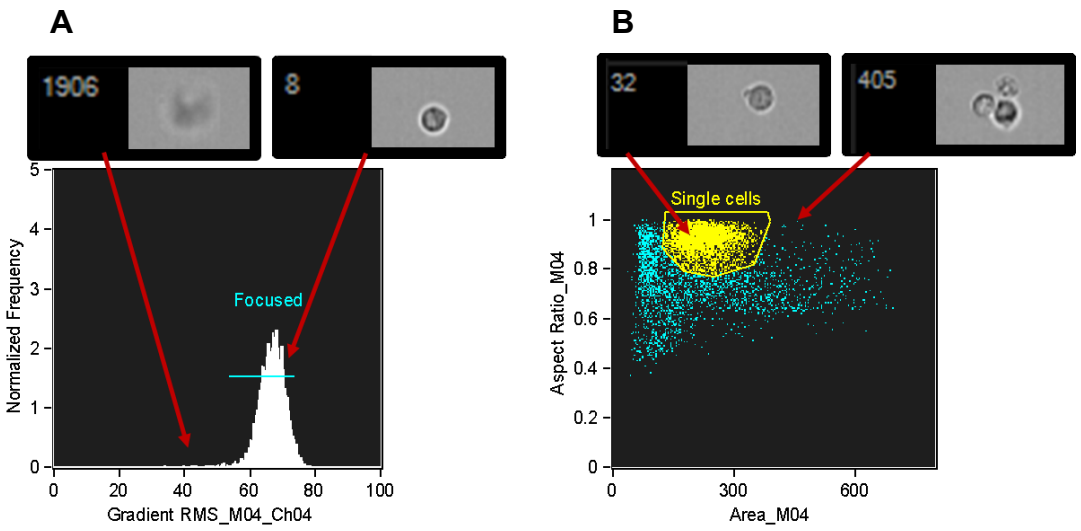

Figure 19. Gating strategy to identifying focused and single cell populations. Fluorescence intensities and image features were analyzed to identify **(A)** focused cells, **(B)** single cells by using a gradient root mean square of the bright field image or bright field area and aspect ratio, respectively.

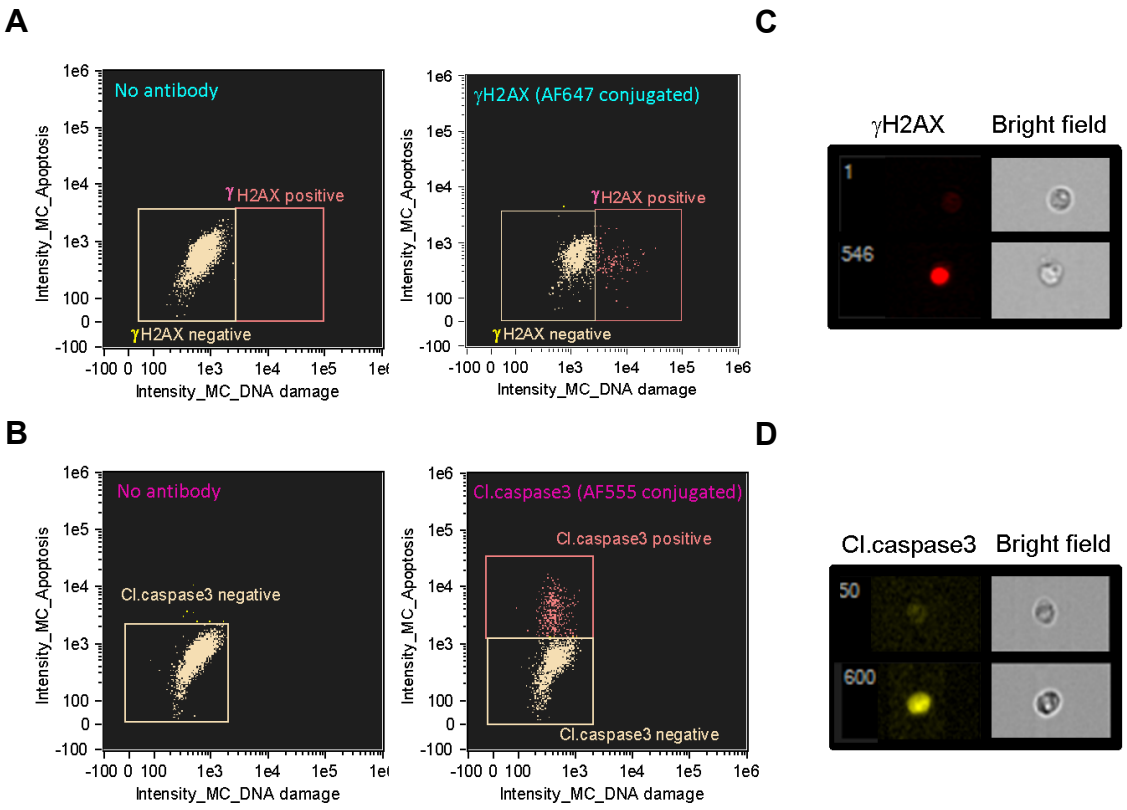

Figure 20. Illustration of cell gating and representative images of DNA damaged and apoptotic cells. The fluorescence intensity of γH2AX-AF647 and Cl.caspase3-AF555 were used to identify **(A**, left**)** γH2AX^{-} and **(A**, right**)** γH2AX^{+} population and **(B**, left**)** Cl.caspase3^{-} and **(B**, right**)** Cl.caspase3^{+} population. Cells from mice injected with AOM (12 hr) were used to detect DNA damage and apoptosis. Cells that are not incubated with antibody were used for gating of γH2AX^{-} population and Cl.caspase3^{-} population. Representative images of **(C)** γH2AX^{+} (#546) and γH2AX^{-} (#1) cells and (D) Cl.caspase3^{+} (#600) and Cl.caspase3^{-} (#50) cells.

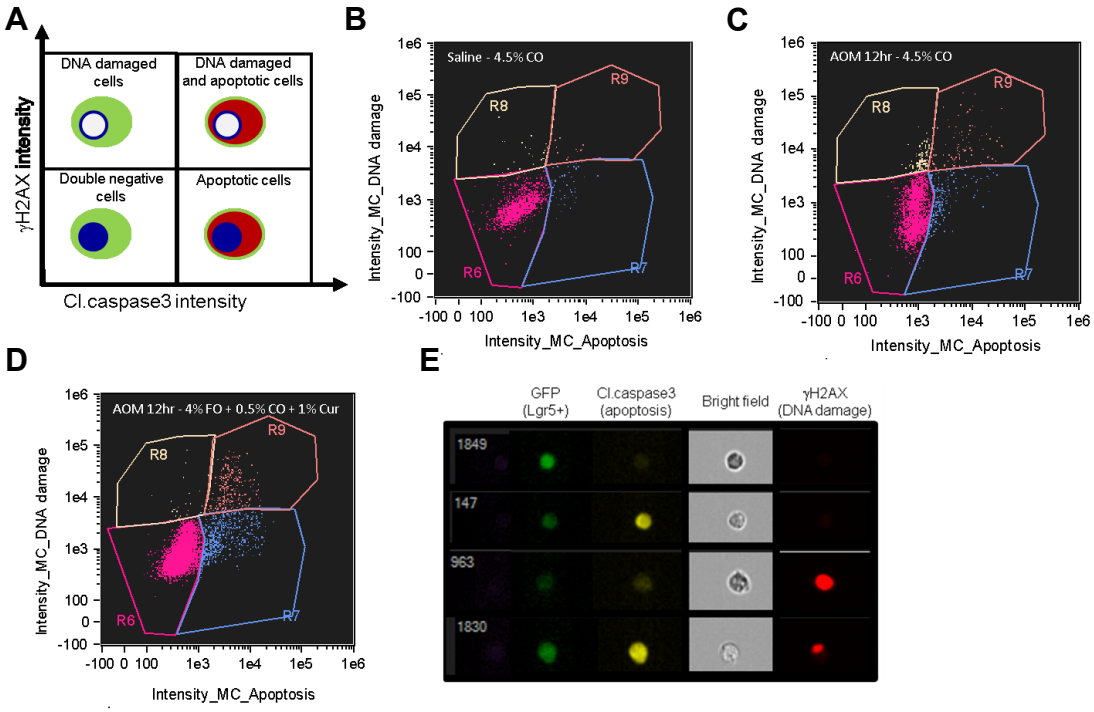

Figure 21. Gating strategy for distinguishing cells double positive (DNA damaged and apoptotic) cells. (A) Schematic illustration showing the gating strategy of the assay. **(B)** Fluorescence intensity of γH2AX-AF647 and Cl.caspase3-AF555 of cells from mice injected with saline (control) used to identify double negative cells. Cells from mice fed 4.5% CO diet, **(C)** and 4% FO + 0.5% CO + 1% Cur diet, **(D)** injected with AOM (12 hr) used to identify DNA damaged (γH2AX^{+}), apoptotic (Cl.caspase3^{+}) and targeted apoptotic (γH2AX^{+}, Cl.caspase3^{+}) cells. **(E)** Representative images of double negative cells (#1849), apoptotic cells (#147), DNA damaged cells (#963) and DNA damaged and apoptotic (#1830) GFP^{high} cells.

4.3.2 Lgr5^{+} stem cells respond to n-3 PUFA and curcumin in a dose-dependent manner in the presence of AOM

In our previous study, we demonstrated that 56%, 18% and 13% of Lgr5^{+} stem cells were DNA damaged, apoptotic and targeted apoptotic cells, respectively in mice fed 5% CO (control) in the presence of AOM, as compared to 22%, 30% and 62% of DNA damaged, apoptotic and targeted apoptotic cells,

respectively, in mice fed 4% FO + 1% CO + 1% Cur in the presence of AOM (Kim et al., 2016b). In comparison, using image-based flow cytometry in this study, 23%, 20% and 35% of $Lgr5^+$ stem cells were DNA damaged, apoptotic and targeted apoptotic cells, respectively, in mice fed 4.5% CO, whereas 5%, 14% and 69% of $Lgr5^+$ stem cells were DNA damaged, apoptotic and targeted apoptotic cells, respectively, in mice fed 4% FO + 0.5% CO + 1% Cur in the presence of AOM (Figure 22). Overall, these cross study trends are consistent and demonstrate that mice fed the chemo-protective diets exhibit lower levels of DNA damaged $Lgr5^+$ stem cells and higher levels of targeted apoptotic $Lgr5^+$ stem cells as compared to control (Figure 22) (Kim et al., 2016b).

Next, we determined the dose effects of n-3 PUFA + curcumin on the % of DNA damaged ($\gamma H2AX^+$), apoptotic (Cl.caspas-3^+) and targeted apoptotic ($\gamma H2AX^+$; Cl.caspas-3^+) in $Lgr5^+$ stem cells (GFP^{high}) in the presence of AOM. As shown in Figure 22A, mice fed 2.8% FO + 0.5% CO + 0.69% Cur and 1.9% FO + 0.5% CO + 0.46% Cur exhibited a marked suppression (5-fold) in DNA damaged ($\gamma H2AX^+$) cells as compared to the control groups. However, no statistically significant chemo-protective effect was detected in mice fed 1.4% FO + 0.5% CO + 0.35% Cur diet as compared to control. In a previous study, the 4% FO + 1% CO + 1% Cur diet increased apoptosis >1.5-fold in $Lgr5^+$ stem cells as compared to control in the presence of AOM (Kim et al., 2016b), however, no statistically significent chemo-protective diet effect was detected in terms of the % of apoptosis (Cl.caspas-3^+) cross all groups as shown in

Figure 22B.

The deletion of damaged Lgr5^{+} stem cells, the cells of origin of colon cancer (Barker et al., 2009), is a critical mechanism to prevent tumorigenesis in the intestine (Leibowitz et al., 2014). We therefore quantified the % of damaged Lgr5^{+} stem cells that are targeted for apoptotic deletion, i.e., γH2AX^{+}, Cl.caspas-3^{+} double-positive cells, as the selective deletion of damaged Lgr5+ stem cells through apoptosis could mitigate the clonal expansion of damaged Lgr5^{+} stem cells. As shown in Figure 22C, mice fed 2.8% FO + 0.5% CO + 0.69% Cur and 1.9% FO + 0.5% CO + 0.46% Cur had markedly increased numbers of targeted apoptotic (γH2AX^{+}, Cl.caspas-3^{+}) Lgr5^{+} stem cells as compared to its control group (2~3-fold). However, no statistically significant chemo-protective effect was detected in mice fed 1.4% FO + 0.5% CO + 0.35% Cur diet as compared to control.

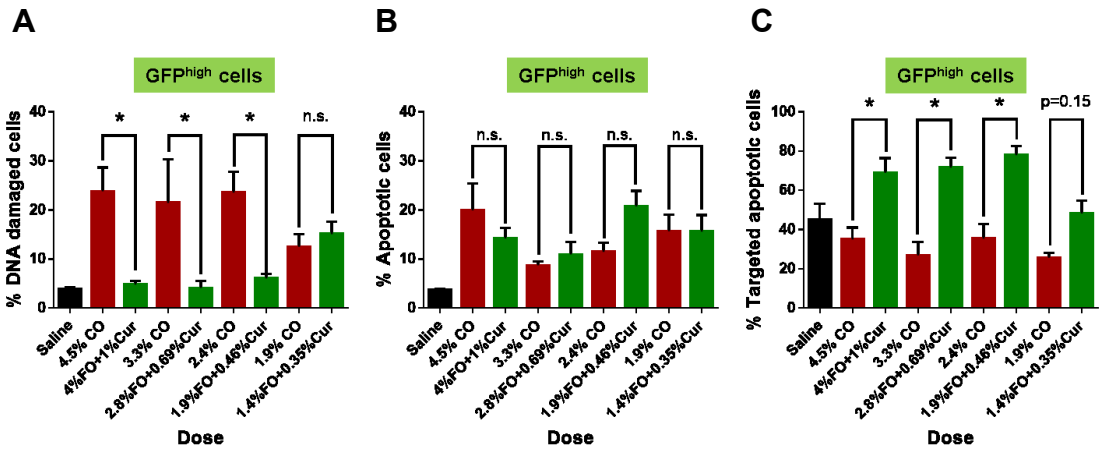

Figure 22. Dose response of GFP^{high} cells to n-3 PUFA + curcumin in the presence of AOM (12 hr). (A) Comparison in % of γH2AX^{+} (DNA damaged) GFP^{high} cells from mice fed varying doses of FO + Cur relative to CO (control) diets. % of DNA damaged cells = # of γH2AX^{+} cells / total # of gated single cells x100. **(B)** Comparison in % of Cl.caspase3^{+} (apoptotic) GFP^{high} cells from mice fed different doses of FO + Cur relative to CO diet. % of apoptotic cells = # of Cl.caspase3^{+} cells / total # of gated single cells x100. **(C)** Comparison in % of γH2AX^{+} Cl.caspase3^{+} (targeted apoptotic, double positive) GFP^{high} cells from mice fed different doses of FO + Cur relative to CO (control) diets. % targeted apoptotic cells = # of double positive cells (γH2AX^{+} Cl.caspase3^{+}) / # of γH2AX^{+} cells x100. GFP^{high} cells were isolated from n=7-8 mice per group and on average 9,000 single cell events per sample were collected. Statistically significant differences between diets were determined using one-way ANOVA followed by Sidak's multiple comparison test adjustment. * Indicates significant difference between treatment groups ($p<0.05$). n.s. indicates not significant.

GFP^{neg} cells represent all populations of colonocytes including Lgr5^{+} stem cells, progenitor cells and differentiated cells due to the mosaic nature of GFP expression in Lgr5-EGFP-IRES-CreER^{T2} knock-in mice (Schuijers et al., 2014). In GFP^{neg} cells, only mice fed the 1.9% FO + 0.5% CO + 0.46% Cur diet had reduced DNA damage as compared to control (Figure 23A) and mice fed 4.5% FO + 0.5% CO + 1% Cur diet exhibited enhanced apoptosis as compared

to control (Figure 23B). However, no other statistically significant chemo-protective effects were detected. This may reflect the dilution of the DNA damaged and apoptotic cell population in crypts, as the majority of AOM induced DNA damaged and apoptotic cells are present in the base of the crypt where $Lgr5^{+}$ stem cells and transit-amplifying (TA) cells reside (Kim et al., 2016a). With respect to the % of targeted apoptotic ($\gamma H2AX^{+}$, Cl.caspas-3^{+}) cells, statistically significent chemo-protective diet effects were detected across all groups compared to control as shown in Figure 23C. These findings indicate that DNA damaged cells (mostly $Lgr5^{+}$ stem cells and transit-amplifying cells) are highly responsive to FO + Cur treatment.

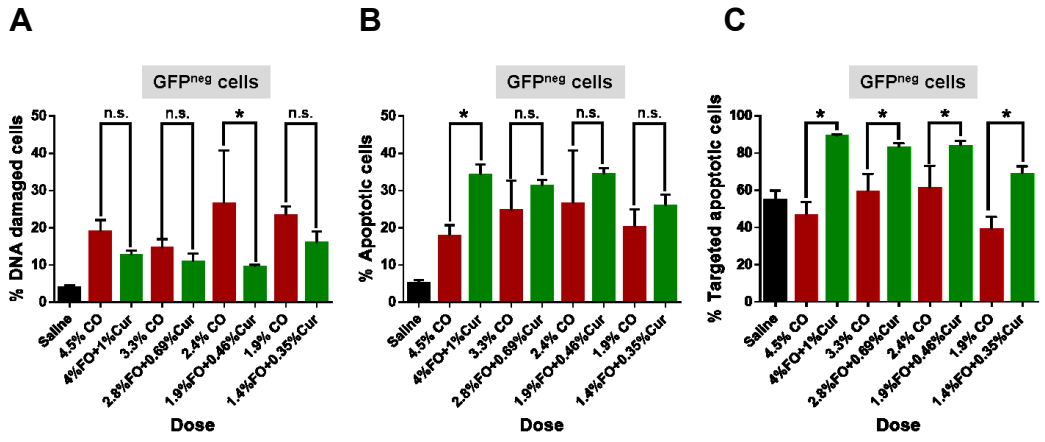

Figure 23. Dose response of GFP^{neg} cells to n-3 PUFA + curcumin in the presence of AOM (12 hr). (A) Comparison in % of γH2AX^{+} (DNA damaged) GFP^{neg} cells from mice fed different doses of FO + Cur relative CO (control) diets. % of DNA damaged cells = # of γH2AX^{+} cells / total # of gated single cells x100. **(B)** Comparison in % of Cl.caspase3^{+} (apoptotic) GFP^{neg} cells from mice fed different doses of FO + Cur relative CO (control) diets. % of apoptotic cells = # of Cl.caspase3^{+} cells / total # of gated single cells x100. **(C)** Comparison in % of γH2AX^{+} Cl.caspase3^{+} (targeted apoptotic, double positive) GFP^{neg} cells from mice fed different doses of FO + Cur relative to CO (control) diets. % of targeted apoptotic cells = # of double positive cells (γH2AX^{+} Cl.caspase3^{+}) / # of γH2AX^{+} cells x100. GFP^{neg} cells were isolated from n=7~8 mice per group and on average 434,301 single cell events per sample were collected. Statistically significant differences between diets were determined using one-way ANOVA followed by Sidak's multiple comparison test adjustment. * Indicates significant difference between treatment groups ($p<0.05$). n.s. indicates not significant.

The median effective dose (ED_{50}), i.e., the dose that produces a chemo-protective effect in 50% of the subjects (Singh et al., 1999) was calculated to be 16 mg of n-3 PUFA and 15.9 mg of curcumin (Figure 24). This corresponds to a daily HED of 3.0 g of n-3 PUFA and 3.0 g of curcumin.

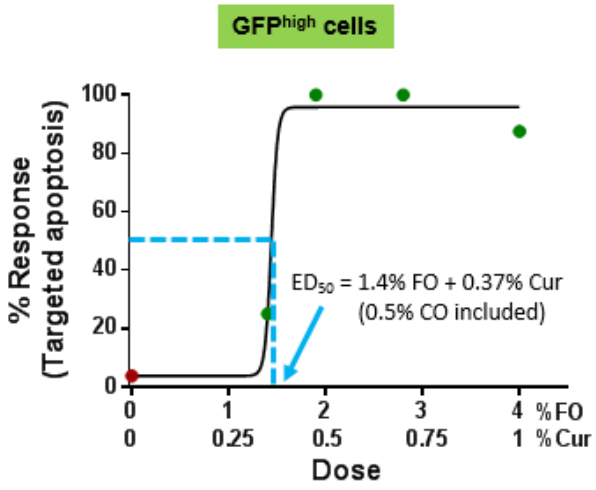

Figure 24. Dose response curves. ED_{50} is indicated in blue arrow.

4.4 Discussion

Drug synergism is of clinical significance when one uses both drugs at lower concentrations to produce better efficacy with lower toxicity than the single drug alone. In our previous mouse study, we demonstrated that AOM-induced DNA damaged $Lgr5^{+}$ stem cells were effectively deleted by targeted apoptosis using a 4% fish oil (1% n-3 PUFA) + 1% curcumin combination diet. This diet also reduced AOM-induced nuclear β-catenin levels in ACF as compared to fish oil or curcumin alone (Kim et al., 2016b). However, the effects of a lower dose of fish oil + curcumin combination diet was not investigated. Therefore, in the present study, we investigated the potential synergistic chemo-protective effects of low dose curcumin and n-3 PUFA combination in the presence of AOM.

The daily dose of the experimental chemo-protective diet (4% fish oil + 1% curcumin) in our previous study (Kim et al., 2016b) was 46 mg of n-3 PUFA and 45 mg of curcumin as described in Figure 17. Therefore, we compared several doses (32 mg n-3 PUFA + 31.7 mg Cur, 21.3 mg n-3 PUFA + 21.1 mg Cur and 16.0 mg n-3 PUFA + 15.9 mg Cur), with an HED of 6.0 g n-3 PUFA + 6.0 g Cur, 4.0 g n-3 PUFA + 4.0 g Cur and 3.0 g n-3 PUFA + 3.0 g Cur, respectively (Figure 17).

Analysis of the impact of the allometric exponent on the conversion of an animal dose to human equivalent dose (HED) utilizes BSA for dose calculations (Reagan-Shaw et al., 2008). The Food and Drug Administration has suggested that the extrapolation of animal dose to human dose is correctly performed only through normalization to body surface area (BSA), which often is represented in mg/ m^2 (Reagan-Shaw et al., 2008). Accordingly, the approach of converting animal doses to an HED based on BSA is standard for estimating starting doses for initial studies in health volunteers. Thus, we extrapolated n-3 PUFA and curcumin dosages in the mouse diet to HED based on BSA (Reagan-Shaw et al., 2008) as shown in Figure 17. In this study, we demonstrated that a significant enhancement in the % of targeted apoptotic $Lgr5^{+}$ stem cells (GFP^{high}) is still observed at a dose of 21.3 mg n-3 PUFA + 21.1 mg Cur (Figure 22), corresponding to an HED of 4.0 g n-3 PUFA + 4.0 g Cur. This is noteworthy, because in human subjects, treatment with 2 g of EPA for 6 months was associated with a 22% reduction in polyp number (West et

al., 2010) and a 40% reduction in ACF number following treatment with a 4 g dose of curcumin (Carroll et al., 2011). In addition, 2.5 g of n-3 PUFA (1.4 g EPA + 1.1 g DHA) significantly reduced proliferative indices in patients with colonic polyps (Anti et al., 1994). With regard to curcumin dose, numerous studies have been conducted to address the pharmacokinetics, safety, and efficacy of curcumin in human subjects. According to the search results on ClinicalTrials.gov, a number of clinical trials utilizing curcumin are underway or have been completed (Li and Zhang, 2014). Curcumin C3 Complex (Sabinsa Corporation, NJ, USA) is known to be well tolerated when taken at high doses (12 g/day) (Cheng et al., 2001; Ireson et al., 2002).

As shown in Figure 22C, 1.9% FO + 0.5% CO + 0.46% Cur diet is the lowest dose that exhibits chemo-protective effects in terms of promoting targeted apoptosis in $Lgr5^{+}$ stem cell. This corresponds to a dose of 21.3 mg n-3 PUFA in combination with 21.1 mg Cur /day or an HED equal to 4.0 g of n-3 PUFA and 4.0 g of curcumin (Figure 17). In summary, the present study provides strong evidence for translating the observed synergistic chemo-protective effects to human trials utilizing a daily dose equivalent to 4.0 g n-3 PUFA + 4.0 g Cur. Although the results from this study are encouraging, the efficacy of n-3 PUFA and curcumin in preventing colon cancer must still be evaluated in prospective controlled trials using ACF or adenoma recurrence as the intermediated end point.

In summary, our data broaden and redefine the physiological dose of n-3 PUFA and curcumin by using mice fed relatively low dose n-3 PUFA and curcumin diets. A daily dose of 21.3 mg of n-3 PUFA in combination with 21.1 mg of curcumin promotes targeted apoptosis in DNA damaged $Lgr5^{+}$ stem cells. This corresponds to a HED of 4.0 g n-3 PUFA + 4.0 g Cur per day and a human ED_{50} equivalent to 3.0 g n-3 PUFA + 3.0 g Cur. These novel findings (i) demonstrate that $Lgr5^{+}$ stem cells are very responsive to low dose dietary cues following the induction of DNA damage, and (ii) provide a therapeutic strategy for eliminating damaged stem cells and reducing colon cancer risk in humans.

5. CHOLESTETOL HOMEOSTASIS IN TUMORIGENESIS

5.1 Introduction

It has been demonstrated that free cholesterol and esterified cholesterol are 1.5~2 fold higher in tumor tissue as compared to uninvolved (normal) tissue in human colon cancer patients (Dessi et al., 1994). Mounting evidence indicates that statins, i.e., cholesterol synthesis inhibitors which selectively target 3-hydroxy-3-methylglutaryl coenzyme A reductase (HMGCR), significantly reduce risk and mortality in colorectal cancer (Cardwell et al., 2014; Lakha et al., 2012; Poynter et al., 2005). In addition, epidemiologic studies suggest that statins may prevent certain malignancies (Hindler et al., 2006), including melanoma (Downs et al., 1998), breast (Boudreau et al., 2004; Cauley et al., 2003) and prostate cancer (Shannon et al., 2005).

Cholesterol serves a structural roles in cell membranes where it forms lipid rafts (liquid ordered domains) (Bloch, 1983). As an important membrane component, cholesterol helps to generate a semipermeable barrier between cellular compartments and to regulate membrane fluidity. Cholesterol also modulates the functions of membrane proteins and participates in several membrane trafficking and transmembrane signaling processes, as exemplified by G protein-coupled receptor signaling (Cherezov et al., 2007; Simons and Vaz, 2004).

Approximately, 90% of free cholesterol is estimated to reside in the plasma membrane (Kim et al., 1991; Lange et al., 1989; Ueland et al., 1986) and membrane cholesterol levels are positively correlated with membrane order (decreased membrane fluidity) (Montero et al., 2008). Highly ordered lipid rafts are increased in many types of cancer (Li et al., 2006b; Patra, 2008) and some drug resistant cancers (Yi et al., 2013). Numerous studies indicate that elevated mitochondrial cholesterol is associated with cancer cell (Montero et al., 2008), can promote increased death resistance and thus malignant cell transformation (Smith and Land, 2012), as well as contribute to chemotherapy resistance (Montero et al., 2008). In addition, there is evidence suggesting that disruption of lipid rafts in cancer can lead to increased responsiveness to anti-cancer therapies (Irwin et al., 2011). For this reason, there is considerable interest in identifying alternative strategies for lowering cholesterol. We have recently demonstrated that n-3 PUFA and curcumin reduce nuclear/cytoplasmic β-catenin in aberrant crypt foci (ACF) (Kim et al., 2016b), and both DHA and curcumin are capable of modulating plasma membrane structure and EGFR function (Soung and Chung, 2011; Turk et al., 2012), which regulates colon cancer stem cell proliferation (Feng et al., 2012). With respect to its membrane targeting properties, curcumin associates with the head group region of the phospholipid bilayer (Barry et al., 2009; Hung et al., 2008), whereas n-3 PUFA interact with the tail group region within rafts (Shaikh et al., 2004; Shaikh et al., 2015; Shaikh et al., 2009a).

Approximately, 80% of human colon cancers have biallelic Apc mutations (Kinzler and Vogelstein, 1996; Sparks et al., 1998), often with complete lack of expression from one allele along with expression of a truncated from the other. In addition, approximately 40% of colon cancers express a mutated form of Kras (Amado et al., 2008; Di Fiore et al., 2007; Kim et al., 2016c). In cell lines, Apc knock-out increases genes involved in the *de novo* synthesis of cholesterol (Dow et al., 2015; Halvey et al., 2012). The intracellular accumulation of cholesterol promotes increased deposition of free cholesterol in the plasma membrane (Kellner-Weibel et al., 1999; Tulenko et al., 1998). However, the link between colon cancer (aberrant Wnt signaling) and membrane biology has not been investigated to date.

We hypothesized that oncogenic Apc and Kras alter plasma membrane order in part by perturbing cholesterol homeostasis. In order to determine the effect of oncogenic Apc and Kras on plasma membrane order, we used tamoxifen (TAM)-regulated Cre transgenic mice, e.g., CDX2P-CreER^{T2}-Apc$^{580S/+}$; Kras$^{LSL\text{-}G12D/+}$ mice, which express Cre in epithelial cells in terminal ileum, cecum, colon and rectum. In this study, we have delineated a mechanism by which oncogenic Apc and Kras modulates plasma membrane order. We also assessed the ability of dietary effect (n-3 PUFA and curcumin) to modulate cholesterol levels and plasma membrane order.

Our novel data provide evidence that oncogenic Apc and Kras directly modulate membrane cholesterol homeostasis, thereby perturbing plasma

membrane order which is positively modulates cell proliferation in our mouse model. Also, we provide evidence that select chemo-protective dietary bioactive compounds (n-3 PUFA and curcumin) can reverse the membrane modifying effects of cancer causing genes.

5.2 Material and methods

5.2.1 Animals

$Kras^{LSL\text{-}G12D/+}$ mice have been described previously (Jackson et al., 2001). To study effects of inactive Apc (Apc $^{580D/+}$) and Kras activation ($Kras^{G12D/+}$) in the large intestine, we crossed $Kras^{LSL\text{-}G12D/+}$ mice with CDX2P-$CreER^{T2}$-Apc $^{580S/+}$ (Shibata et al., 1997) transgenic mice to generate CDX2P-$CreER^{T2}$- Apc $^{580S/+}$; $Kras^{LSL\text{-}G12D/+}$ mice. To study the effects of inactive Apc (Apc $^{580D/+}$) and Kras activation ($Kras^{G12D/+}$) in $Lgr5^{+}$ stem cells, we crossed CDX2P-$CreER^{T2}$-Apc $^{580S/+}$; $Kras^{LSL\text{-}G12D/+}$ mice and Lgr5-EGFP-IRES-$CreER^{T2}$ mice (Barker et al., 2007) to generate Lgr5-EGFP-IRES-CDX2P-$CreER^{T2}$-$Apc^{580S/+}$; $Kras^{LSL\text{-}G12D/+}$ mice. The resultant mice were injected intraperitoneally three times (daily) with tamoxifen (100 mg/kg weight; Sigma-Aldrich, St. Louis, MO) dissolved in corn oil.

5.2.2 Diets

Mice were provided with a Teklad 4% fat rodent diet (Envigo, 7001) to see assess the effect of inactive Apc and oncogenic Kras on cholesterol

homeostasis. In addition, the chemo-protective effect of n-3 PUFA and curcumin, 4% fish oil + 1% curcumin (n-3 PUFA + Cur) diet was examined. Dietary details have been previously reported (Kim et al., 2016b). A complete diet containing 5% corn oil (containing n-6 PUFA) was used as a baseline control, i.e., contained no n-3 PUFA or curcumin. A diet containing 4% (w/w) Menhaden fish oil (enriched in n-3 PUFA) + curcumin diet was used to determine the chemo-protective effects of these dietary bioactives. n-3 PUFA + Cur diet contained 1% corn oil (w/w) to ensure that essential fatty acid requirements were met. Mice were provided with fresh diet every day and the feeders were removed and washed daily. Animals had free access to food and water at all times and 24 hr food intake was measured after 1 week of receiving the diets. The fatty acid composition of the diets was analyzed by gas chromatography and the level of curcumin was quantified by ^{1}H NMR (Jayaprakasha et al., 2013). The fatty acid composition of the crypt was quantified by gas chromatography (Fan et al., 2003) and the level of curcumin was quantified by HPLC (Cuomo et al., 2011; Jayaprakasha et al., 2013).

5.2.3 Total RNA isolation and PCR

DNA from isolated crypts was extracted using RNA miniprep kit (Zymo Research, R1054) following the manufacturer's protocol. Analysis for APC alleles (Apc^{WT}, Apc^{580D}, Apc^{580S}) and KRAS alleles ($Kras^{WT}$, $Kras^{LSL\text{-}G12D}$, $Kras^{G12D}$) were performed by multiplex PCR using primers as described in

Figure 26. Annealing sites for PCR primers used for the detection of each allele are indicated in Figure 26.

5.2.4 RNA sequencing

Total RNA from isolated crypts was isolated using the RNA miniprep kit (Zymo Research, R1054) following the manufacturer's protocol. RNA quantity and quality were measured by nanodrop and Agilent 2100 Bioanalyzers (Agilent Technologies, CA), respectively. Isolated total RNA (250 ng) from each sample was subsequently prepared for sequencing using the TruSeq RNA Library Preparation Kit v2 (RS-122-2002, Illumina). Samples were sequenced for 50 cycles with single index reads on the HiSeq 2500 Sequencing system (Illumina). Following the removal of all genes with CPM (counts-per-million reads) values less than 1, publicly available R software, EdgeR, was used to identify differentially expressed genes.

5.2.5 Ingenuity pathway analysis (IPA)

Genes differentially expressed (FDR < 0.05) were included in pathway and function analyses (Shah et al., 2011; Triff et al., 2013) using Ingenuity software (IPA; Ingenuity® Systems, http://www.ingenuity.com). Statistical significance of the association between each data set and the canonical pathway was determined based on two parameters: (1) ratio of the number of genes from the data set that map to the pathway divided by the total number of

genes that map to the canonical pathway, and (2) p-values calculated using Fischer's exact test determining the probability that the association between the genes in the data set and the canonical pathway is due to chance alone. The upstream regulator analysis function of IPA was subsequently used to identify potential transcriptional regulators that could explain the observed changes in gene expression. The activation z-score was calculated to predict activation or inhibition of transcriptional regulators based on published findings accessible through the Ingenuity knowledge base. Regulators with a z-score greater than 1.96 or less than -1.96 were considered to be significantly activated or inhibited. Functions and pathways with P-value < 0.05 (Fischer's exact test) were considered to be statistically significant.

5.2.6 Fractionation and Western Blot (WB)

Isolated crypts from colon samples were harvested and washed with PBS. The nuclear and cytoplasmic fractions were extracted using NE-PER Nuclear and Cytoplasmic Extraction Reagents (78833, ThermoFisher Scientific, USA) according to the manufacturer's manual. Total lysates were prepared using Pierce RIPA buffer (89901, ThermoFisher Scientific) according to manufacturer's protocol. Samples were quantified by Bradford analysis and measured at 595 nm with a microplate reader. Normalized amounts of the samples were denatured in SDS sample buffer for 10 min at 95°C before being separated by SDS-PAGE and blotted onto polyvinylidene (PVDF) membranes

(Millipore, IPVH00010). Membranes were blocked with 5% non-fat dry milk-TBS at room temperature for 30 min followed by incubation with β-catenin antibody (BD, 610154) at 4° C for overnight. β-actin (AbCam, Ab8227) antibody was used to generate loading controls. After being washed with 0.1% Tris-buffered saline and Tween 20 (TBST), membranes were incubated with horseradish peroxidase labeled Goat anti-rabbit conjugated (HRP) IgG (H+L) (SeraCare, 074-1516) or horseradish peroxidase labeled Goat anti-mouse conjugated (HRP) IgG (H+L) (SeraCare, 074-1806). SuperSignalWestFemtoTrial kit (ThermoFisher, 34094)) was used to detect chemiluminescence, and blots were imaged using a ChemiDoc MP Imaging system (Bio-Rad, USA).

5.2.7 Single cell sorting-ACKG

Lgr5-EGFP-IRES-CreER^{T2}-CDX2P-CreER^{T2} (CG, n=3) and Lgr5-EGFP- IRES-CreER^{T2}-CDX2P-CreER^{T2}- Apc $^{580S/+}$; Kras$^{LSL-G12D/+}$ mice (ACKG, n=3) mice were terminated at 8 wks after 3 daily Tamoxifen (TAM, 100 mg/kg body weight) injections. CG mice were used as a control for the ACKG mice. To examine effects of inactive Apc (Apc$^{580D/+}$) and mutant Kras activation (Kras$^{G12D/+}$) in Lgr5^{+} stem cells compared to all cells, isolated colonocytes from the colon were sorted based on GFP expression using a Beckman Coulter MoFlo Astrios as previously described (Fan et al., 2014). GFP^{high} cells (Lgr5^{+}

stem cells) and GFP^{neg} cells (all cells combined) were sorted for each mouse and used for measuring plasma membrane order and levels of cholesterol.

5.2.8 Membrane order

Live isolated single cells or sorted GFP^{high} cells ($Lgr5^{+}$ stem cells) and GFP^{neg} cells were used for quantifying plasma membrane order. The stock solution of di-4-ANEPPDHQ (ThermoFisher, D36802, 5 μM in DMSO) was stored in a 200 μL aliquots wrapped in aluminum foil at -20° C. Di-4-ANEPPDHQ was mixed with cells (at a final concentration of 1 μM) immediately before imaging to avoid internalization of dye. Cells were transferred onto Cell Imaging Coverglass (8 chamber) slides (Eppendorf, 0030742036) for microscopic analysis using a laser confocal microscope (Leica DMi8 S Platform EII). A 40× oil immersion objective (NA = 1.15) was used with an excitation of 488 nm, and detection ranges for the two channels were set to 500–580 nm and 620–750 nm. Identical microscope settings were maintained for quantitative imaging of membrane components, including the laser power, PMT voltage, and the offset values. After the confocal imaging process, general polarization (GP)-images were generated as previously described (Owen et al., 2011). The image J macro provided by Owen et al. was downloaded and applied.

5.2.9 Filipin III

Isolated single cells or sorted GFP^{high} cells ($Lgr5^{+}$ stem cells) and GFP^{neg} cells were fixed in 1.5% paraformaldehyde for 20 min at room temperature. Cells are rinsed with PBS followed by incubation with Filipin III (Sigma, F4767) at a final concentration of 50 μg/mL for 45 min at room temperature. Cells were washed with PBS and images were captured using an inverted TE 300 Nikon Eclipse fluorescence microscope equipped with 40X/1.30 Nikon Plan Fluor oil immersion objective, a Photometrics Cool Snap EZ digital CCD camera and a SOLA external light source. Images were acquired using a 405 nm laser with 10 ms exposure time to avoid photobleaching. Images were subsequently processed using NIS Image software, version 3.2 (Nikon).

5.2.10 Organoid cultures

Lgr5-EGFP-$CreER^{T2}$ mice were used to isolate a cell population expressing GFP^{high}. Sorted GFP^{high} single cells were embedded in Matrigel on ice and seeded in 12-well plates (200 cells/30 μL of Matrigel per well). The Matrigel was polymerized for 10 min at 37°C, and 500 μL /well basal medium was overlaid for each well. Basal medium contained advanced Dulbecco's modified Eagle medium/F12 supplemented (Gibco, 12634-010) with PenStrep (P/S) (Gibco, 15140-122), 10 mM HEPES (Gibco, H0887), Glutamax glutamax (Gibco, 35050-061), 50 ng/mL murine EGF (LifeTech, PMG8041), 0.2 μM LDN (Noggin replacement) Cellagen Tech, 0.5 μg/mL R-Spondin (Peprotech, 315-

32), 1× N2 (LifeTech, 17502-048), 1× B27 (LifeTech, 12587-010), 1 μM N-acetylcysteine (Sigma, A9165), 30 ng/mL Wnt (TimeBioscience, rmW3aL-002). Media was changed every 48 hr and organoids were passage every 5 days.

5.2.11 Cholesterol loading

Exogenous cholesterol was delivered to cells as a Chol: methyl-β-cyclodextrin (MβCD) complex purchased from Sigma as "water-soluble cholesterol" (Sigma, C4951) containing 40 mg of cholesterol/g solid. All treatment concentrations involving Chol: MβCD were based on cholesterol mass. For this purpose, cholesterol was mixed in a Chol: MβCD molar ratio of 1:7.4, and solubility was increased by adding 351 mg of extra uncomplexed MβCD to produce a molar ratio of 1:10 (Zidovetzki and Levitan, 2007). Cells incubated with media for 24, 48 and 72 hr with 250 μM MβCD (Sigma, C4555) treatment served as control experiments.

5.2.12 Proliferation assay using organoids

To determine whether cholesterol enhanced cell proliferation, organoids were incubated with Chol: MβCD (12.5~100 μM) in organoid complete media for 24, 48 and 72 hr. Media was changed every 24 hr to prevent cholesterol oxidization. To test for proliferation, 10 μM EdU were incubated for 1.5 hr before harvest organoids and the assay was done using the Click-iT Plus EdU Alexa Fluor 647 Imaging kit (Life Technologies, C10640) according to manufacturer's

protocol. Cells incubated with media for 24, 48 and 72 hr with MβCD (125~1000 μM) and cells with no treatment served as control experiments. To quantify EdU^+ cells, imaging is achieved with the imaging flowcytometer FlowSight® (Amnis®, EMDMillipore). Bright field (595-642 nm) and EdU AF647 (632-740 nm) channels were used to collect data. Cells not incubated with AF647 was used for gating EdU negative cells. To quantify EdU^+ cells IDEAS version 6.0 was used.

5.2.13 Cell proliferation assay

Young adult mouse colonic epithelium (YAMC) cells and Immortomouse/Min colon epithelial (IMCE) cells were treated with cholesterol and MβCD for 24, 48 and 72 hr. Rates of cell proliferation were assessed using the CellTiter Blue Cell Viability Assay kit (Promega, G8080), a fluorescent method that is based on the ability of living cells to convert a redox dye (resazurin) into a fluorescent end product (resorufin). Briefly, cells were seeded into 24-well cell-culture plates (3×10^4 per well) and at 0, 24, 48 and 72 hr and cell proliferation was determined.

5.2.14 Measurement of plasma membrane order and cholesterol levels using imaging flow cytometry.

YAMC cells and IMCE cells were seeded into 6-well cell-culture plates (5×10^4 per well) and treated with cholesterol and MβCD for 0, 24, 48 and 72 hr.

Cells were harvested at 0, 24, 48 and 72 hr and harvested cells were used to measure plasma membrane order and cholesterol levels. Analyses were performed using an imaging FlowSight® flowcytometer (Amnis®, EMDMillipore) immediately after adding Di-4-ANEPPDHQ (at a final concentration of 1 μM) to live single cells. A 488 nm laser was used for excitation. Bright field (430-480 nm), ordered (505-560 nm) and disordered (642-740 nm) channels were used to collect data. After collecting images, GP-values were generated (Owen et al., 2011) using IDEAS version 6.0.

Imaging flowcytometry was also used to measure cholesterol levels in the plasma membrane. For this purpose, harvested single cells were fixed in 1.5% PFA for 30 minutes at 4°C, followed by labeling with Filipin III (50 μg/mL) for 45 minutes at room temperature in the dark and washing with PBS. A 403 nm laser was used for excitation. Bright field (560-595 nm) and Filipin III (430-505 nm) channels were used to collect data. Filipin III intensity from the plasma membrane was quantified using the IDEAS feature analysis software. Masks were drawn around each cell to identify the plasma membrane (whole cell – cytoplasm).

5.3 Results

5.3.1 Validation of CDX2P-CreER^{T2}-Apc$^{580D/+}$; Kras$^{LSL-G12D/+}$ mouse model

Tamoxifen (TAM)-regulated inducible CDX2P-CreER^{T2}-Apc$^{580S/+}$; Kras$^{LSL-G12D/+}$ (referred to as ACK) were utilized to express Cre in epithelial cells

in terminal ileum, cecum, colon and rectum. Following TAM injection, Cre expression induced deletion of exon 14 from the Apc^{580S} transcripts, resulting in a frame-shift mutation, Apc^{580D}. Concurrently, Cre-mediated recombination removed transcriptional stop elements and activated a latent oncogenic $Kras^{LSL\text{-}G12D/+}$ allele resulting in the expression $Kras^{LSL\text{-}G12D/+}$ under control of its endogenous regulatory promoter. CDX2P-$CreER^{T2}$ (referred to as Control or WT) mice were used as a control.

Mice were terminated at 4, 8 and 24 wks after 3 TAM injections (Figure 25B) and samples collected as described in Figure 25B. Somatic inactivation of the Apc^{580S} allele and activation of the $Kras^{LSL\text{-}G12D/+}$ allele in the colonic crypt of ACK compared to control mice were assessed using PCR. For both genotype and Cre activity purposes, allele-specific primers were as described is Figure 26 A&B. In control mice, only wild type Apc allele and wild type Kras allele were present across all time points, whereas in ACK mice, mutated allele of Apc and Kras were detected as expected. Animal body weights in ACK compared to control mice were not different (Figure 27A). Since recombinase activity is not 100%, allele carrying floxed region Apc (Apc^{580D}) and Kras ($Kras^{G12D}$) was also detected. We measured the body weight in the mice every week and no difference in ACK compared to control mice (Figure 27A).

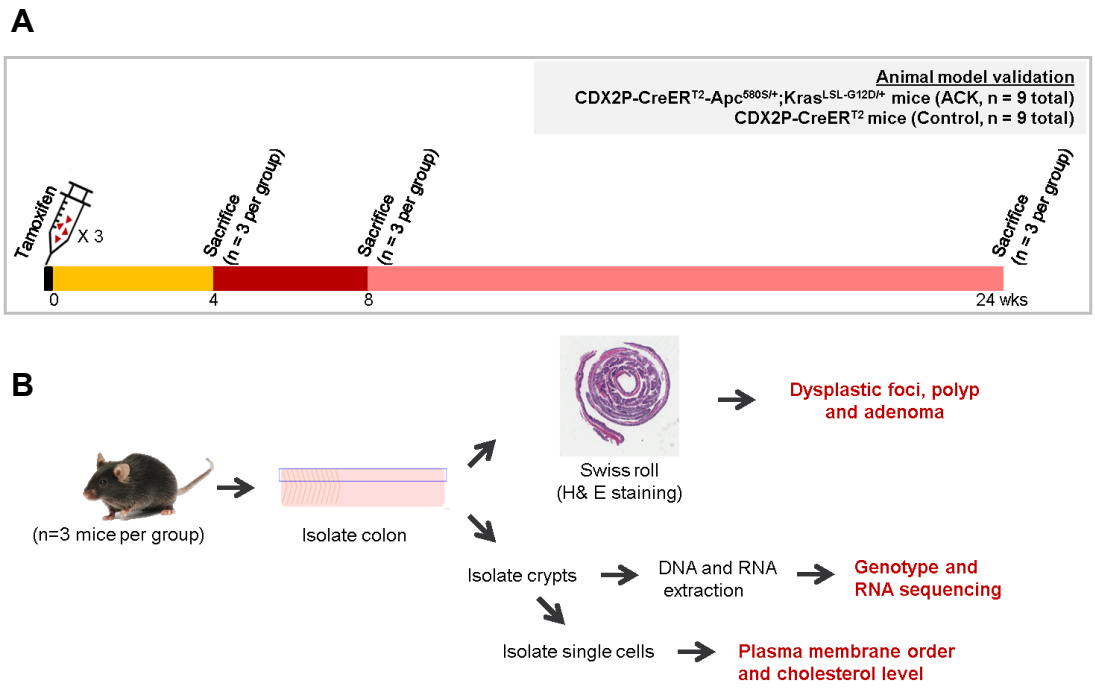

Figure 25. Experimental design and sample preparation. (A) Timeline of the treatments and experimental design. **(B)** Sample preparation.

We then applied a cell fractionation protocol, which separated the nuclear compartment from the cytoplasm of isolated crypts as revealed by western blot analysis to verify the effect of inactive Apc (Apc^{580D}) in ACK mice on Wnt-downstream signaling. As expected, β-catenin was detected in both the nuclear and cytosol fractions in both ACK and control mice across all time points. The relative density of nuclear / cytosolic β-catenin per group was determined and there was no statistically significant change in β-catenin in nuclear/cytoplasmic distribution in ACK mice compared with control mice across all time points (Figure 27D, left). However, when all time points were combined, there was a statistically significant change in β-catenin with respect to its nuclear/cytoplasmic distribution in ACK mice compared to control mice (Figure 27D, right).

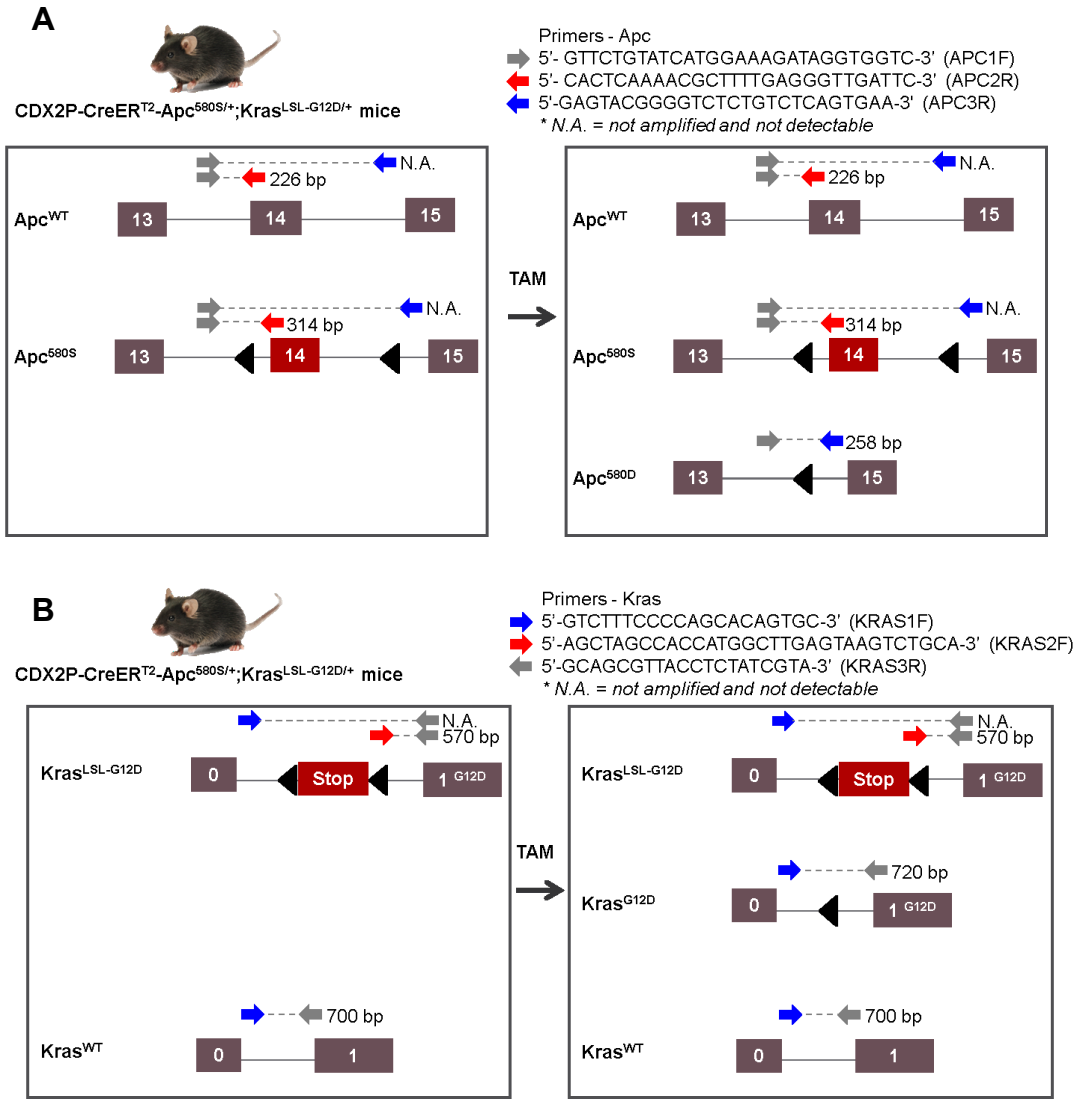

Figure 26. PCR strategy and primers. Positions of Allele-specific primers for Apc **(A)** and Kras **(B)** and estimated size (bp). Apc^{WT}: Apc wild type allele, Kras^{WT}: Kras wild type allele, bp: base pair, N.A.: not amplified.

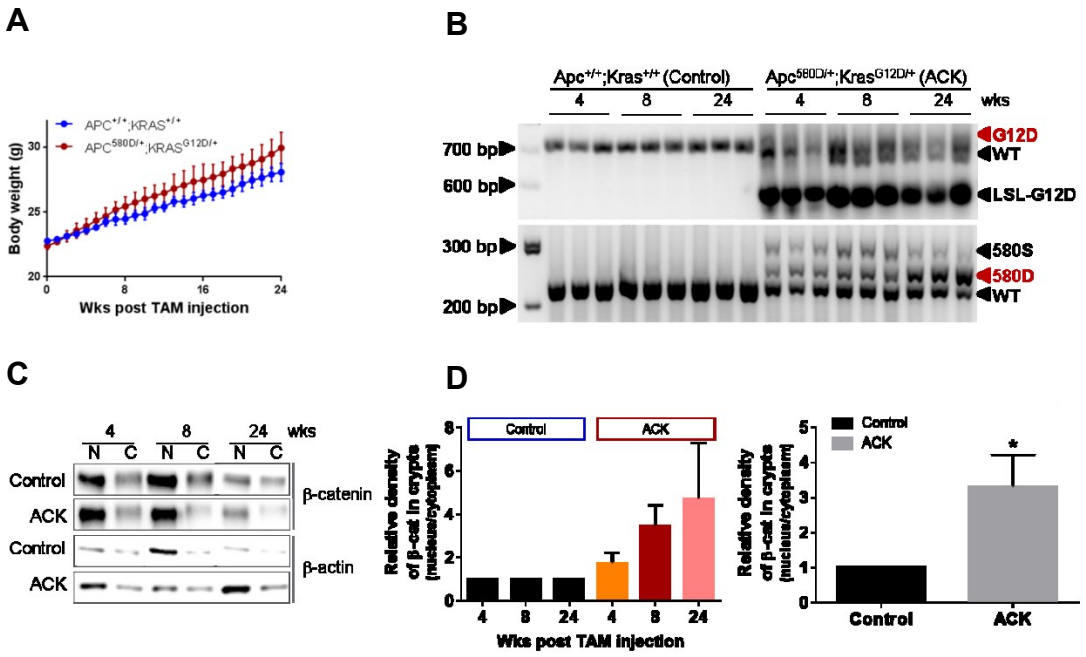

Figure 27. Validation of inactivation of Apc and activation of oncogenic Kras in the ACK mouse model. (A) Animal weight post TAM treatment per group. **(B)** Molecular analysis of Apc and Kras alleles in isolated crypts. CDX2P-CreER^{T2} (Control, n=3 per group) and CDX2P-CreER^{T2}-Apc$^{580S/+}$; Kras$^{LSL-G12D/+}$ (ACK, n=3 per group) mice were terminated at 4, 8 and 24 wks after 3 daily Tamoxifen (TAM, 100 mg/kg body weight) injections. The wild-type Kras allele (Kras^{+}) is represented by a 700 base pair (bp) fragment. The floxed Kras allele (Kras$^{LSL-G12D}$) is represented by a band of 570 bp, whereas the Cre-targeted allele (Kras^{G12D}) is represented by a band of 720 bp. The wild-type Apc (Apc $^{+}$) is represented by a 226 bp fragment. Floxed Apc allele (Apc ^{580S}) is represented by a 314 bp fragment, whereas the Cre-targeted allele (Apc^{580D}) is represented by a band of 258 bp. **(C)** The expression of cytosol and nuclear forms of β-catenin was examined by Western blotting. β-actin served as a loading control. Crypts from control and ACK mice were isolated at 4, 8 and 24 wks post 3 TAM injection and fractionated into nuclear and cytosolic compartments. N = nuclear fraction and C = cytosolic fraction. **(D)** The relative density of nuclear / cytosolic β-catenin of ACK compared to control at 4, 8 and 24 wks post TAM injection (left). The relative density of nuclear / cytosolic β-catenin of ACK compared to control (all time points combined, right) is shown. Values are normalized to the control group. * Indicate significant difference between treatment groups ($p<0.05$).

5.3.2 Dysplastic foci are increased in ACK mice

As a functional validation of our animal model, we immunohistochemically quantified dysplastic foci, polyps and adenoma phenotypes (Di Gregorio et al., 1997; Naini and Odze, 2013; Suzui et al., 2013)

as shown in Figure 28A. Paraffin-embedded, H&E stained colon sections (4 μm) were examined for aberrant crypt foci (ACF) by a blinded veterinary pathologist. Representative images of dysplastic foci, polyps and adenoma are shown in (Figure 28B). (i) Dysplastic foci were defined as regions with an increased nuclear to cytoplasm ratio, loss of apical differentiation, crowding of cells (hyperplasia), and/or irregular lumen diameter with tortuous branching. The lamina propria and submucosa contained a mixed inflammatory infiltrate composed of small numbers of neutrophils with fewer macrophages, lymphocytes and plasma cells. Crypts sometimes contained sloughed degenerate epithelial cells and acellular debris. (ii) Polyps contained a short stalk with a raised, nodular foci of hyperplastic epithelium. They share many of the cellular features of dysplasia but are more nodular and elevated above the surrounding epithelium. (iii) Adenomas were nodular, raised, circumscribed foci of neoplastic epithelial cells arising from the mucosa. Epithelial cells formed irregularly branching tortuous glands that did not extend beyond the muscularis mucosa. The stroma contained a small number of neutrophils, lymphocytes (Di Gregorio et al., 1997; Naini and Odze, 2013; Suzui et al., 2013). Substantial amounts of dysplastic foci were present in ACK mice across all time points (Figure 28C) and polyps and adenomas were detected at 8 and 24 wks, respectively (Figure 28A). In contrast, none of sequential abnormalities were detected in control mice.

A

CDX2P-CreER^{T2}-Apc$^{580S/+}$;Kras$^{LSL-G12D/+}$ mice (ACK)									
	4 wks			8 wks			24 wks		
Animal ID	81	520	527	470	475	497	365	446	447
Dysplastic foci	5	3	4	9	2	8	5	3	2
Polyps	0	0	0	1	0	1	0	2	0
Adenoma	0	0	0	0	0	0	0	1	3
CDX2P-CreER^{T2} mice (control)									
	4 wks			8 wks			24 wks		
None of sequential abnormalities were found in control mice.									

B

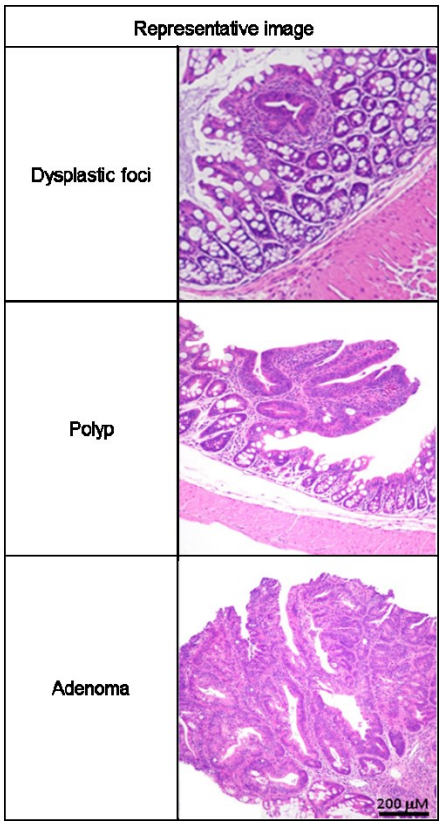

C

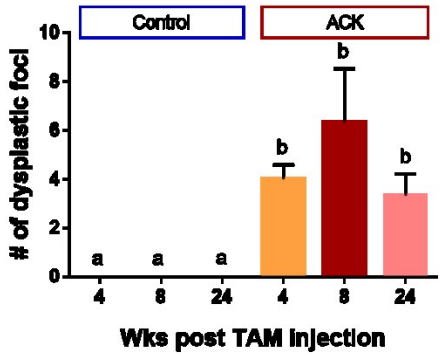

Figure 28. Number of dysplastic foci, polyps and adenomas per animal were increased in ACK mice as compared to control mice. **(A)** Number of dysplastic foci, polyps and adenoma per animal in different group. CDX2P-CreER^{T2} (Control, n=3 per group) and CDX2P-CreER^{T2}-Apc$^{580S/+}$; Kras$^{LSL-G12D/+}$ (ACK, n=3 per group) mice were terminated at 4, 8 and 24 wks after 3 Tamoxifen (TAM, 100 mg/kg body weight) injections. **(B)** Representative images of dysplastic foci, polyps and adenoma and description of it. **(C)** Comparison of number of dysplastic foci per group. Two-way ANOVA followed by the Tukey's multiple comparison test to compare between groups. Bars with different letters are significantly different, $P < 0.05$.

5.3.3 Proliferation is increased in ACK mice as compared to control mice

In familial adenomatous polyposis (FAP), which is associated with germline mutations in APC, the earliest visible change before the development of small, dysplastic adenomas is an upward shift in the proliferative compartment (Potten

et al., 1992). To determine whether the proliferative compartment in the colonic crypt is elongated, the proliferating zone was determined as the distance from the base of the crypt to the highest proliferating cell (EdU^+) cell within in the crypt. For this purpose, the number of EdU^+ cells per crypt, proliferating zone and length of crypt in ACK mice were quantified at 4, 8 and 24 wks after 3 TAM injections. Representative images of Swiss rolls labeled with EdU and counterstained with DAPI are shown in Figure 29D. As expected, the number of EdU^+ cells per crypt (Figure 29A), proliferating zone (Figure 29B) and length of crypt were increased in ACK mice as compared to control across all time points. None of the sequential abnormalities were detected in control mice.

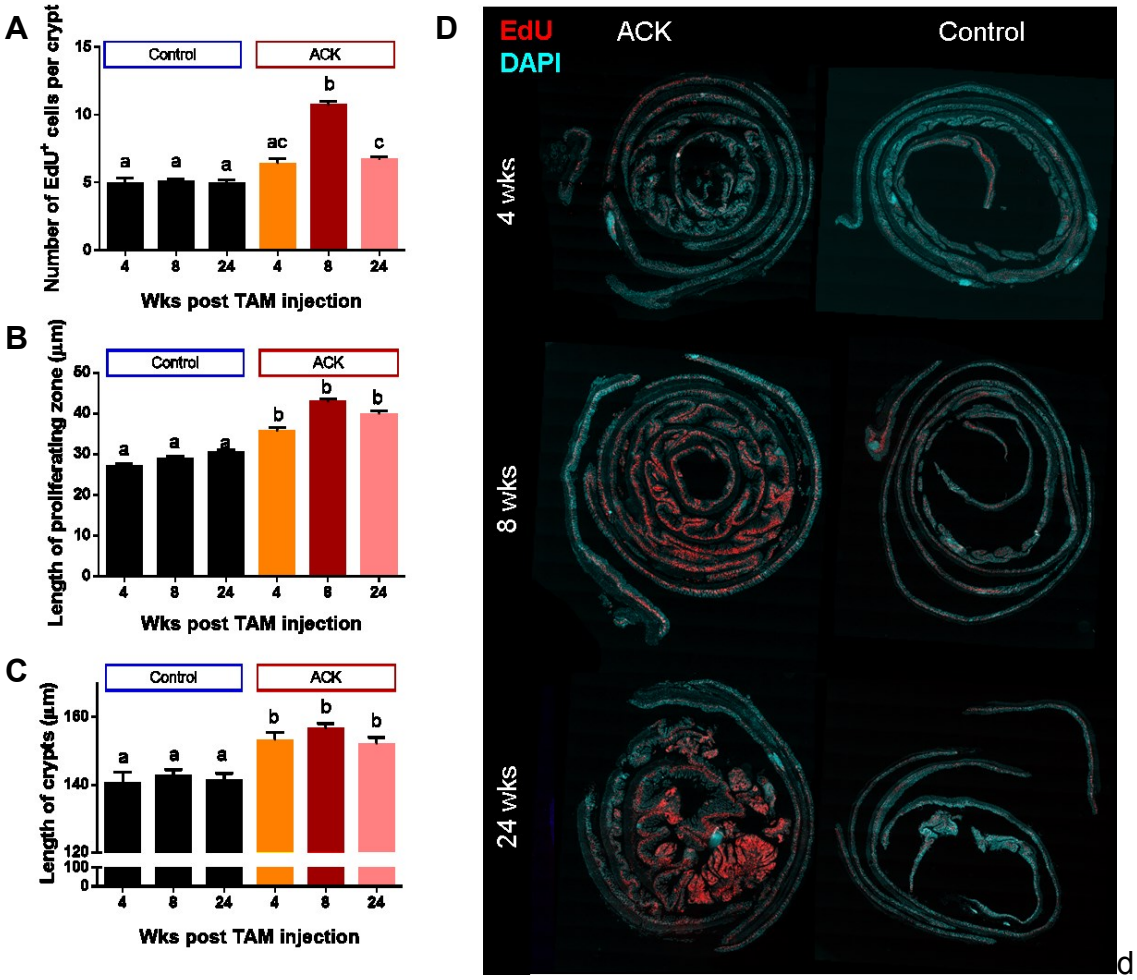

Figure 29. Proliferation is increased in ACK compared to control mice. **(A)** Number of proliferating cells (EdU$^+$) per crypt in the distal colon. CDX2P-CreER^{T2} (Control, n=3 per group) and CDX2P-CreER^{T2}-Apc$^{580S/+}$; Kras$^{LSL-G12D/+}$ (ACK, n=3 per group) mice were terminated at 4, 8 and 24 wks after 3 Tamoxifen (TAM, 100 mg/kg body weight) injections. **(B)** Length of the crypt proliferative zone in the distal colon. **(C)** Length of crypts in the distal colon. **(D)** Swiss roll labeled with DAPI (cyan, nucleus) and EdU (red, proliferating cells). Two-way ANOVA followed by the Tukey's multiple comparison test to compare between groups. Bars with different letters are significantly different, $P < 0.05$.

5.3.4 *Apc$^{580D/+}$ and Kras$^{G12D/+}$ increases cholesterol and plasma membrane order and is positively associated with increased proliferation*

Increased free cholesterol (1.5-fold) and esterified cholesterol (2-fold) in tumor tissue as compared to normal tissue has been reported in human colon cancer patients (Dessi et al., 1994). Statin, a cholesterol antagonist, significantly reduces risk of colorectal cancer (OR=0.33-0.50) and mortality in colorectal cancer patients (Cardwell et al., 2014; Lakha et al., 2012; Poynter et al., 2005) implying an important role for cholesterol in cancer biology. This is noteworthy, because plasma membrane cholesterol is highly correlated with membrane order (Montero et al., 2008), and cholesterol-rich highly ordered lipid rafts are increased in many types of cancer (Li et al., 2006b; Patra, 2008) and some drug resistant cancers (Yi et al., 2013). From a mechanistic perspective, changes in plasma membrane structure alter receptor-mediated cell signaling (Gawrisch et al., 2008).

It has been demonstrated that Apc knock-out mice increase hydroxymethylglutaryl coenzyme A reductase (HMGCR) genes which drive cholesterol synthesis in the colonocyte (Dow et al., 2015). In addition, mutant Kras promotes Wnt signaling through LRP6 phosphorylation (Lemieux et al., 2015), which promotes stemness and malignant transformation. It also has been shown that oncogenic Kras induces cholesterol synthesis (SREBP1/2 and Sqle.1) gene expression in murine lung adenocarcinoma cells (Gouw et al., 2017). However, to date, it has not been determined whether disrupted Wnt

and EGFR signaling pathways modulate colonocyte cholesterol homeostasis in vivo. Thus, we hypothesized that levels of free cholesterol increased by inactive Apc (Apc^{580D}) and oncogenic Kras ($Kras^{G12D}$) will perturb colonic crypt plasma membrane order.

In order to visualize the distribution of plasma membrane free cholesterol, isolated fixed cells from ACK and control mice were labeled with Filipin III (a sterol-binding fluorescent polyene) which selectively binds free cholesterol (Kruth and Vaughan, 1980). Representative images of Filipin III stained cells are shown in Figure 30A and fluorescence intensity of Filipin III from cells was determined using the NIS Image software. Fluorescence microscopy images of cells isolated from ACK mice exhibited an increased staining with Filipin III when compared to cells from control mice (Figure 30B).

From a functional perspective, the cholesterol/phospholipid composition of cellular membranes is known to influence plasma membrane biology and the ability of plasma membrane receptors/signaling proteins to function properly (Griffie et al., 2015; Hou et al., 2016; Phillips et al., 2009). From a biophysical perspective, cholesterol in the plasma membrane increases plasma membrane order (decrease plasma membrane fluidity) (Montero et al., 2008), thus, we examined the effect of cholesterol enrichment on plasma membrane order using colonic epithelial cells isolated from ACK mice as compared to control mice. Representative images of di-4-ANEPPDHQ stained cell are shown in Figure 31A. As expected, plasma membrane order of cells

from ACK mice were increased as compared to control mice across all time points (Figure 31B).

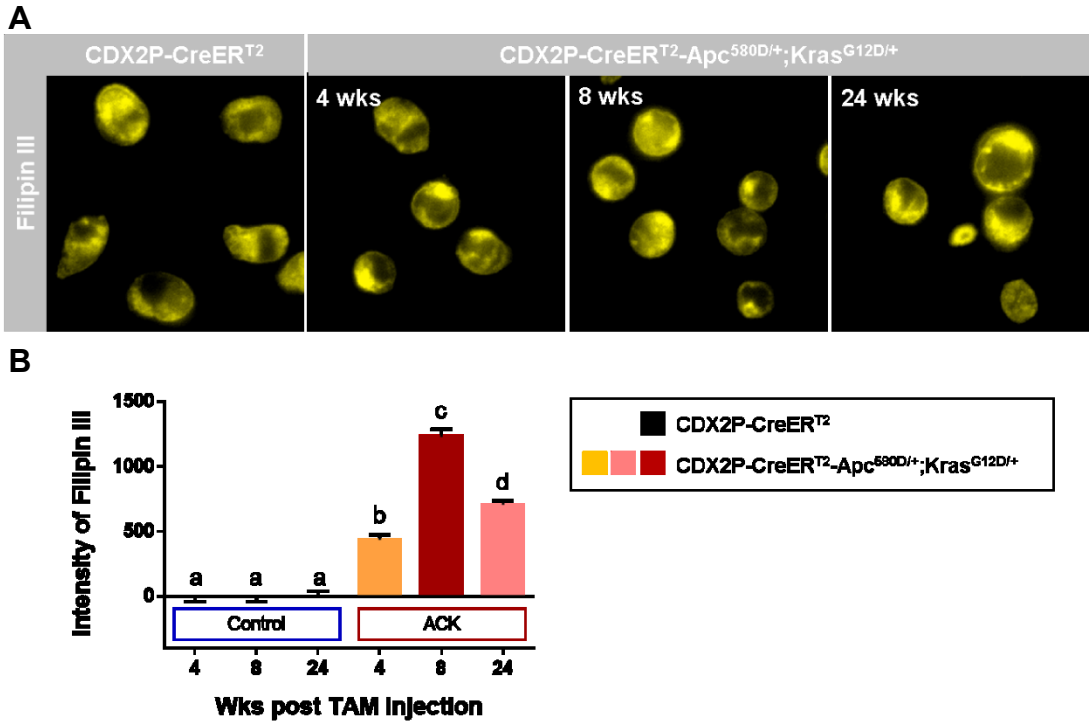

Figure 30. Plasma membrane free cholesterol levels are increased in ACK mice as compared to control mice. (A) Representative images of free cholesterol as indicated by Filipin III fluorescence in colonocyte from each group. **(B)** Mean Filipin III fluorescence in colonocyte from each group. CDX2P-CreER^{T2} and CDX2P-CreER^{T2}-Apc$^{580S/+}$; Kras$^{LSL-G12D/+}$ mice were terminated at 4, 8 and 24 wks after 3 daily Tamoxifen (TAM, 100 mg/kg body weight) injections. Isolated single cells were fixed in 1.5% PFA for 30 minutes at 4°C, followed by labeling of cholesterol with Filipin III (50 μg/mL) for 45 minutes at room temperature in the dark. Images were acquired using a Nikon wide field microscope with 40x oil objective using the DAPI_2 (dedicated DAPI filter, not the quad 4 cube) filter. Images were acquired using the same exposure time (10 ms) to compare relative fluorescence. Intensity of Filipin III was determined using NIS Image software, version 3.2. Two-way ANOVA followed by the Tukey's multiple comparison test to compare between groups. Bars with different letters are significantly different, $P < 0.05$.

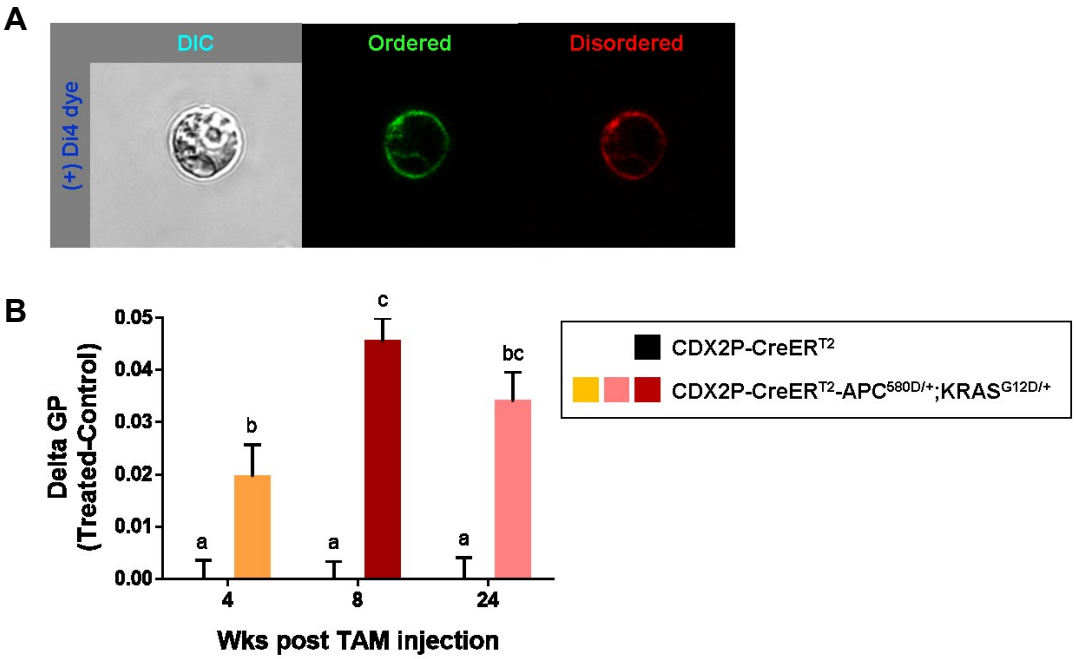

Figure 31. Membrane order of colonocyte is increased in ACK mice compared to control. **(A)** Representative confocal images of colonocyte in the liquid ordered phase (green line) and liquid disordered phase (red line). **(B)** Plasma membrane order of colonocyte isolated from ACK and control mice. CDX2P-CreER^{T2} and CDX2P-CreER^{T2}-Apc$^{580S/+}$; Kras$^{LSL-G12D/+}$ mice were terminated at 4, 8 and 24 wks after 3 daily Tamoxifen (TAM, 100 mg/kg body weight) injections. Imaging was achieved with a Nikon confocal microscope immediately after adding Di-4-ANEPPDHQ to isolated single cells. Generalized Polarization (GP) images were calculated using a custom plugin for ImageJ using the intensity of the ordered phase image (I_O) and a red-shifted image (I_D) from the disordered phase according to the equation, $GP=(I_O-I_D)/(I_O+I_D)$. The GP values ranged from −1 (when all the fluorescence emission is collected in the disordered, long-wavelength channel) to +1 (when all the fluorescence is collected in the ordered, short wavelength channel). I_O: Intensity of the ordered phase image (shorter wavelength, 508-544 nm); I_D: Intensity of the disordered phase image (long-wavelength, 651-695 nm). Statistically significant differences between time were determined using one-way ANOVA followed by Tukey's multiple comparison test adjustment. Bars with different letters are significantly different, $P < 0.05$.

Using a simple linear regression analysis, we determined whether there was any association between the number of EdU$^+$ cells per crypt, membrane cholesterol levels (Figure 32A). In addition, the relationship

between the number of EdU^{+} cells per crypt and plasma membrane order was investigated (Figure 32B). As shown in Figure 32, cholesterol and plasma membrane order exhibited a significant proportional increase dependent on the number of EdU^{+} cells per crypt. This finding implies that Apc^{580S} and Kras^{G12D} play a role in increasing free cholesterol, thereby affecting plasma membrane order, which is associated with increased cell proliferation.

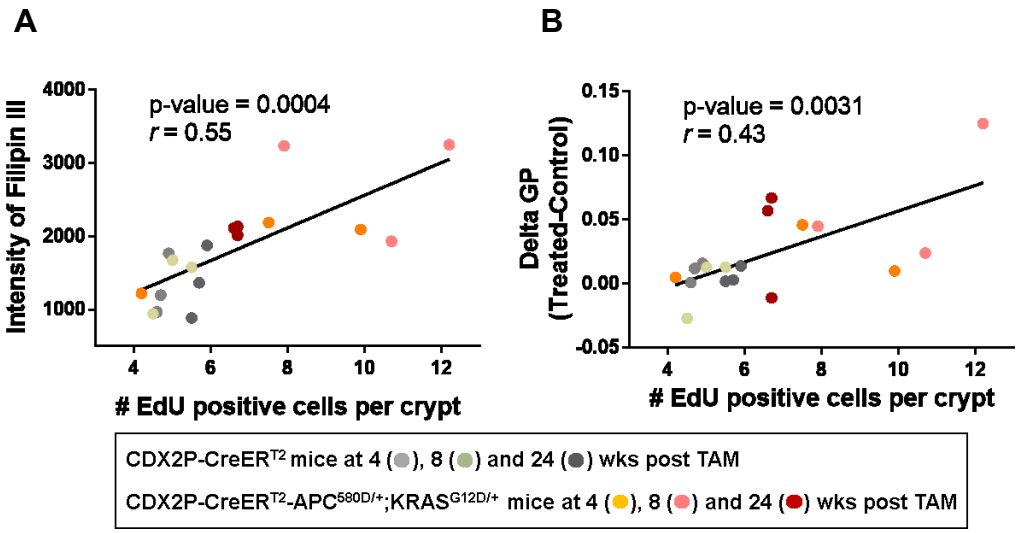

Figure 32. Plasma membrane order and cell proliferation are positively correlated. Association between the number of EdU positive cells and membrane order. **(A)** The association between EdU positive cells and cell cholesterol levels. **(B)** The association between EdU positive cells and cell membrane order. Each point represents an individual animal and wks post Tmx are labeled with different symbols as indicated. Slopes shown are found to be significantly different from 0 at a significant level of 0.05.

5.3.5 Cholesterol directly enhances proliferation – in vitro and ex vivo

Our findings raise the possibility that changes in membrane cholesterol status may directly regulate cell proliferation in the colon. Because proliferating cells, such as cancer cells, are believed to have increased requirements for cholesterol (Menendez and Lupu, 2007), we further elucidated the association of Apc^{580D} and $Kras^{G12D}$ mutation-mediated changes in membrane cholesterol to cell proliferation. To measure the direct effects of cholesterol on cell proliferation, we quantified the proliferation rate following exogenous cholesterol incubation using a model of (i) conditionally immortalized mouse colon epithelial cell lines (in vivo): YAMC (with two wild type Apc alleles) (Whitehead and Robinson, 2009), (ii) IMCE (with one wild type Apc and one mutant Apc^{Min} allele) (Whitehead and Joseph, 1994) and (iii) mouse colonic organoids (ex vivo). Proliferation was determined by the fluorescent CellTiter-Blue method, which is based on the ability of living cells to convert redox dye (resazurin) into a fluorescent end product (resorufin). Nonviable cells rapidly lose metabolic capacity and thus do not generate a fluorescent signal. Cells were either treated with varying concentrations of cholesterol combined with MβCD (water soluble cholesterol) or MβCD as described in Figures 33 and 34. Cells not incubated with cholesterol and MβCD were used as a baseline control. In addition, cholesterol was incubated with media containing lipoprotein depleted serum. Cell viability was monitored every 24 hr over a 72 hr period. YAMC cells increased proliferation in the presence

of 100 μM cholesterol at 72 hr (Figure 33B) whereas, MβCD treated cells exhibited a significant decrease in proliferation as compared to cells with no treatment (cells only) as shown in Figure 33A. Data showing cholesterol incubated cells are separately shown in Figure 33B along with statistical results. As a consequence of cholesterol incubation, levels of cholesterol (Figure 33C) and plasma membrane order (Figure 33D) were also increased as compared to MβCD (alone) incubated cells. In IMCE cells, cholesterol incubation for 72 hr increased proliferation as compared to cells with no treatment in a dose-dependent manner (Figure 34B), in contrast to MβCD treated cells (Figure 34A). These preliminary findings demonstrate that cells increase proliferation in a dose dependent manner, implying a direct role of cholesterol in cell division.

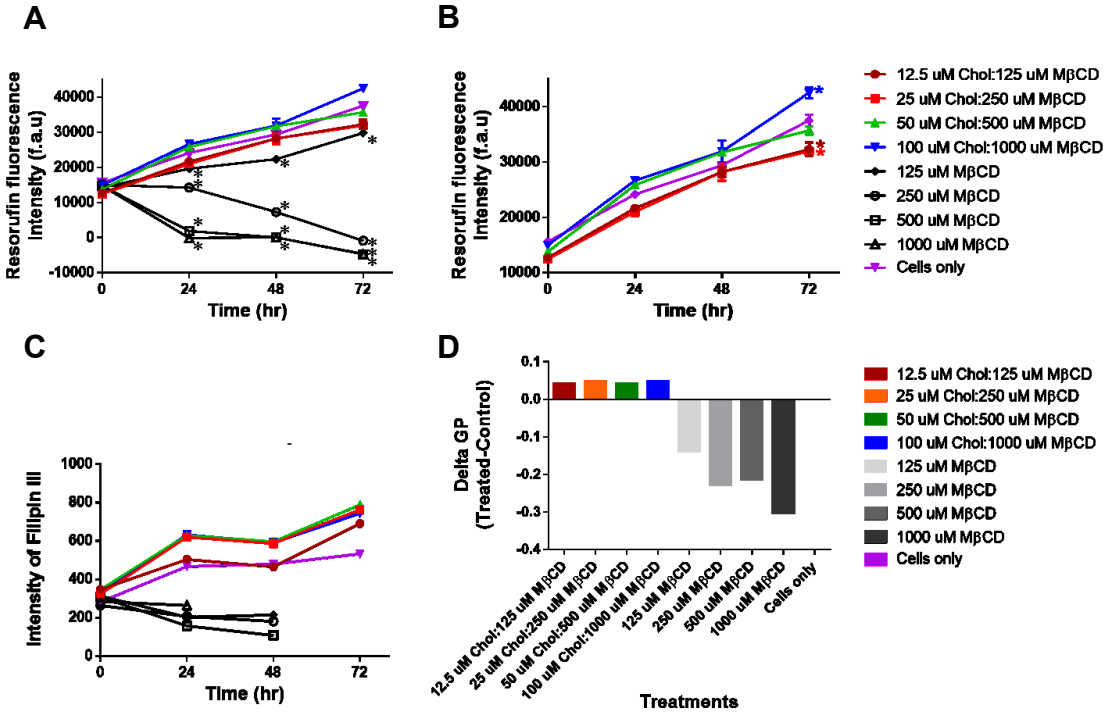

Figure 33. Cholesterol increases proliferative rate in YAMC cells. **(A)** Proliferation rate of YAMC cells upon incubation with different concentrations of cholesterol and MβCD (n=3). **(B)** Statistical summary of cholesterol effects on YAMC cell proliferation (n=3). **(C)** Levels of plasma membrane cholesterol in YAMC cells were exposed to increasing concentrations of cholesterol and MβCD (n=1). Imaging flowcytometry (FlowSight®, Amnis®, EMD Millipore) was used to measure membrane cholesterol levels. For this purpose, harvested single cells were fixed in 1.5% PFA for 30 minutes at 4°C, followed by labeling with Filipin III (50 mg/mL) for 45 minutes at room temperature in the dark followed by washing with PBS. Bright field (560-595 nm) and Filipin III (430-505 nm) channels were used to collect data. Filipin III intensity from cell plasma membranes were quantified using the IDEAS feature analysis software. * Indicates significant difference from cells only. Media was changed every 24 hr to avoid oxidization. No data presented indicates non-viable cultures. Cells not incubated with cholesterol and MβCD were used as a baseline control. **(D)** Plasma membrane order of YAMC cells following incubation with different concentrations of cholesterol and MβCD (n=1). Imaging was achieved immediately after adding Di-4-ANEPPDHQ (at a final concentration of 1 μM) to live single cells. Cells were excited using a 488 nm laser. Bright field (430-480 nm), ordered (505-560 nm) and disordered (642-740 nm) channels were used to collect data. Confocal images were processed to generate GP-values (Owen et al., 2011) using IDEAS version 6.0.

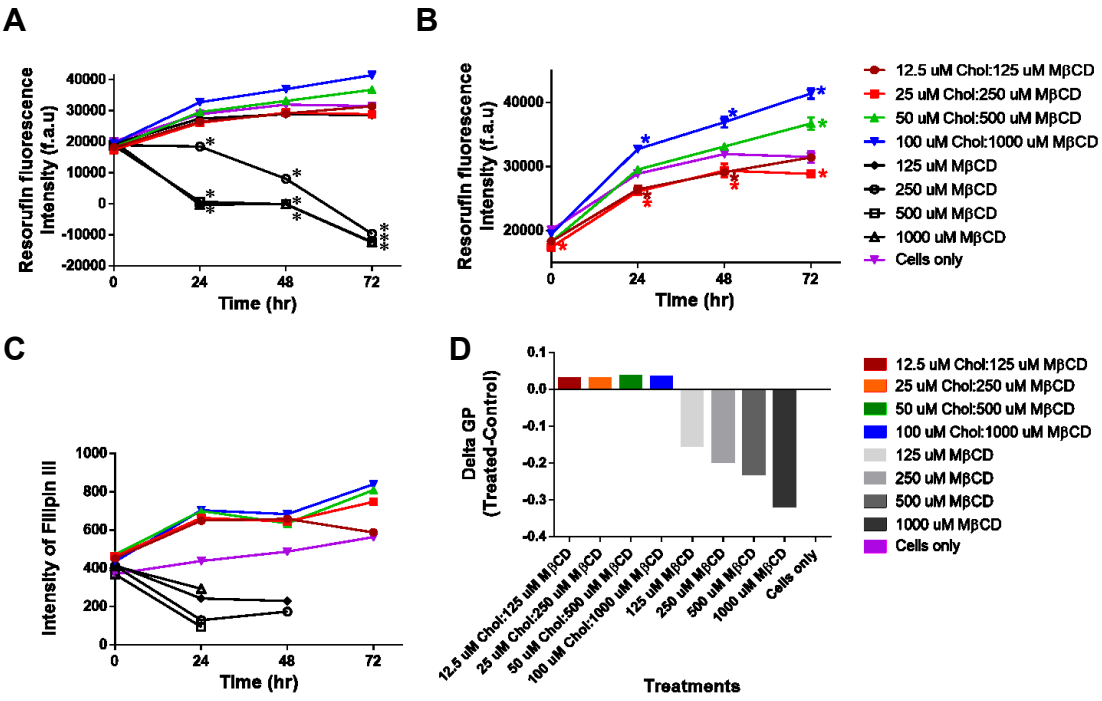

Figure 34. Cholesterol increases proliferative rates in IMCE cells. (A) Proliferation rate of IMCE cells upon cholesterol and MβCD incubation (n=3). **(B)** Effect of cholesterol dose on IMCE cell proliferation rates (n=3). **(C)** Levels of plasma membrane cholesterol in IMCE cells following incubation with increasing concentrations of cholesterol and MβCD (n=1). Plasma membrane cholesterol levels were quantified as described in Figure 34. **(D)** Plasma membrane order of IMCE cells was also quantified using an imaging flowcytometer FlowSight® (Amnis®, EMDMillipore) immediately after adding Di-4-ANEPPDHQ (at a final concentration of 1 μM) to live single cells as described in Figure 33.

We also investigated the effects of exogenous cholesterol on the number of proliferating cells in organoids. For this purpose, organoids were grown using sorted Lgr5 stem cells (GFP^{high}) isolated from Lgr5-EGFP-IRES-$CreER^{T2}$ mice and incubated in media (Table 7) either with 100 μM cholesterol or 1000 μM MβCD for 72 hr. A predetermined cholesterol (100 μM) dose was selected

based on our cell line proliferation data (Figure 33B and 34B). MβCD (1 mM) was used as a control (Figure 33A and 34A). Proliferating cells were labeled using EdU assay and the % of EdU positive cells were quantified using a Millipore FlowSight imaging flow cytometer. As shown in Figure 35A, less than 5% of EdU positive cells were found in organoids incubated without cholesterol (no Chol, 72 hr), whereas 25% of EdU positive cells were detected in organoids incubated with cholesterol (Chol, 72 hr), further demonstrating the ability of cholesterol to directly modulate colonocyte proliferation. Consistent with these findings, membrane cholesterol levels and plasma membrane order were increased upon cholesterol incubation for 72 hr as expected (Figure 35B and 35C). In summary, our data demonstrate a direct effect of cholesterol on enhancing proliferation and plasma membrane order in vitro (Figure 33A and 34A) and ex vivo (Figure 35A). These findings support our hypothesis that cholesterol mediated changes in plasma membrane order may modulate cell proliferation.

Organoid media	Final concentration	500 µL/well
EGF (100µg/mL)	50 ng/mL	0.25
LDN (Noggin replacement (0.2 mM)	0.2 mM, ~ 81.3 ng/mL	0.5
R-Spondin (1 mg/ml)	1x	0.25
N2 supplement (100x)	1x	5
B27 supplement (50x)	1x	10
N-Acetylcys (400 µM) (A)	1 mM	1.25
ADF+ (w/ Gln, HEPES)		482.5
Wnt (100 ug/ml)	50 ng/ml	0.25
Total volume		500

Table 7. Organoid culture media.

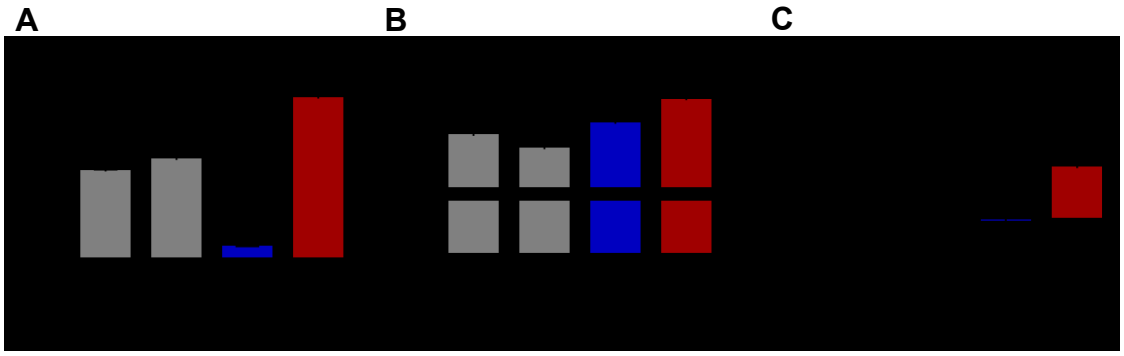

Figure 35. Cholesterol increases the percentage of proliferating cells in organoids. (A) % EdU positive cells in organoids incubated with 100 μM cholesterol for 72 hr. Organoids were derived from sorted GFP^{high} cells isolated from Lgr5-EGFP-$CreER^{T2}$ crypt cells. To quantify EdU^{+} cells, FlowSight® (Amnis®, EMDMillipore) images were obtained following excitation with 647 nm. Bright field (595-642 nm) and EdU AF647 (632-740 nm) channels were used to collect data. Cells not incubated with AF647 were used for gating EdU negative cells. Cholesterol **(B)** and plasma membrane order **(C)** in organoids incubated with 100 mM cholesterol for 72 hr. * Indicates significant difference between groups. Refer to Figure 30 and 31 for additional details.

5.3.6 $Apc^{580D/+}$ and $Kras^{G12D/+}$ regulate a canonical cancer driver gene associated with cholesterol homeostasis

To further elucidate the effect of $Apc^{580D/+}$ and $Kras^{G12D/+}$ on modulating cholesterol homeostasis, global transcriptional profiles in ACK mice and control mice were assessed by RNA sequencing on isolated crypt cells. Mice were terminated at 4, 8 and 24 wks after 3 daily TAM injections and samples were collected as described in Figure 25B. ACK mice terminated at 4, 8 and 24 wks post TAM were compared with control mice terminated at 4, 8 and 24 wks, respectively. IPA was subsequently used to identify potential transcriptional

regulators inferred from differentially expressed genes. Interestingly, Myc was the number one ranked upstream regulator (highest z-score) in ACK mice at 4 and 8 wks as compared to control mice, and was the second highest ranked upstream regulator at 24 wks (Table 8). This is highly relevant, since Myc is a well-known marker gene associated with inactive Apc and is overexpressed in approximately 70% of colorectal tumors (Erisman et al., 1985). Oncogenic Myc is known to regulate the expression of HMGCR in esophageal epithelial cells (SHEE) cells (Zhong et al., 2014), thereby increasing cholesterol. Cholesterol is synthesized from acetyl-CoA, which is condensed to form HMG-CoA and is subsequently reduced to mevalonate by HMGCR. HMGCR is rate-limiting in the cholesterol synthesis pathway; hence, HMGCR is essential for Myc-driven cancer as it mediates the phosphorylation and transactivation of Myc (Cao et al., 2011). In summary, our novel findings indicate that $Apc^{580D/+}$ and $Kras^{G12D/+}$ regulate a canonical cancer driver gene associated with cholesterol homeostasis.

Using bioinformatic analysis, we have identified a total of 66 Myc target genes that were differentially expressed in ACK mice as compared to control mice across all time points. Myc target genes expressed in at 4, 8 and 24 wks are listed in Table 8. Many of these genes regulate the cell cycle and mitotic regulation including Cyclin A2 (CCNA2) (Pagano et al., 1992), cyclin B1 (CCNB1) (Wang et al., 1997), cyclin E (CCNE) (Bondi et al., 2005), cyclin D2 (CCND2) (Mermelshtein et al., 2005), cyclin-dependent kinase 1 (CDK1)

(Castedo et al., 2002), and cyclin-dependent kinase 4 (CDK4) (O'Leary et al., 2016) (marked with green) (Tables 8 & 9).

Proliferation of epithelial crypt cells is Wnt dependent (Schuijers et al., 2015) and Wnt-driven target gene expressed in colon cancer and in crypts has been categorized (Van der Flier et al., 2007). Among them ASCL2, CD44 and Myc (marked in orange), main Wnt target gene, are also shown in our ACK mouse model (Table 8 and Table9) implying activation of Wnt signaling by inactive Apc. It also implying that colonocyte in ACK mice are globally affected by inactive Apc because ASCL2, Myc and CD44 are is expressed highly restricted fashion in intestinal stem cells (Barker et al., 2007; Fevr et al., 2007; ten Kate et al., 1989).

Other notable Myc target genes include Solute carrier family 2 member 1 (SLC2A1, GLUT1, marked in violet) (Tables 8 & 9). SLC2A1 is a glucose transporter expressed in colorectal carcinoma from patients (Haber et al., 1998). This finding is consistent with the link between Myc and metabolic reprogramming, a hallmark of cancer (Hanahan and Weinberg, 2011).

Comparison	ACK/Control mice		
Wks post TAM injection	4	8	24
Upstream Regulator		Myc	
Fold change (ACK/Control)	1.0	1.4	2.8
Activation z-score	4.2	7.0	4.2
p-value of overlap	4.42E-14	2.41E-17	2.08E-18
Target genes of Myc (total of 66 genes)	ANGPT2	BUB1	ANGPT2
	CAD	CCNA2	ASCL2
	Ccl6	CCNB1	CAD
	CCND2	CCNE2	Ccl6
	CCNE1	CD44	CCND2
	CD44	CDK1	CCNE1
	DUSP2	CDKN2A	CD44
	ENO1	COMMD3-BMI1	CDK4
	GATA4	ENO1	CDKN2A
	GPT	EPHB3	CIDEC
	LDHB	FOXA2	COMMD3-BMI1
	ME2	GOT1	ENO1
	NFATC3	GPT	FABP4
	ODC1	HIF1A	FOXA2
	PARP1	Hnrnpa1	GATA4
	PML	LDHA	GFPT1
	RRM2	MAD2L1	GLUD1
	SLC16A1	MCM5	GOT1
	SLC16A3	MCM7	HIF1A
	SLC1A5	ME2	HMGA1
	SLC2A1	MYC	Igha
	SLC38A1	ODC1	ME2
	SLC7A5	PDK1	MYC
	SRM	PGK1	ODC1
	TIAM1	PML	PA2G4
	TNFRSF12A	RRM2	PDK1
		SERPINE1	PFKL
		SLC16A3	PKM
		SLC1A5	RRM2
		SLC2A1	SERPINE1
		SLC7A5	SLC16A3
		SRM	SLC1A5
		TFRC	SLC2A1
		TNFRSF12A	SLC3A2
			SLC7A5
			SRM
			TCF3
			Tcf7
			THBS1
			TNFRSF12A
			TNFRSF19
			TP53
			YY1

Table 8. IPA upstream regulator analysis. Direct target genes of Myc that are differentially expressed in ACK mice as compared to control mice. CDX2P-CreER^{T2} (Control) and CDX2P-CreER^{T2}-Apc$^{580S/+}$; Kras$^{LSL-G12D/+}$ (ACK) mice were terminated at 4, 8 and 24 wks after 3 daily Tamoxifen (TAM, 100 mg/kg body weight) injections. n=3 mice per group.

Comparison	ACK/Control					
Wks post TAM injection	4		8		24	
Target gene	Fold change	FDR	Fold change	FDR	Fold change	FDR
Ccna2	0.8	-	1.6	**	0.9	-
Ccnb1	0.8	-	1.6	**	0.9	-
Ccnd2	1.6	**	1.1	-	1.3	**
Ccne1	1.4	**	1.3	*	1.6	**
Ccne2	1.1	-	1.6	**	1.1	-
Cdk1	0.9	-	1.8	**	1.0	-
Cdk4	1.1	-	1.3	*	1.4	**
Ascl2	1.3	-	1.0	-	1.8	**
Cd44	1.6	**	1.5	**	2.4	**
Myc	1.0	-	1.4	**	2.8	**
Slc2a1	1.9	**	1.5	**	1.9	**

Table 9. Myc target genes transcriptionally modulated in ACK mice as compared to control. Fold change of gene expression in ACK mice as compared to control mice. CDX2P-CreER^{T2} (Control) and CDX2P-CreER^{T2}-Apc$^{580S/+}$; Kras$^{LSL-G12D/+}$ (ACK) mice were terminated at 4, 8 and 24 wks after 3 daily Tamoxifen (TAM, 100 mg/kg body weight) injections, n=3 mice per group. FDR values less than 0.05 are noted by two asterisks (**), FDR values less than 0.01 are noted by a single asterisk (*), and FDR values greater than 0.1 are marked with a dash (-).

Since membrane free cholesterol levels and plasma membrane order are elevated in ACK mice, we looked at genes known to modulate cholesterol metabolism. Cells can increase their cholesterol content either via *de novo* synthesis (i.e., mevalonate pathway), by increasing uptake of extracellular cholesterol via the low-density lipoprotein receptor, or by decreasing expression of a rate-limiting cholesterol exporter, e.g., ATP binding cassette transporter A1 (ABCA1) (Ikonen, 2008). As shown in Table 10, Low-density lipoprotein (LDL) receptor (Ldlr) was increased by 1.4-fold in ACK mice as compared to control mice at 4 wks. Also, Very Low Density Lipoprotein Receptor (Vldlr) and Proprotein convertase subtilisin/kexin type 9 (Pcsk9) were increased in ACK mice as compared to control mice at 8 and 24 wks. Ldlr, Vldlr

and Pcsk9 are known to increase cell cholesterol (Go and Mani, 2012; Takahashi et al., 1995; Tao et al., 2010). These data imply that increases in cholesterol and plasma membrane order in ACK mice (Figure 30 and 31) were in part attributed to elevation in cholesterol uptake.

Comparison	ACK/Control					
Wks post TAM injection	4		8		24	
Target gene	Fold change	FDR	Fold change	FDR	Fold change	FDR
Ldlr	1.427	**	1.014	–	0.959	–
Lrp10	1.140	–	0.797	–	0.884	–
Lrp12	1.121	–	1.172	–	1.086	–
Lrp6	0.874	–	0.675	**	0.797	–
Olr1	2.867	–	4.733	–	4.382	–
Stab1	1.025	–	1.449	–	1.464	–
Stab2	5.404	–	0.878	–	3.201	–
Vldlr	1.142	–	1.299	*	1.799	**
Lrpap1	0.839	–	0.827	–	0.754	**
Pcsk9	1.239	–	1.940	**	2.264	**
Snx17	1.039	–	0.893	–	1.044	–
Ankra2	0.731	*	1.292	–	0.938	–
Colec12	0.388	–	2.062	–	0.634	–
Nccrp1	0.313	**	0.215	**	0.138	**
Scarf1	0.690	–	0.435	**	0.333	**
Sorl1	1.119	–	0.752	–	1.152	–
Apoa1	2.767	–	3.532	–	2.535	–
Apod	0.853	–	1.809	–	2.230	–

Table 10. Genes associated with cholesterol uptake that are transcriptionally modulated in ACK mice as compared to control. See Table 9 for details.

Examination of genes involved in the efflux of cholesterol were assessed in ACK mice. As shown in Table 11, only the ATP binding cassette transporter A1 (Abca1) was differentially expressed in ACK mice as compared to control mice. Abca1 mediates the transfer of cellular cholesterol across the plasma membrane to apolipo-protein A-I (ApoAI), the major apolipoprotein component of high-density lipoprotein (HDL) (Attie, 2007). The increased levels of Abca1 (2.4-fold) in ACK mice at 24 wks suggests that cholesterol efflux does not

contribute to increased cholesterol and plasma membrane order observed in ACK mice (Figure 30 and 31).

Comparison	ACK/Control					
Wks post TAM injection	4		8		24	
Target gene	Fold change	FDR	Fold change	FDR	Fold change	FDR
Abca1	0.533	**	0.604	**	2.422	**
Abcg1	0.774	–	0.701	–	0.618	*
Apoe	0.806	–	0.720	–	0.794	–
Pltp	0.940	–	0.644	–	1.172	–
Stard3	0.926	–	0.782	**	0.960	–
Npc1l1	0.634	–	0.840	–	1.545	–
Osbpl5	0.986	–	0.819	–	0.837	–

Table 11. Abca1 associated with cholesterol export is transcriptionally modulated in ACK mice as compared to control. See Table 9 for details.

Lastly, we examined genes involved in cholesterol *de novo* synthesis. Interestingly, hydroxymethylglutaryl coenzyme A reductase (HMGCR) was increased by1.4-fold in ACK mice as compared to control at 8 wks (Table 12). HMGCR catalyzes the conversion of HMG-CoA to mevalonate, a rate-determining step in the synthesis of cholesterol (Goldstein and Brown, 1990) and is regulated by Myc in esophageal epithelial cells (Zhong et al., 2014). CCHC-type zinc finger nucleic acid binding protein (CNBP, also named ZNF9) was also increased by 1.7-fold in ACK mice as compared to control at 8 wks (Table 12). CNBP was originally identified as a transcription factor bound to the sterol regulatory element (SRE) of the hydroxymethylglutaryl coenzyme A (HMGCOA) gene (Rajavashisth et al., 1989). Also, peroxisome proliferator-activated receptor (PPARα), known to lower the synthesis of cholesterol (Konig et al., 2007), was reduced by 0.5-fold in ACK mice at 8 wks as compared to

control mice (Table 12). Overall, our RNAseq data provide evidence that the elevated colonocyte membrane cholesterol level and plasma membrane order in ACK mice is the result a perturbation in cholesterol homeostasis.

Comparison	ACK/Control					
Wks post TAM injection	4		8		24	
Target gene	Fold change	FDR	Fold change	FDR	Fold change	FDR
Cyp39a1	0.811	–	0.958	–	0.624	**
Trerf1	1.345	–	1.550	–	0.799	–
Ldlrap1	1.598	**	1.551	**	2.547	**
Acaa2	0.838	–	0.965	–	0.944	–
Cnbp	0.944	–	1.690	**	1.250	–
Cyb5r3	1.361	*	0.996	–	1.334	*
Cyp51	0.684	–	1.167	–	1.005	–
Dhcr24	1.223	–	0.958	–	1.991	***
Dhcr7	1.030	–	0.616	**	0.928	–
Ebp	1.376	**	0.996	–	0.863	–
Fdft1	1.540	**	1.441	**	1.313	*
Fdps	1.161	–	1.273	*	1.070	–
Ggps1	0.778	–	1.435	–	1.025	–
Hmgcr	1.212	–	1.389	**	1.244	–
Hmgcs1	1.133	–	1.139	–	0.911	–
Hmgcs2	0.682	**	0.677	**	0.804	–
Idi1	0.715	–	1.669	*	1.187	–
Mvd	1.209	–	1.122	–	1.345	**
Mvk	0.995	–	1.170	–	1.265	–
Nsdhl	0.939	–	1.175	–	1.357	**
Pmvk	0.686	**	0.880	–	0.824	–
Prkaa1	0.995	–	1.008	–	1.131	–
Prkaa2	0.875	–	0.996	–	1.147	–
Prkag2	0.917	–	1.009	–	1.093	–
Sc5d	1.046	–	1.038	–	0.935	–
Scd1	0.673	**	0.922	–	1.048	–
Tm7sf2	0.984	–	1.041	–	1.158	–
Abca2	1.421	–	1.059	–	1.103	–
Apob	1.393	**	0.988	–	1.801	**
Cyp11a1	2.579	–	1.017	–	3.467	–
Cyp7b1	0.955	–	1.596	–	1.186	–
Hdlbp	1.331	–	0.971	–	1.014	–
Il4	0.593	–	1.336	–	1.487	–
Insig1	0.942	–	1.491	–	1.053	–
Insig2	0.812	–	1.237	–	0.951	–
Lipe	1.061	–	0.633	**	0.841	–
Mbtps1	1.231	–	0.913	–	1.127	–
Nr1h4	0.613	**	1.117	–	0.567	**
Osbpl1a	0.729	–	1.194	–	1.179	–
Ppara	0.845	–	0.500	**	0.779	–
Ppard	0.931	–	0.628	*	0.612	**
Pparg	0.881	–	1.329	–	1.453	**
Scap	1.309	–	0.973	–	1.437	*
Soat2	0.439	**	1.265	–	1.330	–
Srebf1	1.113	–	0.801	–	1.259	–
Srebf2	1.200	–	0.939	–	1.291	–

Table 12. Genes associated with cholesterol synthesis are transcriptionally modulated in ACK mice as compared to control. See Table 9 for details.

Sphingolipid enriched plasma membrane domains (Pike, 2005) are also known to increase plasma membrane order (Brown and London, 2000; Simons and Sampaio, 2011). Therefore, we also examined genes involved in sphingolipid metabolism. As shown Table 13, no sphinogolipid metabolism related genes were modulated in ACK mice as compared to control mice across all time points. This finding suggest that increases in plasma membrane order are associated with perturbations in cholesterol homeostasis.

Comparison	ACK/Control					
Wks post TAM injection	4		8		24	
Target gene	Fold change	FDR	Fold change	FDR	Fold change	FDR
Cerk	1.001	–	0.802	–	0.768	–
Sgpp1	0.653	**	1.029	–	0.770	**
Sgpp2	0.972	–	0.797	–	0.706	–
Sphk2	0.886	–	0.697	**	1.023	–
Xbp1	0.713	**	1.041	–	0.714	**

Table 13. Genes associated with sphingolipid synthesis are transcriptionally modulated in ACK mice as compared to control. See Table 9 for details.

5.3.7 Proliferation induced by compound Apc^{580D} and Kras^{G12D} mutations is ameliorated by n-3 PUFA + curcumin feeding.

Highly ordered lipid rafts are increased in many types of cancer (Li et al., 2006b; Patra, 2008) and some drug resistant cancers (Yi et al., 2013). There is also evidence suggesting that disruption of lipid rafts in cancer can lead to increased responsiveness to anti-cancer therapies (Irwin et al., 2011). With respect to diet and membrane therapy, it has been demonstrated that DHA suppresses EGFR-mediated cell proliferation by translocating EGFR from lipid

raft to non-lipid raft domains in the plasma membrane (Turk et al., 2012). Curcumin and n-3 PUFA are also known to modulate plasma membrane order: the ordering effect of curcumin is strongest in the head group region of the phospholipid bilayer (Barry et al., 2009; Hung et al., 2008), whereas n-3 PUFA acyl chains impact the organization of the tail group region within rafts (Shaikh et al., 2004; Shaikh et al., 2015; Shaikh et al., 2009a) implying a synergistic effect. For this reason, we evaluated the effects of n-3 PUFA combined with curcumin on plasma membrane order in colonocyte harvested from ACK mice. For this purpose, we examined whether increased plasma membrane order due to Apc^{580D} and $Kras^{G12D}$ is reduced by dietary n-3 PUFA + curcumin enriched diet (4% fish oil + 1% corn oil + 1% curcumin). An n-6 PUFA enriched diet (5% corn oil diet) was used as a control (Figure 36B).

A

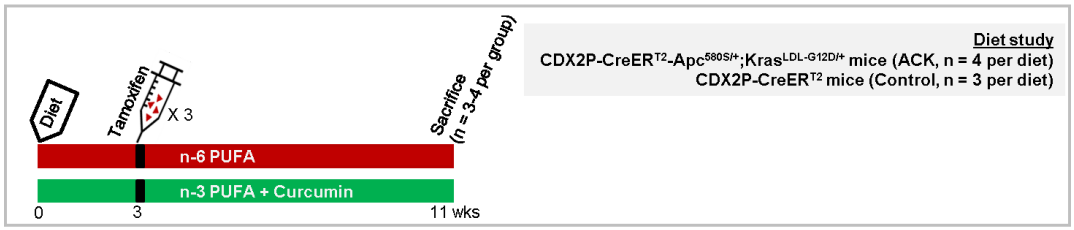

B

Ingredients	Diet (g/100 g)	
	n-6 PUFA	n-3 PUFA + Cur
Sucrose	42	41
Casein	20	20
DL-methionine	0.3	0.3
AIN-76 Mineral mix	3.5	3.5
AIN-76 Vitamin mix	1	1
Choline Chloride	0.2	0.2
Corn Starch	22	22
Cellulose	6	6
Curcumin	0	1
Fish oil	0	4
Corn oil	5	1
Total	100	100

Figure 36. Experimental design and sample preparation. (A) Timeline of the treatments and experimental design. **(B)** Experimental diets.

ACK and control mice were fed either a n-3 PUFA + curcumin containing diet (referred to as n-3 PUFA + Cur) or a n-6 PUFA containing diet (referred to as the n-6 PUFA control diet), and terminated at 8 wks after 3 daily TAM injections (Figure 36A). Samples were collected as described in Figure 25B. Initially, for validation purposes, the effect of n-3 PUFA + Cur on dysplastic foci in ACK mice was assessed. As shown in Figure 37, ACK mice fed n-3 PUFA + Cur diet exhibited a 50% reduction in the number of dysplastic foci as compared to ACK mice fed the control diet.

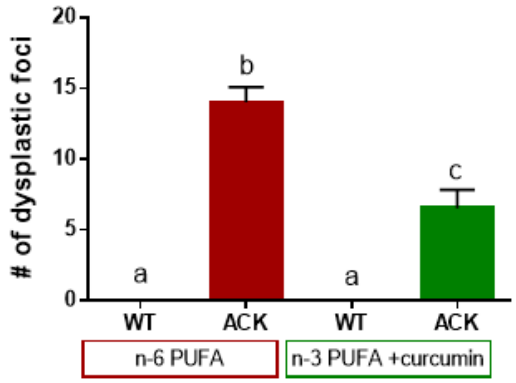

Figure 37. **ACK mice fed n-3 PUFA + Curcumin exhibit a reduced number of dysplastic foci**. CDX2P-CreER^{T2} (WT or control, n=3 per group) and CDX2P-CreER^{T2}-Apc$^{580S/+}$; Kras$^{LSL-G12D/+}$ (ACK, n=4 per group) mice were fed n-3 PUFA + Curcumin (4% fish oil + 1% corn oil + 1% curcumin diet) or n-6 PUFA (5% corn oil diet) for 3 wks prior to TAM injection. Mice were terminated 8 wks following Cre induction. Data from ACK mice fed n-6 PUFA and n-3 PUFA + Cur were normalized to control mice (WT) fed n-6 PUFA and n-3 PUFA + Cur, respectively.

To determine the chemo-protective effect of n-3 PUFA + Cur in ACK mice, the number of EdU$^+$ cells per crypt, proliferative zone and length of crypt were quantified. As expected, n-3 PUFA + Cur feeding reduced the number of EdU$^+$ cells per crypt (Figure 38A), proliferative zone (Figure 38B) and crypt length (Figure 38C) by 30%, 20% and 5 %, respectively, as compared to ACK mice fed the control diet. For control mice (WT), no significant diet effect was detected.

The location of colonic Lgr5 stem cells at the bottom of the crypt is well defined. Sasaki et al. measured LGR5-GFP signal in Lgr5-EGFP-IRES-CreER^{T2} derived live cells and demonstrated that the stem cell zone lies within 35 μm of the bottom of the crypt (Sasaki et al., 2016). In a complementary

study, the Lgr5 stem cells zone in fixed tissue was found within 20 μm of the bottom of the crypt (Kim et al., 2016b). Thus, we defined the stem cell zone as the cells located within 20 μm of the bottom of the crypt. To determine location-specific diet effects, we measured the number of EdU^+ cells in 20 μm segments from the base to the top of crypts in the distal colon. As shown in Figure 38D, no location-specific diet effect in the stem cell zone was detected.

A **B**

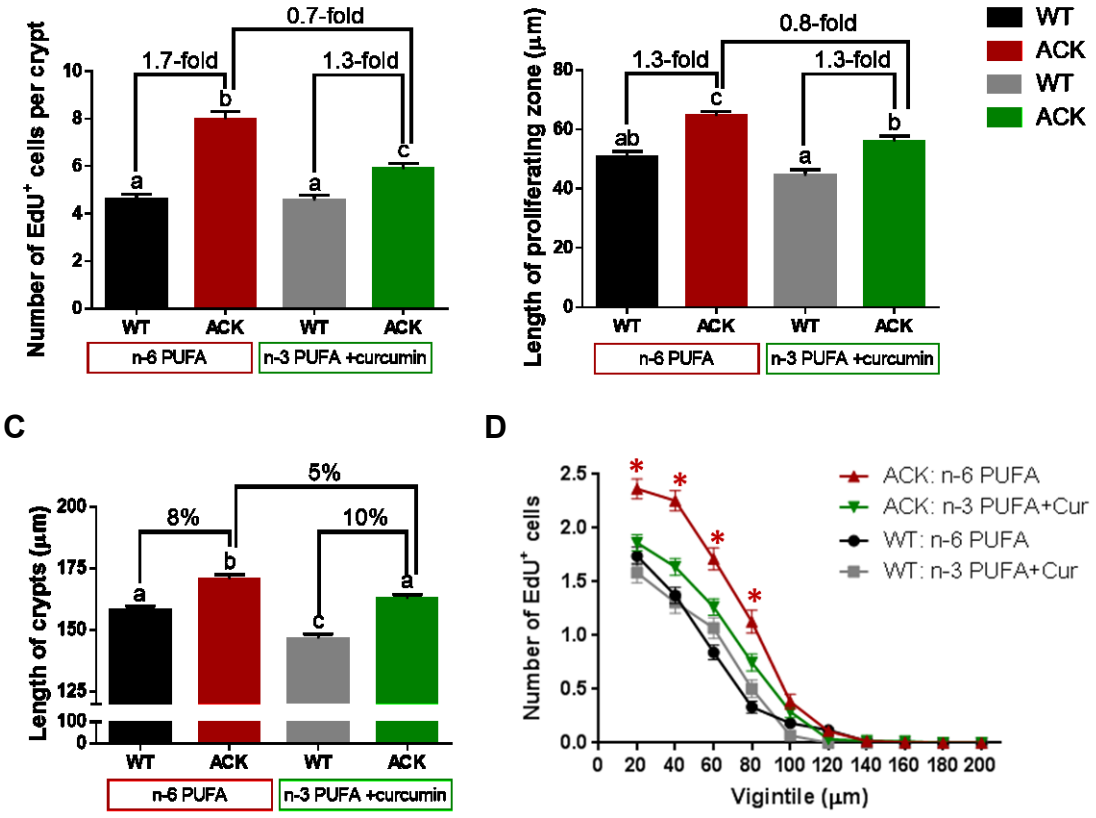

Figure 38. Reduced cell proliferation in ACK mice fed n-3 PUFA + Curcumin. **(A)** Number of proliferating cells (EdU$^+$) per crypt in the distal colon. **(B)** Length of proliferative zone per crypt in the distal colon. **(C)** Length of crypts in the distal colon. **(D)** Number of EdU$^+$ cells in 20 µm intervals along the vertical crypt axis. Refer to Figures 30 and 31 for analytical details.

5.3.8 *Increased plasma membrane order associated with compound Apc^{580D} and Kras^{G12D} mice is ameliorated by n-3 PUFA + curcumin feeding.*

Next, we determined the effect of n-3 PUFA + Cur on plasma membrane properties in colonocytes isolated from ACK mice. As shown in Figure 39A, the increased free cholesterol associated with ACK mice compared to control mice

was reduced (by 50%) following n-3 PUFA + Cur feeding. Figure 39B shows that ACK mice fed n-3 PUFA + Cur as are resistant to change in plasma membrane due to Apc^{580D} and $Kras^{G12D}$ as compared to ACK mice fed a control diet. Changes in plasma membrane order in mice fed n-3 PUFA + Cur were significantly less than n-6 PUFA fed mice (Figure 39B).

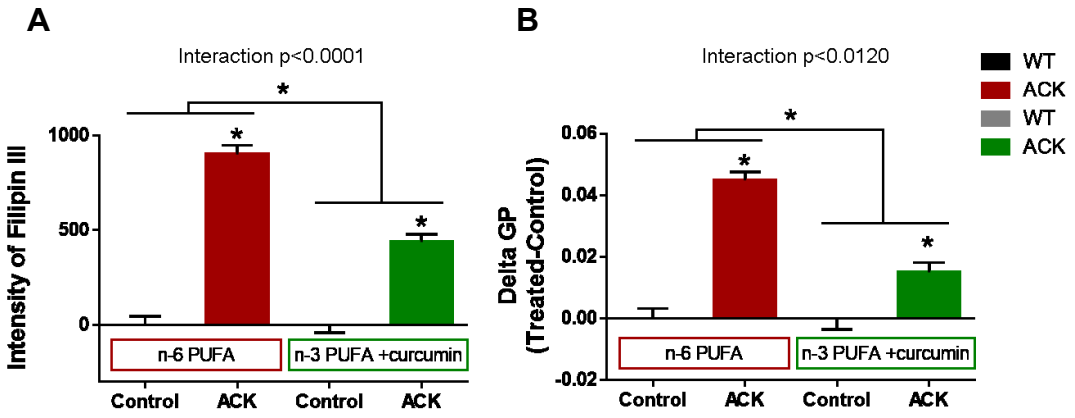

Figure 39. Chemo-protective diet effects on membrane parameters in ACK mice compared to control mice. (A) Cholesterol and **(B)** plasma membrane order of colonocyte from ACK and control mice fed with experiment diet. Mice were terminated at 8 wks after 3 Tamoxifen (TAM, 100 mg/kg body weight) injections. Refer to Figures 30 and 31 for analytical details.

To determine whether n-3 PUFA + Cur diet reduces the positive association between EdU^{+} cell number per crypt and cholesterol level (Figure 40A) and plasma membrane order (Figure 40B), we performed a simple linear regression analysis. As shown in Figure 40B, a positive association of plasma

membrane order and the number of EdU^{+} cells per crypt was found in n-6 PUFA fed mice with a p-value of 0.07. In contrast, the n-3 PUFA + Cur group had a p-value of 0.41.

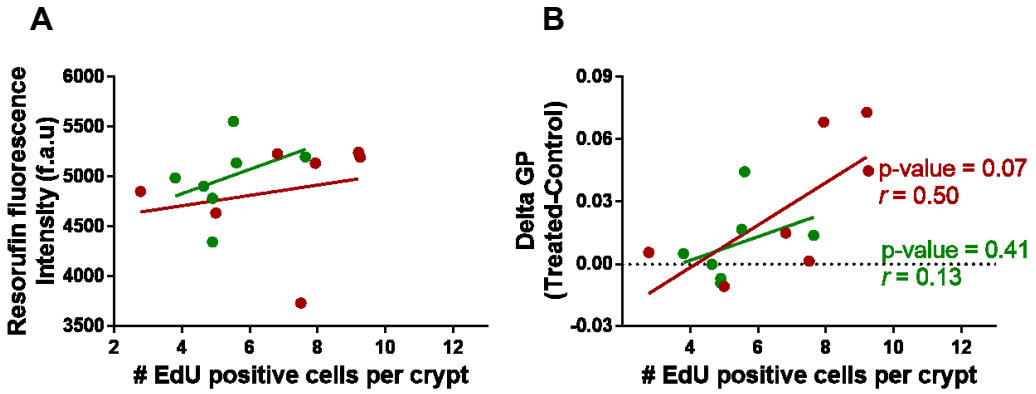

Figure 40. Linear regression analysis. Association between the number of EdU positive cells and cholesterol level **(A)** and association between EdU positive cells and membrane order **(B)**. Mice were terminated at 8 wks after 3 daily Tamoxifen (TAM, 100 mg/kg body weight) injections. Each point represents an individual animal. n-3 PUFA + Cur containing diet is highlighted in green and n-6 PUFA containing diet is labeled with red. ACK and control mice fed same diet were combined for this analysis.

5.3.9 Increased cholesterol and plasma membrane order is not cell type specific effect.

Lgr5-EGFP-IRES-CreER^{T2}-CDX2P-CreER^{T2}-Apc$^{580S/+}$; Kras$^{LSL-G12D/+}$ mice (ACKG, n=3) mice were used to measure the effect of Apc$^{580S/+}$; Kras$^{LSL-G12D/+}$ on cholesterol and plasma membrane order homeostasis. Lgr5-EGFP-IRES-CreER^{T2} (CG, n=3) mice were used as a control (Figure 41A). Mice were provided a Teklad 4% fat rodent diet (Envigo, 7001). ACKG and CG mice were

terminated at 8 wks following 3 daily Tamoxifen (TAM, 100 mg/kg body weight) injections. Live GFP^{high} cells (stem cells) and GFP^{neg} cells (all cells combined) from each mouse were sorted using a MoFlow fluorescent cell sorter. Half of sorted cells were used to measure plasma membrane order and the other half of cells were fixed cells with 4% PFA to measure cholesterol level.

Di-4-ANEPPDHQ dye used for measuring plasma membrane order was excited at 488 nm. Since the EGFP signal from GFP^{high} cells and it emission wave length overlap, 5% laser power was utilized for di-4-ANEPPDHQ dye excitation. As shown in Figure 41B, only di-4-ANEPPDHQ signal is detected at this level. EGFP signal was detectable only when laser power was increased to 50% (GFP-50%).

A

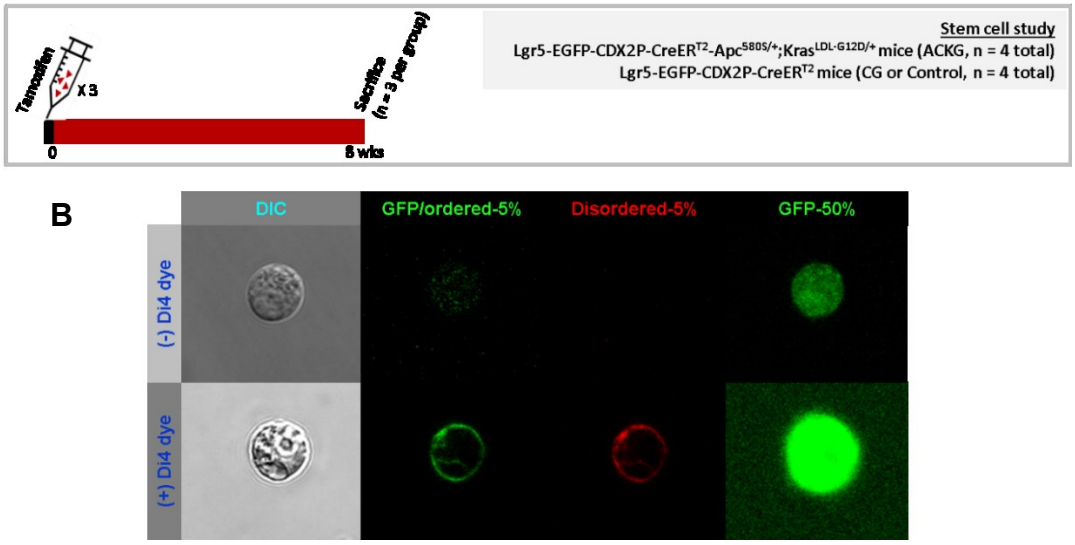

Figure 41. Experimental design and validation. (A) Timeline of the treatments and experimental design. **(B)** Representative confocal images of Lgr5^{+} cell (GFP^{high}) in liquid ordered phase (green line) and liquid disordered phase (red line) using 5% or 50% laser power.

Next, we determined plasma membrane properties of colonic stem cells, i.e., GFP^{high} (Lgr5^{+}), from ACK mice as compared to GFP^{high} cells from control mice. GFP^{neg} cell (all cells combined) from ACK mice were also compared to GFP^{neg} cells from control mice. As shown in Figure 42, altered free cholesterol and plasma membrane order due to inactive Apc and active Kras do not appear to be stem cell (GFP^{high} cell) specific.

A **B**

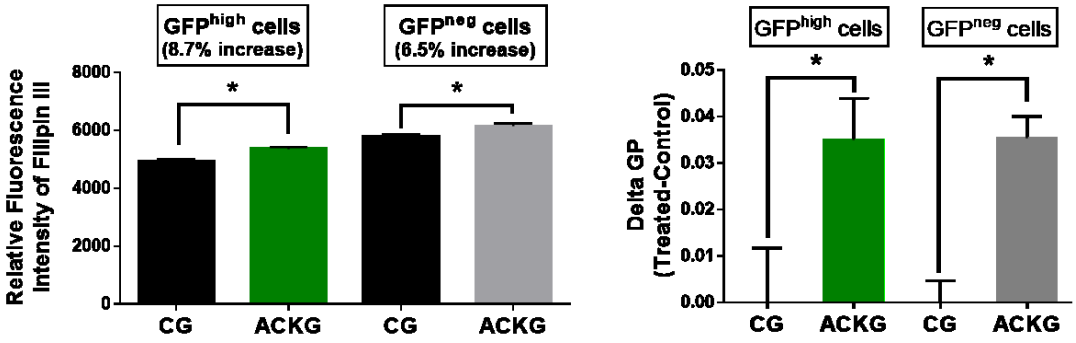

Figure 42. Cholesterol level and plasma membrane order of GFP^{high} and GFP^{neg} cells from ACK mice compared to control (CG) mice. Lgr5-EGFP-CDX2P-CreER^{T2} (CG) and Lgr5-EGFP-CDX2P-CreER^{T2}-Apc$^{580S/+}$; Kras$^{LSL-G12D/+}$ (ACKG) mice were terminated at 8 wks after 3 daily Tamoxifen (TAM, 100 mg/kg body weight) injections. Refer to Figures 31 and 32 for analytical details.

5.2 Discussion

To our knowledge, this is the first time that the effect of Apc and Kras mutations on plasma membrane order in the context of colon tumorigenesis has been assessed. We utilized a novel mouse model, CDX2P-CreER^{T2}-Apc$^{580S/+}$; Kas$^{LSL-G12D/+}$ (ACK), in which Cre expression induced by TAM injection results in the simultaneous deletion of Apc (Apc$^{580D/+}$) and activation of Kras$^{G12D/+}$. ACK mice does not develop tumors in 6 month window post TAM injection but develop dysplastic foci, polyps and some adenomas, indicating that it can be used to study chemo-prevention at the pre-tumor stage.

The role of Apc and Kras mutation in promoting proliferation in colon cancer is well defined. In this study, that the Apc and oncogenic Kras mutations linked to increased cholesterol and plasma membrane order (Figure 30 and

31) are positively associated with cell proliferation (Figure 32). Global transcriptome data provide evidence that that genes involved in cholesterol synthesis (Table 12) and cholesterol uptake (Table 10) are increased in ACK mice as compared to control mice. It is noteworthy, that genes involved in sphingolipid metabolism are not modulated at the mRNA level, suggesting that the altered plasma membrane order observed in this study is in part mediated by effects on cholesterol homeostasis (Table 13).

We next demonstrated that YAMC and IMCE cells respond to exogenous cholesterol by enhancing proliferation in a dose-dependent manner (Figure 33 and 34). Similar results were observed using mouse colonic organoids (Figure 35). These findings suggest that the elevated cell proliferation phenotype observed in ACK mice are in part mediated by increased membrane cholesterol levels. Clearly, further work is required to elucidate the mechanism(s) by which cholesterol modulates plasma membrane-mediated signaling in the presence of oncogenic Apc and Kras.

Cell growth and division rely on new membrane synthesis, which requires energy. Fatty acids (FA) are the main components of phospholipids, which make up cell membranes and triglycerides, the major form of energy storage in the cell. Cholesterol, a lipid sterol derivative, maintains membrane integrity and regulates its fluidity. Given the importance of lipid in cell growth, fatty acid and cholesterol metabolism is strictly regulated in normal cells and

often upregulated in rapidly growing cancer cells (Clendening et al., 2010; Kuhajda et al., 1994; Santos and Schulze, 2012; Yoon et al., 2007).

Early global mapping of Myc target genes has revealed that genes involved in fatty acid metabolism are regulated by Myc (Lin et al., 2012; Priolo et al., 2014; Zeller et al., 2006). Metabolomic analysis also suggests high levels of Myc are linked to elevated fatty acid synthesis (Priolo et al., 2014). In this study, we demonstrate that Myc is increasing cholesterol in part by induce mRNA levels of HMGCR. It is noteworthy because HMGCR is rate-limiting in the cholesterol synthesis pathway; hence, HMGCR has been documented to be essential for Myc-driven liver cancer as it mediates the phosphorylation and transactivation of Myc (Cao et al., 2011). Our data suggest that Myc is a major upstream transcription factor modulating cholesterol homeostasis thereby alters plasma membrane properties.

We have demonstrated that a diet containing 4% fish oil (enriched in n-3 PUFA) combined with 1% curcumin synergistically reduces nuclear/cytosolic β-catenin in aberrant crypt foci (ACF) in the mouse colon (Kim et al., 2016b). Since n-3 PUFA acyl chains impact the organization of the tail group region within plasma membrane (Shaikh et al., 2004; Shaikh et al., 2015; Shaikh et al., 2009a) and curcumin can modify plasma membrane structure by targeting head group region of the phospholipid bilayer (Barry et al., 2009; Hung et al., 2008), we determined whether these bioactives can modulate plasma membrane order. In our study, we found that plasma membrane order induced

by compound Apc^{580D} and $Kras^{G12D}$ mutations is ameliorated by n-3 PUFA + curcumin feeding. Recent evidence further suggests that DHA can perturb lipid rafts (Chapkin et al., 2008; Kim et al., 2008; Shaikh et al., 2009b). DHA, due to its high degree of unsaturation, is sterically incompatible with cholesterol (Wassall et al., 2004), a major constituent of rafts. However, further work is required to pinpoint the mechanism by which n-3 PUFA and curcumin modulate cholesterol, plasma membrane order and plasma membrane-mediated signaling pathways.

In conclusion, our novel data provide evidence that compound Apc^{580D} and $Kras^{G12D}$ mutations mediate perturbations in cholesterol homeostasis, contributing to an increase in plasma membrane order and the promotion of cell proliferation (a colon cancer risk factor). The direct dose-dependent effect of exogenous cholesterol on membrane cholesterol, lipid order and cell proliferation was documented in multiple in vitro models (YAMC, IMCE and organoids). In addition, we provide cogent evidence that dietary bioactive compounds (n-3 PUFA and curcumin) can modulate plasma membrane order. These findings imply that n-3 PUFA and curcumin may suppress tumorigenesis in part by targeting the plasma membrane.

6. SUMMARY AND CONCLUSIONS

6.1 Summary

We have demonstrated that $Lgr5^+$ stem cells, the cells of origin of colon cancer, preferentially promote damage-induced apoptosis in response to carcinogen. n-3 PUFA and curcumin synergize to promote targeted apoptosis of damaged $Lgr5^+$ stem cells in part by enhancing p53 signaling in $Lgr5^+$ stem cells at the tumor initiation stage and reduce nuclear/cytoplasmic β-catenin in ACF, surrogate marker of colon cancer at the pre-tumor stage. $Lgr5^+$ stem cells also respond to low dose combination diet reducing carcinogen-induced DNA damage by enhancing apoptosis, which may lower HED ultimately. Additionally, we found that oncogenic Apc and Kras increase plasma membrane order (fluidity) by perturbing cholesterol homeostasis at pre-tumor stage. Myc was identified as an upstream regulator modulating genes associated with cholesterol homeostasis and cholesterol promotes cell proliferation in dose-dependent manner. We also demonstrated that the altered plasma membrane order and cholesterol homeostasis associated with oncogenic Apc and Kras is ameliorated by n-3 PUFA + curcumin feeding.

6.2 Conclusions

Historically, alkylating agents are known to produce gastrointestinal tumors in rodents (Hawks and Magee, 1974; James and Autrup, 1983) and to cause cancer in humans as a result of lifetime environmental exposures (Hall

et al., 1991). Notably, azoxymethane (AOM) - induced DNA damage is clinically relevant because AOM hyper-activates β-catenin and Kras signaling, which are dysregulated in sporadic colorectal cancer in humans (Hata et al., 2004; Takahashi and Wakabayashi, 2004). Thus, the deletion of damaged cells at the tumor initiation stage is a critical mechanism to prevent tumorigenesis in the intestine (Leibowitz et al., 2014).

Highly ordered lipid rafts (Li et al., 2006b; Patra, 2008) and cholesterol levels (Dessi et al., 1994) are increased in many types of cancer and some drug resistant cancers (Yi et al., 2013). Increased plasma membrane order (decreased membrane fluidity) is positively correlated with cholesterol levels (Montero et al., 2008) and altered membrane fluidity is associated with modulation of plasma membrane-mediated signaling pathways (Cherezov et al., 2007; Simons and Vaz, 2004). However, the link between plasma membrane order and cancer biology is poorly understood.

The transformation of $Lgr5^+$ stem cells drives intestinal neoplasia, indicating that $Lgr5^+$ crypt stem cells are the cell-of-origin of cancer (Barker et al., 2009). Thus, it is important to understand how $Lgr5^+$ stem cells phenotypically respond to AOM (associated with DNA damage response).

Because of the broad-acting effects of n-3 PUFA and curcumin on mammalian physiology, it has been postulated that these dietary fatty acids act at a fundamental level common to all cells from initiation to the pre-tumor stage of colon tumorigenesis, i.e., by promoting cell apoptosis and suppressing

proliferation (Altenburg et al., 2011; Carroll et al., 2011; Jia et al., 2011; Saw et al., 2010; Siddiqui et al., 2013; Swamy et al., 2008; West et al., 2010) and by altering the physical properties of biological membranes (Barry et al., 2009; Chapkin et al., 2008; Hung et al., 2008; Shaikh et al., 2009b; Wassall et al., 2004; Wassall and Stillwell, 2008). A wealth of published literature supports the hypothesis that n-3 PUFA and curcumin play an important role in modulating apoptotic genes as well as plasma membrane fluidity. Despite cogent scientific evidence indicating the protective effect of n-3 PUFA and curcumin, there is a lack of data regarding the additive/synergistic effects of these two dietary components in terms of colon tumorigenesis, especially with respect to $Lgr5^+$ stem cell biology.

In the absence of comprehensive human data, the AOM chemical carcinogenesis model serves as one of the most definitive means of assessing human colon cancer risk (Ahnen, 1985; Reddy, 1994). Therefore, the first portion of the study was designed to determine the response of $Lgr5^+$ stem cells in mice exposed to AOM. We demonstrate that DNA damage occurs to a greater degree in $Lgr5^+$ stem cells (located at the base of the crypt) as compared to differentiated cells. We also demonstrate that colonic $Lgr5^+$ stem cells uniquely respond to AOM by inducing targeted apoptosis, which is positively associated with induced γH2AX, whereas differentiated cells do not exhibit this response. Specifically, “untargeted” apoptosis ($TUNEL^+$, $\gamma H2AX^-$) in $Lgr5^+$ stem cells was 2.2-fold higher than “targeted” apoptosis ($TUNEL^+$,

γH2AX$^+$), implying an inefficient removal of damaged Lgr5$^+$ stem cells via programmed cell death. These observations are important because the deletion of damaged cells is a critical mechanism to prevent tumorigenesis in the intestine (Leibowitz et al., 2014).

To further elucidate the unique properties of colonic Lgr5$^+$ stem cells in terms of their response to bioactive compounds in the presence of carcinogen, the second portion of the study was designed to determine the chemo-protective effects of combinatorial bioactives in AOM-induced DNA damaged Lgr5$^+$ stem cells as compared to differentiated cells. We demonstrate that DNA damaged Lgr5$^+$ stem cells uniquely respond to n-3 PUFA and curcumin, and n-3 PUFA and curcumin synergize to promote the deletion of DNA damaged Lgr5$^+$ stem cell in part by enhancing p53 signaling pathway. This was exemplified, in part, by the induction of Bax at the mRNA and protein levels, a major mediator of p53-mediated apoptosis. These findings are relevant in view of the fact that the absence of an acute apoptotic response to AOM in p53-deficient mice is associated with an increased tumor incidence (Davidson et al., 2015; Hu et al., 2005).

Consistent with these observations, curcumin combined with n-3 PUFA synergistically reduces AOM-induced nuclear β-catenin levels in ACF at the pre-tumor stage. This is noteworthy because elevated nuclear β-catenin levels are associated with higher mortality in selected groups of colorectal cancer patients (Hao et al., 2001; Takayama et al., 2001; Wanitsuwan et al., 2008),

and various attempts have been made to identify and characterize pharmacological inhibitors of β-catenin (Thakur and Mishra, 2013). Consistent with this notion, it has been shown that n-3 PUFA or curcumin reduce polyps or adenoma in Apc mutated mice (Collett et al., 2001; Fini et al., 2010) and inhibit nuclear location of β-catenin in colon cancer cells and breast cancer stem cells (Calviello et al., 2007; Mukherjee et al., 2014).

The daily dose of the experimental chemo-protective diet (4% fish oil + 1% curcumin) was 46 mg of n-3 PUFA and 45 mg of curcumin, which corresponds to an HED of 8.6 g n-3 PUFA + 8.5 g Curcumin. In contrast, corn oil control diets contain only trace amounts of n-3 PUFA and no curcumin. In terms of human consumption, curcumin and n-3 PUFA intake vary greatly. Curcumin C3 Complex (Sabinsa Corporation, NJ, USA) is known to be well tolerated when taken at high doses (12 g/day) (Cheng et al., 2001; Ireson et al., 2002) and the maximal tolerable dose for EPA and DHA is 17.6 g n-3 PUFA/day in humans (Skarke et al., 2015). Therefore, our experimental diets contain quantities of n-3 PUFA and curcumin well within the range that can be consumed in the human diet. However, the HED of n-3 PUFA is higher than the FDA recommended (3g/day) level and curcumin has not yet been approved as a therapeutic agent because of relatively low bioavailability and intense staining color of curcumin (Anand et al., 2007).

To address bioactive dose dependency, we assessed the dietary threshold for phenotypically significant responses by administering lower levels

of n-3 PUFA and curcumin. We demonstrate that the median effective dose (ED_{50}), i.e., the dose that produces a chemo-protective effect in 50% of the subjects (Singh et al., 1999), is 16 mg of n-3 PUFA and 15.9 mg of curcumin. This corresponds to a daily HED of 3.0 g of n-3 PUFA and 3.0 g of curcumin. These finding provides a therapeutic strategy for eliminating damaged stem cells and reducing colon cancer risk in humans by using lower doses of n-3 PUFA and curcumin.

To further elucidate the biophysical properties of plasma membrane in pre tumor stage of colon tumorigenesis, we generated conditional CDX2P-$CreER^{T2}$-$Apc^{580S/+}$; $Kras^{LSL-G12D/+}$ transgenic mice to delineate the mechanism by which oncogenic Apc and Kras modulate colonocyte plasma membrane order. We demonstrate that oncogenic Apc and Kras perturb plasma membrane order (fluidity) by perturbing cholesterol homeostasis, which is associated with elevated levels of cell proliferation. We also analyzed gene expression datasets obtained from the RNAseq. The upstream regulator analysis function of IPA was used to identify potential transcriptional regulators which explain the observed changes in gene expression. Interestingly, Myc was the major upstream regulator modulating cholesterol homeostasis associated genes such as HMGCR and LDLR. This is noteworthy because HMGCR is a rate-limiting step in the cholesterol synthesis pathway. Overall, the knowledge obtained from our studies provides a solid mechanistic underpinning for the role

of Myc in increasing plasma membrane order by modulating cholesterol associated genes.

Our findings raise the possibility that changes in membrane cholesterol status and plasma membrane order may directly regulate cell proliferation in the colon. This is supported by our data demonstrating that cholesterol dose-dependently promotes cell proliferation in YAMC, IMCE and mouse colonic organoid cultures.

We also investigated the effects of chemo-protective dietary agents on cholesterol homeostasis, plasma membrane order and dysplastic foci in CDX2P-CreER^{T2}-Apc$^{580S/+}$; Kras$^{LSL-G12D/+}$ transgenic mice. Our data demonstrate that perturbed plasma membrane order and cholesterol homeostasis as well as dysplastic formation due to compound Apc^{580D} and Kras^{G12D} mutations are ameliorated by n-3 PUFA + curcumin feeding. These findings indicate that n-3 PUFA combined with curcumin modulate plasma membrane order, thereby affecting plasma membrane-mediated signaling resulting in the suppression of dysplastic foci formation. These findings are consistent with the fact that DHA and curcumin are capable of modulating plasma membrane structure and EGFR function (Soung and Chung, 2011; Turk et al., 2012), which regulates colon cancer stem cell proliferation (Feng et al., 2012).

To further elucidate the unique properties of colonic Lgr5^{+} stem cells in response to oncogenic Apc and Kras in terms of cholesterol levels and plasma membrane order, Lgr5-EGFP-IRES-CreER^{T2}-CDX2P-CreER^{T2}-Apc$^{580S/+}$; Kras$^{LSL\text{-}G12D/+}$ mice were used. We demonstrate that altered cholesterol and plasma membrane order due to compound Apc^{580D} and Kras^{G12D} mutations do not appear to be Lgr5^{+} stem cell specific.

In summary, our results indicate for the first time that fish oil plus curcumin synergistically protect Lgr5^{+} stem cells in part by modulating apoptosis during the initiation of tumorigenesis following carcinogen exposure. We have established an HED for curcumin and n-3 PUFA, and propose a novel membrane order related mechanism of action. This body of work is important for overall human health, and will likely assist future researchers in understanding the role that dietary n-3 PUFA and curcumin play in chronic disease prevention.

6.3 Future directions

The research presented herein set the groundwork for a number of future studies that could further delve into the effects of DHA and curcumin on receptor signaling and function.

6.3.1 DNA damage response of Lgr5^{+} stem cells

We demonstrated that Lgr5^{+} stem cells preferentially promote damage-

induced apoptosis in response to carcinogen. Human embryonic stem cells have constitutively active Bax at the Golgi, and active Bax translocates from Golgi to mitochondria after DNA damage in a p53-dependent manner, triggering a rapid apoptotic response (Dumitru et al., 2012). Additionally, AOM-induced apoptosis is p53-dependent whereas spontaneous apoptosis is p53-independent (Hu et al., 2005). Therefore, future studies should focus on whether the induced apoptosis in Lgr5^{+} stem cells is promoted due to p53-dependent mitochondrial priming. This type of study would help delineate how Lgr5^{+} stem cells uniquely respond to external cues.

6.3.2 Mechanism of bystander effect in Lgr5^{+} stem cells

We demonstrated that the majority of apoptosis occurs in undamaged GFP^{high} Lgr5^{+} stem cells following AOM exposure. Based on the proximity of γH2AX^{+} cells to TUNEL^{+}, γH2AX^{-} Lgr5^{+} stem cells, we have proposed the involvement of an AOM-induced bystander effect (BE). This unexpected outcome suggests that undamaged 'bystander' Lgr5^{+} stem cells are being indirectly influenced by the intestinal niche. For example, numerous studies have shown that irradiated/damaged colonic cells can induce secondary apoptosis (Furlong et al., 2013) and γH2AX foci in non-irradiated cells via bystander effects (Dickey et al., 2011). This process, in part, may be mediated by lipid rafts (Burdak-Rothkamm et al., 2007) via the absorption of exosomes by naïve bystander cells (Al-Mayah et al., 2012) or intestinal commensal

bacteria by triggering macrophages (Yang et al., 2013). It is noteworthy that bystander cells exhibit a significant pro-apoptotic gene expression profile compared to cells directly impacted by radiation (Furlong et al., 2013). From a mechanistic perspective, soluble mediators induced by AOM such as PGE_2 may partly mediate this process (Riehl et al., 2006; Zhou et al., 2005). Therefore, future studies should focus on molecules mediating BE to reduce propagation of DNA damage and undesired apoptosis in $Lgr5^+$ stem cells. These proposed experiments would further elucidate the mechanism of the alkylation-induced bystander effects.

6.3.3 Human study

We demonstrated that 1.9% FO + 0.5% CO + 0.46% Cur diet is the lowest dose that exhibits chemo-protective effects in terms of promoting targeted apoptosis in $Lgr5^+$ stem cells. This corresponds to a dose of 21.3 mg n-3 PUFA in combination with 21.1 mg Cur /day or an HED equal to 4.0 g of n-3 PUFA and 4.0 g of curcumin. However, the efficacy of n-3 PUFA and curcumin in preventing colon cancer must still be evaluated in prospective controlled human trials using ACF or adenoma recurrence as the intermediate end point.

6.3.4 Mechanism(s) by which cholesterol modulates plasma membrane-mediated signaling

We demonstrated that YAMC and IMCE cells respond to exogenous cholesterol by enhancing proliferation in a dose-dependent manner. Similar results were observed using mouse colonic organoids. These findings suggest that the elevated cell proliferation phenotype observed in ACK mice is in part mediated by increased membrane cholesterol levels. Clearly, further work is required to elucidate the mechanism(s) by which cholesterol modulates plasma membrane-mediated signaling in the presence of oncogenic Apc and Kras.

6.3.5 Mechanism by which n-3 PUFA and curcumin modulate plasma membrane order

In our study, we found that plasma membrane order induced by compound Apc^{580D} and $Kras^{G12D}$ mutations is ameliorated by n-3 PUFA + curcumin feeding. Recent evidence suggests that both DHA and curcumin are capable of modulating plasma membrane structure and EGFR function (Soung and Chung, 2011; Turk et al., 2012), which regulate colon cancer stem cell proliferation (Feng et al., 2012). Therefore, future studies should focus on the mechanism by which n-3 PUFA and curcumin modulate cholesterol, plasma membrane order and plasma membrane-mediated signaling pathways. It also important to determine whether low doses of n-PUFA and curcumin

exhibit similar effects in terms of modulating plasma membrane order and plasma membrane-mediated signaling pathways.

REFERENCES

Ahnen, D.J. (1985). Are animal models of colon cancer relevant to human disease. Digestive diseases and sciences *30*, 103S-106S.

Al-Mayah, A.H., Irons, S.L., Pink, R.C., Carter, D.R., and Kadhim, M.A. (2012). Possible role of exosomes containing RNA in mediating nontargeted effect of ionizing radiation. Radiation research *177*, 539-545.

Altenburg, J.D., Bieberich, A.A., Terry, C., Harvey, K.A., Vanhorn, J.F., Xu, Z., Jo Davisson, V., and Siddiqui, R.A. (2011). A synergistic antiproliferation effect of curcumin and docosahexaenoic acid in SK-BR-3 breast cancer cells: unique signaling not explained by the effects of either compound alone. BMC cancer *11*, 149.

Altmann, G.G. (1983). Morphological observations on mucus-secreting nongoblet cells in the deep crypts of the rat ascending colon. Am J Anat *167*, 95-117.

Amado, R.G., Wolf, M., Peeters, M., Van Cutsem, E., Siena, S., Freeman, D.J., Juan, T., Sikorski, R., Suggs, S., Radinsky, R.*, et al.* (2008). Wild-type KRAS is required for panitumumab efficacy in patients with metastatic colorectal cancer. Journal of clinical oncology : official journal of the American Society of Clinical Oncology *26*, 1626-1634.

Anand, P., Kunnumakkara, A.B., Newman, R.A., and Aggarwal, B.B. (2007). Bioavailability of curcumin: problems and promises. Mol Pharm *4*, 807-818.

Anti, M., Armelao, F., Marra, G., Percesepe, A., Bartoli, G.M., Palozza, P., Parrella, P., Canetta, C., Gentiloni, N., De Vitis, I.*, et al.* (1994). Effects of different doses of fish oil on rectal cell proliferation in patients with sporadic colonic adenomas. Gastroenterology *107*, 1709-1718.

Asfaha, S., Hayakawa, Y., Muley, A., Stokes, S., Graham, T.A., Ericksen, R.E., Westphalen, C.B., von Burstin, J., Mastracci, T.L., Worthley, D.L.*, et al.* (2015). Krt19(+)/Lgr5(-) Cells Are Radioresistant Cancer-Initiating Stem Cells in the Colon and Intestine. Cell stem cell *16*, 627-638.

Ashton, G.H., Morton, J.P., Myant, K., Phesse, T.J., Ridgway, R.A., Marsh, V., Wilkins, J.A., Athineos, D., Muncan, V., Kemp, R.*, et al.* (2010). Focal adhesion kinase is required for intestinal regeneration and tumorigenesis downstream of Wnt/c-Myc signaling. Dev Cell *19*, 259-269.

Attie, A.D. (2007). ABCA1: at the nexus of cholesterol, HDL and atherosclerosis. Trends Biochem Sci *32*, 172-179.

Avery, O.T., Macleod, C.M., and McCarty, M. (2000). Studies on the chemical nature of the substance inducing transformation of pneumococcal types: Induction of transformation by a desoxyribonucleic acid fraction isolated from Pneumococcus type III. Oswald Theodore Avery (1877-1955). Clin Orthop Relat Res, S3-8.

Bailey, C.E., Hu, C.Y., You, Y.N., Bednarski, B.K., Rodriguez-Bigas, M.A., Skibber, J.M., Cantor, S.B., and Chang, G.J. (2015). Increasing disparities in the age-related incidences of colon and rectal cancers in the United States, 1975-2010. JAMA Surg *150*, 17-22.

Ballschmiter, K. (2003). Pattern and sources of naturally produced organohalogens in the marine environment: biogenic formation of organohalogens. Chemosphere *52*, 313-324.

Barker, N., and Clevers, H. (2007). Tracking down the stem cells of the intestine: strategies to identify adult stem cells. Gastroenterology *133*, 1755-1760.

Barker, N., and Clevers, H. (2010). Leucine-rich repeat-containing G-protein-coupled receptors as markers of adult stem cells. Gastroenterology *138*, 1681-1696.

Barker, N., Huch, M., Kujala, P., van de Wetering, M., Snippert, H.J., van Es, J.H., Sato, T., Stange, D.E., Begthel, H., van den Born, M.*, et al.* (2010). Lgr5(+ve) stem cells drive self-renewal in the stomach and build long-lived gastric units in vitro. Cell Stem Cell *6*, 25-36.

Barker, N., Ridgway, R.A., van Es, J.H., van de Wetering, M., Begthel, H., van den Born, M., Danenberg, E., Clarke, A.R., Sansom, O.J., and Clevers, H. (2009). Crypt stem cells as the cells-of-origin of intestinal cancer. Nature *457*, 608-611.

Barker, N., van Es, J.H., Kuipers, J., Kujala, P., van den Born, M., Cozijnsen, M., Haegebarth, A., Korving, J., Begthel, H., Peters, P.J., *et al.* (2007). Identification of stem cells in small intestine and colon by marker gene Lgr5. Nature *449*, 1003-1007.

Barry, J., Fritz, M., Brender, J.R., Smith, P.E., Lee, D.K., and Ramamoorthy, A. (2009). Determining the effects of lipophilic drugs on membrane structure by solid-state NMR spectroscopy: the case of the antioxidant curcumin. J Am Chem Soc *131*, 4490-4498.

Becker, K., Dosch, J., Gregel, C.M., Martin, B.A., and Kaina, B. (1996). Targeted expression of human O(6)-methylguanine-DNA methyltransferase (MGMT) in transgenic mice protects against tumor initiation in two-stage skin carcinogenesis. Cancer research *56*, 3244-3249.

Beneteau, M., Pizon, M., Chaigne-Delalande, B., Daburon, S., Moreau, P., De Giorgi, F., Ichas, F., Rebillard, A., Dimanche-Boitrel, M.T., Taupin, J.L., *et al.* (2008). Localization of Fas/CD95 into the lipid rafts on down-modulation of the phosphatidylinositol 3-kinase signaling pathway. Mol Cancer Res *6*, 604-613.

Beranek, D.T. (1990). Distribution of methyl and ethyl adducts following alkylation with monofunctional alkylating agents. Mutation research *231*, 11-30.

Beroukhim, R., Mermel, C.H., Porter, D., Wei, G., Raychaudhuri, S., Donovan, J., Barretina, J., Boehm, J.S., Dobson, J., Urashima, M., *et al.* (2010).

The landscape of somatic copy-number alteration across human cancers. Nature *463*, 899-905.

Beyaz, S., Mana, M.D., Roper, J., Kedrin, D., Saadatpour, A., Hong, S.J., Bauer-Rowe, K.E., Xifaras, M.E., Akkad, A., Arias, E.*, et al.* (2016). High-fat diet enhances stemness and tumorigenicity of intestinal progenitors. Nature *531*, 53-58.

Bhanja, P., Saha, S., Kabarriti, R., Liu, L., Roy-Chowdhury, N., Roy-Chowdhury, J., Sellers, R.S., Alfieri, A.A., and Guha, C. (2009). Protective role of R-spondin1, an intestinal stem cell growth factor, against radiation-induced gastrointestinal syndrome in mice. PloS one *4*, e8014.

Bleeker, W.A., Hayes, V.M., Karrenbeld, A., Hofstra, R.M., Hermans, J., Buys, C.C., and Plukker, J.T. (2000). Impact of KRAS and TP53 mutations on survival in patients with left- and right-sided Dukes' C colon cancer. Am J Gastroenterol *95*, 2953-2957.

Blough, M.D., Zlatescu, M.C., and Cairncross, J.G. (2007). O6-methylguanine-DNA methyltransferase regulation by p53 in astrocytic cells. Cancer research *67*, 580-584.

Boldogh, I., Ramana, C.V., Chen, Z., Biswas, T., Hazra, T.K., Grosch, S., Grombacher, T., Mitra, S., and Kaina, B. (1998). Regulation of expression of the DNA repair gene O6-methylguanine-DNA methyltransferase via protein kinase C-mediated signaling. Cancer research *58*, 3950-3956.

Bondi, J., Husdal, A., Bukholm, G., Nesland, J.M., Bakka, A., and Bukholm, I.R. (2005). Expression and gene amplification of primary (A, B1, D1, D3, and E) and secondary (C and H) cyclins in colon adenocarcinomas and correlation with patient outcome. J Clin Pathol *58*, 509-514.

Boudreau, D.M., Gardner, J.S., Malone, K.E., Heckbert, S.R., Blough, D.K., and Daling, J.R. (2004). The association between 3-hydroxy-3-methylglutaryl conenzyme A inhibitor use and breast carcinoma risk among postmenopausal women: a case-control study. Cancer *100*, 2308-2316.

Brodeur, G.M., Seeger, R.C., Schwab, M., Varmus, H.E., and Bishop, J.M. (1984). Amplification of N-myc in untreated human neuroblastomas correlates with advanced disease stage. Science *224*, 1121-1124.

Buchanan, F.G., Holla, V., Katkuri, S., Matta, P., and DuBois, R.N. (2007). Targeting cyclooxygenase-2 and the epidermal growth factor receptor for the prevention and treatment of intestinal cancer. Cancer research *67*, 9380-9388.

Burdak-Rothkamm, S., Short, S.C., Folkard, M., Rothkamm, K., and Prise, K.M. (2007). ATR-dependent radiation-induced gamma H2AX foci in bystander primary human astrocytes and glioma cells. Oncogene *26*, 993-1002.

Cai, T., Li, X., Ding, J., Luo, W., Li, J., and Huang, C. (2011). A cross-talk between NFAT and NF-kappaB pathways is crucial for nickel-induced COX-2 expression in Beas-2B cells. Curr Cancer Drug Targets *11*, 548-559.

Calviello, G., Resci, F., Serini, S., Piccioni, E., Toesca, A., Boninsegna, A., Monego, G., Ranelletti, F.O., and Palozza, P. (2007). Docosahexaenoic acid induces proteasome-dependent degradation of beta-catenin, down-regulation of survivin and apoptosis in human colorectal cancer cells not expressing COX-2. Carcinogenesis *28*, 1202-1209.

Cao, Z., Fan-Minogue, H., Bellovin, D.I., Yevtodiyenko, A., Arzeno, J., Yang, Q., Gambhir, S.S., and Felsher, D.W. (2011). MYC phosphorylation, activation, and tumorigenic potential in hepatocellular carcinoma are regulated by HMG-CoA reductase. Cancer research *71*, 2286-2297.

Cardwell, C.R., Hicks, B.M., Hughes, C., and Murray, L.J. (2014). Statin use after colorectal cancer diagnosis and survival: a population-based cohort study. Journal of clinical oncology : official journal of the American Society of Clinical Oncology *32*, 3177-3183.

Carmon, K.S., Gong, X., Lin, Q., Thomas, A., and Liu, Q. (2011). R-spondins function as ligands of the orphan receptors LGR4 and LGR5 to regulate Wnt/beta-catenin signaling. Proceedings of the National Academy of Sciences of the United States of America *108*, 11452-11457.

Carroll, R.E., Benya, R.V., Turgeon, D.K., Vareed, S., Neuman, M., Rodriguez, L., Kakarala, M., Carpenter, P.M., McLaren, C., Meyskens, F.L., Jr.*, et al.* (2011). Phase IIa clinical trial of curcumin for the prevention of colorectal neoplasia. Cancer prevention research *4*, 354-364.

Castedo, M., Perfettini, J.L., Roumier, T., and Kroemer, G. (2002). Cyclin-dependent kinase-1: linking apoptosis to cell cycle and mitotic catastrophe. Cell Death Differ *9*, 1287-1293.

Cauley, J.A., Zmuda, J.M., Lui, L.Y., Hillier, T.A., Ness, R.B., Stone, K.L., Cummings, S.R., and Bauer, D.C. (2003). Lipid-lowering drug use and breast cancer in older women: a prospective study. J Womens Health (Larchmt) *12*, 749-756.

Chambers, A.F., Groom, A.C., and MacDonald, I.C. (2002). Dissemination and growth of cancer cells in metastatic sites. Nature reviews Cancer *2*, 563-572.

Chandler, J.M., and Lagasse, E. (2010). Cancerous stem cells: deviant stem cells with cancer-causing misbehavior. Stem cell research & therapy *1*, 13.

Chang, W.L., Chapkin, R.S., and Lupton, J.R. (1998). Fish oil blocks azoxymethane-induced rat colon tumorigenesis by increasing cell differentiation and apoptosis rather than decreasing cell proliferation. The Journal of nutrition *128*, 491-497.

Chapkin, R.S., Hong, M.Y., Fan, Y.Y., Davidson, L.A., Sanders, L.M., Henderson, C.E., Barhoumi, R., Burghardt, R.C., Turner, N.D., and Lupton, J.R. (2002). Dietary n-3 PUFA alter colonocyte mitochondrial membrane composition and function. Lipids *37*, 193-199.

Chapkin, R.S., and Lupton, J.R. (1999). Colonic cell proliferation and apoptosis in rodent species. Modulation by diet. Advances in experimental medicine and biology *470*, 105-118.

Chapkin, R.S., McMurray, D.N., Davidson, L.A., Patil, B.S., Fan, Y.Y., and Lupton, J.R. (2008). Bioactive dietary long-chain fatty acids: emerging mechanisms of action. The British journal of nutrition *100*, 1152-1157.

Charalambous, M.P., Maihofner, C., Bhambra, U., Lightfoot, T., Gooderham, N.J., and Colorectal Cancer Study, G. (2003). Upregulation of cyclooxygenase-2 is accompanied by increased expression of nuclear factor-kappa B and I kappa B kinase-alpha in human colorectal cancer epithelial cells. British journal of cancer *88*, 1598-1604.

Chen, A., Xu, J., and Johnson, A.C. (2006). Curcumin inhibits human colon cancer cell growth by suppressing gene expression of epidermal growth factor receptor through reducing the activity of the transcription factor Egr-1. Oncogene *25*, 278-287.

Chen, E.C., Karl, T.A., Kalisky, T., Gupta, S.K., O'Brien, C.A., Longacre, T.A., van de Rijn, M., Quake, S.R., Clarke, M.F., and Rothenberg, M.E. (2015). KIT Signaling Promotes Growth of Colon Xenograft Tumors in Mice and Is Up-Regulated in a Subset of Human Colon Cancers. Gastroenterology *149*, 705-717 e702.

Cheng, A.L., Hsu, C.H., Lin, J.K., Hsu, M.M., Ho, Y.F., Shen, T.S., Ko, J.Y., Lin, J.T., Lin, B.R., Ming-Shiang, W.*, et al.* (2001). Phase I clinical trial of

curcumin, a chemopreventive agent, in patients with high-risk or pre-malignant lesions. Anticancer research *21*, 2895-2900.

Cherezov, V., Rosenbaum, D.M., Hanson, M.A., Rasmussen, S.G., Thian, F.S., Kobilka, T.S., Choi, H.J., Kuhn, P., Weis, W.I., Kobilka, B.K.*, et al.* (2007). High-resolution crystal structure of an engineered human beta2-adrenergic G protein-coupled receptor. Science *318*, 1258-1265.

Cherukuri, D.P., Goulet, A.C., Inoue, H., and Nelson, M.A. (2005). Selenomethionine regulates cyclooxygenase-2 (COX-2) expression through nuclear factor-kappa B (NF-kappaB) in colon cancer cells. Cancer biology & therapy *4*, 175-180.

Ciccia, A., and Elledge, S.J. (2010). The DNA damage response: making it safe to play with knives. Molecular cell *40*, 179-204.

Clendening, J.W., Pandyra, A., Boutros, P.C., El Ghamrasni, S., Khosravi, F., Trentin, G.A., Martirosyan, A., Hakem, A., Hakem, R., Jurisica, I.*, et al.* (2010). Dysregulation of the mevalonate pathway promotes transformation. Proceedings of the National Academy of Sciences of the United States of America *107*, 15051-15056.

Clevers, H. (2013). The intestinal crypt, a prototype stem cell compartment. Cell *154*, 274-284.

Colak, S., Zimberlin, C.D., Fessler, E., Hogdal, L., Prasetyanti, P.R., Grandela, C.M., Letai, A., and Medema, J.P. (2014). Decreased mitochondrial

priming determines chemoresistance of colon cancer stem cells. Cell Death Differ *21*, 1170-1177.

Collett, G.P., Robson, C.N., Mathers, J.C., and Campbell, F.C. (2001). Curcumin modifies Apc(min) apoptosis resistance and inhibits 2-amino 1-methyl-6-phenylimidazo[4,5-b]pyridine (PhIP) induced tumour formation in Apc(min) mice. Carcinogenesis *22*, 821-825.

Colussi, C., Fiumicino, S., Giuliani, A., Rosini, S., Musiani, P., Macri, C., Potten, C.S., Crescenzi, M., and Bignami, M. (2001). 1,2-Dimethylhydrazine-induced colon carcinoma and lymphoma in msh2(-/-) mice. Journal of the National Cancer Institute *93*, 1534-1540.

Coquerelle, T., Dosch, J., and Kaina, B. (1995). Overexpression of N-methylpurine-DNA glycosylase in Chinese hamster ovary cells renders them more sensitive to the production of chromosomal aberrations by methylating agents--a case of imbalanced DNA repair. Mutation research *336*, 9-17.

Corpet, D.E., and Pierre, F. (2005). How good are rodent models of carcinogenesis in predicting efficacy in humans? A systematic review and meta-analysis of colon chemoprevention in rats, mice and men. Eur J Cancer *41*, 1911-1922.

Cuomo, J., Appendino, G., Dern, A.S., Schneider, E., McKinnon, T.P., Brown, M.J., Togni, S., and Dixon, B.M. (2011). Comparative absorption of a standardized curcuminoid mixture and its lecithin formulation. Journal of natural products *74*, 664-669.

Dalerba, P., Kalisky, T., Sahoo, D., Rajendran, P.S., Rothenberg, M.E., Leyrat, A.A., Sim, S., Okamoto, J., Johnston, D.M., Qian, D.*, et al.* (2011). Single-cell dissection of transcriptional heterogeneity in human colon tumors. Nat Biotechnol *29*, 1120-1127.

Dang, C.V. (2012). MYC on the path to cancer. Cell *149*, 22-35.

Dasari, A., and Messersmith, W.A. (2010). New strategies in colorectal cancer: biomarkers of response to epidermal growth factor receptor monoclonal antibodies and potential therapeutic targets in phosphoinositide 3-kinase and mitogen-activated protein kinase pathways. Clinical cancer research : an official journal of the American Association for Cancer Research *16*, 3811-3818.

Davidson, L.A., Callaway, E.S., Kim, E., Weeks, B.R., Fan, Y.Y., Allred, C.D., and Chapkin, R.S. (2015). Targeted Deletion of p53 in Lgr5-Expressing Intestinal Stem Cells Promotes Colon Tumorigenesis in a Preclinical Model of Colitis-Associated Cancer. Cancer research *75*, 5392-5397.

de Lau, W., Barker, N., Low, T.Y., Koo, B.K., Li, V.S., Teunissen, H., Kujala, P., Haegebarth, A., Peters, P.J., van de Wetering, M.*, et al.* (2011). Lgr5 homologues associate with Wnt receptors and mediate R-spondin signalling. Nature *476*, 293-297.

de Lau, W., Peng, W.C., Gros, P., and Clevers, H. (2014). The R-spondin/Lgr5/Rnf43 module: regulator of Wnt signal strength. Genes & development *28*, 305-316.

Dean, M., Fojo, T., and Bates, S. (2005). Tumour stem cells and drug resistance. Nature reviews Cancer *5*, 275-284.

Deans, A.J., and West, S.C. (2011). DNA interstrand crosslink repair and cancer. Nature reviews Cancer *11*, 467-480.

DeClercq, V., McMurray, D.N., and Chapkin, R.S. (2015). Obesity promotes colonic stem cell expansion during cancer initiation. Cancer letters *369*, 336-343.

Deng, G., Bell, I., Crawley, S., Gum, J., Terdiman, J.P., Allen, B.A., Truta, B., Sleisenger, M.H., and Kim, Y.S. (2004). BRAF mutation is frequently present in sporadic colorectal cancer with methylated hMLH1, but not in hereditary nonpolyposis colorectal cancer. Clinical cancer research : an official journal of the American Association for Cancer Research *10*, 191-195.

Deschner, E.E., and Long, F.C. (1977). Colonic neoplasms in mice produced with six injections of 1,2-dimethylhydrazine. Oncology *34*, 255-257.

Dessi, S., Batetta, B., Pulisci, D., Spano, O., Anchisi, C., Tessitore, L., Costelli, P., Baccino, F.M., Aroasio, E., and Pani, P. (1994). Cholesterol content in tumor tissues is inversely associated with high-density lipoprotein cholesterol in serum in patients with gastrointestinal cancer. Cancer *73*, 253-258.

DeVita, V.T., Jr., Young, R.C., and Canellos, G.P. (1975). Combination versus single agent chemotherapy: a review of the basis for selection of drug treatment of cancer. Cancer *35*, 98-110.

Di Fiore, F., Blanchard, F., Charbonnier, F., Le Pessot, F., Lamy, A., Galais, M.P., Bastit, L., Killian, A., Sesboue, R., Tuech, J.J.*, et al.* (2007). Clinical relevance of KRAS mutation detection in metastatic colorectal cancer treated by Cetuximab plus chemotherapy. British journal of cancer *96*, 1166-1169.

Di Gregorio, C., Losi, L., Fante, R., Modica, S., Ghidoni, M., Pedroni, M., Tamassia, M.G., Gafa, L., Ponz de Leon, M., and Roncucci, L. (1997). Histology of aberrant crypt foci in the human colon. Histopathology *30*, 328-334.

Dickey, J.S., Zemp, F.J., Altamirano, A., Sedelnikova, O.A., Bonner, W.M., and Kovalchuk, O. (2011). H2AX phosphorylation in response to DNA double-strand break formation during bystander signalling: effect of microRNA knockdown. Radiation protection dosimetry *143*, 264-269.

Dienstmann, R., and Tabernero, J. (2011). BRAF as a target for cancer therapy. Anticancer Agents Med Chem *11*, 285-295.

Donnenberg, V.S., and Donnenberg, A.D. (2005). Multiple drug resistance in cancer revisited: the cancer stem cell hypothesis. Journal of clinical pharmacology *45*, 872-877.

Dow, L.E., O'Rourke, K.P., Simon, J., Tschaharganeh, D.F., van Es, J.H., Clevers, H., and Lowe, S.W. (2015). Apc Restoration Promotes Cellular Differentiation and Reestablishes Crypt Homeostasis in Colorectal Cancer. Cell *161*, 1539-1552.

Downs, J.R., Clearfield, M., Weis, S., Whitney, E., Shapiro, D.R., Beere, P.A., Langendorfer, A., Stein, E.A., Kruyer, W., and Gotto, A.M., Jr. (1998). Primary prevention of acute coronary events with lovastatin in men and women with average cholesterol levels: results of AFCAPS/TexCAPS. Air Force/Texas Coronary Atherosclerosis Prevention Study. Jama *279*, 1615-1622.

Duckett, D.R., Drummond, J.T., Murchie, A.I., Reardon, J.T., Sancar, A., Lilley, D.M., and Modrich, P. (1996). Human MutSalpha recognizes damaged DNA base pairs containing O6-methylguanine, O4-methylthymine, or the cisplatin-d(GpG) adduct. Proceedings of the National Academy of Sciences of the United States of America *93*, 6443-6447.

Dumitru, R., Gama, V., Fagan, B.M., Bower, J.J., Swahari, V., Pevny, L.H., and Deshmukh, M. (2012). Human embryonic stem cells have constitutively active Bax at the Golgi and are primed to undergo rapid apoptosis. Mol Cell *46*, 573-583.

Erisman, M.D., Rothberg, P.G., Diehl, R.E., Morse, C.C., Spandorfer, J.M., and Astrin, S.M. (1985). Deregulation of c-myc gene expression in human colon carcinoma is not accompanied by amplification or rearrangement of the gene. Mol Cell Biol *5*, 1969-1976.

Esteller, M., Toyota, M., Sanchez-Cespedes, M., Capella, G., Peinado, M.A., Watkins, D.N., Issa, J.P., Sidransky, D., Baylin, S.B., and Herman, J.G. (2000). Inactivation of the DNA repair gene O6-methylguanine-DNA

methyltransferase by promoter hypermethylation is associated with G to A mutations in K-ras in colorectal tumorigenesis. Cancer research *60*, 2368-2371.

Fan, X.S., Wu, H.Y., Yu, H.P., Zhou, Q., Zhang, Y.F., and Huang, Q. (2010). Expression of Lgr5 in human colorectal carcinogenesis and its potential correlation with beta-catenin. International journal of colorectal disease *25*, 583-590.

Fan, Y.Y., Davidson, L.A., Callaway, E.S., Goldsby, J.S., and Chapkin, R.S. (2014). Differential effects of 2- and 3-series E-prostaglandins on in vitro expansion of Lgr5+ colonic stem cells. Carcinogenesis *35*, 606-612.

Fan, Y.Y., McMurray, D.N., Ly, L.H., and Chapkin, R.S. (2003). Dietary (n-3) polyunsaturated fatty acids remodel mouse T-cell lipid rafts. The Journal of nutrition *133*, 1913-1920.

Fearon, E.R., and Vogelstein, B. (1990). A genetic model for colorectal tumorigenesis. Cell *61*, 759-767.

Femia, A.P., and Caderni, G. (2008). Rodent models of colon carcinogenesis for the study of chemopreventive activity of natural products. Planta medica *74*, 1602-1607.

Feng, Y., Dai, X., Li, X., Wang, H., Liu, J., Zhang, J., Du, Y., and Xia, L. (2012). EGF signalling pathway regulates colon cancer stem cell proliferation and apoptosis. Cell Prolif *45*, 413-419.

Fevr, T., Robine, S., Louvard, D., and Huelsken, J. (2007). Wnt/beta-catenin is essential for intestinal homeostasis and maintenance of intestinal stem cells. Mol Cell Biol *27*, 7551-7559.

Fiala, E.S. (1977). Investigations into the metabolism and mode of action of the colon carcinogens 1,2-dimethylhydrazine and azoxymethane. Cancer *40*, 2436-2445.

Fini, L., Piazzi, G., Ceccarelli, C., Daoud, Y., Belluzzi, A., Munarini, A., Graziani, G., Fogliano, V., Selgrad, M., Garcia, M.*, et al.* (2010). Highly purified eicosapentaenoic acid as free fatty acids strongly suppresses polyps in Apc(Min/+) mice. Clinical cancer research : an official journal of the American Association for Cancer Research *16*, 5703-5711.

Fitzgerald, J.B., Schoeberl, B., Nielsen, U.B., and Sorger, P.K. (2006). Systems biology and combination therapy in the quest for clinical efficacy. Nature chemical biology *2*, 458-466.

Furlong, H., Mothersill, C., Lyng, F.M., and Howe, O. (2013). Apoptosis is signalled early by low doses of ionising radiation in a radiation-induced bystander effect. Mutation research *741-742*, 35-43.

Gajate, C., and Mollinedo, F. (2011). Lipid rafts and Fas/CD95 signaling in cancer chemotherapy. Recent patents on anti-cancer drug discovery *6*, 274-283.

Gama, V., and Deshmukh, M. (2012). Human embryonic stem cells: living on the edge. Cell cycle *11*, 3905-3906.

Gawrisch, K., Soubias, O., and Mihailescu, M. (2008). Insights from biophysical studies on the role of polyunsaturated fatty acids for function of G-protein coupled membrane receptors. Prostaglandins, leukotrienes, and essential fatty acids *79*, 131-134.

Gerson, S.L., Allay, E., Vitantonio, K., and Dumenco, L.L. (1995). Determinants of O6-alkylguanine-DNA alkyltransferase activity in human colon cancer. Clinical cancer research : an official journal of the American Association for Cancer Research *1*, 519-525.

Glinka, A., Dolde, C., Kirsch, N., Huang, Y.L., Kazanskaya, O., Ingelfinger, D., Boutros, M., Cruciat, C.M., and Niehrs, C. (2011). LGR4 and LGR5 are R-spondin receptors mediating Wnt/beta-catenin and Wnt/PCP signalling. EMBO Rep *12*, 1055-1061.

Glinka, A., Wu, W., Delius, H., Monaghan, A.P., Blumenstock, C., and Niehrs, C. (1998). Dickkopf-1 is a member of a new family of secreted proteins and functions in head induction. Nature *391*, 357-362.

Go, G.W., and Mani, A. (2012). Low-density lipoprotein receptor (LDLR) family orchestrates cholesterol homeostasis. Yale J Biol Med *85*, 19-28.

Goldstein, J.L., and Brown, M.S. (1990). Regulation of the mevalonate pathway. Nature *343*, 425-430.

Gouw, A.M., Eberlin, L.S., Margulis, K., Sullivan, D.K., Toal, G.G., Tong, L., Zare, R.N., and Felsher, D.W. (2017). Oncogene KRAS activates fatty acid synthase, resulting in specific ERK and lipid signatures associated with lung

adenocarcinoma. Proceedings of the National Academy of Sciences of the United States of America *114*, 4300-4305.

Grady, W.M., and Carethers, J.M. (2008). Genomic and epigenetic instability in colorectal cancer pathogenesis. Gastroenterology *135*, 1079-1099.

Gravitz, L. (2011). Chemoprevention: First line of defence. Nature *471*, S5-7.

Gregorieff, A., and Clevers, H. (2005). Wnt signaling in the intestinal epithelium: from endoderm to cancer. Genes & development *19*, 877-890.

Griffie, J., Burn, G., and Owen, D.M. (2015). The nanoscale organization of signaling domains at the plasma membrane. Curr Top Membr *75*, 125-165.

Guo, L.D., Chen, X.J., Hu, Y.H., Yu, Z.J., Wang, D., and Liu, J.Z. (2013). Curcumin inhibits proliferation and induces apoptosis of human colorectal cancer cells by activating the mitochondria apoptotic pathway. Phytother Res *27*, 422-430.

Haber, R.S., Rathan, A., Weiser, K.R., Pritsker, A., Itzkowitz, S.H., Bodian, C., Slater, G., Weiss, A., and Burstein, D.E. (1998). GLUT1 glucose transporter expression in colorectal carcinoma: a marker for poor prognosis. Cancer *83*, 34-40.

Hall, C.N., Badawi, A.F., O'Connor, P.J., and Saffhill, R. (1991). The detection of alkylation damage in the DNA of human gastrointestinal tissues. British journal of cancer *64*, 59-63.

Halvey, P.J., Zhang, B., Coffey, R.J., Liebler, D.C., and Slebos, R.J. (2012). Proteomic consequences of a single gene mutation in a colorectal cancer model. Journal of proteome research *11*, 1184-1195.

Hamilton, J.T., McRoberts, W.C., Keppler, F., Kalin, R.M., and Harper, D.B. (2003). Chloride methylation by plant pectin: an efficient environmentally significant process. Science *301*, 206-209.

Hanahan, D., and Weinberg, R.A. (2011). Hallmarks of cancer: the next generation. Cell *144*, 646-674.

Hao, X.P., Pretlow, T.G., Rao, J.S., and Pretlow, T.P. (2001). Beta-catenin expression is altered in human colonic aberrant crypt foci. Cancer research *61*, 8085-8088.

Hata, K., Yamada, Y., Kuno, T., Hirose, Y., Hara, A., Qiang, S.H., and Mori, H. (2004). Tumor formation is correlated with expression of beta-catenin-accumulated crypts in azoxymethane-induced colon carcinogenesis in mice. Cancer science *95*, 316-320.

Hawkins, N., Norrie, M., Cheong, K., Mokany, E., Ku, S.L., Meagher, A., O'Connor, T., and Ward, R. (2002). CpG island methylation in sporadic colorectal cancers and its relationship to microsatellite instability. Gastroenterology *122*, 1376-1387.

Hawks, A., and Magee, P.N. (1974). The alkylation of nucleic acids of rat and mouse in vivo by the carcinogen 1,2-dimethylhydrazine. British journal of cancer *30*, 440-447.

He, T.C., Sparks, A.B., Rago, C., Hermeking, H., Zawel, L., da Costa, L.T., Morin, P.J., Vogelstein, B., and Kinzler, K.W. (1998). Identification of c-MYC as a target of the APC pathway. Science *281*, 1509-1512.

Hecht, S.S. (1999). DNA adduct formation from tobacco-specific N-nitrosamines. Mutation research *424*, 127-142.

Hindler, K., Cleeland, C.S., Rivera, E., and Collard, C.D. (2006). The role of statins in cancer therapy. Oncologist *11*, 306-315.

Hirose, Y., Yoshimi, N., Makita, H., Hara, A., Tanaka, T., and Mori, H. (1996). Early alterations of apoptosis and cell proliferation in azoxymethane-initiated rat colonic epithelium. Japanese journal of cancer research : Gann *87*, 575-582.

Hong, M.Y., Chapkin, R.S., Barhoumi, R., Burghardt, R.C., Turner, N.D., Henderson, C.E., Sanders, L.M., Fan, Y.Y., Davidson, L.A., Murphy, M.E.*, et al.* (2002). Fish oil increases mitochondrial phospholipid unsaturation, upregulating reactive oxygen species and apoptosis in rat colonocytes. Carcinogenesis *23*, 1919-1925.

Hong, M.Y., Chapkin, R.S., Davidson, L.A., Turner, N.D., Morris, J.S., Carroll, R.J., and Lupton, J.R. (2003). Fish oil enhances targeted apoptosis during colon tumor initiation in part by downregulating Bcl-2. Nutrition and cancer *46*, 44-51.

Hong, M.Y., Chapkin, R.S., Wild, C.P., Morris, J.S., Wang, N., Carroll, R.J., Turner, N.D., and Lupton, J.R. (1999). Relationship between DNA adduct

levels, repair enzyme, and apoptosis as a function of DNA methylation by azoxymethane. Cell growth & differentiation : the molecular biology journal of the American Association for Cancer Research *10*, 749-758.

Hong, M.Y., Lupton, J.R., Morris, J.S., Wang, N., Carroll, R.J., Davidson, L.A., Elder, R.H., and Chapkin, R.S. (2000). Dietary fish oil reduces O6-methylguanine DNA adduct levels in rat colon in part by increasing apoptosis during tumor initiation. Cancer epidemiology, biomarkers & prevention : a publication of the American Association for Cancer Research, cosponsored by the American Society of Preventive Oncology *9*, 819-826.

Hong, M.Y., Turner, N.D., Murphy, M.E., Carroll, R.J., Chapkin, R.S., and Lupton, J.R. (2015). In Vivo Regulation of Colonic Cell Proliferation, Differentiation, Apoptosis, and P27Kip1 by Dietary Fish Oil and Butyrate in Rats. Cancer prevention research *8*, 1076-1083.

Hou, T.Y., Davidson, L.A., Kim, E., Fan, Y.Y., Fuentes, N.R., Triff, K., and Chapkin, R.S. (2016). Nutrient-Gene Interaction in Colon Cancer, from the Membrane to Cellular Physiology. Annu Rev Nutr *36*, 543-570.

Hsieh, A.L., Walton, Z.E., Altman, B.J., Stine, Z.E., and Dang, C.V. (2015). MYC and metabolism on the path to cancer. Semin Cell Dev Biol *43*, 11-21.

Hu, Y., Le Leu, R.K., and Young, G.P. (2005). Absence of acute apoptotic response to genotoxic carcinogens in p53-deficient mice is associated with increased susceptibility to azoxymethane-induced colon

tumours. International journal of cancer Journal international du cancer *115*, 561-567.

Hu, Y., Martin, J., Le Leu, R., and Young, G.P. (2002). The colonic response to genotoxic carcinogens in the rat: regulation by dietary fibre. Carcinogenesis *23*, 1131-1137.

Hua, G., Thin, T.H., Feldman, R., Haimovitz-Friedman, A., Clevers, H., Fuks, Z., and Kolesnick, R. (2012). Crypt base columnar stem cells in small intestines of mice are radioresistant. Gastroenterology *143*, 1266-1276.

Hung, W.C., Chen, F.Y., Lee, C.C., Sun, Y., Lee, M.T., and Huang, H.W. (2008). Membrane-thinning effect of curcumin. Biophys J *94*, 4331-4338.

Iacopetta, B. (2002). Are there two sides to colorectal cancer? Int J Cancer *101*, 403-408.

Ikenoue, T., Kanai, F., Hikiba, Y., Obata, T., Tanaka, Y., Imamura, J., Ohta, M., Jazag, A., Guleng, B., Tateishi, K.*, et al.* (2005). Functional analysis of PIK3CA gene mutations in human colorectal cancer. Cancer research *65*, 4562-4567.

Ikonen, E. (2008). Cellular cholesterol trafficking and compartmentalization. Nature reviews Molecular cell biology *9*, 125-138.

Ireland, H., Kemp, R., Houghton, C., Howard, L., Clarke, A.R., Sansom, O.J., and Winton, D.J. (2004). Inducible Cre-mediated control of gene expression in the murine gastrointestinal tract: effect of loss of beta-catenin. Gastroenterology *126*, 1236-1246.

Ireson, C.R., Jones, D.J., Orr, S., Coughtrie, M.W., Boocock, D.J., Williams, M.L., Farmer, P.B., Steward, W.P., and Gescher, A.J. (2002). Metabolism of the cancer chemopreventive agent curcumin in human and rat intestine. Cancer Epidemiol Biomarkers Prev *11*, 105-111.

Irwin, M.E., Mueller, K.L., Bohin, N., Ge, Y., and Boerner, J.L. (2011). Lipid raft localization of EGFR alters the response of cancer cells to the EGFR tyrosine kinase inhibitor gefitinib. Journal of cellular physiology *226*, 2316-2328.

Iwamoto, M., Ahnen, D.J., Franklin, W.A., and Maltzman, T.H. (2000). Expression of beta-catenin and full-length APC protein in normal and neoplastic colonic tissues. Carcinogenesis *21*, 1935-1940.

Jackson, E.L., Willis, N., Mercer, K., Bronson, R.T., Crowley, D., Montoya, R., Jacks, T., and Tuveson, D.A. (2001). Analysis of lung tumor initiation and progression using conditional expression of oncogenic K-ras. Genes & development *15*, 3243-3248.

Jaks, V., Barker, N., Kasper, M., van Es, J.H., Snippert, H.J., Clevers, H., and Toftgard, R. (2008). Lgr5 marks cycling, yet long-lived, hair follicle stem cells. Nat Genet *40*, 1291-1299.

James, J.T., and Autrup, H. (1983). Methylated DNA adducts in the large intestine of ICR/Ha and C57BL/Ha mice given 1,2-dimethylhydrazine. Journal of the National Cancer Institute *70*, 541-546.

Jancik, S., Drabek, J., Radzioch, D., and Hajduch, M. (2010). Clinical relevance of KRAS in human cancers. J Biomed Biotechnol *2010*, 150960.

Jayaprakasha, G.K., Nagana Gowda, G.A., Marquez, S., and Patil, B.S. (2013). Rapid separation and quantitation of curcuminoids combining pseudo two-dimensional liquid flash chromatography and NMR spectroscopy. J Chromatogr B Analyt Technol Biomed Life Sci *937*, 25-32.

Jemal, A., Bray, F., Center, M.M., Ferlay, J., Ward, E., and Forman, D. (2011). Global cancer statistics. CA: a cancer journal for clinicians *61*, 69-90.

Jia, Q., Ivanov, I., Zlatev, Z.Z., Alaniz, R.C., Weeks, B.R., Callaway, E.S., Goldsby, J.S., Davidson, L.A., Fan, Y.Y., Zhou, L.*, et al.* (2011). Dietary fish oil and curcumin combine to modulate colonic cytokinetics and gene expression in dextran sodium sulphate-treated mice. The British journal of nutrition *106*, 519-529.

Jiao, Y.F., Nakamura, S., Sugai, T., Yamada, N., and Habano, W. (2008). Serrated adenoma of the colorectum undergoes a proliferation versus differentiation process: new conceptual interpretation of morphogenesis. Oncology *74*, 127-134.

Kaina, B., Fritz, G., Mitra, S., and Coquerelle, T. (1991). Transfection and expression of human O6-methylguanine-DNA methyltransferase (MGMT) cDNA in Chinese hamster cells: the role of MGMT in protection against the genotoxic effects of alkylating agents. Carcinogenesis *12*, 1857-1867.

Kantara, C., Moya, S.M., Houchen, C.W., Umar, S., Ullrich, R.L., Singh, P., and Carney, D.H. (2015). Novel regenerative peptide TP508 mitigates radiation-induced gastrointestinal damage by activating stem cells and

preserving crypt integrity. Laboratory investigation; a journal of technical methods and pathology *95*, 1222-1233.

Karran, P., and Bignami, M. (1992). Self-destruction and tolerance in resistance of mammalian cells to alkylation damage. Nucleic acids research *20*, 2933-2940.

Kazanskaya, O., Glinka, A., del Barco Barrantes, I., Stannek, P., Niehrs, C., and Wu, W. (2004). R-Spondin2 is a secreted activator of Wnt/beta-catenin signaling and is required for Xenopus myogenesis. Dev Cell *7*, 525-534.

Kee, Y., and D'Andrea, A.D. (2010). Expanded roles of the Fanconi anemia pathway in preserving genomic stability. Genes & development *24*, 1680-1694.

Kellner-Weibel, G., Yancey, P.G., Jerome, W.G., Walser, T., Mason, R.P., Phillips, M.C., and Rothblat, G.H. (1999). Crystallization of free cholesterol in model macrophage foam cells. Arterioscler Thromb Vasc Biol *19*, 1891-1898.

Kenyon, J., and Gerson, S.L. (2007). The role of DNA damage repair in aging of adult stem cells. Nucleic acids research *35*, 7557-7565.

Kesse, E., Clavel-Chapelon, F., and Boutron-Ruault, M.C. (2006). Dietary patterns and risk of colorectal tumors: a cohort of French women of the National Education System (E3N). American journal of epidemiology *164*, 1085-1093.

Kim, E., Davidson, L.A., Zoh, R.S., Hensel, M.E., Patil, B.S., Jayaprakasha, G.K., Callaway, E.S., Allred, C.D., Turner, N.D., Weeks, B.R., *et al.* (2016a). Homeostatic responses of colonic LGR5+ stem cells following acute in vivo exposure to a genotoxic carcinogen. Carcinogenesis *37*, 206-214.

Kim, E., Davidson, L.A., Zoh, R.S., Hensel, M.E., Salinas, M.L., Patil, B.S., Jayaprakasha, G.K., Callaway, E.S., Allred, C.D., Turner, N.D., *et al.* (2016b). Rapidly cycling Lgr5+ stem cells are exquisitely sensitive to extrinsic dietary factors that modulate colon cancer risk. Cell Death Dis *7*, e2460.

Kim, H.S., Heo, J.S., Lee, J., Lee, J.Y., Lee, M.Y., Lim, S.H., Lee, W.Y., Kim, S.H., Park, Y.A., Cho, Y.B., *et al.* (2016c). The impact of KRAS mutations on prognosis in surgically resected colorectal cancer patients with liver and lung metastases: a retrospective analysis. BMC cancer *16*, 120.

Kim, J.A., Maxwell, K., Hajjar, D.P., and Berliner, J.A. (1991). Beta-VLDL increases endothelial cell plasma membrane cholesterol. J Lipid Res *32*, 1125-1131.

Kim, K.A., Zhao, J., Andarmani, S., Kakitani, M., Oshima, T., Binnerts, M.E., Abo, A., Tomizuka, K., and Funk, W.D. (2006). R-Spondin proteins: a novel link to beta-catenin activation. Cell cycle *5*, 23-26.

Kim, W., Fan, Y.Y., Barhoumi, R., Smith, R., McMurray, D.N., and Chapkin, R.S. (2008). n-3 polyunsaturated fatty acids suppress the localization and activation of signaling proteins at the immunological synapse in murine

CD4+ T cells by affecting lipid raft formation. Journal of immunology *181*, 6236-6243.

Kim, W., Fan, Y.Y., Smith, R., Patil, B., Jayaprakasha, G.K., McMurray, D.N., and Chapkin, R.S. (2009). Dietary curcumin and limonin suppress CD4+ T-cell proliferation and interleukin-2 production in mice. The Journal of nutrition *139*, 1042-1048.

Kinzler, K.W., and Vogelstein, B. (1996). Lessons from hereditary colorectal cancer. Cell *87*, 159-170.

Kondo, N., Takahashi, A., Ono, K., and Ohnishi, T. (2010). DNA damage induced by alkylating agents and repair pathways. Journal of nucleic acids *2010*, 543531.

Konig, B., Koch, A., Spielmann, J., Hilgenfeld, C., Stangl, G.I., and Eder, K. (2007). Activation of PPARalpha lowers synthesis and concentration of cholesterol by reduction of nuclear SREBP-2. Biochem Pharmacol *73*, 574-585.

Koo, B.K., Spit, M., Jordens, I., Low, T.Y., Stange, D.E., van de Wetering, M., van Es, J.H., Mohammed, S., Heck, A.J., Maurice, M.M.*, et al.* (2012). Tumour suppressor RNF43 is a stem-cell E3 ligase that induces endocytosis of Wnt receptors. Nature *488*, 665-669.

Korinek, V., Barker, N., Moerer, P., van Donselaar, E., Huls, G., Peters, P.J., and Clevers, H. (1998). Depletion of epithelial stem-cell compartments in the small intestine of mice lacking Tcf-4. Nat Genet *19*, 379-383.

Korinek, V., Barker, N., Morin, P.J., van Wichen, D., de Weger, R., Kinzler, K.W., Vogelstein, B., and Clevers, H. (1997). Constitutive transcriptional activation by a beta-catenin-Tcf complex in APC-/- colon carcinoma. Science *275*, 1784-1787.

Kruth, H.S., and Vaughan, M. (1980). Quantification of low density lipoprotein binding and cholesterol accumulation by single human fibroblasts using fluorescence microscopy. J Lipid Res *21*, 123-130.

Kruyt, F.A., and Schuringa, J.J. (2010). Apoptosis and cancer stem cells: Implications for apoptosis targeted therapy. Biochemical pharmacology *80*, 423-430.

Kuhajda, F.P., Jenner, K., Wood, F.D., Hennigar, R.A., Jacobs, L.B., Dick, J.D., and Pasternack, G.R. (1994). Fatty acid synthesis: a potential selective target for antineoplastic therapy. Proceedings of the National Academy of Sciences of the United States of America *91*, 6379-6383.

Kuhnert, F., Davis, C.R., Wang, H.T., Chu, P., Lee, M., Yuan, J., Nusse, R., and Kuo, C.J. (2004). Essential requirement for Wnt signaling in proliferation of adult small intestine and colon revealed by adenoviral expression of Dickkopf-1. Proceedings of the National Academy of Sciences of the United States of America *101*, 266-271.

Kuo, L.J., and Yang, L.X. (2008). Gamma-H2AX - a novel biomarker for DNA double-strand breaks. In vivo *22*, 305-309.

Kycler, W., Szarzynska, B., Lozinski, C., Korski, K., and Lamperska, K. (2012). Analysis of O6-methylguanine-DNA methyltransferase methylation status in sporadic colon polyps. Reports of practical oncology and radiotherapy : journal of Greatpoland Cancer Center in Poznan and Polish Society of Radiation Oncology *17*, 13-18.

Lakha, F., Theodoratou, E., Farrington, S.M., Tenesa, A., Cetnarskyj, R., Din, F.V., Porteous, M.E., Dunlop, M.G., and Campbell, H. (2012). Statin use and association with colorectal cancer survival and risk: case control study with prescription data linkage. BMC cancer *12*, 487.

Lange, S.S., Takata, K., and Wood, R.D. (2011). DNA polymerases and cancer. Nature reviews Cancer *11*, 96-110.

Lange, Y., Swaisgood, M.H., Ramos, B.V., and Steck, T.L. (1989). Plasma membranes contain half the phospholipid and 90% of the cholesterol and sphingomyelin in cultured human fibroblasts. The Journal of biological chemistry *264*, 3786-3793.

Leibowitz, B., Qiu, W., Buchanan, M.E., Zou, F., Vernon, P., Moyer, M.P., Yin, X.M., Schoen, R.E., Yu, J., and Zhang, L. (2014). BID mediates selective killing of APC-deficient cells in intestinal tumor suppression by nonsteroidal antiinflammatory drugs. Proceedings of the National Academy of Sciences of the United States of America *111*, 16520-16525.

Lemieux, E., Cagnol, S., Beaudry, K., Carrier, J., and Rivard, N. (2015). Oncogenic KRAS signalling promotes the Wnt/beta-catenin pathway through LRP6 in colorectal cancer. Oncogene *34*, 4914-4927.

Lengauer, C., Kinzler, K.W., and Vogelstein, B. (1997). Genetic instability in colorectal cancers. Nature *386*, 623-627.

Li, L., and Clevers, H. (2010). Coexistence of quiescent and active adult stem cells in mammals. Science *327*, 542-545.

Li, Q., Zhang, Q., Wang, C., Jiang, S., Li, N., and Li, J. (2011). The response of intestinal stem cells and epithelium after alemtuzumab administration. Cell Mol Immunol *8*, 325-332.

Li, W.Q., Kawakami, K., Ruszkiewicz, A., Bennett, G., Moore, J., and Iacopetta, B. (2006a). BRAF mutations are associated with distinctive clinical, pathological and molecular features of colorectal cancer independently of microsatellite instability status. Molecular cancer *5*, 2.

Li, Y., and Zhang, T. (2014). Targeting cancer stem cells by curcumin and clinical applications. Cancer letters *346*, 197-205.

Li, Y.C., Park, M.J., Ye, S.K., Kim, C.W., and Kim, Y.N. (2006b). Elevated levels of cholesterol-rich lipid rafts in cancer cells are correlated with apoptosis sensitivity induced by cholesterol-depleting agents. The American journal of pathology *168*, 1107-1118; quiz 1404-1105.

Lin, C.Y., Loven, J., Rahl, P.B., Paranal, R.M., Burge, C.B., Bradner, J.E., Lee, T.I., and Young, R.A. (2012). Transcriptional amplification in tumor cells with elevated c-Myc. Cell *151*, 56-67.

Lindblom, A. (2001). Different mechanisms in the tumorigenesis of proximal and distal colon cancers. Curr Opin Oncol *13*, 63-69.

Liu, J.C., Guan, X., Ryan, J.A., Rivera, A.G., Mock, C., Agrawal, V., Letai, A., Lerou, P.H., and Lahav, G. (2013). High mitochondrial priming sensitizes hESCs to DNA-damage-induced apoptosis. Cell stem cell *13*, 483-491.

Loeb, L.A., and Harris, C.C. (2008). Advances in chemical carcinogenesis: a historical review and prospective. Cancer research *68*, 6863-6872.

Magnuson, B.A., South, E.H., Exon, J.H., Dashwood, R.H., Xu, M., Hendrix, K., and Hubele, S. (2000). Increased susceptibility of adult rats to azoxymethane-induced aberrant crypt foci. Cancer letters *161*, 185-193.

Markowitz, S.D., Dawson, D.M., Willis, J., and Willson, J.K. (2002). Focus on colon cancer. Cancer Cell *1*, 233-236.

McClanahan, T., Koseoglu, S., Smith, K., Grein, J., Gustafson, E., Black, S., Kirschmeier, P., and Samatar, A.A. (2006). Identification of overexpression of orphan G protein-coupled receptor GPR49 in human colon and ovarian primary tumors. Cancer biology & therapy *5*, 419-426.

Medema, J.P. (2013). Cancer stem cells: the challenges ahead. Nature cell biology *15*, 338-344.

Meikrantz, W., Bergom, M.A., Memisoglu, A., and Samson, L. (1998). O6-alkylguanine DNA lesions trigger apoptosis. Carcinogenesis *19*, 369-372.

Menendez, J.A., and Lupu, R. (2007). Fatty acid synthase and the lipogenic phenotype in cancer pathogenesis. Nature reviews Cancer *7*, 763-777.

Mermelshtein, A., Gerson, A., Walfisch, S., Delgado, B., Shechter-Maor, G., Delgado, J., Fich, A., and Gheber, L. (2005). Expression of D-type cyclins in colon cancer and in cell lines from colon carcinomas. British journal of cancer *93*, 338-345.

Metcalfe, C., Kljavin, N.M., Ybarra, R., and de Sauvage, F.J. (2014). Lgr5+ stem cells are indispensable for radiation-induced intestinal regeneration. Cell Stem Cell *14*, 149-159.

Meyskens, F.L., Jr., McLaren, C.E., Pelot, D., Fujikawa-Brooks, S., Carpenter, P.M., Hawk, E., Kelloff, G., Lawson, M.J., Kidao, J., McCracken, J., *et al.* (2008). Difluoromethylornithine plus sulindac for the prevention of sporadic colorectal adenomas: a randomized placebo-controlled, double-blind trial. Cancer prevention research *1*, 32-38.

Meza, R., Jeon, J., Renehan, A.G., and Luebeck, E.G. (2010). Colorectal cancer incidence trends in the United States and United kingdom:

evidence of right- to left-sided biological gradients with implications for screening. Cancer research *70*, 5419-5429.

Mi, B., Wang, X., Bai, Y., Gong, W., Wang, X., Geng, Y., Wang, J., Zhang, H., and Jiang, B. (2009). Beta-catenin expression is altered in dysplastic and nondysplastic aberrant crypt foci of human colon. Appl Immunohistochem Mol Morphol *17*, 294-300.

Mojas, N., Lopes, M., and Jiricny, J. (2007). Mismatch repair-dependent processing of methylation damage gives rise to persistent single-stranded gaps in newly replicated DNA. Genes & development *21*, 3342-3355.

Montero, J., Morales, A., Llacuna, L., Lluis, J.M., Terrones, O., Basanez, G., Antonsson, B., Prieto, J., Garcia-Ruiz, C., Colell, A.*, et al.* (2008). Mitochondrial cholesterol contributes to chemotherapy resistance in hepatocellular carcinoma. Cancer Res *68*, 5246-5256.

Montesano, R., Hall, J., Hollstein, M., Mironov, N., and Wild, C.P. (1990). Alkylation repair in human tissues. Basic life sciences *53*, 437-452.

Moran, A., Ortega, P., de Juan, C., Fernandez-Marcelo, T., Frias, C., Sanchez-Pernaute, A., Torres, A.J., Diaz-Rubio, E., Iniesta, P., and Benito, M. (2010). Differential colorectal carcinogenesis: Molecular basis and clinical relevance. World J Gastrointest Oncol *2*, 151-158.

Mori, H., Yamada, Y., Kuno, T., and Hirose, Y. (2004). Aberrant crypt foci and beta-catenin accumulated crypts; significance and roles for colorectal carcinogenesis. Mutation research *566*, 191-208.

Morin, P.J., Sparks, A.B., Korinek, V., Barker, N., Clevers, H., Vogelstein, B., and Kinzler, K.W. (1997). Activation of beta-catenin-Tcf signaling in colon cancer by mutations in beta-catenin or APC. Science *275*, 1787-1790.

Mukherjee, S., Mazumdar, M., Chakraborty, S., Manna, A., Saha, S., Khan, P., Bhattacharjee, P., Guha, D., Adhikary, A., Mukhjerjee, S.*, et al.* (2014). Curcumin inhibits breast cancer stem cell migration by amplifying the E-cadherin/beta-catenin negative feedback loop. Stem cell research & therapy *5*, 116.

Munemitsu, S., Albert, I., Souza, B., Rubinfeld, B., and Polakis, P. (1995). Regulation of intracellular beta-catenin levels by the adenomatous polyposis coli (APC) tumor-suppressor protein. Proceedings of the National Academy of Sciences of the United States of America *92*, 3046-3050.

Naini, B.V., and Odze, R.D. (2013). Advanced precancerous lesions (APL) in the colonic mucosa. Best Pract Res Clin Gastroenterol *27*, 235-256.

Nam, J.S., Turcotte, T.J., Smith, P.F., Choi, S., and Yoon, J.K. (2006). Mouse cristin/R-spondin family proteins are novel ligands for the Frizzled 8 and LRP6 receptors and activate beta-catenin-dependent gene expression. The Journal of biological chemistry *281*, 13247-13257.

Nau, M.M., Brooks, B.J., Battey, J., Sausville, E., Gazdar, A.F., Kirsch, I.R., McBride, O.W., Bertness, V., Hollis, G.F., and Minna, J.D. (1985). L-myc,

a new myc-related gene amplified and expressed in human small cell lung cancer. Nature *318*, 69-73.

Niture, S.K., Velu, C.S., Smith, Q.R., Bhat, G.J., and Srivenugopal, K.S. (2007). Increased expression of the MGMT repair protein mediated by cysteine prodrugs and chemopreventative natural products in human lymphocytes and tumor cell lines. Carcinogenesis *28*, 378-389.

Noffsinger, A.E. (2009). Serrated polyps and colorectal cancer: new pathway to malignancy. Annu Rev Pathol *4*, 343-364.

O'Leary, B., Finn, R.S., and Turner, N.C. (2016). Treating cancer with selective CDK4/6 inhibitors. Nat Rev Clin Oncol *13*, 417-430.

O'Neill, J.P. (2000). DNA damage, DNA repair, cell proliferation, and DNA replication: how do gene mutations result? Proceedings of the National Academy of Sciences of the United States of America *97*, 11137-11139.

Ochs, K., and Kaina, B. (2000). Apoptosis induced by DNA damage O6-methylguanine is Bcl-2 and caspase-9/3 regulated and Fas/caspase-8 independent. Cancer research *60*, 5815-5824.

Owen, D.M., Rentero, C., Magenau, A., Abu-Siniyeh, A., and Gaus, K. (2011). Quantitative imaging of membrane lipid order in cells and organisms. Nat Protoc *7*, 24-35.

Paek, A.L., Liu, J.C., Loewer, A., Forrester, W.C., and Lahav, G. (2016). Cell-to-Cell Variation in p53 Dynamics Leads to Fractional Killing. Cell *165*, 631-642.

Pagano, M., Pepperkok, R., Verde, F., Ansorge, W., and Draetta, G. (1992). Cyclin A is required at two points in the human cell cycle. EMBO J *11*, 961-971.

Patra, S.K. (2008). Dissecting lipid raft facilitated cell signaling pathways in cancer. Biochimica et biophysica acta *1785*, 182-206.

Pegg, A.E., and Byers, T.L. (1992). Repair of DNA containing O6-alkylguanine. FASEB journal : official publication of the Federation of American Societies for Experimental Biology *6*, 2302-2310.

Phillips, R., Ursell, T., Wiggins, P., and Sens, P. (2009). Emerging roles for lipids in shaping membrane-protein function. Nature *459*, 379-385.

Pinto, D., Gregorieff, A., Begthel, H., and Clevers, H. (2003). Canonical Wnt signals are essential for homeostasis of the intestinal epithelium. Genes & development *17*, 1709-1713.

Pisco, A.O., and Huang, S. (2015). Non-genetic cancer cell plasticity and therapy-induced stemness in tumour relapse: 'What does not kill me strengthens me'. British journal of cancer *112*, 1725-1732.

Potten, C.S., Booth, C., and Pritchard, D.M. (1997). The intestinal epithelial stem cell: the mucosal governor. Int J Exp Pathol *78*, 219-243.

Potten, C.S., Kellett, M., Rew, D.A., and Roberts, S.A. (1992). Proliferation in human gastrointestinal epithelium using bromodeoxyuridine in vivo: data for different sites, proximity to a tumour, and polyposis coli. Gut *33*, 524-529.

Potter, J.D. (1999). Colorectal cancer: molecules and populations. Journal of the National Cancer Institute *91*, 916-932.

Poynter, J.N., Gruber, S.B., Higgins, P.D., Almog, R., Bonner, J.D., Rennert, H.S., Low, M., Greenson, J.K., and Rennert, G. (2005). Statins and the risk of colorectal cancer. The New England journal of medicine *352*, 2184-2192.

Pozharisski, K.M., Kapustin, Y.M., Likhachev, A.J., and Shaposhnikov, J.D. (1975). The mechanism of carcinogenic action of 1,2-dimethylhydrazine (SDMH) in rats. Int J Cancer *15*, 673-683.

Pretlow, T.P., and Pretlow, T.G. (2005). Mutant KRAS in aberrant crypt foci (ACF): initiation of colorectal cancer? Biochimica et biophysica acta *1756*, 83-96.

Priolo, C., Pyne, S., Rose, J., Regan, E.R., Zadra, G., Photopoulos, C., Cacciatore, S., Schultz, D., Scaglia, N., McDunn, J.*, et al.* (2014). AKT1 and MYC induce distinctive metabolic fingerprints in human prostate cancer. Cancer research *74*, 7198-7204.

Psaty, B.M., and Potter, J.D. (2006). Risks and benefits of celecoxib to prevent recurrent adenomas. The New England journal of medicine *355*, 950-952.

Puszynski, K., Bertolusso, R., and Lipniacki, T. (2009). Crosstalk between p53 and nuclear factor-B systems: pro- and anti-apoptotic functions of NF-B. IET Syst Biol *3*, 356-367.

Qiu, W., Wang, X., Leibowitz, B., Liu, H., Barker, N., Okada, H., Oue, N., Yasui, W., Clevers, H., Schoen, R.E.*, et al.* (2010). Chemoprevention by nonsteroidal anti-inflammatory drugs eliminates oncogenic intestinal stem cells via SMAC-dependent apoptosis. Proceedings of the National Academy of Sciences of the United States of America *107*, 20027-20032.

Quiros, S., Roos, W.P., and Kaina, B. (2010). Processing of O6-methylguanine into DNA double-strand breaks requires two rounds of replication whereas apoptosis is also induced in subsequent cell cycles. Cell cycle *9*, 168-178.

Rajagopalan, H., Bardelli, A., Lengauer, C., Kinzler, K.W., Vogelstein, B., and Velculescu, V.E. (2002). Tumorigenesis: RAF/RAS oncogenes and mismatch-repair status. Nature *418*, 934.

Rajavashisth, T.B., Taylor, A.K., Andalibi, A., Svenson, K.L., and Lusis, A.J. (1989). Identification of a zinc finger protein that binds to the sterol regulatory element. Science *245*, 640-643.

Reagan-Shaw, S., Nihal, M., and Ahmad, N. (2008). Dose translation from animal to human studies revisited. FASEB journal : official publication of the Federation of American Societies for Experimental Biology *22*, 659-661.

Reddy, B.S. (1994). Chemoprevention of colon cancer by dietary fatty acids. Cancer metastasis reviews *13*, 285-302.

Richards, T.C. (1977). Early changes in the dynamics of crypt cell populations in mouse colon following administration of 1,2-dimethylhydrazine. Cancer research *37*, 1680-1685.

Riehl, T.E., George, R.J., Sturmoski, M.A., May, R., Dieckgraefe, B., Anant, S., and Houchen, C.W. (2006). Azoxymethane protects intestinal stem cells and reduces crypt epithelial mitosis through a COX-1-dependent mechanism. American journal of physiology Gastrointestinal and liver physiology *291*, G1062-1070.

Rogers, K.J., and Pegg, A.E. (1977). Formation of O6-methylguanine by alkylation of rat liver, colon, and kidney DNA following administration of 1,2-dimethylhydrazine. Cancer research *37*, 4082-4087.

Roos, W.P., Nikolova, T., Quiros, S., Naumann, S.C., Kiedron, O., Zdzienicka, M.Z., and Kaina, B. (2009). Brca2/Xrcc2 dependent HR, but not NHEJ, is required for protection against O(6)-methylguanine triggered apoptosis, DSBs and chromosomal aberrations by a process leading to SCEs. DNA Repair (Amst) *8*, 72-86.

Rosenberg, D.W., Giardina, C., and Tanaka, T. (2009). Mouse models for the study of colon carcinogenesis. Carcinogenesis *30*, 183-196.

Rothenberg, M.E., Nusse, Y., Kalisky, T., Lee, J.J., Dalerba, P., Scheeren, F., Lobo, N., Kulkarni, S., Sim, S., Qian, D.*, et al.* (2012). Identification of a cKit(+) colonic crypt base secretory cell that supports Lgr5(+) stem cells in mice. Gastroenterology *142*, 1195-1205 e1196.

Rubinfeld, B., Robbins, P., El-Gamil, M., Albert, I., Porfiri, E., and Polakis, P. (1997). Stabilization of beta-catenin by genetic defects in melanoma cell lines. Science *275*, 1790-1792.

Rubinfeld, B., Souza, B., Albert, I., Muller, O., Chamberlain, S.H., Masiarz, F.R., Munemitsu, S., and Polakis, P. (1993). Association of the APC gene product with beta-catenin. Science *262*, 1731-1734.

Rudolph, R.E., Dominitz, J.A., Lampe, J.W., Levy, L., Qu, P., Li, S.S., Lampe, P.D., Bronner, M.P., and Potter, J.D. (2005). Risk factors for colorectal cancer in relation to number and size of aberrant crypt foci in humans. Cancer epidemiology, biomarkers & prevention : a publication of the American Association for Cancer Research, cosponsored by the American Society of Preventive Oncology *14*, 605-608.

Russell, S.J., Ye, Y.W., Waber, P.G., Shuford, M., Schold, S.C., Jr., and Nisen, P.D. (1995). p53 mutations, O6-alkylguanine DNA alkyltransferase activity, and sensitivity to procarbazine in human brain tumors. Cancer *75*, 1339-1342.

Rydberg, B., and Lindahl, T. (1982). Nonenzymatic methylation of DNA by the intracellular methyl group donor S-adenosyl-L-methionine is a potentially mutagenic reaction. EMBO J *1*, 211-216.

Sahlberg, S.H., Spiegelberg, D., Glimelius, B., Stenerlow, B., and Nestor, M. (2014). Evaluation of cancer stem cell markers CD133, CD44,

CD24: association with AKT isoforms and radiation resistance in colon cancer cells. PloS one *9*, e94621.

Saif, M.W., and Chu, E. (2010). Biology of colorectal cancer. Cancer J *16*, 196-201.

Sansom, O.J., Meniel, V.S., Muncan, V., Phesse, T.J., Wilkins, J.A., Reed, K.R., Vass, J.K., Athineos, D., Clevers, H., and Clarke, A.R. (2007). Myc deletion rescues Apc deficiency in the small intestine. Nature *446*, 676-679.

Santos, C.R., and Schulze, A. (2012). Lipid metabolism in cancer. FEBS J *279*, 2610-2623.

Sasaki, N., Sachs, N., Wiebrands, K., Ellenbroek, S.I.J., Fumagalli, A., Lyubimova, A., Begthel, H., van den Born, M., van Es, J.H., Karthaus, W.R.*, et al.* (2016). Reg4+ deep crypt secretory cells function as epithelial niche for Lgr5+ stem cells in colon. Proceedings of the National Academy of Sciences *113*, E5399-E5407.

Sato, T., Vries, R.G., Snippert, H.J., van de Wetering, M., Barker, N., Stange, D.E., van Es, J.H., Abo, A., Kujala, P., Peters, P.J.*, et al.* (2009). Single Lgr5 stem cells build crypt-villus structures in vitro without a mesenchymal niche. Nature *459*, 262-265.

Saw, C.L., Huang, Y., and Kong, A.N. (2010). Synergistic anti-inflammatory effects of low doses of curcumin in combination with polyunsaturated fatty acids: docosahexaenoic acid or eicosapentaenoic acid. Biochemical pharmacology *79*, 421-430.

Schepers, A.G., Vries, R., van den Born, M., van de Wetering, M., and Clevers, H. (2011). Lgr5 intestinal stem cells have high telomerase activity and randomly segregate their chromosomes. EMBO J *30*, 1104-1109.

Schuijers, J., Junker, J.P., Mokry, M., Hatzis, P., Koo, B.K., Sasselli, V., van der Flier, L.G., Cuppen, E., van Oudenaarden, A., and Clevers, H. (2015). Ascl2 acts as an R-spondin/Wnt-responsive switch to control stemness in intestinal crypts. Cell Stem Cell *16*, 158-170.

Schuijers, J., van der Flier, L.G., van Es, J., and Clevers, H. (2014). Robust cre-mediated recombination in small intestinal stem cells utilizing the olfm4 locus. Stem cell reports *3*, 234-241.

Schulz, M.D., Atay, C., Heringer, J., Romrig, F.K., Schwitalla, S., Aydin, B., Ziegler, P.K., Varga, J., Reindl, W., Pommerenke, C.*, et al.* (2014). High-fat-diet-mediated dysbiosis promotes intestinal carcinogenesis independently of obesity. Nature *514*, 508-512.

Schwitalla, S., Fingerle, A.A., Cammareri, P., Nebelsiek, T., Goktuna, S.I., Ziegler, P.K., Canli, O., Heijmans, J., Huels, D.J., Moreaux, G.*, et al.* (2013a). Intestinal tumorigenesis initiated by dedifferentiation and acquisition of stem-cell-like properties. Cell *152*, 25-38.

Schwitalla, S., Ziegler, P.K., Horst, D., Becker, V., Kerle, I., Begus-Nahrmann, Y., Lechel, A., Rudolph, K.L., Langer, R., Slotta-Huspenina, J.*, et al.* (2013b). Loss of p53 in enterocytes generates an inflammatory

microenvironment enabling invasion and lymph node metastasis of carcinogen-induced colorectal tumors. Cancer Cell *23*, 93-106.

Sedgwick, B., Bates, P.A., Paik, J., Jacobs, S.C., and Lindahl, T. (2007). Repair of alkylated DNA: recent advances. DNA Repair (Amst) *6*, 429-442.

Shah, M.S., Schwartz, S.L., Zhao, C., Davidson, L.A., Zhou, B., Lupton, J.R., Ivanov, I., and Chapkin, R.S. (2011). Integrated microRNA and mRNA expression profiling in a rat colon carcinogenesis model: effect of a chemo-protective diet. Physiological genomics *43*, 640-654.

Shaikh, S.R., Dumaual, A.C., Castillo, A., LoCascio, D., Siddiqui, R.A., Stillwell, W., and Wassall, S.R. (2004). Oleic and docosahexaenoic acid differentially phase separate from lipid raft molecules: a comparative NMR, DSC, AFM, and detergent extraction study. Biophys J *87*, 1752-1766.

Shaikh, S.R., Kinnun, J.J., Leng, X., Williams, J.A., and Wassall, S.R. (2015). How polyunsaturated fatty acids modify molecular organization in membranes: insight from NMR studies of model systems. Biochimica et biophysica acta *1848*, 211-219.

Shaikh, S.R., Locascio, D.S., Soni, S.P., Wassall, S.R., and Stillwell, W. (2009a). Oleic- and docosahexaenoic acid-containing phosphatidylethanolamines differentially phase separate from sphingomyelin. Biochimica et biophysica acta *1788*, 2421-2426.

Shaikh, S.R., Rockett, B.D., Salameh, M., and Carraway, K. (2009b). Docosahexaenoic acid modifies the clustering and size of lipid rafts and the

lateral organization and surface expression of MHC class I of EL4 cells. The Journal of nutrition *139*, 1632-1639.

Shannon, J., Tewoderos, S., Garzotto, M., Beer, T.M., Derenick, R., Palma, A., and Farris, P.E. (2005). Statins and prostate cancer risk: a case-control study. American journal of epidemiology *162*, 318-325.

Shao, J., Fujiwara, T., Kadowaki, Y., Fukazawa, T., Waku, T., Itoshima, T., Yamatsuji, T., Nishizaki, M., Roth, J.A., and Tanaka, N. (2000). Overexpression of the wild-type p53 gene inhibits NF-kappaB activity and synergizes with aspirin to induce apoptosis in human colon cancer cells. Oncogene *19*, 726-736.

Shibata, H., Toyama, K., Shioya, H., Ito, M., Hirota, M., Hasegawa, S., Matsumoto, H., Takano, H., Akiyama, T., Toyoshima, K.*, et al.* (1997). Rapid colorectal adenoma formation initiated by conditional targeting of the Apc gene. Science *278*, 120-123.

Siddiqui, R.A., Harvey, K.A., Walker, C., Altenburg, J., Xu, Z., Terry, C., Camarillo, I., Jones-Hall, Y., and Mariash, C. (2013). Characterization of synergistic anti-cancer effects of docosahexaenoic acid and curcumin on DMBA-induced mammary tumorigenesis in mice. BMC cancer *13*, 418.

Simons, K., and Vaz, W.L. (2004). Model systems, lipid rafts, and cell membranes. Annu Rev Biophys Biomol Struct *33*, 269-295.

Singh, G.J., Adams, W.P., Lesko, L.J., Shah, V.P., Molzon, J.A., Williams, R.L., and Pershing, L.K. (1999). Development of in vivo

bioequivalence methodology for dermatologic corticosteroids based on pharmacodynamic modeling. Clinical pharmacology and therapeutics *66*, 346-357.

Skarke, C., Alamuddin, N., Lawson, J.A., Li, X., Ferguson, J.F., Reilly, M.P., and FitzGerald, G.A. (2015). Bioactive products formed in humans from fish oils. J Lipid Res *56*, 1808-1820.

Smakman, N., Borel Rinkes, I.H., Voest, E.E., and Kranenburg, O. (2005). Control of colorectal metastasis formation by K-Ras. Biochimica et biophysica acta *1756*, 103-114.

Smith, B., and Land, H. (2012). Anticancer activity of the cholesterol exporter ABCA1 gene. Cell Rep *2*, 580-590.

Snippert, H.J., Haegebarth, A., Kasper, M., Jaks, V., van Es, J.H., Barker, N., van de Wetering, M., van den Born, M., Begthel, H., Vries, R.G.*, et al.* (2010). Lgr6 marks stem cells in the hair follicle that generate all cell lineages of the skin. Science *327*, 1385-1389.

Snippert, H.J., van Es, J.H., van den Born, M., Begthel, H., Stange, D.E., Barker, N., and Clevers, H. (2009). Prominin-1/CD133 marks stem cells and early progenitors in mouse small intestine. Gastroenterology *136*, 2187-2194 e2181.

Sohn, O.S., Fiala, E.S., Requeijo, S.P., Weisburger, J.H., and Gonzalez, F.J. (2001). Differential effects of CYP2E1 status on the metabolic activation of

the colon carcinogens azoxymethane and methylazoxymethanol. Cancer research *61*, 8435-8440.

Solomon, S.D., McMurray, J.J., Pfeffer, M.A., Wittes, J., Fowler, R., Finn, P., Anderson, W.F., Zauber, A., Hawk, E., Bertagnolli, M.*, et al.* (2005). Cardiovascular risk associated with celecoxib in a clinical trial for colorectal adenoma prevention. The New England journal of medicine *352*, 1071-1080.

Soung, Y.H., and Chung, J. (2011). Curcumin inhibition of the functional interaction between integrin alpha6beta4 and the epidermal growth factor receptor. Molecular cancer therapeutics *10*, 883-891.

Sparks, A.B., Morin, P.J., Vogelstein, B., and Kinzler, K.W. (1998). Mutational analysis of the APC/beta-catenin/Tcf pathway in colorectal cancer. Cancer research *58*, 1130-1134.

Staszewski, O., Nikolova, T., and Kaina, B. (2008). Kinetics of gamma-H2AX focus formation upon treatment of cells with UV light and alkylating agents. Environmental and molecular mutagenesis *49*, 734-740.

Stracquadanio, G., Wang, X., Wallace, M.D., Grawenda, A.M., Zhang, P., Hewitt, J., Zeron-Medina, J., Castro-Giner, F., Tomlinson, I.P., Goding, C.R.*, et al.* (2016). The importance of p53 pathway genetics in inherited and somatic cancer genomes. Nature reviews Cancer *16*, 251-265.

Stratton, M.R., Campbell, P.J., and Futreal, P.A. (2009). The cancer genome. Nature *458*, 719-724.

Su, L.K., Johnson, K.A., Smith, K.J., Hill, D.E., Vogelstein, B., and Kinzler, K.W. (1993). Association between wild type and mutant APC gene products. Cancer research *53*, 2728-2731.

Sugai, T., Habano, W., Jiao, Y.F., Tsukahara, M., Takeda, Y., Otsuka, K., and Nakamura, S. (2006). Analysis of molecular alterations in left- and right-sided colorectal carcinomas reveals distinct pathways of carcinogenesis: proposal for new molecular profile of colorectal carcinomas. J Mol Diagn *8*, 193-201.

Suzui, M., Morioka, T., and Yoshimi, N. (2013). Colon preneoplastic lesions in animal models. J Toxicol Pathol *26*, 335-341.

Swamy, M.V., Citineni, B., Patlolla, J.M., Mohammed, A., Zhang, Y., and Rao, C.V. (2008). Prevention and treatment of pancreatic cancer by curcumin in combination with omega-3 fatty acids. Nutr Cancer *60 Suppl 1*, 81-89.

Swann, P.F. (1990). Why do O6-alkylguanine and O4-alkylthymine miscode? The relationship between the structure of DNA containing O6-alkylguanine and O4-alkylthymine and the mutagenic properties of these bases. Mutation research *233*, 81-94.

Takahashi, M., and Wakabayashi, K. (2004). Gene mutations and altered gene expression in azoxymethane-induced colon carcinogenesis in rodents. Cancer science *95*, 475-480.

Takahashi, S., Suzuki, J., Kohno, M., Oida, K., Tamai, T., Miyabo, S., Yamamoto, T., and Nakai, T. (1995). Enhancement of the binding of

triglyceride-rich lipoproteins to the very low density lipoprotein receptor by apolipoprotein E and lipoprotein lipase. The Journal of biological chemistry *270*, 15747-15754.

Takayama, T., Katsuki, S., Takahashi, Y., Ohi, M., Nojiri, S., Sakamaki, S., Kato, J., Kogawa, K., Miyake, H., and Niitsu, Y. (1998). Aberrant crypt foci of the colon as precursors of adenoma and cancer. The New England journal of medicine *339*, 1277-1284.

Takayama, T., Ohi, M., Hayashi, T., Miyanishi, K., Nobuoka, A., Nakajima, T., Satoh, T., Takimoto, R., Kato, J., Sakamaki, S.*, et al.* (2001). Analysis of K-ras, APC, and beta-catenin in aberrant crypt foci in sporadic adenoma, cancer, and familial adenomatous polyposis. Gastroenterology *121*, 599-611.

Taketo, M.M. (2006). Mouse models of gastrointestinal tumors. Cancer Sci *97*, 355-361.

Tao, H., Aakula, S., Abumrad, N.N., and Hajri, T. (2010). Peroxisome proliferator-activated receptor-gamma regulates the expression and function of very-low-density lipoprotein receptor. Am J Physiol Endocrinol Metab *298*, E68-79.

Taverna, P., and Sedgwick, B. (1996). Generation of an endogenous DNA-methylating agent by nitrosation in Escherichia coli. Journal of bacteriology *178*, 5105-5111.

ten Kate, J., Eidelman, S., Bosman, F.T., and Damjanov, I. (1989). Expression of c-myc proto-oncogene in normal human intestinal epithelium. J Histochem Cytochem *37*, 541-545.

Tetteh, P.W., Basak, O., Farin, H.F., Wiebrands, K., Kretzschmar, K., Begthel, H., van den Born, M., Korving, J., de Sauvage, F., van Es, J.H.*, et al.* (2016). Replacement of Lost Lgr5-Positive Stem Cells through Plasticity of Their Enterocyte-Lineage Daughters. Cell Stem Cell *18*, 203-213.

Thakur, R., and Mishra, D.P. (2013). Pharmacological modulation of beta-catenin and its applications in cancer therapy. J Cell Mol Med *17*, 449-456.

Thompson, C.B. (1995). Apoptosis in the pathogenesis and treatment of disease. Science *267*, 1456-1462.

Tomasetti, C., and Vogelstein, B. (2015). Cancer etiology. Variation in cancer risk among tissues can be explained by the number of stem cell divisions. Science *347*, 78-81.

Tominaga, Y., Tsuzuki, T., Shiraishi, A., Kawate, H., and Sekiguchi, M. (1997). Alkylation-induced apoptosis of embryonic stem cells in which the gene for DNA-repair, methyltransferase, had been disrupted by gene targeting. Carcinogenesis *18*, 889-896.

Triff, K., Konganti, K., Gaddis, S., Zhou, B., Ivanov, I., and Chapkin, R.S. (2013). Genome-wide analysis of the rat colon reveals proximal-distal

differences in histone modifications and proto-oncogene expression. Physiol Genomics *45*, 1229-1243.

Tulenko, T.N., Chen, M., Mason, P.E., and Mason, R.P. (1998). Physical effects of cholesterol on arterial smooth muscle membranes: evidence of immiscible cholesterol domains and alterations in bilayer width during atherogenesis. J Lipid Res *39*, 947-956.

Turk, H.F., Barhoumi, R., and Chapkin, R.S. (2012). Alteration of EGFR spatiotemporal dynamics suppresses signal transduction. PLoS One *7*, e39682.

Ueland, P.M., Refsum, H., Male, R., and Lillehaug, J.R. (1986). Disposition of endogenous homocysteine by mouse fibroblast C3H/10T1/2 Cl 8 and the chemically transformed C3H/10T1/2 MCA Cl 16 cells following methotrexate exposure. Journal of the National Cancer Institute *77*, 283-289.

van de Wetering, M., Sancho, E., Verweij, C., de Lau, W., Oving, I., Hurlstone, A., van der Horn, K., Batlle, E., Coudreuse, D., Haramis, A.P.*, et al.* (2002). The beta-catenin/TCF-4 complex imposes a crypt progenitor phenotype on colorectal cancer cells. Cell *111*, 241-250.

Van der Flier, L.G., Sabates-Bellver, J., Oving, I., Haegebarth, A., De Palo, M., Anti, M., Van Gijn, M.E., Suijkerbuijk, S., Van de Wetering, M., Marra, G.*, et al.* (2007). The Intestinal Wnt/TCF Signature. Gastroenterology *132*, 628-632.

van Es, J.H., Haegebarth, A., Kujala, P., Itzkovitz, S., Koo, B.K., Boj, S.F., Korving, J., van den Born, M., van Oudenaarden, A., Robine, S.*, et al.* (2012). A critical role for the Wnt effector Tcf4 in adult intestinal homeostatic self-renewal. Mol Cell Biol *32*, 1918-1927.

Van Schoore, G., Mendive, F., Pochet, R., and Vassart, G. (2005). Expression pattern of the orphan receptor LGR4/GPR48 gene in the mouse. Histochem Cell Biol *124*, 35-50.

Verzi, M.P., and Shivdasani, R.A. (2010). Stem cells: The intestinal-crypt casino. Nature *467*, 1055-1056.

Vogelstein, B., Fearon, E.R., Hamilton, S.R., Kern, S.E., Preisinger, A.C., Leppert, M., Nakamura, Y., White, R., Smits, A.M., and Bos, J.L. (1988). Genetic alterations during colorectal-tumor development. N Engl J Med *319*, 525-532.

Vogelstein, B., Fearon, E.R., Kern, S.E., Hamilton, S.R., Preisinger, A.C., Nakamura, Y., and White, R. (1989). Allelotype of colorectal carcinomas. Science *244*, 207-211.

Vogelstein, B., and Kinzler, K.W. (2004). Cancer genes and the pathways they control. Nat Med *10*, 789-799.

Vogelstein, B., and Kinzler, K.W. (2012). Winning the war: science parkour. Science translational medicine *4*, 127ed122.

Vogelstein, B., Lane, D., and Levine, A.J. (2000). Surfing the p53 network. Nature *408*, 307-310.

Wang, A., Yoshimi, N., Ino, N., Tanaka, T., and Mori, H. (1997). Overexpression of cyclin B1 in human colorectal cancers. Journal of cancer research and clinical oncology *123*, 124-127.

Wanitsuwan, W., Kanngurn, S., Boonpipattanapong, T., Sangthong, R., and Sangkhathat, S. (2008). Overall expression of beta-catenin outperforms its nuclear accumulation in predicting outcomes of colorectal cancers. World J Gastroenterol *14*, 6052-6059.

Wassall, S.R., Brzustowicz, M.R., Shaikh, S.R., Cherezov, V., Caffrey, M., and Stillwell, W. (2004). Order from disorder, corralling cholesterol with chaotic lipids. The role of polyunsaturated lipids in membrane raft formation. Chem Phys Lipids *132*, 79-88.

Wassall, S.R., and Stillwell, W. (2008). Docosahexaenoic acid domains: the ultimate non-raft membrane domain. Chem Phys Lipids *153*, 57-63.

Watson, J.D., and Crick, F.H. (1953). Molecular structure of nucleic acids; a structure for deoxyribose nucleic acid. Nature *171*, 737-738.

West, N.J., Clark, S.K., Phillips, R.K., Hutchinson, J.M., Leicester, R.J., Belluzzi, A., and Hull, M.A. (2010). Eicosapentaenoic acid reduces rectal polyp number and size in familial adenomatous polyposis. Gut *59*, 918-925.

Whitehead, R.H., and Joseph, J.L. (1994). Derivation of conditionally immortalized cell lines containing the Min mutation from the normal colonic mucosa and other tissues of an "Immortomouse"/Min hybrid. Epithelial Cell Biol *3*, 119-125.

Whitehead, R.H., and Robinson, P.S. (2009). Establishment of conditionally immortalized epithelial cell lines from the intestinal tissue of adult normal and transgenic mice. American journal of physiology Gastrointestinal and liver physiology *296*, G455-460.

Worthley, D.L., and Leggett, B.A. (2010). Colorectal cancer: molecular features and clinical opportunities. The Clinical biochemist Reviews / Australian Association of Clinical Biochemists *31*, 31-38.

Wu, S., Powers, S., Zhu, W., and Hannun, Y.A. (2016). Substantial contribution of extrinsic risk factors to cancer development. Nature *529*, 43-47.

Xu, G., Ren, G., Xu, X., Yuan, H., Wang, Z., Kang, L., Yu, W., and Tian, K. (2010). Combination of curcumin and green tea catechins prevents dimethylhydrazine-induced colon carcinogenesis. Food Chem Toxicol *48*, 390-395.

Yamada, Y., Yoshimi, N., Hirose, Y., Matsunaga, K., Katayama, M., Sakata, K., Shimizu, M., Kuno, T., and Mori, H. (2001). Sequential analysis of morphological and biological properties of beta-catenin-accumulated crypts, provable premalignant lesions independent of aberrant crypt foci in rat colon carcinogenesis. Cancer research *61*, 1874-1878.

Yang, Y., Wang, X., Huycke, T., Moore, D.R., Lightfoot, S.A., and Huycke, M.M. (2013). Colon Macrophages Polarized by Commensal Bacteria Cause Colitis and Cancer through the Bystander Effect. Translational oncology *6*, 596-606.

Yi, J.S., Mun, D.G., Lee, H., Park, J.S., Lee, J.W., Lee, J.S., Kim, S.J., Cho, B.R., Lee, S.W., and Ko, Y.G. (2013). PTRF/cavin-1 is essential for multidrug resistance in cancer cells. Journal of proteome research *12*, 605-614.

Yoon, S., Lee, M.Y., Park, S.W., Moon, J.S., Koh, Y.K., Ahn, Y.H., Park, B.W., and Kim, K.S. (2007). Up-regulation of acetyl-CoA carboxylase alpha and fatty acid synthase by human epidermal growth factor receptor 2 at the translational level in breast cancer cells. The Journal of biological chemistry *282*, 26122-26131.

Yuen, S.T., Davies, H., Chan, T.L., Ho, J.W., Bignell, G.R., Cox, C., Stephens, P., Edkins, S., Tsui, W.W., Chan, A.S.*, et al.* (2002). Similarity of the phenotypic patterns associated with BRAF and KRAS mutations in colorectal neoplasia. Cancer research *62*, 6451-6455.

Zaidi, N.H., Liu, L., and Gerson, S.L. (1996). Quantitative immunohistochemical estimates of O6-alkylguanine-DNA alkyltransferase expression in normal and malignant human colon. Clinical cancer research : an official journal of the American Association for Cancer Research *2*, 577-584.

Zaidi, N.H., Pretlow, T.P., O'Riordan, M.A., Dumenco, L.L., Allay, E., and Gerson, S.L. (1995). Transgenic expression of human MGMT protects against azoxymethane-induced aberrant crypt foci and G to A mutations in the K-ras oncogene of mouse colon. Carcinogenesis *16*, 451-456.

Zedeck, M.S., Grab, D.J., and Sternberg, S.S. (1977). Differences in the acute response of the various segments ofrat intestine to treatment with the

intestinal carcinogen, methylazoxymethanol acetate. Cancer research *37*, 32-36.

Zell, J.A., Pelot, D., Chen, W.P., McLaren, C.E., Gerner, E.W., and Meyskens, F.L. (2009). Risk of cardiovascular events in a randomized placebo-controlled, double-blind trial of difluoromethylornithine plus sulindac for the prevention of sporadic colorectal adenomas. Cancer prevention research *2*, 209-212.

Zeller, K.I., Zhao, X., Lee, C.W., Chiu, K.P., Yao, F., Yustein, J.T., Ooi, H.S., Orlov, Y.L., Shahab, A., Yong, H.C.*, et al.* (2006). Global mapping of c-Myc binding sites and target gene networks in human B cells. Proceedings of the National Academy of Sciences of the United States of America *103*, 17834-17839.

Zhong, C., Fan, L., Yao, F., Shi, J., Fang, W., and Zhao, H. (2014). HMGCR is necessary for the tumorigenecity of esophageal squamous cell carcinoma and is regulated by Myc. Tumour biology : the journal of the International Society for Oncodevelopmental Biology and Medicine *35*, 4123-4129.

Zhou, H., Ivanov, V.N., Gillespie, J., Geard, C.R., Amundson, S.A., Brenner, D.J., Yu, Z., Lieberman, H.B., and Hei, T.K. (2005). Mechanism of radiation-induced bystander effect: role of the cyclooxygenase-2 signaling pathway. Proceedings of the National Academy of Sciences of the United States of America *102*, 14641-14646.

Zidovetzki, R., and Levitan, I. (2007). Use of cyclodextrins to manipulate plasma membrane cholesterol content: evidence, misconceptions and control strategies. Biochimica et biophysica acta *1768*, 1311-1324.

APPENDIX A

MAKING “SWISS ROLLS” FROM INTESTINAL SECTIONS

Purpose: To make Swiss rolls using 1/2 ~ 1/3 of isolated colon.

Materials: PBS (Gibco, 21600-069), dissection kit (scissor, forceps, blade), 10 mL syringes, biomedical needle, histology paper (OBEX Industries, 245, cassette (Simport, M498-6), straw (4 mm diameters, 3 cm long), 20% PFA (Electron Microscopy Science, 15713), Swiss roll tube, 100% Ethanol (KOPEC, V1001).

Procedure:

(1) Chill 70% and 50% ethanol at 4° C.
(2) Cut histology paper in half.
(3) Isolate colon and flush with PBS.
(4) Open colon along with Taeniae coli. Epiploic appendix (fat filled pouches) is lining close to Taeniae coli.

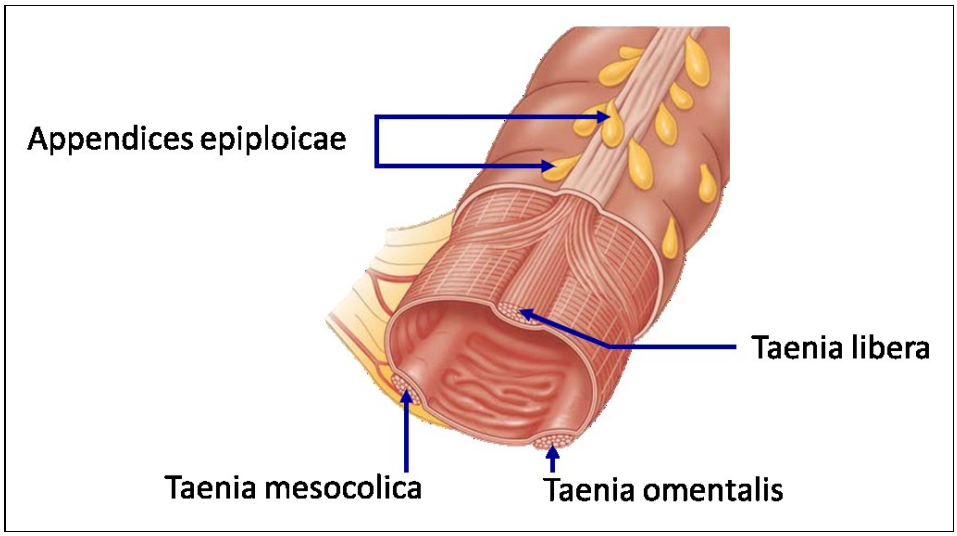

External appearance of colon

(5) Put colon on the PBS-wetted histology paper and cut the 1/2 ~ 1/3 of colon longitudinally.

Note: Keep luminal side facing up.

(6) Wrap the edge of the histology paper close to proximal colon end around the straw and slowly rolling the straw with fingers to roll the colon around the straw to form a Swiss roll.
(7) Drop the Swiss roll only (without the straw) into Swiss roll tube prefilled with

6 mL 4% PFA and incubate for 4 hr at 4° C.

(8) Dump PFA and wash with 50% and 70% ethanol every 20 min on ice.
Note: keep tissue and ethanol at 4° C.

(9) Store in 70% ethanol overnight at 4° C.

---

(10) Next day, label big cassette using HB1 pencil: solution to fix tissue, Animal ID and date.
Note: Be careful, only #1 pencil works

(11) Cut out square in the middle of sponge and locate it in the cassette. The hole is preventing Swissroll from unrolling.

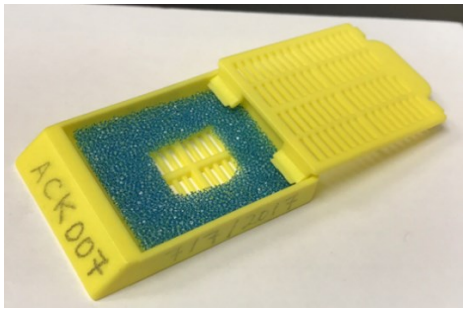

(12) Remove straw from the Swissroll and transfer it to the middle of sponge.
(13) Place it in a container with pre-chilled 70% ethanol.
(14) Take it to histology lab.

References:
Bialkowska AB, Ghaleb AM, Nandan MO, Yang VW. (2016) Improved Swiss-rolling Technique for Intestinal Tissue Preparation for Immunohistochemical and Immunofluorescent Analyses.J Vis Exp. (113).

APPENDIX B

QUANTIFICATION OF APOPTOTIC CELLS IN DNA DAMAGED LGR5^{+} STEM CELLS

Purpose: To quantify cells that are double positive to DNA damage and apoptosis.

Materials: Rabbit monoclonal phospho-gamma H2AX (γH2AX) Ser139 antibody (Cell Signaling 9718), goat polyclonal to GFP (Abcam, ab6673), Jackson donkey anti rabbit 649 (711-605-152) for H2AX, Jackson Donkey anti Goat 488 (705-545-147) for GFP, TUNEL assay kit: TACS 2TdT Replenisher Kit (Trevigen, 4810-30-R), Strepttavidine-Cy3 (ThermoFisher, 438315), sodium citrate tribasic (Sigma, S4641), Xylene (Fisher, X2P-1GAL), 100% Ethanol (KOPEC, V1001), 90% Ethanol (KOPEC, V1101), PAP pen (Invitrogen, 008899), TBST buffer (1X TBS with 0.1% Tween-20), Tween-20 (Sigma, P9416), IgG-free BSA (Roche, 9048-46-8, at 4° C), PBS (Gibco, 21600-069), donkey serum (Millipore, S30-100ml), Cell Signaling antibody diluent (Cell signaling, 8112), TritonX-100 (Sigma, 9002-93), ddH2O (Gibco, 15230-170), ProLong AntiFade (LifeTech, P36935), coverslip (VWR, 16004-336), metal pot, the immune stain moisture chamber and coplin jars (it is in the shelf labeled with Immunohistochemistry supplies).

Solutions:

10 X Tris Buffered Saline (TBS):

24.2 g Trizma® base ($C_4H_{11}NO_3$) (Fisher, BP154-1) + 80 g sodium chloride (NaCl) (Sigma, S3014) / 1 L dH2O. Adjust pH to 7.6. = 0.2 M Tris+1.36 M Nacl

Note: do not use BSA or milk to block. There is cross reactivity with the goat secondary.

Procedure:

1st day

(1) Prepare 1.2 L of 10 mM sodium citrate, pH 6.0 (3.52 g sodium citrate trisodium ($C_6H_5Na_3O_7 \cdot 2H_2O$) in 850 mL dd$H_2O$, adjust pH to 6.0 and then take final volume to 1.2 L). Preheat on hot plate by bringing to a boil at the level 10 on Thermolyne heat plate and once boiling, switch to level 5.9.
Note: Make sure the solution is NOT bubbling at all once the tissues go in the metal pot.

Deparaffinization/Rehydration

(2) Wash slides in Xylene 3 X 5 min.

(3) Circle with PAP pen if needed.
Note: Make a thick circle and dry out completely.

(4) Wash slides in 100% ethanol 3 X 4 min.
Note: Do not allow slides to dry at any time from this procedure.
(5) Wash slides in 95% ethanol 3 X 4 min.
(6) Wash slides in 70% ethanol 2 x 4 min.
(7) Wash slides in dH_2O 3 X 3 min.
Note: If paraffin is not completely removed, you will see non-specific signal.

Antigen Unmasking

(8) 20 min in sub-boiling 10 mM sodium citrate in metal pot on top of heat plate setting at 5.9. Cool metal pot (with slide inside) for additional 20 min in tub of tap water.
Note: If these steps are not performed, the antibodies will not have complete access to antigens in the tissue and will be unable to bind to the correct epitopes.

TUNEL assay to detect apoptotic cells

Note: Thaw reagents, except TdT enzyme (keep at -20° C) at 4° C. Warm up 10 x Labeling and Stop buffers at 25° C (room temperature, RT). Set oven temp to 37° C for the TdT step.
(9) Wash slides in dH_2O 1 X 5 min.
(10) Wash slides in PBS, 2 X 5 min.
(11) Blot excess liquid, then cover specimen with 13.3 μg/mL Proteinase K, 30 min, at RT.
per 3 sections (1:75 dilution) = 2.0 μL 1 mg/mL proteinase K + 150 μL good bottle dH_2O = 152 μL
Note: Spin proteinase K prior to taking aliquot.
(12) Wash slides in dd H_2O 3 X 2 min each.
(13) Immerse in 1 X 0.22 μm filtered 1X labeling buffer (diluted in dH_2O) for 5 min at RT.
(14) Prepare TdT mixture.
Note: Spin reagents prior to taking aliquot.
Note: Remove TdT enzyme from freezer only briefly.
per 3 sections = 3.0 μL TdT-dNTP + 150 μL 1X labeling buffer + 3.0 μL Mn_2 + 3.0 μL TdT enzyme = 159 μL
Negative control = exclude TdT enzyme. Keep mix on ice.
(15) Blot (50 μL) of TdT mixture carefully around each tissue section. Add TdT labeling mixture.
Note: make sure mixture covers whole tissue.

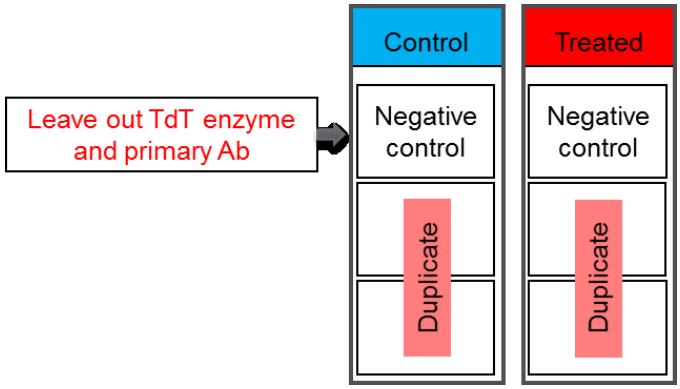

(16) Place slides in humidified chamber at 37° C, 1 hr.
(17) Transfer slides to 1 X 0.22 μm filtered Stop buffer which is diluted in dH_2O, RT, 5 min.
(18) Wash slides in PBS 2 X 2 min.
Note: Keep samples in the dark for the following steps.
(19) Prepare Streptavidin-Cy3 (1:60 dilution).
Note: Spin SA-Cy3 prior to taking aliquot to avoid debris.
per 3 sections = 147.5 μL PBS/0.05% tween + 2.5 μL Strepavidin-Cy3 = 150 μL
Note: Spin reagents prior to use.
(20) Blot (50 μL of Streptavidine-Cy3 in PBS/0.05% tween) around tissue section and apply Strepavidin mix to slide.
Incubate in a humidified chamber for 30 min at RT in the dark.
(21) Wash slides in PBS 3 X 2 min.
(22) Wash slides in dH_2O 3 X 5 min.

Label with H2AX to detect DNA damaged cells
(23) Wash slides in TBST 2 X 5 min.
(24) 5% donkey serum in TBST (blocking solution) 30 min at RT.
2.25 mL donkey serum + 42.75 mL TBST = 45 mL
(25) Prepare 1° antibody (phospho-γH2AX).
1:200 in Cell Signaling antibody diluent.
per 3 sections = 1 μL H2AX antibody (Ab) + 199 μL diluent = 200 μL
Neg control = use antibody diluent
(26) Incubate overnight at 4° C in a humidified chamber.

2nd day

(27) Wash slides in TBST 4 X 3 min.

(28) Prepare 2° Ab (Jackson donkey anti rabbit IgG – 649).
1:400 in 1% donkey serum/0.3% Triton in PBS for 1 hr at RT.
per 3 sections 0.5 μL 2° Ab + 2 μL donkey serum + 6 μL 10% Triton + 191.5 μL PBS = 200 μL

Label with GFP to detect LGR5^{+} stem cells

(29) Wash slides in dH_2O 2 X 5 min.

(30) Wash slides in TBST 4 X 5 min.

(31) Block in 5% donkey serum in TBST for 15 min at room temperature.
2.25 mL donkey serum + 43.75 mL TBST= 45 mL

(32) Prepare 1° antibody (GFP)
1:400 in PBS / 1% donkey serum.
per 3 sections = 0.5 μL GFP Ab + 2 μL donkey serum + 197.5 μL PBS = 200 μL
Neg control = use antibody diluent

(33) Incubate overnight at 4° C in a humidified chamber.
Note: The solution beads up (on some steps) into a little ball. You have to really drag it with a pipet tip to cover the tissue. And you need to look very closely to make sure the outer edge is covered with solution. This is the distal end which we want to score so we don't want it to dry out and give artifact.

3rd day

(34) Wash slides in TBST 4 X 3 min.

(35) Prepare 2° Ab (Jackson donkey anti goat IgG – 488).
1:400 in 1% donkey serum / 0.3% Triton in PBS for 30 min - 1 hr at RT.
per 3 sections = 0.5 μL GFP Ab + 2 μL donkey serum + 6 μL 10% Triton + 191.5 μL PBS =200 μL

(36) Wash slides in TBST 4 X 5 min.

(37) Wash slides in dH_2O 3 X 5 min.

(38) Coverslip with ProLong AntiFade + DAPI.

Capture image of entire Swiss roll

(1) All immunofluorescent images of colonic crypts were captured using an inverted TE 300 Nikon Eclipse fluorescence microscope equipped with

40X/1.30 Nikon Plan Fluor oil immersion objective and a Photometrics Cool Snap EZ digital CCD camera and a SOLA external light source.

(2) Images are processed using the NIS Image software, version 3.2 (Nikon).

(3) Start scanning from the distal colon and find a GFP positive good structured crypt in distal colon. Capture image of GFP positive good structured crypt.

Analysis

(1) Using NIS element, open up image you captured.

(2) Count number of cells positive to TUNEL, γH2AX and both positive to TUNEL and γH2AX and DAPI per crypt.

(3) Calculate % Apoptotic cells per crypt = # of $TUNEL^+$ stem or differentiated cells / total # of stem or differentiated cells per crypt x 100

(4) Calculate % DNA damaged cells per crypt = # of $\gamma H2AX^+$ stem or differentiated cells / total # of stem or differentiated cells per crypt x 100

(5) Calculate % Non-targeted apoptosis = # of $TUNEL^+$ and $\gamma H2AX^-$ stem or differentiated cells / total # of $\gamma H2AX^-$ stem or differentiated cells x 100

(6) Calculate % Targeted apoptosis = # of double positive $TUNEL^+$ and $\gamma H2AX^+$ stem or differentiated cells / total # of $\gamma H2AX^+$ stem or differentiated cells x 100

(7) Perform statistical analysis using GraphPad Prism 6.

References:

Hua G, Thin TH, Feldman R, Haimovitz-Friedman A, Clevers H, Fuks Z, Kolesnick R. (2012) Crypt base columnar stem cells in small intestines of mice are radioresistant.Gastroenterology. 143(5):1266-1276.

APPENDIX C

QUANTIFICATION OF PROLIFERATING CELLS IN DNA DAMAGED LGR5^{+} STEM CELLS

Purpose: To quantify cells double positive for DNA damage and proliferation.

Materials: Rabbit monoclonal phospho-gamma H2AX (γH2AX) Ser139 antibody (Cell Signaling #9718), Jackson donkey anti rabbit 649 (711-605-152) for H2AX, goat polyclonal to GFP (Abcam #ab6673), Alexa-488 rabbit anti goat IgG (Invitrogen A-21222) for GFP, Click-It Plus EdU Alexa Fluor imaging kit (Thermofisher, C10640), sodium citrate tribasic (Sigma, S4641), Xylene (Fisher, X2P-1GAL), 100% Ethanol (KOPEC, V1001), 90% Ethanol (KOPEC, V1101), PAP pen (Invitrogen, 008899), TBST buffer (1X TBS with 0.1% Tween-20), Tween-20 (Sigma, P9416), BSA (Roche, 9048-46-8, at 4°C), PBS (Gibco, 21600-069), donkey serum (Millipore, S30-100ml), rabbit serum (Invitrigen, 10510), Cell Signaling antibody diluent (Cell signaling, #8112), TritonX-100 (Sigma, 9002-93), dH2O (Gibco, 15230-170), ProLong AntiFade (LifeTech, P36935), coverslip (VWR, 16004-336), metal pot, the immune stain moisture chamber and coplin jars are in the shelf labeled with Immunohistochemistry supplies.

Solutions:
10 X Tris Buffered Saline (TBS):
24.2 g Trizma® base ($C_4H_{11}NO_3$) (Fisher, BP154-1) + 80 g sodium chloride (NaCl) (Sigma, S3014) / 1 L dH2O. Adjust pH to 7.6. = 0.2 M Tris+1.36 M Nacl
Note: do not use BSA or milk to block. There is cross reactivity with the goat secondary.

Procedure:
1st day

(1) Prepare 1.2 L of 10 mM sodium citrate, pH 6.0 (3.52 g sodium citrate trisodium ($C_6H_5Na_3O_7 \cdot 2H_2O$) in 850 mL H_2O, adjust pH to 6.0 and then take final volume of 1.2 L). Preheat on hot plate by bringing to a boil at the level 10 on Thermolyne heat plate and once boiling, switch to level 5.9.
Note: Make sure the solution is NOT bubbling at all once the tissues go in the metal pot.

Deparaffinization/Rehydration

(2) Wash slides in Xylene 3 X 5 min.
(3) Circle with PAP pen if needed. Note: Make a thick circle and dry out completely.

(4) Wash slides in 100% ethanol 3 X 4 min.
Note: Do not allow slides to dry at any time from this procedure.
(5) Wash slides in 95% ethanol 3 X 4 min.
(6) Wash slides in 70% ethanol 2 x 4 min.
(7) Wash slides in dH_2O 3 X 3 min.
Note: If paraffin is not completely removed, you will see non-specific signal.

Antigen Unmasking

(8) 20 min in sub-boiling citrate in metal pot. Cool metal pot for 20 min in tub of tap water.
Note: If these steps are not performed, the antibodies will not have complete access to antigens in the tissue and will be unable to bind to the correct epitopes.

Label with H2AX to detect DNA damaged cells

(9) Wash slides in TBST 2 X 5 min.
(10) 5% donkey serum in TBST (blocking solution) 30 min at RT.
2.25 mL donkey serum + 42.75 mL TBST = 45 mL
(11) Prepare 1° antibody (phospho-γH2AX).
1:200 in Cell Signaling antibody diluent.
per 3 sections = 1 μL H2AX antibody (Ab) + 199 μL diluent = 200 μL
Neg control = use antibody diluent

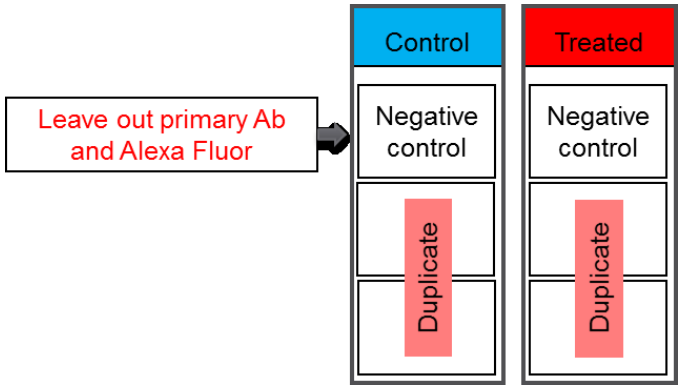

(12) Incubate overnight at 4° C in a humidified chamber.

2nd day

(13) Wash slides in TBST 4 X 3 min.
(14) Prepare 2° Ab (Jackson donkey anti rabbit IgG – 649).

1:400 in 1% donkey serum/0.3% Triton in PBS for 1 hr at RT.
per 3 sections 0.5 μL 2° Ab + 2 μL donkey serum + 6 μL 10% Triton + 191.5 μL PBS = 200 μL

Label with GFP to detect LGR5^{+} stem cells

(15) Wash slides in dH_2O 2 X 5 min.
(16) Wash slides in TBST 4 X 5 min.
(17) Block in 10% rabbit serum in TBST for 1 hr at RT.
2.25 mL donkey serum + 43.75 mL TBST= 45 mL
(18) Prepare 1° antibody (GFP)
1:400 in PBS / 1% donkey serum.
per 3 sections = 0.5 μL GFP Ab + 2 μL donkey serum + 197.5 μL PBS = 200 μL
Neg control = leave out 1° antibody
(19) Incubate overnight at 4° C in a humidified chamber.
Note: The solution beads up (on some steps) into a little ball. You have to really drag it with a pipet tip to cover the tissue. And you need to look very closely to make sure the outer edge is covered with solution. This is the distal end which we want to score so we don't want it to dry out and give artifact.

3rd day

(20) Wash slides in TBST 4 X 3 min.
(21) Prepare 2° Ab (Alexa-488 rabbit anti goat IgG).
1:400 in 1% rabbit serum / 1% BSA/ 0.3% Triton in PBS for 1 hr at RT.
per 3 sections = 0.5 μL GFP Ab + 2 μL rabbit serum + 20 μL 10% BSA + 6 μL 10% Triton + 171.5 μL PBS = 200 μL
(22) Wash slides in TBST 4 X 5 min.

Label EdU to detect proliferating cells

(23) Wash slides in dH2O 1 X 3 min.
(24) Wash slides in 3% BSA in PBS (dip 3-4 times).
(25) Incubate slides in 0.5% Triton X-100 in PBS, 20 min.
(26) Prepare Click-It Reaction Cocktail, Table below. Add reagents in order.
For negative control, omit Alexa.

Per 5 sections	
10X Rxn buffer (D)	43.75 µl
Water	396.25 µl
CuSO4 (E)	10 µl
Alexa Fluor 647(B)	1.2 µl
10X Rxn buffer additive (F)	5 µl
Water	45 µl
Total	501.2µl

(27) Store in the dark and use within 15 minutes.
Note: don't use until indicated below.
(28) Wash slides in 3% BSA in PBS, wash (dip 3-4 times).
(29) Add 100 µl Click-It reaction cocktail to each sample, incubate 30 min RT, in the immune stain moisture chamber.
(30) Tap off slide and wash slides in 3% BSA in PBS wash (dip 2-3 times)
(31) Wash slides in PBS, 1 X 30 sec
(32) Coverslip with ProLong AntiFade + DAPI.

Capture image of entire Swiss roll

(1) All immunofluorescent images of colonic crypts were captured using an inverted TE 300 Nikon Eclipse fluorescence microscope equipped with 40X/1.30 Nikon Plan Fluor oil immersion objective and a Photometrics Cool Snap EZ digital CCD camera and a SOLA external light source.
(2) Images are processed using the NIS Image software, version 3.2 (Nikon).
(3) Start scanning from the distal colon and find a GFP positive good structured crypt in distal colon. Capture image of GFP positive good structured crypt.

Analysis

(1) Using NIS element, open up image you captured.
(2) Count number of cells positive to TUNEL, γH2AX and both positive to TUNEL and γH2AX and DAPI per crypt.
(3) Calculate % proliferating cells per crypt = # of EdU^+ stem or differentiated cells / total # of stem or differentiated cells per crypt x 100
(4) Calculate % DNA damaged cells per crypt = # of $\gamma H2AX^+$ stem or differentiated cells / total # of stem or differentiated cells per crypt x 100
(5) Calculate % proliferating cells with no DNA damage = # of EdU^+ and $\gamma H2AX^-$ stem or differentiated cells / total # of $\gamma H2AX^-$ stem or differentiated cells x 100
(6) Calculate % proliferating cells with DNA damage = # of double positive EdU^+ and $\gamma H2AX^+$ stem or differentiated cells / total # of $\gamma H2AX^+$ stem or differentiated cells x 100
(7) Perform statistical analysis using GraphPad Prism 6.

Click-It Reaction (https://www.youtube.com/watch?v=AZ35QQDPlH8)
In this assay the modified thymidine analogue EdU is efficiently incorporated into newly synthesized DNA and fluorescently labeled with a bright, photostable Alexa Fluor® dye in a fast, highly-specific click reaction. This fluorescent labeling of proliferating cells is accurate and compatible with antibody methods due to the mild click protocol. EdU (5-ethynyl-2'-deoxyuridine) is a nucleoside analog of thymidine and is incorporated into DNA during active DNA synthesis. With Click-iT® EdU, mild fixation and detergent permeabilization is sufficient for the small molecule-based Click-iT® EdU detection reagent to gain access to the DNA. Click it reaction: Detection is based on a click reaction, a copper catalyzed covalent reaction between a picolyl azide and an alkyne. In this application, the alkyne is found in the ethynyl moiety of EdU, while the picolyl azide is coupled to Alexa Fluor™ 488 dye.

References:

Hua G, Thin TH, Feldman R, Haimovitz-Friedman A, Clevers H, Fuks Z, Kolesnick R. (2012) Crypt base columnar stem cells in small intestines of mice are radioresistant.Gastroenterology. 143(5):1266-1276.

APPENDIX D

QUANTIFYING CELLS DOUBLE POSITIVE FOR DNA DAMAGE AND MGMT IN LGR5^{+} STEM CELLS

Purpose: To quantify cells double positive for DNA damage and DNA adduct repairing enzyme.

Materials: Rabbit monoclonal phospho-gamma H2AX (γH2AX) Ser139 antibody (Cell Signaling #9718), goat polyclonal to GFP (Abcam #ab6673), Jackson donkey anti rabbit 649 (711-605-152) for H2AX, Jackson Donkey anti Goat 488 (705-545-147) for GFP, Mouse monoclonal to MGMT (AbCam cat# ab54306), Donkey anti-mouse 546 (Invitrogen A10036) for MGMT, sodium citrate tribasic (Sigma, S4641), Xylene (Fisher, X2P-1GAL), 100% Ethanol (KOPEC, V1001), 90% Ethanol (KOPEC, V1101), PAP pen (Invitrogen, 008899), TBST buffer (1X TBS with 0.1% Tween-20), Tween-20 (Sigma, P9416), BSA (Roche, 9048-46-8, at 4°C), PBS (Gibco, 21600-069), donkey serum (Millipore, S30-100ml), Cell Signaling antibody diluent (Cell signaling, #8112), TritonX-100 (Sigma, 9002-93), dH2O (Gibco, 15230-170), ProLong AntiFade (LifeTech, P36935), coverslip (VWR, 16004-336), metal pot, the immune stain moisture chamber and coplin jars are in the shelf labeled with Immunohistochemistry supplies.

Solutions:

<u>10 X Tris Buffered Saline (TBS):</u>

24.2 g Trizma® base ($C_4H_{11}NO_3$) (Fisher, BP154-1) + 80 g sodium chloride (NaCl) (Sigma, S3014) / 1 L dH2O. Adjust pH to 7.6. = 0.2 M Tris+1.36 M Nacl

Note: do not use BSA or milk to block. There is cross reactivity with the goat secondary.

Procedure:

1st day

(1) Prepare 1.2 L of 10 mM sodium citrate, pH 6.0 (3.52 g sodium citrate trisodium ($C_6H_5Na_3O_7 \cdot 2H_2O$) in 850 mL H_2O, adjust pH to 6.0 and then take final volume of 1.2 L). Preheat on hot plate by bringing to a boil at the level 10 on Thermolyne heat plate and once boiling, switch to level 5.9.

Note: Make sure the solution is NOT bubbling at all once the tissues go in the metal pot.

Deparaffinization/Rehydration

(2) Wash slides in Xylene 3 X 5 min.

(3) Circle with PAP pen if needed. Note: Make a thick circle and dry out completely.
(4) Wash slides in 100% ethanol 3 X 4 min.
Note: Do not allow slides to dry at any time from this procedure.
(5) Wash slides in 95% ethanol 3 X 4 min.
(6) Wash slides in 70% ethanol 2 x 4 min.
(7) Wash slides in dH_2O 3 X 3 min.
Note: If paraffin is not completely removed, you will see non-specific signal.

Antigen Unmasking

(8) 20 min in sub-boiling citrate in metal pot. Cool metal pot for 20 min in tub of tap water.
Note: If these steps are not performed, the antibodies will not have complete access to antigens in the tissue and will be unable to bind to the correct epitopes.

Label with H2AX to detect DNA damaged cells

(9) Wash slides in TBST 2 X 5 min.
(10) 5% donkey serum in TBST (blocking solution) 30 min at RT.
2.25 mL donkey serum + 42.75 mL TBST = 45 mL
(11) Prepare 1° antibody (phospho-γH2AX).
1:200 in Cell Signaling antibody diluent.
per 3 sections = 1 μL H2AX antibody (Ab) + 199 μL diluent = 200 μL
Neg control = use antibody diluent

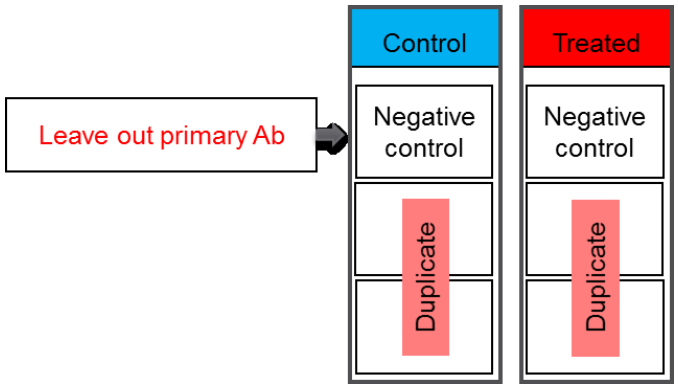

(12) Incubate overnight at 4° C in a humidified chamber.

2nd day

(13) Wash slides in TBST 4 X 3 min.

(14) Prepare 2° Ab (Jackson donkey anti rabbit IgG – 649).
1:400 in 1% donkey serum/0.3% Triton in PBS for 1 hr at RT.
per 3 sections 0.5 μL 2° Ab + 2 μL donkey serum + 6 μL 10% Triton + 191.5 μL PBS = 200 μL

Label with GFP to detect LGR5^{+} stem cells

(39) Wash slides in dH_2O 2 X 5 min.

(40) Wash slides in TBST 4 X 5 min.

(41) Block in 5% donkey serum in TBST for 15 min at room temperature.
2.25 mL donkey serum + 43.75 mL TBST= 45 mL

(42) Prepare 1° antibody (GFP)
1:400 in PBS / 1% donkey serum.
per 3 sections = 0.5 μL GFP Ab + 2 μL donkey serum + 197.5 μL PBS = 200 μL
Neg control = leave out 1° antibody

(43) Incubate overnight at 4° C in a humidified chamber.
Note: The solution beads up (on some steps) into a little ball. You have to really drag it with a pipet tip to cover the tissue. And you need to look very closely to make sure the outer edge is covered with solution. This is the distal end which we want to score so we don't want it to dry out and give artifact.

3rd day

(44) Wash slides in TBST 4 X 3 min.

(45) Prepare 2° Ab (Jackson donkey anti goat IgG – 488).
1:400 in 1% donkey serum / 0.3% Triton in PBS for 30 min - 1 hr at RT.
per 3 sections = 0.5 μL 2° Ab + 2 μL donkey serum + 6 μL 10% Triton + 191.5 μL PBS =200 μL

Label with MGMT to detect repairing cells

(46) Wash slides in dH_2O 2 X 5 min.

(47) Wash slides in TBST 4 X 5 min.

(48) Block in 5% donkey serum in TBST for 15 min at room temperature.
2.25 mL donkey serum + 43.75 mL TBST= 45 mL

(49) Incubate with 1° antibody (MGMT)

Drop 1-2 drop per sample

(50) Incubate overnight at 4° C in a humidified chamber.

4th day

(51) Wash slides in TBST 4 X 3 min.

(52) Prepare 2° Ab (Donkey anti-mouse 546).
1:400 in 1% donkey serum / 0.3% Triton in PBS for 30 min - 1 hr at RT.
per 3 sections = 0.5 μL 2° Ab + 2 μL donkey serum + 6 μL 10% Triton + 191.5 μL PBS =200 μL

(53) Wash slides in TBST 4 X 5 min.

(54) Wash slides in dH_2O 3 X 5 min.

(55) Coverslip with ProLong AntiFade + DAPI.

Capture image of entire Swiss roll

(1) All immunofluorescent images of colonic crypts were captured using an inverted TE 300 Nikon Eclipse fluorescence microscope equipped with 40X/1.30 Nikon Plan Fluor oil immersion objective and a Photometrics Cool Snap EZ digital CCD camera and a SOLA external light source.

(2) Images are processed using the NIS Image software, version 3.2 (Nikon).

(3) Start scanning from the distal colon and find a GFP positive good structured crypt in distal colon. Capture image of GFP positive good structured crypt.

References:

Hua G, Thin TH, Feldman R, Haimovitz-Friedman A, Clevers H, Fuks Z, Kolesnick R. (2012) Crypt base columnar stem cells in small intestines of mice are radioresistant.Gastroenterology. 143(5):1266-1276.

APPENDIX E

QUANTIFYING CELLS DOUBLE POSITIVE FOR DNA DAMAGE AND BAX IN LGR5^{+} STEM CELLS

Purpose: To immunohistochemically quantify Bax expression.

Materials: Rabbit monoclonal to Bax (Cell Signaling #14796), Jackson donkey anti rabbit 649 (711-605-152) for Bax, Goat polyclonal to GFP (Abcam #ab6673), Jackson Donkey anti Goat 488 (705-545-147) for GFP, sodium citrate tribasic (Sigma, S4641), Xylene (Fisher, X2P-1GAL), 100% Ethanol (KOPEC, V1001), 90% Ethanol (KOPEC, V1101), PAP pen (Invitrogen, 008899), TBST buffer (1X TBS with 0.1% Tween-20), Tween-20 (Sigma, P9416), BSA (Roche, 9048-46-8, at 4°C), PBS (Gibco, 21600-069), donkey serum (Millipore, S30-100ml), Cell Signaling antibody diluent (Cell signaling, #8112), TritonX-100 (Sigma, 9002-93), dH2O (Gibco, 15230-170), ProLong AntiFade (LifeTech, P36935), coverslip (VWR, 16004-336), metal pot, the immune stain moisture chamber and coplin jars are in the shelf labeled with Immunohistochemistry supplies.

Solutions:
10 X Tris Buffered Saline (TBS):
24.2 g Trizma® base ($C_4H_{11}NO_3$) (Fisher, BP154-1) + 80 g sodium chloride (NaCl) (Sigma, S3014) / 1 L dH2O. Adjust pH to 7.6. = 0.2 M Tris+1.36 M Nacl
Note: do not use BSA or milk to block. There is cross reactivity with the goat secondary.

Procedure:
1st day

(1) Prepare 1.2 L of 10 mM sodium citrate, pH 6.0 (3.52 g sodium citrate trisodium ($C_6H_5Na_3O_7 \cdot 2H_2O$) in 850 mL H_2O, adjust pH to 6.0 and then take final volume of 1.2 L). Preheat on hot plate by bringing to a boil at the level 10 on Thermolyne heat plate and once boiling, switch to level 5.9.
Note: Make sure the solution is NOT bubbling at all once the tissues go in the metal pot.

Deparaffinization/Rehydration

(2) Wash slides in Xylene 3 X 5 min.
(3) Circle with PAP pen if needed. Note: Make a thick circle and dry out completely.
(4) Wash slides in 100% ethanol 3 X 4 min.
Note: Do not allow slides to dry at any time from this procedure.

(5) Wash slides in 95% ethanol 3 X 4 min.
(6) Wash slides in 70% ethanol 2 x 4 min.
(7) Wash slides in dH_2O 3 X 3 min.
Note: If paraffin is not completely removed, you will see non-specific signal.

Antigen Unmasking

(8) 20 min in sub-boiling citrate in metal pot. Cool metal pot for 20 min in tub of tap water.
Note: If these steps are not performed, the antibodies will not have complete access to antigens in the tissue and will be unable to bind to the correct epitopes.

Label with GFP to detect $LGR5^+$ stem cells

(9) Wash slides in dH_2O 2 X 5 min.
(10) Wash slides in TBST 4 X 5 min.
(11) Block in 5% donkey serum in TBST for 15 min at room temperature.
2.25 mL donkey serum + 43.75 mL TBST= 45 mL
(12) Prepare 1° antibody (GFP)
1:400 in PBS / 1% donkey serum.
per 3 sections = 0.5 µL GFP Ab + 2 µL donkey serum + 197.5 µL PBS = 200 µL
Neg control = leave out 1° antibody

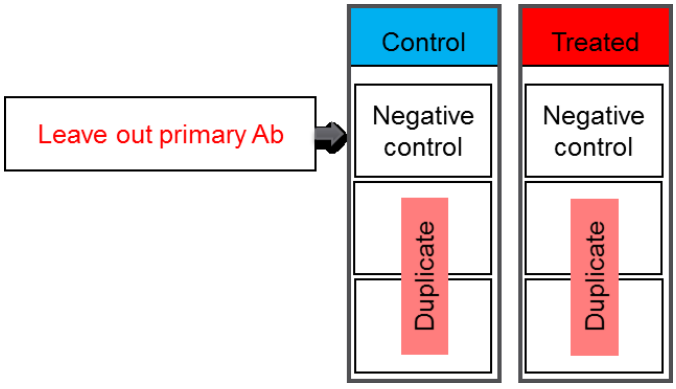

Incubate overnight at 4° C in a humidified chamber.
Note: The solution beads up (on some steps) into a little ball. You have to really drag it with a pipet tip to cover the tissue. And you need to look very closely to make sure the outer edge is covered with solution. This is the

distal end which we want to score so we don't want it to dry out and give artifact.

2nd day

(13) Wash slides in TBST 4 X 3 min.
(14) Prepare 2° Ab (Jackson donkey anti goat IgG – 488).
1:400 in 1% donkey serum/0.3% Triton in PBS for 1 hr at RT.
per 3 sections 0.5 μL 2° Ab + 2 μL donkey serum + 6 μL 10% Triton + 191.5 μL PBS = 200 μL

Label with Bax

(15) Wash slides in dH_2O 2 X 5 min.
(16) Wash slides in TBST 4 X 5 min.
(17) Block in 5% donkey serum in TBST for 15 min at room temperature.
2.25 mL donkey serum + 43.75 mL TBST= 45 mL
(18) Prepare 1° antibody (Bax, 1:400) in Cell Signaling antibody diluent (#8112)
per 3 sections = 0.5 μL Bax Ab + 199.5 μL antibody diluent = 200 μL
Neg control = leave out 1° antibody
Incubate overnight at 4° C in a humidified chamber.
(19) Incubate overnight at 4° C in a humidified chamber.

3rd day

(20) Wash slides in TBST 4 X 3 min.
(21) Prepare 2° Ab (Jackson donkey anti rabbit IgG – 649).
1:400 in 1% donkey serum / 0.3% Triton in PBS for 30 min - 1 hr at RT.
per 3 sections = 0.5 μL 2° Ab + 2 μL donkey serum + 6 μL 10% Triton + 191.5 μL PBS =200 μL
(22) Wash slides in TBST 4 X 5 min.
(23) Wash slides in dH_2O 3 X 5 min.
(24) Coverslip with ProLong AntiFade + DAPI.

Capture image of entire Swiss roll

(1) All immunofluorescent images of colonic crypts were captured using an inverted TE 300 Nikon Eclipse fluorescence microscope equipped with 40X/1.30 Nikon Plan Fluor oil immersion objective and a Photometrics Cool Snap EZ digital CCD camera and a SOLA external light source.
(2) Images are processed using the NIS Image software, version 3.2 (Nikon).

(3) Start scanning from the distal colon and find a GFP positive good structured crypt in distal colon. Capture image of GFP positive good structured crypt.

Analysis

(8) Using NIS element, open file you with to analyze.
(9) Draw ROI of GFP^{high} cells to quantify intensity of Bax in Lgr5 stem cell region. Go to Simple ROI Editor - Bezier.
(10) Draw ROI of GFP^{neg} cells to quantify intensity of Bax in non-Lgr5 stem cell region. Go to Simple ROI Editor - Bezier. Click finish when you are done with drawing.
(11) Quantify its intensity. Go to Automated Measurement Result.
(12) Click Update measurement in Automated Measurement Result panel. This will give you a mean intensity for each of the ROI.
(13) Calculate the relative intensity of Bax in GFP^{high} / GFP^{neg} cells.
(14) Perform statistical analysis using GraphPad Prism 6.

References:

Dumitru R, Gama V, Fagan BM, Bower JJ, Swahari V, Pevny LH, Deshmukh M. (2012) Human embryonic stem cells have constitutively active Bax at the Golgi and are primed to undergo rapid apoptosis.Mol Cell. 46(5):573-583.

APPENDIX F

QUANTIFYING NUCLEAR/CYTOSOLIC β-CATENIN IN ACF

Purpose: Labeling β-catenin inn GI sections (Swiss Roll).

Materials: Mouse monoclonal β-catenin antibody (BD Transduction, 610154/dilution 1:500), Anti-mouse Alexa 546 (Life Technologies, A10036/dilution 1:200), 0.05 M Tris pH 7.6, TBST buffer (1X TBS with 0.1% Tween-20), Tween-20 (Sigma, P9416), donkey serum (Millipore, S30-100ml), BSA (Roche, 9048-46-8, at 4°C), PBS (Gibco, 21600-069), sodium citrate tribasic (Sigma, S4641), Xylene (Fisher, X2P-1GAL), 100% Ethanol (KOPEC, V1001), 90% Ethanol (KOPEC, V1101), PAP pen (Invitrogen, 008899), TritonX-100 (Sigma, 9002-93), dH2O (Gibco, 15230-170), ProLong AntiFade (LifeTech, P36935), coverslip (VWR, 16004-336), metal pot, the immune stain moisture chamber and coplin jars are in the shelf labeled with Immunohistochemistry supplies, H&E stained slide.
Note: H&E stained slide and β-catenin stain slide has to be serial section so that we can measure intensity of β-catenin of ACF.

Solutions:
10X Tris Buffered Saline (TBS):
24.2 g Trizma® base ($C_4H_{11}NO_3$) (Fisher, BP154-1) + 80 g sodium chloride (NaCl) (Sigma, S3014) / 1 L dH2O. Adjust pH to 7.6. = 0.2 M Tris+1.36 M Nacl
0.05 M Tris-HCl buffer:
6.057g Tris (Fisher. BP154-1) / 1L dH2O. Adjust pH to 7.6.
2% BSA:
2g BSA + 100ml 0.05 M Tris-HCl buffer (pH 7.6)
Note: Do not use BSA or milk to block. There is cross reactivity with the goat secondary ab.

Procedure:
1st day

(1) Prepare 1.2 L of 10 mM sodium citrate, pH 6.0 (3.52 g sodium citrate trisodium ($C_6H_5Na_3O_7 \cdot 2H_2O$) in 850 mL H_2O, adjust pH to 6.0 and then take final volume of 1.2 L). Preheat on hot plate by bringing to a boil at the level 10 on Thermolyne heat plate and once boiling, switch to level 5.9.
Note: Make sure the solution is NOT bubbling at all once the tissues go in the metal pot.

Deparaffinization/Rehydration

(2) Wash slides in Xylene 3 X 5 min.

(3) Circle with PAP pen if needed.
Note: Make a thick circle and dry out completely.
(4) Wash slides in 100% ethanol 3 X 4 min.
Note: Do not allow slides to dry at any time from this procedure.
(5) Wash slides in 95% ethanol 3 X 4 min.
(6) Wash slides in 70% ethanol 2 x 4 min.
(7) Wash slides in dH_2O 3 X 3 min.
Note: If paraffin is not completely removed, you will see non-specific signal.

Antigen Unmasking

(8) 20 min in sub-boiling citrate in metal pot. Cool metal pot for 20 min in tub of tap water.
Note: If these steps are not performed, the antibodies will not have complete access to antigens in the tissue and will be unable to bind to the correct epitopes.

Label β-catenin

(9) Wash slides in dH_2O 2 X 5 min.
(10) Wash slides in TBST 2X 5 min.
(11) Block in 5% donkey serum in TBST for 40 min at RT.
(12) Wash slides in 0.05 M Tris-HCl buffer (pH 7.6) 2 x 5 min
(13) Tap serum off
(14) Put slides in the immune stain moisture chamber and add primary antibody
(15) Prepare 1° antibody (β-catenin)
1:500 in PBS / 2% BSA in 0.05 M Tris-HCl buffer (pH 7.6)
per 5 sections = 0.5 μL β-catenin Ab + 249.5 μL 2% BSA in 0.05 M Tris-HCl = 250 μL
Neg control = leave out 1° antibody

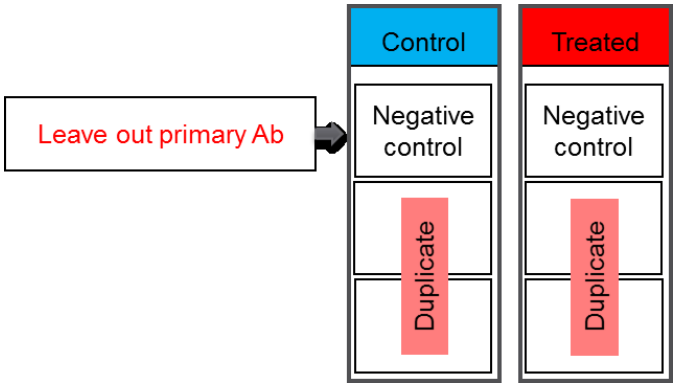

Incubate overnight at 4° C in a humidified chamber.

Note: The solution beads up (on some steps) into a little ball. You have to really drag it with a pipet tip to cover the tissue. And you need to look very closely to make sure the outer edge is covered with solution. This is the distal end which we want to score so we don't want it to dry out and give artifact.

2nd day

(16) Wash in 0.05 M Tris-HCl buffer (pH 7.6) 3 X 5 min
(17) Prepare 2° Ab (Anti-mouse Alexa 546).
1:200 in 2% BSA in 0.05 M Tris-HCl buffer (pH 7.6) for 1 hr at RT.
per 5 sections = 1.25 μL 2° Ab + 248.75 μL 2% BSA in 0.05 M Tris-HCl = 250 μL
(18) Wash slides in 0.05 M Tris-HCl buffer (pH 7.6) 3 X 5 min
(19) Wash slides in dH_2O 3 X 5 min.
(20) Coverslip with ProLong AntiFade + DAPI.

Imaging

(1) Have pathologist record number and location of ACF using H&E stained slide.
(2) Find the ACF on β-catenin stained slide and capture image.
(3) All immunofluorescent images of colonic crypts were captured using an inverted TE 300 Nikon Eclipse fluorescence microscope equipped with × 40/1.30 Nikon Plan Fluor oil immersion objective and a Photometrics Cool Snap EZ digital CCD camera and a SOLA external light source (Nikon, Melville, NY, USA), TRITC filter.
(4) Images are processed using the NIS Image software, version 3.2 (Nikon).

Analysis

(1) Using NIS element, open file you with to analyze.
(2) Find ACF on β-catenin stained slide. Draw β-catenin positive region of ACF you want to analyze to quantify intensity of cellular β-catenin in ACF. Go to Simple ROI Editor - Bezier. Draw ACF.
(3) Draw region of nucleus with in the ACF to quantify intensity of β-catenin in nucleus. Go to DAPI channel to visualize nucleus. Go to Simple ROI Editor - Bezier. Draw each nucleus. Click finish when you are done with drawing.
(4) Quantify its intensity. Go to Automated Measurement Result.
(5) Click Update measurement in Automated Measurement Result panel. This will give you a mean intensity for each of the ROI.

(6) Calculate the intensity of nucleus and cytosolic β-catenin in ACF. Subtract intensity of nucleic β-catenin from cellular β-catenin to quantify intensity of cytosolic β-catenin.
(7) Perform statistical analysis using GraphPad Prism 6.

References:

McGinley JN, Thompson MD, Thompson HJ. (2010) A method for serial tissue processing and parallel analysis of aberrant crypt morphology, mucin depletion, and Beta-catenin staining in an experimental model of colon carcinogenesis.Biol Proced Online. 12(1):9032.

APPENDIX G

SINGLE CELL ISOLATION

Purpose: Isolate single cells from mouse colon crypts.

Materials: ADF (Gibco, SILAC Advanced DMEM/F-12 Flex; no glucose included, A24943-01), PenStrep (P/S) (Gibco, 15140-122), HEPES (Gibco, H0887), Glucose (Gibco, A24940-01), 12x75 mm polypropylene tube (BD, 352063), FBS (HyClone, SH30084.03), EDTA (Sigma, ED4SS), 2mM EGTA pH 8.0 (Sigma, E4378), 0.25% trypsin (Gibco, 25200-056), sodium butyrate (Sigma, B5887), Y-27632 (Sigma, Y0503), N-Acetyl-L-cysteine (Sigma, A9165), 10% BSA (Roche, 9048-46-8, at 4°C) in PBS (Gibco, 21600-069), 0.5% BSA in PBS, 20 unit/μl DNase (Sigma, D5025) diluted in PBS, 20-gauge needle (BD, 305176), 5ml syringe (BD, 309646), 40 μm cell strainer (Falcon, 352340), 20 μm cell strainer (Partec, 04-0042-2305), Propidium Iodide staining solution.

The day before:

(1) Chill Ca/Mg free PBS in cell culture fridge and lab fridge.
(2) Prepare ADF^+ = 50 mL ADF + 0.5 mL glutamax + 0.5 mL P/S + 0.5 mL HEPES + 0.5mL Glucose.
(3) Precoat flow collection tubes 12 X 75 mm polypropylene tube with 2% FBS in ADF^+.
    Note: keep in 4° C fridge.

The day of isolation:

(1) Make 20 mM EDTA in PBS, pH 7.4 solution fresh immediately before use.
    6 colons (30 mL/ colon) = 180 mL PBS + 1.52 g EDTA
    (add 6 drops 10 M HCl + 6 drops 1 M HCl to reach pH to 7.4)
(2) Warm EDTA to 37° C in cell culture room.
(3) Pre-warm 0.25% trypsin to RT.
(4) Make 0.055 g sodium butyrate in 1.0 mL PBS (500 mM stock).
(5) Thaw FBS (1 mL per colon).
(6) Turn on 'Centrifuge 5920R' and pre-cool to 4° C.

Isolate crypts from colon

(1) Remove colon from mouse and place in cold Ca/Mg Free PBS in weigh boat.
(2) Using gavage needle, perfuse with 10 mL cold PBS, cut the colon longitudinally (see APPENDIX A) and drop into 50 mL tube with 30 mL cold PBS containing 1X Pen/Strep (0.3 mL).
(3) Vortex colon to remove remaining debris, 6 x 5 sec each at setting 10.
    Note: Replace with fresh cold PBS and repeat to help remove bacteria, 3 X 5 sec each.

(4) Incubate the intestine in a 50 mL tube of 2 mM EGTA at 37° C for 20 min. (EGTA is dissociating cell-cell interaction by depleating Ca^{2+}, I added this step to increase the yield. 1-2 mM of EGTA is also used to separate colonal crypt (Ikuma et al., 1998; Kaaij et al., 2013; Robert et al., 2001; van der Wurff et al., 1998)).

(5) Incubate the intestine in a 50 ml tube of 20 mM EDTA at 37° C for 15 min. (EDTA is dissociating basolateral membrane of crypt from stroma by depleating Ca^{2+} (Munoz et al., 2012; Sato et al., 2011)).

(6) Meanwhile prepare single cell cocktail (1 mL/ colon).

1 mL of single cell cocktail = 1 mL ADF^+ + 1 μL 10 mM Y-27632 + 2.5 μL 400 μM N-Ac + 30 μL 10% BSA + 10 μL DNase (20 unit/μL) + 8 μL 0.25 M EGTA + 1 μL 500 mM butyrate.

(7) After 35 min, transfer the suspended tissue to a fresh tube of 30 mL cold PBS + 30 μL butyrate and vortex (setting 10 for 2 X 5 sec) to release crypts.

Dissociate single cells from crypt

(8) Remove colon and add FBS to tube of crypts to 2% (0.6 mL) and spin down the crypts at 300 x g, 5 min at 4° C.

(9) Aspirate solution and gently resuspend crypts with 10 mL cold ADF^+ + 10 μL butyrate. (Or vortex for 5 sec X 2 at setting 7).

(10) Spin at 200 x g, 2 min at 4° C (helps prevent pelleting of single cells).

(11) Aspirate and gently resuspend in 10 mL ADF^++10 μL butyrate. (Or vortex for 5 sec X 2 at setting 7).
Note: Take a 10 μL aliquot to count.

(11) Spin at 300 x g, 3 min at 4° C.

(12) Aspirate and resuspend (or vortex for 5 sec X 2 at setting 7) crypts in 5 ml 0.25% trypsin + 50 μL of DNase (20 unit/μL).

(13) Incubate at 37° C water bath for 7 min.

Isolate single cells from crypt

(14) After incubation, pass suspension through 20-gauge needle gently 3x to aid complete dissociation. Let sit 1 min then pass each sample thru needle 1x more.

(15) Add 10 mL ice cold ADF^+ + 250 μL FBS (final 1% FBS) + 1.5 mL 20 mM EGTA (final 1.2 mM EGTA) to stop reaction.

(16) Pass through 40 μm cell strainer, changing strainer when it becomes too slow.

(17) Add additional 10 mL ADF^+ and 2 μL Y-27632 + 20 μL butyrate + 80 μL 0.25 M EGTA.
(This may be a problem step. I'm dropping 5% FBS to 1% because it may cause problem in spinning cells down. If cells don't filter well, need to dilute with larger volume.)

(18) Spin down at 500 X g, 3 min. Make sure you see pellet. If there is still fluffy stuff, spin at 550 X g, 1 min. If you still don't have a pellet, go up to 600 X g for 1-2 min.
(19) Carefully aspirate and resuspend in 200 μL single cell cocktail (prepared above) to achieve 4 ~ 5 x 10^6 cells/mL.
(20) 200 μL of single cell cocktail will be added when you sort single cell (APPENDIX H).

References:

Ikuma, M., Binder, H.J., and Geibel, J. (1998). Role of apical H-K exchange and basolateral K channel in the regulation of intracellular pH in rat distal colon crypt cells. J Membr Biol *166*, 205-212.

Kaaij, L.T., van de Wetering, M., Fang, F., Decato, B., Molaro, A., van de Werken, H.J., van Es, J.H., Schuijers, J., de Wit, E., de Laat, W., et al. (2013). DNA methylation dynamics during intestinal stem cell differentiation reveals enhancers driving gene expression in the villus. Genome Biol 14, R50.

Munoz, J., Stange, D.E., Schepers, A.G., van de Wetering, M., Koo, B.K., Itzkovitz, S., Volckmann, R., Kung, K.S., Koster, J., Radulescu, S., et al. (2012). The Lgr5 intestinal stem cell signature: robust expression of proposed quiescent '+4' cell markers. The EMBO journal 31, 3079-3091.

Robert, M.E., Singh, S.K., Ikuma, M., Jain, D., Ardito, T., and Binder, H.J. (2001). Morphology of isolated colonic crypts. Cells Tissues Organs 168, 246-251.

Sato, T., Stange, D.E., Ferrante, M., Vries, R.G., Van Es, J.H., Van den Brink, S., Van Houdt, W.J., Pronk, A., Van Gorp, J., Siersema, P.D., et al. (2011). Long-term expansion of epithelial organoids from human colon, adenoma, adenocarcinoma, and Barrett's epithelium. Gastroenterology 141, 1762-1772.

van der Wurff, A.A., ten Kate, J., Marx, P.T., van der Linden, E.P., Beek, C.C., Bovelander, F.J., Dekker, J., Dinjens, W.N., von Meyenfeldt, M.F., Arends, J.W., et al. (1998).

APPENDIX H

SORTING CELLS USING THE MOFLOW CELL SORTER

Purpose: Sorting cells using fluorescence intensity on the MoFlow.

Materials: 20 μm cell strainer (Partec, 04-0042-2305), Propidium Iodide staining solution, PI (BD, 51-66211E), single cell cocktail, Precoated flow collection tubes (12x75 mm polypropylene tube) with 2% FBS in ADF^+ kept in 4° C fridge.

Procedure:

(1) Isolate single cells (APPENDIX G).

Take to Vet School: 20 μm cell strainer, Lab book or old flow runs, extra flow tubes, gloves, 1000 and 10 μL Pipets and tips, PI, coated flow tubes, PBS/ADF^+ to collect into (1 mL per sample), sharpie & pen

Note: pipet gently about 3-4 times with P-1000. Excessive pipetting is not needed and is harmful.

(2) At flow lab, filter again thru 20 μm cell strainer into coated tube, rinsing with a 200 μL of single cell cocktail.

(3) Add PI to detect dead cells (5 μL of 100 μg /mL PI per 500 μL cells) and vortex to mix it with cells.
Note: DO NOT ADD PI if sorting with tomato. Tomato cells show up in same area as PI (562-588nm) positive cells.

(4) Add 500 μL of single cell cocktail into a pre-coated tube and collect sorted cells into it using Beckman Coulter MoFlo (Indianapolis, IN, USA).

References:

Fan YY, Davidson LA, Callaway ES, Wright GA, Safe S, Chapkin RS. (2015) A bioassay to measure energy metabolism in mouse colonic crypts, organoids, and sorted stem cells. Am J Physiol Gastrointest Liver Physiol. 309(1):G1-9.

APPENDIX I

QUANTIFYING SINGLE CELLS POSITIVE FOR γH2AX AND CLEAVED CASPASE-3

Purpose: To quantify DNA damaged cells undergoing apoptosis using the FlowSight imaging flow cytometer.

Materials: Phospho γH2AX-AF647 conjugated antibody (Cell Signaling, #9720), cleaved caspase3-AF555 conjugated antibody (Cell Signaling, #9604), 20% PFA (Electron Microscopy Science, 15713), rabbit serum (Invitrigen, 10510), 200 proof pure Ethanol (KOPTEC, 64-17-5), BSA (Roche, 9048-46-8, at 4°C).
Note: Ethanol has to be kept in -20° C.

Procedure:

(1) Prepare single cells (APPENDIX G) or sorted cells (APPENDIX H).
(2) Add the same volume of 8 % PFA (diluted from the 20% PFA stock in PBS) to the tube containing sorted single cells right after the cells were collected to make 4% PFA.
(3) Fix cells for 20 min at RT.
(4) Remove PFA by centrifugation (1000 X g for 5 min) and resuspend cells in pre-chilled 1.5 mL PBS. Keep it on ice from this step.
(5) Transfer cells in PBS into 5 mL tube and permeabilize cells by adding 3.5 mL of ice-cold 100% ethanol drop by drop slowly to pre-chilled cells, while gently invert tube up and down to a final concentration of 70% ethanol.
(6) Incubate 24 hr at -20° C. PFA-fixed sorted cells in 70% ethanol can be store at -20° C up to 1 month.
(7) Spin the cells at 1000 X g for 10 min to remove the ethanol at 4° C.
(8) Rehydrate the cells with 3 mL pre-chilled PBS (the volume?) for 10 on ice min and spin down at 1000 x g for 10 min at 4° C. Repeat.
(9) Blocking the cells with 5 mL 5% rabbit serum buffer (diluted in PBST, 0.1% Tween 20) for 30 min on ice and wash by centrifugation (1000 X g for 5 min at 4° C).
(10) Resuspend cells in 100 μL pre-chilled incubation buffer on ice (0.5% BSA in PBS).
(11) Add 2 μL of γH2AX (1:50) and/ or 2 μL of Caspase-3 (1:50) Ab into sample tubes.
(12) Incubate on rotator for overnight at 4° C.

---

(13) Next day, wash sample by centrifugation (1000 X g for 5 min at 4° C) in 1 mL incubation buffer (2 times).

(14) Resuspend cells in 25 μL PBS (recommended concentration of cells by Amnis is 1 x 10^6 cells/50 μL PBS).
(15) Add 2.5 μL of DAPI (10x) to the 25 μL of samples. Keep on ice.
(16) Run FlowSight.

References:

Heo SK, Noh EK, Yoon DJ, Jo JC, Choi Y, Koh S, Baek JH, Park JH, Min YJ, Kim H. (2015) Radotinib Induces Apoptosis of CD11b+ Cells Differentiated from Acute Myeloid Leukemia Cells. PLoS One. 10(6):e0129853.

APPENDIX J

MEASUREMENT OF CELLULAR FREE CHOLESTEROL LEVELS

Purpose: To label sorted cells with Filipin III to measure free cholesterol levels in the cell.

Materials: 0.5 mg/mL Filipin III stock (10X), 1 mg of Filipin III from *Streptomyces filipinesis* (Sigma, F4767), DMSO, PBS (Gibco, 21600-069), 20% PFA (Electron Microscopy Science, 15713), 1.5 mL Low Retantion Microtubes (Phenix, MAX-815S), Cell Imaging Coverglass (8 chamber) slides (Eppendorf, 0030742036).
Note: Filipin III stock preparation is described after procedure

Procedure:

(1) Transfer single cells (APPENDIX G) or sorted cells (APPENDIX H) in 1.5 mL Low Retantion Microtubes (10^5 cells/ mL).
(2) Rinse cells with 1 mL PBS (300 X g for 3 min at 4° C) and fix with 1.5% paraformaldehyde (PFA) for 30 min at room temperature.
(3) Rinse again with 1 mL PBS (1000 X g for 10 min at RT) and resuspend cells in PBS.
(4) Resuspend cells in 100 μL PBS
(5) Incubate cells with Filipin at a final concentration of 50 μg/mL in PBS for 45 min at RT. Add 90 μL cells in PBS + 10 μL of 0.5 mg/ml Filipin III stock in 1.5 mL Low Retantion Microtubes.
(6) Transfer 100 μL cells onto Cell Imaging Coverglass (8 chamber) slides for microscopic analysis.
(7) Acquire images using 360/40 nm excitation and 480/40 nm emission filters with a 365 nm dichroic long pass filter. (Other similar UV filters should work.)
(8) It is very important to use a low level (10 ms) of exposure time. Depending on lamp, filters, etc., you can attenuate excitation by 90–99% with a neutral density filter. This reduced excitation will slow photobleaching.

Making 0.5 mg/ml Filipin III stock solution:

Materials: 1 mg of Filipin III from *Streptomyces filipinesis* (Sigma, F4767), DMSO, PBS (Gibco, 21600-069), DMSO safe acrodisk filter (VWR, PN4433), Acrodisk filter (VWR, PN4192), 20-gauge needle (BD, 305176), 5mL syringe (BD, 309646), 1mL syringe (BD, 309659),

Procedure:

(1) Prepare 0.6 mL tubes for aliquot.

(10 tubes X 33 μL stock, 10 tubes X 44ul stock, 10 tubes X 55 μL stock, 10 tubes X 66 μL stock)

(2) Filter 500 μL DMSO and 2 mL 1 X PBS into 2 mL eppy tube separately. (Use DMSO safe acrodisk filter and acrodisk filter to filter DMSO and PBS respectively)

(3) Fill syringe with 400 μL filtered DMSO and inject it into Filipin III vial and invert it to mix.
(Use 20G needle on 1mL syringe).

(4) Fill syringe with 1.6 mL filtered PBS and inject it into Filipin III vial (Use 20G needle on 5 mL syringe) and dissolve Filipin III for 2-3 min by inverting it.

(5) Take Filipin III vial, prepared tubes, 200p pipet and 200 tips into chemical hood.

(6) Aliquot dissolved Filipin III into prepared tubes.
Note: Flush nitrogen gas before close the lid to eliminate oxygen in epi tube.

(7) Wrap with foil to protect it from lights.

(8) Keep it in a box containing desiccant pack at -20° C.

Note: The aliquoted Filipin III won't freeze at -20°C. The freezing point of DMSO is greatly decreased by the presence of water, requiring much lower temperatures to freeze the sample. Company recommend to use Fillipin III in DMSO (80% hydration) and it is not frozen in -20°C. Do not surprised that DMSO Fillipin III in DMSO is not frozen at -20°C.

Reference:

Maxfield FR, Wüstner D. (2012) Analysis of cholesterol trafficking with fluorescent probes. Methods Cell Biol. 108:367-393.

Norman AW, Demel RA, de Kruyff B, van Deenen LL. (1972) Studies on the biological properties of polyene antibiotics. Evidence for the direct interaction of filipin with cholesterol. J Biol Chem. 247(6):1918-1929.

Schroeder F, Holland JF, Bieber LL. (1971) Fluorometric evidence for the binding of cholesterol to the filipin complex. J Antibiot (Tokyo). 24(12):846-849.

APPENDIX K

MEASUREMENT OF PLASMA MEMBRANE ORDER

Purpose: To measure membrane order using confocal microscope

Materials:
5 mM Di4-ANEPPDHQ (ThermoFisher, D36802), Cell Imaging Coverglass (8 chamber) slides (Eppendorf, 0030742036), Leibovitz's L-15 Medium, no phenol red (Gibco, 21083-027)
Note: 5 mM Di4-4-ANEPPDHQ is stored in a 200 μL aliquots wrapped in aluminum foil at -20° C.

Procedure:

(1) Prepare single cells (APPENDIX G) or sorted cells (APPENDIX H) in Leibovitz's L-15 Medium (10^5 cells/ mL).
(2) Bring cells and Di4 dye to the microscope room.
Note: Keep cells and Di4 Dye wrapped in aluminum foil on ice.
(3) Setting up the microscope

Dye	Excitation	Emission (Ordered)	Emission (Disordered)
Di-4-ANEPPDHQ	488	520-600	620-700

Note: These ordered and disorder emissions are arbitrary and can vary, however the included reference has excellent guidelines

(4) Di-4-ANEPPDHQ is mixed with cells (at a final concentration of 1 μM)
(5) Cells are transferred onto Cell Imaging Coverglass (8 chamber) slides for microscopic analysis using a laser confocal microscope (Leica DMi8 S Platform EII).
(6) Immediately image cells to avoid internalization of dye.

Generation of general polarization (GP) images:

1. Download and install FIJI (FIJI Is Just ImageJ) software. Fiji is an image processing package — a "batteries-included" distribution of ImageJ, bundling a lot of plugins which facilitate scientific image analysis. (https://fiji.sc/)
2. Install General Polarization Plug in. (https://github.com/dwaithe/GP-plugin)
3. Place all the images you would like to analyze in one folder.
4. Using FIJI convert all images in the folder to tiffs. Process → Batch→ Convert. Then select the folder the images are in as the “Input” and then create a new folder “Raw Tiffs” as the “Output”. Make sure interpolation is set to “None”. See the example below.

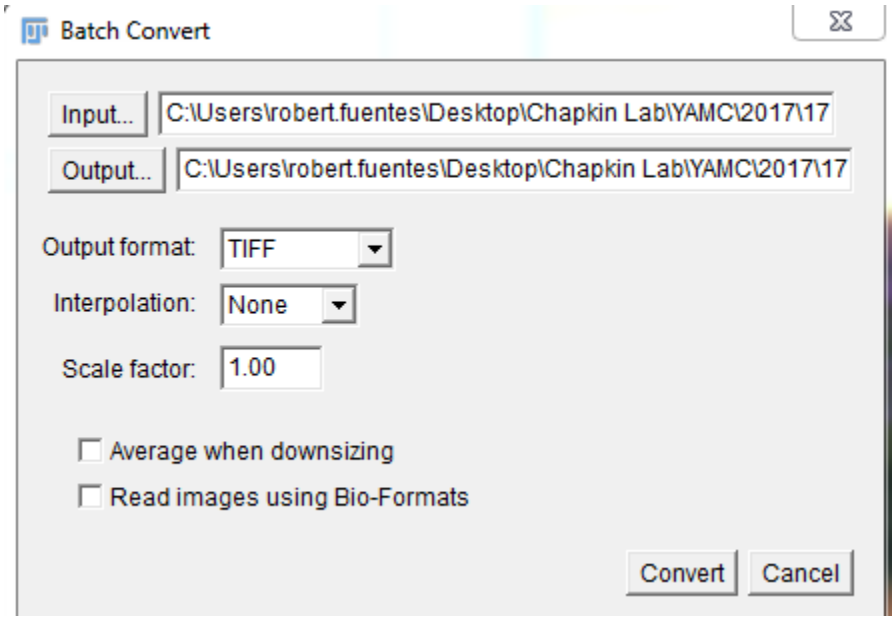

5. To generate GP images. Process → Batch → Macro. Paste the "GP macro" text into the white area. Select the "Raw Tiffs" folder as the "Input" and then create a new folder "GP images" as the "Output". Then select "Process". Note: A threshold will need to be selected. Open an image, place the mouse in an area that has no cells, to determine the background intensity. Sum the intensity for the order and disordered channel, and then use this as a guide. Do the same for a region that has a strong membrane signal and record the values. It is usually best to set the threshold at a value that falls above the background sum but below the sum membrane signal.

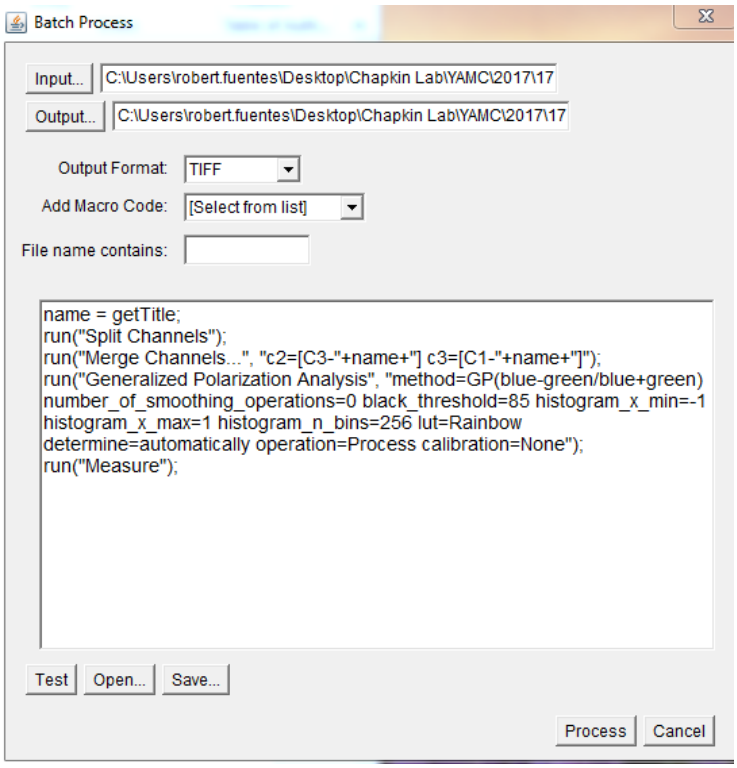

6. The “GP” folder will now contain GP images.

Analysis of general polarization (GP) images

1. To draw regions of interest (ROIs) on the images. Analyze → Tools → ROI Manger.
2. Select the polygon tool, and draw and ROI. Then on the ROI manger select “Add”.
3. Repeat this process until you collect all the necessary ROIs. Then on the ROI Manger select “Measure”. This will generate a list of measurements that can be copied and pasted into excel, and used for analysis.

Reference:

Ashdown GW, Owen DM. (2015) Imaging membrane order using environmentally sensitive fluorophores. Methods Mol Biol. 1232:115-122.

Owen DM, Rentero C, Magenau A, Abu-Siniyeh A, Gaus K. (2011) Quantitative imaging of membrane lipid order in cells and organisms. Nat Protoc. 7(1):24-35.

Sáenz JP, Sezgin E, Schwille P, Simons K. (2012) Functional convergence of hopanoids and sterols in membrane ordering. Proc Natl Acad Sci U S A. 109(35):14236-14240.

APPENDIX L

MAKING A CHOLESTEROL STOCK SOLUTION

Purpose: Preparation of 10 mM MβCD:cholesterol stock solution

Materials: MβCD:cholesterol (Sigma, C4951), MβCD (Sigma, C4555).

Procedure:

(1) MβCD:cholesterol (Sigma, C4951-30MG) contains 40 mg of cholesterol and 1000 mg of MβCD in a bottle.
(2) Molar ratio of MβCD:cholesterol is 7.4:1 and, solubility is increased by adding extra uncomplexed MβCD to make molar ratio of 10:1.
(3) Add 351 mg of uncomplexed MβCD powder (Sigma, C4555) into cholesterol:MβCD (Sigma, C4951-30MG) container and add 9.34 mL cholesterol free organoid media (APPENDIX N) to dissolve it. It will come up with 10 mM cholesterol in 10.34 mL media.

Note: 10 mM MβCD:cholesterol is stored in a 100 μL aliquots wrapped in aluminum foil at -20° C.

Note: Flush nitrogen gas before close the lid to eliminate oxygen in epi tube.

Note: 5 mM MβCD:600 μM (cholesterol molar ratio of 8:1) or 2.5 mM MβCD:250 μM (cholesterol molar ratio of 10:1) is known to be a soluble form and deliver cholesterol in both Fu5AH and CHO cells.

References:

Zidovetzki R, Levitan I. (2007) Use of cyclodextrins to manipulate plasma membrane cholesterol content: evidence, misconceptions and control strategies. Biochim Biophys Acta. 1768(6):1311-1324.

APPENDIX M

CHOLESTEROL INCUBATION WITH ORGANOIDS

Purpose: To incubate cholesterol with organoids in culture.

Materials: ADF (Gibco, SILAC Advanced DMEM/F-12 Flex, A24943-01), PenStrep (P/S) (Gibco, 15140-122), HEPES (Gibco, H0887), Glucose (Gibco, A24940-01), 100 µg/mL EGF mouse recombinant (LifeTech, PMG8041, 100 µg EGF/ 1 mL PBS + 0.5% FBS), 0.2 mM LDN/Noggin replacement (Cellagen Tech, 0.2 mM stock in PBS + 0.5% FBS), 1 mg/mL R-Spondin mouse (Sino Biological Lnc., 50316-M08S, 0.5 µg/mL final concentration), N2 supplement (LifeTech, 17502-048, 100X), B27 supplement (LifeTech, 12587-010, 50X), N-Acetyl-L-cysteine (Sigma, A9165), 100 µg/mL Wnt (TimeBioscience, rmW3aL-002, final 30 ng/mL), 10mM MβCD:cholesterol stock solution (APPENDIX L).

Solutions:

(1) Prepare ADF^+ = 50 mL ADF + 0.5 mL glutamax + 0.5 mL P/S + 0.5 mL HEPES + 0.5 mL Glucose.

(2) Make cholesterol free media.
Note: L-WRN media contains cholesterol so do not use it. Instead Wnt, R-Spondin and Noggins has to be added to the ADF^+ media separately.

Organoid media	Final concentration	500 µL/well
EGF (100 µg/mL)	50 ng/mL	0.25
LDN (Noggin replacement (0.2 mM)	0.2 µM ~ 81.3 ng/mL	0.5
R-Spondin (1 mg/mL)	1x	0.25
N2 supplement (100x)	1x	5
B27 supplement (50x)	1x	10
N-Acetylcys (400 µM) (A)	1 µM	1.25
ADF^+ (w/ Gln, HEPES)		482.5
Wnt (100 ug/mL)	50 ng/mL	0.25
Total volume		500

Procedure:

(1) Prepare organoid (200 organoid per well).
Note: Replace media with cholesterol containing media 24 hr after seeding cells.

(2) Prepare cholesterol containing media = 5 µL of 10mM MβCD:cholesterol stock solution (APPENDIX M) + 495 µL cholesterol free media per well.

(3) Remove media and replace with cholesterol containing media.

(4) Change media every 24 hr to avoid oxidization.

(5) Harvest organoid upon cholesterol incubation for 72 hr.

References: McFarlane MR, Cantoria MJ, Linden AG, January BA, Liang G, Engelking LJ. (2015) Scap is required for sterol synthesis and crypt growth in intestinal mucosa. J Lipid Res. 56(8):1560-15671.

APPENDIX N

QUANTIFYING PROLIFERATING CELLS FOLLOWING CHOLESTEROL INCUBATION WITH ORGANOIDS

Purpose: To determine whether increased cholesterol promotes cell proliferation in organoids culture.

Reagents: ADF (Gibco, SILAC Advanced DMEM/F-12 Flex, A24943-01), PenStrep (P/S) (Gibco, 15140-122), HEPES (Gibco, H0887), Glucose (Gibco, A24940-01), FBS (HyClone, SH30084.03), 0.25% trypsin (Gibco, 25200-056), 100 μg/mL EGF mouse recombinant (LifeTech, PMG8041, 100 μg EGF/ 1 mL PBS + 0.5% FBS), 0.2 mM LDN/Noggin replacement (Cellagen Tech, 0.2 mM stock in PBS + 0.5% FBS), 1 mg/mL R-Spondin mouse (Peprotech, 315-32, 0.5 μg/mL final concentration), N2 supplement (LifeTech, 17502-048, 100X), B27 supplement (LifeTech, 12587-010, 50X), N-Acetyl-L-cysteine (Sigma, A9165), 100 μg/mL Wnt (TimeBioscience, rmW3aL-002, final 30 ng/mL), 50 mM cholesterol (Sigma, C4951), 40 mM EdU stock (Life Technologies, A10044) in PBS (Gibco, 21600-069), Click-iT™ Plus EdU Alxa Fluor™ 647 Imaging Kit (ThermoFisher, C10640), 4% PFA (Electron Microscopy Science, 15713) in PBS, 3% BSA (Roche, 9048-46-8, at 4°C) in PBS, 0.5% TritonX-100 (Sigma, 9002-93) in PBS, DAPI (LifeTech, H3570), 10mM MβCD:cholesterol stock solution (APPENDIX L).

Organoid preparation:

Prepare organoid incubated with or without cholesterol (APPENDIX N).

EdU preparation:

(1) Make 10 mg/mL EdU solution (40 mM stock solution) in saline, heat in water bath until dissolved (37° C for 20-30 min).
(2) Aliquot 1 mL of 10 mg/mL EdU into 2.0 ml tubes. Avoid multiple freeze/thaws.
(3) Store at -20° C protected from light.
(4) Can be stored at -20° C for 6 months from time of preparation.
(5) Prepare a working solution of 1X Click–iT EdU reaction buffer (Component D)
(6) Transfer the solution (4 mL) in the Component D bottle to 36 mL of deionized water.
(7) To make a 10X stock solution of the Click-iT EdU buffer additive (Component F, 400 mg)
(8) Add 2 mL deionized water to the vial, then mix until fully dissolved.
(9) After use, store any remaining solution at $\leq -20^{\circ}$ C. (need to aliquot it if you won't use it with in one year)

Note: When stored as directed, this stock solution is stable for up to 1 year. If the solution develope a brown color, it has degraded and should be discarded.

Label EdU:

(1) Prepare a 5 mM solution of EdU using EdU stock solution (40 mM), then mix well.
32 samples (32 μL) = 4 μL of 5 mM EdU + 28 μL ADF^+
(2) After use, store any remaining stock solution at ≤−20°C. When stored as directed, this stock solution is stable for up to 1 year.
(3) Directly add 0.5 μL 5 mM EdU to 500 μL cholesterol containing media in 24 well (5 μM final concentration).
(4) Incubate the cells for 1.5 hours (1~2 hr is recommended).
Note: incubation time and concentration of EdU is different depending on experiment and cell. For mouse study we inject EdU 2 hr before terminate it however, organoid grow faster upon cholesterol incubation so I reduced incubation time down to 1.5 hr to avoid saturated EdU^+ cellstype.
(5) Aspirate culture medium, add 0.5 ml ice cold ADF^+ and mechanically pipette and scrap the matrigel with a P1000 on ice.
(6) Transfer the dissociated matrigel into a 2 ml tube (pooling 3 wells for 1 sample).
(7) Use another 0.5 ml cold ADF+ to finish transfer of all material from the wells.
(8) Spin down the organoids at short (5000 X g for 4 sec at 4° C) . Remove media (may see a glutinous Matrigel area above pellet. Careful not to aspirate organoids!)
(9) Resuspend organoids in 0.3 ml 0.25% EDTA-Trypsin and incubate at 37 °C for 8~12 min using heat block.
(10) Every 2 minutes, pipet solution well (6 to 10 times).
(11) Add 900 μL cold 10% FBS ADF^+ solution to stop reaction.

EdU reaction:

(1) Spin down at 500 X g (or 600 X g) for 3 min at 4 °C.
(2) Remove supernatant as much as possible
(3) Resuspend dissociated cells completely in 500 μL PBS.
(4) Note: resuspend organoid well to prevent fixing organoid without dissociation
(5) Add 500 μL 8.0% PFA in PBS to dissociated cells in 500 μL PBS (4% PFA final). Incubate 15 min at room temperature.
(6) Spin down to remove PFA (1500 x g, 2 minat RT), wash once with 1mL 3% BSA in PBS.
(7) Spin and remove BSA. (Note: once organoids are PFA fixed, you can use a faster speed to centrifuge them, 1500 x g for 2 minutes, and operate fixed cells at RT).
(8) Add 1 mL 0.5% Triton X-100 in PBS. Incubate 20 min at RT to permeabilize.

(9) Prepare Click-iT reaction cocktail during triton incubation. All reagent should warm to RT before use.
(10) Add reagents in order shown. Store in the dark until ready to use and use within 15 minutes.

Per 5 sections	
10X Rxn buffer (D)	43.75 µl
Water	396.25 µl
CuSO4 (E)	10 µl
Alexa Fluor 647(B)	1.2 µl
10X Rxn buffer additive (F)	5 µl
Water	45 µl
Total	501.2 µl

(11) Spin down to remove 0.5% Triton X-100 from cells.
(12) Wash once in 3% BSA in PBS. Spin down to remove wash solution.
(13) Add 100 µL Click-It reaction cocktail to each sample. Pipet gently to make sure all cells are exposed to buffer.
(14) Incubate 30 min RT, in the DARK.
(15) Spin down to remove reaction cocktail.
(16) Wash once with 1 mL 3% BSA in PBS, transfer to 1.7 mL eppy tube. Spin down to remove wash solution.
(17) Resuspend pellet in 20 µL cold ADF^+ (total volume should less than 50 µL).
(18) As soon as possible, analyze the stained cells by flowsight, measuring the fluorescence emission at 675 using 640 nm excitation.
(19) Power setting for Flowsight machine: 640 nm: 5%.
(20) If cells contain GFP, 488 nm: 40% or even higher (Fixed GFP is very weak!).

References: McFarlane MR, Cantoria MJ, Linden AG, January BA, Liang G, Engelking LJ. (2015) Scap is required for sterol synthesis and crypt growth in intestinal mucosa. J Lipid Res. 56(8):1560-15671.

APPENDIX O

MEASURING PLASMA MEMBRANE ORDER AND CHOLESTEROL LEVELS IN ORGANOIDS

Purpose: To assess the effect of exogenous cholesterol on plasma membrane order using organoids.

Reagents: ADF (Gibco, SILAC Advanced DMEM/F-12 Flex, A24943-01), PenStrep (P/S) (Gibco, 15140-122), HEPES (Gibco, H0887), Glucose (Gibco, A24940-01), FBS (HyClone, SH30084.03), 0.25% trypsin (Gibco, 25200-056), 100 μg/mL EGF mouse recombinant (LifeTech, PMG8041, 100 μg EGF/ 1mL PBS + 0.5% FBS), 0.2 mM LDN/Noggin replacement (Cellagen Tech, 0.2 mM stock in PBS + 0.5% FBS), 1 mg/mL R-Spondin mouse (Peprotech, 315-32, 0.5 μg/mL final concentration), N2 supplement (LifeTech, 17502-048, 100X), B27 supplement (LifeTech, 12587-010, 50X), N-Acetyl-L-cysteine (Sigma, A9165), 100 μg/mL Wnt (TimeBioscience, rmW3aL-002, final 30 ng/mL), 50 mM cholesterol (Sigma, C4951), 40 mM EdU stock (Life Technologies Cat #A10044) in PBS (Gibco, 21600-069), Click-iT™ Plus EdU Alxa Fluor™ 647 Imaging Kit (ThermoFisher, C10640), 4% PFA (Electron Microscopy Science, 15713) in PBS, 3% BSA (Roche, 9048-46-8, at 4°C) in PBS, 0.5% TritonX-100 (Sigma, 9002-93) in PBS, DAPI (LifeTech, H3570), 10 mM MβCD:cholesterol stock solution (APPENDIX L).

Procedure:

(1) Prepare organoid incubated with or without cholesterol in 1.5 mL (APPENDIX M).
(2) Aspirate culture medium, add 0.5 mL ice cold ADF$^+$ and mechanically pipette and scrap the matrigel with a P1000 on ice.
(3) Transfer the dissociated matrigel into a 2 mL tube (pooling 3 wells for 1 sample).
(4) Use another 0.5 mL cold ADF$^+$ to finish transfer of all material from the wells.
(5) Spin down the organoids at short (5000 X g for 4 sec at 4° C). Remove media (may see a glutinous Matrigel area above pellet. Careful not to aspirate organoids!)
(6) Resuspend organoids in 0.3 mL 0.25% EDTA-Trypsin and incubate at 37 °C for 8~12 min using heat block.
(7) Every 2 minutes, pipet solution well (6 to 10 times).
(8) Add 900 μL cold 10% FBS ADF$^+$ solution to stop reaction.
(9) Spin down at 500 g for 3 min at 4° C and carefully aspirate.
(10) Add 200 μL of ADF$^+$ media, resuspend with cells.
(11) Take 50 μL of cells in the media is for measuring plasma membrane order.
(12) Measure plasma membrane order (APPENDIX K).
(13) Measure cholesterol levels in the plasma membrane (APPENDIX J).

References:
Maxfield FR, Wüstner D. (2012) Analysis of cholesterol trafficking with fluorescent probes. Methods Cell Biol. 108:367-393.
Norman AW, Demel RA, de Kruyff B, van Deenen LL. (1972) Studies on the biological properties of polyene antibiotics. Evidence for the direct interaction of filipin with cholesterol. J Biol Chem. 247(6):1918-1929.
Schroeder F, Holland JF, Bieber LL. (1971) Fluorometric evidence for the binding of cholesterol to the filipin complex. J Antibiot (Tokyo). 24(12):846-849.
Ashdown GW, Owen DM. (2015) Imaging membrane order using environmentally sensitive fluorophores. Methods Mol Biol. 1232:115-122.
Owen DM, Rentero C, Magenau A, Abu-Siniyeh A, Gaus K. (2011) Quantitative imaging of membrane lipid order in cells and organisms. Nat Protoc. 7(1):24-35.
Sáenz JP, Sezgin E, Schwille P, Simons K. (2012) Functional convergence of hopanoids and sterols in membrane ordering. Proc Natl Acad Sci U S A. 109(35):14236-14240.

APPENDIX P

GENERAL CHOLESTEROL INCUBATION WITH YAMC/ IMCE CELLS

Purpose: To stimulate cholesterol activation in YAMC/ IMCE cells.

Materials: Trypsin-EDTA (Gibco, #25300-054), 500 mL RPMI without glutamine (Mediatech, 15- 040 CV), 26.6 mL Fetal Bovine Serum (Hyclone, AK 12434), 5.3 mL Glutamax (Gibco, 35050-061), 0.532 mL ITS "-" minus (Insulin, Transferrin, Selenious acid without Linoleic acid) (Collaborative Biomed products, 4351), γ-Interferon (Gibco BRL, 13284-021), Lipoprotein free serum (Kalen Biomedical, 880100-1), 10mM MβCD:cholesterol stock solution (APPENDIX L).

Solution:

Reconstitution of ITS "-":

Add 5 mL of sterile distilled water into lysophylized powder. Aliquot and store at -20°C.

500 mL of RPMI complete media:

500 mL RPMI without glutamine + 26.6 mL Fetal Bovine Serum + 5.3 mL Glutamax + 0.532 mL ITS "-" minus

Note: Add 1μL of γ-Interferon (γ-IFN, 10 μL aliquot in -20° C) per 10 mL of complete RPMI 1640 medium just prior to use.

50 mL of cholesterol free RPMI complete media:

50 mL RPMI without glutamine + 2.66 mL Lipoprotein free serum + 0.53 mL Glutamax + 53.2 μL ITS "-" minus

Note: Add 1μL of γ-Interferon (γ-IFN) per 10 mL of complete RPMI 1640 medium just prior to use.

Lipoprotein free serum (Kalen Biomedical, 880100-1): Lipoprotein depleted FBS contains *0.04 mg/mL of cholesterol* whereas normal FBS contains *1.4 mg/mL of cholesterol*. Using HDL and LDL/VLDL cholesterol assay kit from abcam (ab65390), Kalen Biomedical reported that 35-fold reduction in cholesterol of Lipoprotein depleted FBS is found as compared to traditional FBS. (https://kalenbiomed.com/products/lipoprotein-depleted-fetal-bovine-serum).

Note: 0.3 mg/mL cholesterol in FBS also reported (Gstraunthaler, 2003).

Concentration of cholesterol in serum and 5% FBS media:

0.04 mg/mL (10 μM) cholesterol in serum = 0.5 μM cholesterol in 5% FBS media

0.3 mg/mL (75 μM) cholesterol in serum = 3.75 μM cholesterol in 5% FBS media

1.4 mg/mL (350 μM) cholesterol in serum = 17.5 μM cholesterol in 5% FBS media

---

Procedure:

(1) Culture YAMC and IMCE cells in a T-75 flask in complete media at 33° C and 5% CO_2 until they become ~70% confluent.
(2) Add 15 mL RPMI complete media in a 50 mL conical tube (to spin cells) – always use at least 2X as much media as trypsin to stop the trypsinization.
(3) Add 25 mL cholesterol free complete RPMI 1640 medium plus 2.5 μL γ-IFN to a 50 mL conical tube (to grow cells).
(4) Warm both conical tubes of media in water bath (37° C).
(5) Aspirate old media from flask.
(6) Rinse monolayer of cells with 10 mL PBS by adding and aspirating gently without disturbing the cell monolayer.
(7) Add 5 mL Trypsin-EDTA to the flask and incubate cells at 37° C for 3 min or until > 90% cells are lifted. Gently tap the bottom of the flask to assist in cells lifting.
(8) Add the 15 mL RPMI complete media from the conical tube to the flask of trypsinized cells (add by rapidly dispensing the media and moving the pipette in a back and forth motion across the flask to dislodge any stuck cells). Then, transfer the media and trypsin to the 50 mL conical tube.
(9) Transfer 10 μL of the cell suspension onto each end of the hemacytometer.

Note: Cell number (per mL) = $\frac{\text{Living cells count x 10,000}}{\text{\# Squares counted}}$

(10) Centrifuge cells at 200 x g (1096 rpm, countertop centrifuge for 5 min).
(11) Vacuum aspirate supernatant (media with trypsin), taking care not to disturb the pellet.
(12) Seed cell according to desired density in cholesterol free RPMI complete media with γ-IFN.

Culture plates	Surface area (cm^2)	Seeding density	Cells at confluency	Growth medium (mL)
6-well (plasma membrane order and Filipin III experiment)	9	0.05×10^6	1.2×10^6	3–5
24-well (proliferation rate using CellTiter Blue)	2	0.03×10^6	0.2×10^6	0.5–1.0

(13) Add 10 μL of 10 mM cholesterol per 1 mL of cholesterol free complete RPMI 1640 medium (final concentration = 100 μM).
(14) Change cholesterol containing media every 24 hr to avoid oxidization.
(15) Harvest cells every 24 hr and measure plasma membrane order, cholesterol level in plasma membrane and proliferation rate.

References: Zhao C, Deng Y, Liu L, Yu K, Zhang L, Wang H, He X, Wang J, Lu C, Wu LN, Weng Q, Mao M, Li J, van Es JH, Xin M, Parry L, Goldman SA, Clevers H, Lu QR. (2016) Dual regulatory switch through interactions of Tcf7l2/Tcf4 with stage-specific partners propels oligodendroglial maturation.Nat Commun. 7:10883.
Gstraunthaler G.(2003) Alternatives to the use of fetal bovine serum: serum-free cell culture.ALTEX. 20(4):275-281.

APPENDIX Q

DETERMINE CELL PROLIFERATION RATES USING CELLTITER-BLUE

Purpose: To determine proliferation rates of YAMC/IMCE cells upon cholesterol incubation.

Materials: Trypsin-EDTA (Gibco, #25300-054), 500 mL RPMI without glutamine (Mediatech, 15- 040 CV), 26.6 mL Fetal Bovine Serum (Hyclone, AK 12434), 5.3 mL Glutamax (Gibco, 35050-061), 0.532 mL ITS "-" minus (Insulin, Transferrin, Selenious acid without Linoleic acid) (Collaborative Biomed products, 4351), γ-Interferon (Gibco BRL, 13284-021), Lipoprotein free serum (Kalen Biomedical, 880100-1), 10mM MβCD:cholesterol stock solution (APPENDIX L). CellTiter-Blue Cell Viability Assay (Promega, G8080), Microplate Reader (BMG LABTECH, CLARIOstar).

Procedure: (perform all step in sterile hood, as the cells will continue 4 hr incubation after the addition of Cell titer Blue)

(1) Prepare cells incubated with or without cholesterol (APPENDIX Q).
(2) Thaw CellTiter-Blue Reagent and bring to ambient temperature. A 33° C water bath may be used to thaw the reagent.
    Note: protect the CellTiter-Blue Reagent from direct light.
(3) Remove 24 well plate from 33° C incubator and add CellTiter-Blue Reagent (6X stock solution) to appropriate wells. 100 μL CellTiter-Blue Reagent + 500 μL RPMI media with or without cholesterol.
    Negative control: 3 wells with CellTiter-Blue Reagent + media without cells
    Note: leave 3 empty wells for the subtraction of the background fluorescence.
(4) Incubate in 33° C incubator for 4 hr (1~4 hr is recommended).
(5) Shake/swirl plate for 10 sec and record fluorescence at 560/590 nm.
    Note: Fluorescence filter set at 530-570 nm for excitation and 580-620 nm for fluorescence emission.

References:

Habermann N, Christian B, Luckas B, Pool-Zobel BL, Lund EK, Glei M. (2009) Effects of fatty acids on metabolism and cell growth of human colon cell lines of different transformation state. Biofactors. 35(5):460-467.

APPENDIX R

ASSESSMENT OF PLASMA MEMBRANE ORDER AND CHOLESTEROL LEVELS IN CELL PLASMA MEMBRANE USING FLOWSIGHT

Purpose: Determine membrane order (Di4) and free cholesterol levels (Filipin) in cell lines or single cells from mice using the FlowSight imaging flow cytometer.

Materials: 5 μM Di4-ANEPPDHQ (ThermoFisher, D36802), 1 mg of Filipin III from *Streptomyces filipinesis* (Sigma, F4767), DMSO, PBS (Gibco, 21600-069), 4% PFA (Electron Microscopy Science, 15713) in PBS

Procedure:

(1) Prepare single cells incubated with or without cholesterol (APPENDIX Q).
(2) If you use cells from same well, take 75% of cells in the media, fix in 1.5% paraformaldehyde for 20 min at RT for the measuring cholesterol in the plasma membrane. 25% of cells in the media is for measuring plasma membrane order.

Membrane order:

(1) Turn on FlowSight, Run start up, and Calibration.
(2) Load template. Robert → Template → Single Cell Di4 (1μM).
(3) This template should have the 488 laser on.
(4) Take 36 μL single cells 10^5 cells/ mL and add 4μL Di4 (10 μM) to make a final concentration of 1μM. Note: This must be done immediately before running on the FlowSight.
(5) Run on FlowSight. Note: Make sure the signal is not saturated in the disordered channel. If it is you can lower the laser power.
(6) Use the Ideas analysis template. (170724 YAMC post di4.ist).
Note: This was generated by Michael and has different mask that analyze the whole cells, just the membrane, or the internal membrane. Although it is not truly just the internal membrane since it is a wide field image.
(7) Batch the data with the template to generate all the statistics.

Filipin III:

(1) In a 1.7 mL eppy tube, fix the remaining cells (~150 μL) in 4% PFA for 15 min on ice.
Note: I do this by adding equal parts 8% PFA to the same volume of cells to make 4% PFA.
(2) Add 1 mL PBS to the fixed cells, and spin down at 1000 g for 5 min at 4° C.
Note: The fix cells are fine at this speed and they make a nice pellet.
(3) Aspirate carefully and do not disturb the pellet.
(4) Add 1.5 mL PBS to wash the pellet.
(5) Spin down at 1000 g for 5 min at 4° C.

(6) Carefully aspirate the media.
(7) Re-suspend the pellet in 40 μL PBS.
(8) Transfer 36 μL of cells to a new 1.7 mL eppy tube.
(9) Add 4 μL of Filipin (500 μg/mL) to make a final concentration of 50 μg/mL.
Note: Filipin photo bleaches very easy so keep the samples protected from light from now on when possible.
(10) Incubate on ice covered in the dark for 45 minutes.
(11) Add 1.5 mL PBS, and spin down at 1000 g for 5 min at 4° C.
Note: This washes out excess Filipin III.
(12) Aspirate carefully and do not disturb the pellet. Repeat the wash and spin.
(13) Resuspend the pellet in 40 μL PBS.
(14) Load the Filipin template: Robert → Template → Fillipin III.
Note: The 405 Laser should turn on and will be at 100%, since the 405 barely excites Filipin III.
(15) Run the sample on the FlowSight.
(16) Use the Ideas analysis template. (170724 YAMC Filipin.ist).
Note: This was generated by Michael and has different mask that analyze the whole cells, just the membrane, or the internal membrane. Although it is not truly just the internal membrane since it is a wide field image.
(17) Batch the data with the template to generate all the statistics.

References: Chapkin lab developed the protocol.

APPENDIX S

EXTRACTION OF DNA AND RNA USING RNA ISOLATION KIT

Purpose: Extract DNA and RNA from isolated GI crypts using the RNA miniprep kit (Zymo Research, R1050).

Materials: RNA miniprep kit (Zymo Research, R1050), 100% RNase free ethanol (KOPEC, V1001), DNA-free DNA removal kit (Ambion, AM1906).

Note: all steps at RT, unless specified.

Procedure:

(1) Make sure to add ethanol to RNA Wash Buffer concentrate.
(2) Preheat DNase/RNase-free water to 75° C for elution (~ 60 μL/sample).
(3) Prepare cells in RNA lysis buffer.
(4) Transfer the lysed cell solution to a Zymo-Spin IIICG column in a RNase free collection tube (max 700 μL at a time). Collection tube should be a RNase-free 2mL round bottom tube.
(5) Centrifuge at 30 sec at 13,000 X g. Repeat loading if necessary. Do not discard flow thru.
(6) DNA is on a collection tube. Flow thru is for the isolating RNA.

DNA extraction:

(7) Place a column in a new collection tube that comes with a kit.
(8) Add 400 μL RNA Prep buffer to the column.
(9) Centrifuge for 30 sec at 13,000 X g. Discard flow thru.
(10) Add 700 μL RNA Wash buffer to the column.
(11) Centrifuge for 30 sec at 13,000 X g. Discard flow thru.
(12) Add 400 μL RNA Wash buffer to the column.
(13) Centrifuge for 30 sec at 13,000 X g first, then centrifuge for 2 min at 13,000 X g, to ensure complete removal of the wash buffer. Discard flow thru.
(14) Place the column in RNase-free 1.7 mL eppy tube (not provided in the kit).
(15) Add 30 ~ 60 μL pre-heated DNase/RNase-free water directly to the matrix.
(16) Centrifuge for 30 sec at 16,000 X g.
(17) The flow thru is the isolated DNA.
(18) You can repeat the elution again to get more yield, but the concentration will decrease. Minimum elution volume is 30 μL.

RNA extraction:

(1) Add same volume of 95 ~ 100% ethanol to the sample in RNA lysis buffer (1:1). Mix well.
(2) Transfer the mixture to a Zymo-Spin IC Column in a Collection Tube.

(3) Centrifuge at 30 sec at 13,000 X g. Discard flow thru. Repeat loading if necessary.
(4) Add 400 μL RNA Prep buffer to the column.
(5) Centrifuge for 30 sec at 13,000 X g. Discard flow thru.
(6) Add 700 μL RNA Wash buffer to the column.
(7) Centrifuge for 30 sec at 13,000 X g. Discard flow thru.
(8) Add 400 μL RNA Wash buffer to the column.
(9) Centrifuge for 2 min at 13,000 X g to ensure complete removal of the wash buffer. Discard flow thru.
(8) Place the column in RNase-free 1.7 mL eppy tube (not provided in the kit).
(9) Add ~ 10 μL (at least 6 μL) pre-heated DNase/RNase-free water directly to the matrix.
(10) Centrifuge for 30 sec at 16,000 X g.
(11) The flow thru is the isolated RNA.
(12) You can repeat the elution again to get more yield, but the concentration will decrease. Minimum elution volume is 6 μL.

DNase I treatment:
(13) Use DNA Free kit from Ambion (Ambion, AM1906), not the one in the Zymo kit).
(14) Add 0.1 volume (of the RNA eluate) of 10X DNase I buffer and 1 μL of DNase I to the RNA eluate.
(15) Mix gently.
(16) Incubate at 37° C for 20 min.
(17) Vortex DNase Inactivation Reagent to disperse the slurry before use.
(18) Add 0.1 volume (of RNA/DNase mixture) of DNase Inactivation Reagent to the mixture.
(19) Mix gently by flicking the tube, incubate at RT for 2 min.
(20) Flick the tube once more during the incubation.
(21) Centrifuge at 13,000 x g for 1.5 min. Transfer supernatant to a new RNase-free tube.
(22) Now ready for RT-PCR.
(23) Measure the concentration in Nano drop, and check the quality in Agilent Bioanalyzer.

Remove Guanidine after isolating RNA using Zymo Quick-RNA MicroPrep kit (Cat# R1050)
(1) Add 100 μL RNA lysis buffer. Mix well.
(2) Transfer the mixture to a Zymo-Spin IC Column in a Collection Tube.
(3) Centrifuge at 30 sec at 13,000 X g. Discard flow thru. Repeat loading if necessary.
(4) Add 400 μL RNA Prep buffer to the column.
(5) Centrifuge for 30 sec at 13,000 X g. Discard flow thru.

(6) Add 700 μL RNA Wash buffer to the column.
(7) Centrifuge for 30 sec at 13,000 X g. Discard flow thru.
(8) Add 400 μL RNA Wash buffer to the column.
(9) Centrifuge for 2 min at 13,000 X g to ensure complete removal of the wash buffer. Discard flow thru.
(10) Place the column in RNase-free 1.7 mL eppy tube (not provided in the kit).
(11) Add ~ 10 μL (at least 6 μL) pre-heated DNase/RNase-free water directly to the matrix.
(12) Centrifuge for 30 sec at 16,000 X g.
(13) The flow thru is the isolated RNA.
(14) You can repeat the elution again to get more yield, but the concentration will decrease. Minimum elution volume is 6 μL.

References:
https://www.zymoresearch.com/rna/total-rna-purification/cell-soft-tissue-rna/quick-rna-microprep

APPENDIX T

GENOTYPING OF KRAS MICE

Purpose: Detecting wild type KRAS, LSL-G12D Kras (floxed but not recombined) and G12D-Kras (recombined) allele using DNA extracted from crypts isolated from CDX2P-CreER^{T2}-Apc$^{580D/+}$; Kras$^{G12D/+}$ mouse colon.

Materials: 2X master mix (Denville Hot Start, CB4030-4), 10μM primers (order from https://www.idtdna.com/Primerquest/Home/Index), PCR machine (AB, 2720 Thermocycler), dH_2O (Gibco, 15230-170).

Solution:
Dissolve primer in TE buffer to make 100 μM stock primer, aliquot into 10 μL and keep it in -80° C.
Dilute100 μM stock primer in TE buffer to make 10 μM.

Source of primers: Jackson lab (https://jacks-lab.mit.edu/protocols/genotyping/kras_cond) and Hinoi et al., 2007

Kras Jackson F1 (P1)	5'-GTCTTTCCCCAGCACAGTGC-3′
Kras 1AS (Reverse)	5′-GCAGCGTTACCTCTATCGTA-3′
Kras Jackson F2 (P3)	5'-AGCTAGCCACCATGGCTTGAGTAAGTCTGCA-3′

Reaction Mix (30 μL reaction):

Reaction mix	Volume (μl)
Master mix (2X)	15
10 μM Kras P1 (0.5 μM final concentration)	1.5
10 μM Kras P2 (0.5 μM final concentration)	1.5
10 μM Kras P3 (0.5 μM final concentration)	1.5
DNA (25 ng)	4
Water	6.5
Total	30

PCR parameters:

95°C	2 min	Initialization

35 cycles of:

95°C	30 sec	Denaturation
61°C	30 sec	Annealing
72°C	45 sec	Extension/elongation

72°C	10 min	Final elongation
4°C	keep	Final hold

Amplified fragments:

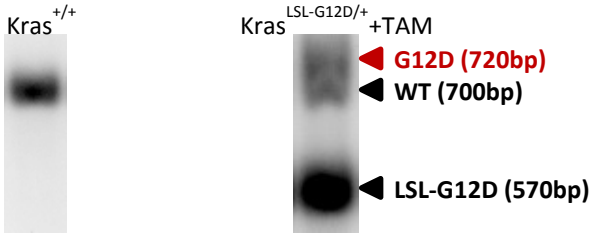

Note: 20 bp difference between G12D and WT can be acquired when you run samples for 1.5 hr in 1.5% gel.
Note: Recombination efficiency is not 100% so, you will see both LSL-G12D and G12D.

References:

Jackson lab (https://jacks-lab.mit.edu/protocols/genotyping/kras_cond),
Hinoi, T., Akyol, A., Theisen, B.K., Ferguson, D.O., Greenson, J.K., Williams, B.O., Cho, K.R., and Fearon, E.R. (2007). Mouse model of colonic adenoma-carcinoma progression based on somatic Apc inactivation. Cancer research 67, 9721-9730.

APPENDIX U

GENOTYPING OF APC MICE

Purpose: Detecting wild type Apc, Apc^{580S} (floxed but not recombined) and APC^{580D} (recombined) allele using DNA extracted from crypts isolated from CDX2P-$CreER^{T2}$-$Apc^{580D/+}$; $Kras^{G12D/+}$ mouse colon

Materials: 2X master mix (Denville Hot Start, CB4030-4), 10μM primers (order from https://www.idtdna.com/Primerquest/Home/Index), PCR machine (AB, 2720 Thermocycler), dH_2O (Gibco, 15230-170).

Solution:
Dissolve primer in TE buffer to make 100 μM stock primer, aliquot into 10 μL and keep it in -80° C.
Dilute100 μM stock primer in TE buffer to make 10 μM.

Source of primers: Shibata et al., 1997

Apc F1 (P3)	5′- GTTCTGTATCATGGAAAGATAGGTGGTC-3′
Apc R1 (P4)	5′- CACTCAAAACGCTTTTGAGGGTTGATTC -3′
Apc R2 (P5)	5'-GAGTACGGGGTCTCTGTCTCAGTGAA-3'

Rxn Mix (30 μL reaction):

Reaction mix	Volume (μl)
Master mix (2X)	15
10 μM Apc F1 (P3) (0.5 μM final concentration)	1
10 μM Apc R1 (P4) (0.5 μM final concentration)	1
10 μM Apc R2 (P5) (0.5 μM final concentration)	1
DNA	4
Water	8
Total	30

PCR parameters:

95°C	3 min	Initialization

35 cycles of:

95°C	30 sec	Denaturation
59°C	30 sec	Annealing
72°C	40 sec	Extension/elongation

72°C	2 min	Final elongation
4°C	keep	Final hold

Amplified fragments:

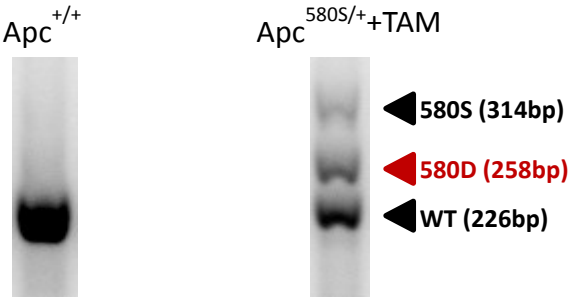

Note: Recombination efficiency is not 100% so, you will see both 580D and 580S.

References:

Shibata, H., Toyama, K., Shioya, H., Ito, M., Hirota, M., Hasegawa, S., Matsumoto, H., Takano, H., Akiyama, T., Toyoshima, K., et al. (1997). Rapid colorectal adenoma formation initiated by conditional targeting of the Apc gene. Science 278, 120-123.

APPENDIX V

PREPARATION OF TOTAL CELL LYSATES

Purpose: To isolate cell lysates from mouse colonic crypts.

Materials:

5 mL of Homogenization buffer (HB)	Final concentration
500 μL of 500 mM Tris-HCl (Sigma, T1503)	50 mM
1.25 mL of 1 M sucrose (Sigma, S9278)	250 nM
50 μl of 200 mM EDTA(Sigma, ED4SS)	2 mM
50 μl of 100 mM EGTA (Sigma, 34596)	1 mM
500 μl of 10% Triton-X (Sigma, T6878)	1%
0.625 μl of 0.4 M NaF (Sigma, S6521)	50 μM
2395.875 μl of double distilled water	
50 μl of 10 mM activated sodium orthovanadate (Sigma, S6508)	100 μM
200 μl of protease inhibitor cocktail (Sigma, P8340)	
3.5 μl of 14.2 M β-mercaptoethanol (Bio-Rad, 161-0710)	10 mM
* Items in red are to be added on the day of use	

Procedure:

(1) Harvest crypts according to the SINGLE CELL ISOLATION protocol
(2) Transfer extracted crypts into 1.7 mL eppy tubes and add 100 μl of HB.
(3) Pass through 29G needle once into the same set of 1.7 mL eppy tubes, flush the suspension very hard to sheer the cells (perform on ice).
(4) Incubate the total lysate in ice for 30 min.
(5) Centrifuge at 16,000 X g at 4° C for 20 min.
(6) Transfer the supernatant (lysate) to clean 1.7 mL eppy-tube and pipette up and down to mix.
(7) Quantify levels of protein using Coomassie Plus and immunoblotting.

References:

Turk HF, Barhoumi R, Chapkin RS. (2012) Alteration of EGFR spatiotemporal dynamics suppresses signal transduction. PLoS One. 2012;7(6):e39682.

APPENDIX W

NUCLEAR AND CYTOPLASMIC PROTEIN EXTRACTION

Purpose: Quantify nuclear/cytosolic beta-catenin protein levels.

Aim: Extract cytoplasmic and nuclear protein fractions from isolated crypts.

Reagents: ADF (Gibco, SILAC Advanced DMEM/F-12 Flex; no glucose included, A24943-01), PenStrep (P/S) (Gibco, 15140-122), HEPES (Gibco, H0887), Glucose (Gibco, A24940-01), EDTA (Sigma, ED4SS), 2mM EGTA pH 8.0 (Sigma, E4378), NE-PER Nuclear and Cytoplasmic Extraction (Thermofisher, 78833), Protease inhibitors (e.g., Thermo Scientific™ Halt™ Protease Inhibitor Cocktail, Product No. 78425 or 78437), 10 mM activated sodium orthovanadate (Sigma #S6508), 0.4 M NaF (Sigma, S6521)

Procedure:
Extract cytosolic proteins:

(1) Transfer crypts in PBS to a pre-weighed 1.7 mL eppy tube and pellet by centrifugation at 500 X g for 5 min.
(2) Use a pipette to carefully remove and discard the supernatant, leaving the cell pellet as dry as possible. Weigh the 1.7 mL epi-tube with cells.
(3) Add ice-cold CER I to the cell pellet (Table below). Proceed to Cytoplasmic and Nuclear Protein Extraction, using the reagent volumes indicated in Table below.
(4) Vortex the tube vigorously on the highest setting for 15 sec to fully suspend the cell pellet.
(5) Incubate the tube on ice for 10 minutes.
(6) Add ice-cold CER II to the tube.
(7) Vortex the tube for 5 sec on the highest setting.
(8) Incubate tube on ice for 1 min.
(9) Vortex the tube for 5 sec on the highest setting.
(10) Centrifuge at 16,000 X g at 4° C for 5 min
(11) Immediately transfer the supernatant (cytoplasmic extract) to a clean pre-chilled tube.
Note: Keep pellet fraction for nuclear extraction below
(12) Place this tube on ice until use or storage extracts at -80° C until use.

Tissue Weight (mg)	CER I (µL)	CER II (µL)	NER (µL)
20	200	11	100
40	400	22	200
80	800	44	400
100	1000	55	500

Note: Scale this protocol depending on the cell pellet volume (Tables above). Maintain the volume ratio of CER I:CER II:NER reagents at 200:11:100µL, respectively.

Extract nuclear proteins:

(13) Suspend the insoluble (pellet) fraction, which contains nuclei, in ice-cold NER.
(14) Vortex on the highest setting for 15 seconds. Place the sample on ice and continue vortexing for 15 seconds every 10 minutes, for a total of 40 minutes.
(15) Centrifuge at 16,000 X g at 4° C for 10 min.
(16) Immediately transfer the supernatant (nuclear extract) fraction to a clean pre-chilled 1.7 mL eppy tube. Place on ice.
(17) Store extracts at -80° C until use.

Note: Extracts obtained with this product generally have less than 10% contamination between nuclear and cytoplasmic fractions, which is sufficient purity for most experiments involving nuclear extracts.

References:

Calviello G, Resci F, Serini S, Piccioni E, Toesca A, Boninsegna A, Monego G, Ranelletti FO, Palozza P. (2007) Docosahexaenoic acid induces proteasome-dependent degradation of beta-catenin, down-regulation of survivin and apoptosis in human colorectal cancer cells not expressing COX-2. Carcinogenesis. 28(6):1202-1209.

APPENDIX X

COOMASSIE PROTEIN ASSAY

Purpose: To determine the protein concentration of samples.

Materials:
Homogenization buffer (whichever was used to collect samples), EIA/RIA clear polystyrene 96-well plate (Corning #9017), Coomassie Plus assay reagent (ThermoFisher #23238), Disposable borosilicate glass tubes (VWR #47729-572)

Procedure:
(1) Use this assay with homogenization buffer (HB) used to collect the total cell lysate (TCL).
(2) Before beginning, turn on SpectroMax and prepare a template.
(3) Prepare samples and standards in glass tubes by mixing the amounts of standard/sample, water, HB, and reagent listed below. Make triplicates of all samples and standards.
(4) After adding everything to each tube, vortex tubes for 3 sec and transfer 300 mL of standard/sample to the designated well on the 96-well plate.
(5) Immediately after adding all standard and samples to the plate, bring to the SpectroMax plate reader and read at 595 nm.

Standard curve (μg protein)	0.25 μg/μL BSA	1 μg/μL BSA	2 μg/μL BSA	dH_2O	HB	Reagent	Well position
0	0			497.5	2.5	500	A1-A3
0.5	2			495.5	2.5	500	B1-B3
1	4			493.5	2.5	500	C1-C3
2		2		495.5	2.5	500	D1-D3
4		4		493.5	2.5	500	E1-E3
10		10		487.5	2.5	500	F1-F3
20			10	487.5	2.5	500	G1-G3

Samples: 2.5 μL sample + 497.5 μL dH_2O + 500 μL Reagent

References:
Turk HF, Barhoumi R, Chapkin RS. (2012) Alteration of EGFR spatiotemporal dynamics suppresses signal transduction. PLoS One. 2012;7(6):e39682.

APPENDIX Y

WESTERN BLOTTING

Purpose: To measure the amount of total or phosphorylated proteins in cell lysates.

Materials: Protein loading buffer (Tribioscience, TBS5014), Protein marker (Invitrogen, LC5602), 4-12% pre-made gel (Expedeon, NXG41212), running buffer (RunBlue, NXB60500), a pair of forceps, a tray for transfer, transfer buffer (VWR, 0783-5L), methanol (Fisher, A4333P-4), 0.45 μm PVDF membrane (millipore, IPVH00020), filter paper (MIDSCI, 6MW-2020), stir bar, instant dry milk powder, β-catenin antibody (BD, 610154), β-actin (AbCam, Ab8227), horseradish peroxidase labeled Goat anti-rabbit conjugated (HRP) IgG (H+L) (SeraCare, 074-1516), horseradish peroxidase labeled Goat anti-mouse conjugated (HRP) IgG (H+L) (SeraCare, 074-1806), SuperSignalWestFemtoTrial kit (ThermoFisher, 34094).

Preparation:
(1) Thaw samples on ice.
(2) Label 0.6 mL eppy tubes.
(3) Turn heating block on and set temperature to 98° C.
(4) Prepare the western template sheet.
(5) Cut PVDF membrane and filter papers ready.

Procedure:
Sample preparation
(1) Thaw the samples on ice while you turn on the heating block and set the temperature to 98°C (takes about 15 min).
(2) Dye used for the sample dilution is 5X Pyronin. Use 1X of the dye based on the total volume of sample required (usually 25 mL total).
(3) With the aid of western template sheet make the necessary dilution (if required) and add the calculated amount of dye and water to the samples and standard.
(4) Quick spin.
(5) Boil the samples for 5~10 min depending on the volume of the samples (25 mL volume boil for 10 min). Do not boil the marker.
(6) Quick- spin of the samples on the tabletop.

Gel unit set up
(1) Take the pre-made gel (usually 4~20%) and carefully rip off and discard the white tape and the comb. Mark the lanes on the plate.
(2) Attach the gel to the gel rack align 3rd with the lower gasket and clamp the

unit. (Note that the red clip should have the broad end facing you, broad ends face outside on all 4 clips). Either run a gel on each side or attach the white space holder on the empty side.
(3) Pour running buffer to fill the stand and the trough up to the top mark.
(4) Use gel-loading tips (or 10 mL XL tips) and load the complete sample volume.
(5) Close the unit with the lid and check the leads and make sure black-to-black and red-to-red.
(6) In the cold room run the gel at 125 V for as long as needed. Check after 10 minutes to make sure it is running.
(7) After about 1 h check every 15 min.
(8) Stop the gel when it has run as far as needed.

Gel transfer

(1) Crack open the plate with a scalpel between the markings on the plate all around by keeping the large side of the gel down.
(2) Cut the gel just above the bottom.
(3) Carefully separate the gel from the plate and cut the gel at lane one to identify the side (left end).
(4) Take the gel transfer unit in a staining tray and pour transfer buffer into it and the trough. Allow gel to equilibrate in transfer buffer for 15-30 min. Wet membrane with methanol then equilibrate in transfer buffer for ~5 min.
(5) Take the cassette and lay it open.
(6) Put a sponge on the black side of the cassette and place a filter paper on top of it.
(7) Pour transfer buffer to keep it wet.
(8) Take the gel plate out of the running through and transfer the running buffer into the bottle for reuse.
(9) Place the gel on the filter paper with lane one on the right (protein side facing the membrane.
(10) Cut the right hand top corner of the membrane to identify the side.
(11) Place the membrane on the gel and place the other filter paper on the membrane. Now, use a roller on the filter paper to eliminate any air bubbles in between.
(12) Place the sponge and close the white side of the cassette and clip it.
(13) Place the cassette in the transfer unit with the hinges facing the top and black side facing back.
(14) Put a stir bar into the transfer trough.
(15) Fill the trough with transfer buffer just enough to cover the hinges of the cassette. Check the terminals black to black correspond.
(16) Place it on the cold room stir plate.
(17) Connect black-to-black and red-to-red and set current to 400 milliamps and let it transfer for at least 90 min.

Blocking

(1) At the end of 90 min- make 4% nonfat dry milk/ PBST in a 50 mL tube (to 30 mL of PBST and add 1.2 g of pre-weighted milk powder). Mix gently by inverting. If 5% BSA is required, add 1.5 g IgG free BSA to 30 mL PBST.
(2) Pour the milk into a dish and keep ready to transfer the membrane into it.
(3) After the transfer is complete- open the gel unit and transfer the transfer buffer into the bottle.
(4) Use a pair of forceps to take the membrane and place the membrane into the milk dish (with the side facing gel-protein side now facing top)
(5) Place it on the shaker for 1 hr at room temperature.

Primary antibody

(1) Take a dish with 1.2 gm dry milk powder and 30 mL PBST. Mix and pour into a new dish.
(2) Transfer the membrane from the blocking buffer into the dish with fresh milk.
(3) Now, add the appropriate volume of the primary antibody (based on the dilution and add it into the dish).
(4) Close the lid of the dish and shake it gently on the cold room shaker overnight.

Washing

(1) The next day take the membrane and give a quick wash with PBST.
(2) Then replace the membrane in fresh PBST in the dish and keep on the shaker at room temp for 10 min. Let it shake vigorously.
(3) Repeat the wash 2 times at 5-10 min interval.

Secondary antibody

(4) Make 30 mL milk/ PBST and pour into the dish after the second wash.
(5) Add the required volume of secondary antibody based on the dilution.
(6) Set on shaker for 1 hr at room temperature.
(7) Repeat washing with PBST 3 times.
(8) While the 1 wash of 2° antibody is going on turn on the imager and set focus.

Developing

(9) Cut an acetate sheet into 2 halves and remove the black sheet.
(10) Mix equal parts of chemiluminescent super signal reagent A and reagent B in an eppy tube. Mix gently by inversion.
(11) Transfer the membrane between the layers of the acetate sheet and evenly disperse the developing solution across on the top of the membrane.
(12) Slowly close the top layer so that the solution gets evenly distributed on the membrane.
(13) Expose for 5 minutes and then transfer the membrane on to the clean acetate sheet.
(14) Transfer it into the BioRad imager for imaging immediately.

Imaging

(15) Turn on switch and make sure the lever on the hood is at chemiluminescence.
(16) Select QuantityOne on program on desktop.
(17) Select scanner – click on chemidoc.xrs.
(18) Step 1- option is chemiluminescences.
(19) Step 2 – live focus. Focus with a printed sheet and set the iris as you need for brightness. Zoom and focus, as you need for clarification.
(20) Freeze. Put the gel in the imager and zoom and freeze again. Close the door.
(21) Click on live acquire.
(22) Set the Starting exposure time, Total exposure time, and Number of exposures as needed.

References:

Turk HF, Barhoumi R, Chapkin RS. (2012) Alteration of EGFR spatiotemporal dynamics suppresses signal transduction. PLoS One. 2012;7(6):e39682.